Dually Functionalized Cryptophane-[223] Derivatives : Elaboration of Hydrosoluble 129-Xe Biosensors and Chiroptical Aspects

Orsola Baydoun

Numéro National de Thèse : 2019LYSEN064

THESE de DOCTORAT DE L'UNIVERSITE DE LYON
opérée par
l'Ecole Normale Supérieure de Lyon

Ecole Doctorale N° 206
Ecole Doctorale de Chimie (Chimie, Procédés, Environnement)

Discipline : Chimie

Soutenue publiquement le 25/11/2019, par :

Orsola BAYDOUN

Dually Functionalized Cryptophane-[223] Derivatives: Elaboration of Hydrosoluble ^{129}Xe Biosensors and Chiroptical Aspect

Cryptophanes-[223] Doublement Fonctionnalisés : Elaboration de Biosondes au ^{129}Xe et Propriétés Chiroptiques

---

Devant le jury composé de :

Zehnacker-Rentien Anne	Directrice de Recherche	Institut des Sciences Moléculaires d'Orsay	Rapporteure
Chambron Jean-Claude	Directeur de Recherche	Institut de Chimie de Strasbourg	Rapporteur
Martinez Alexandre	Professeur	Institut des Sciences Moléculaires de Marseille	Examinateur
Lesage Anne	Ingénieure de Recherche	Institut des Sciences Analytiques, Lyon	Examinatrice
Brotin Thierry	Directeur de Recherche	Ecole Normale Supérieur de Lyon	Directeur de thèse
De Rycke Nicolas	Maître de conférences	Ecole Normale Supérieur de Lyon	Co-encadrant

Cryptophanes-[223]

Doublement Fonctionnalisés :

Elaboration de Biosondes au

^{129}Xe et Propriétés

Chiroptiques

Acknowledgment

I would like to express my deepest gratitude to my supervisor Dr. Thierry Brotin for his continuous support and kindness. His patience and enthusiasm to science have always inspired me to tackle difficulties. I really appreciate his caring character for little details to get things as perfect as possible. Dr. Brotin monitored my work carefully through our weekly discussions till writing my dissertation. He was always there to answer my questions and give me a lot of time even in the most stressful moments. I am really fortunate to have him as a supervisor and without his support this work would not reach completion.

Deep thanks to Dr. Nicolas De Rycke for his resolute support. His passion in organic syntheses and his smart fresh ideas helped me look to things from different perspectives. His fruitful comments enriched my view to things and his joyful spirit made even the hardest things easy to handle.

I would like to thank Dr. Chantal Andraud, the director of the chemistry laboratory at ENS for giving me the chance to train in my M2 internship and then my PhD.

I would like to thank Dr. Jean-Claude Chambron and Dr. Anne Zehnacker-Rentien for accepting to be my thesis referees and for the time they spent on qualifying my work. My warm thanks to Pr. Alexander Martinez and Dr. Anne Lesage for accepting to be a part of my thesis jury.

Profound appreciation goes for Dr. Christophe Bucher, who gave me the chance to be a part of the supramolecular chemistry group, and placed me on the right track to establish my research career. The warmest "thank you" is for Dr. Jean-Pierre Dutasta for his support, the endless knowledge he offered in our weekly group meetings and for the kindest spirit he used to spread and for Dr. Laure Guy for giving me a lot of advice at the scientific and technical levels. Many thanks for Delphine and Jean-Christophe who kindly answered my questions and of course for the kindest: Christian for his help in computer issues and for the funny jokes he always makes.

Not to forget Dr. Patrick Berthault and his welcoming team Gaspard, Céline and Estelle who hosted me in the CEA, Paris-Saclay and gave me the chance to learn and perform experiments with hyperpolarized ^{129}Xe.

I would like to thank Pr. Jens Hasserodt, Dr. Sébastian Vidal, Dr. Cyrille Monnereau and finally Dr. Patrick Berthault for accepting to be a part of the commette de thèse members and who evaluated my work during my thesis.

Big "thank you" to my colleagues, Mathieu, Maxime, Corentin, Alexander and Maëlle who were always there to help me at the professional and personal levels. Of course, I will not forget to thank my kindest friends and officemates; Jean for his generous soul, endless assistance and for sure for the nice informative conversations we carried; Caroline for her strong confident character, which inspired me a lot and for being always available to give me valuable advices and finally the kindest Ting Ting for her support and tender heart. I would like to thank also my colleagues, Janah, Sylvan, Amandine, Jeremy, lulu, Maher, Damien, Quentin, Clement, Martin, Alix, Junchao, Youssef, Alysa, Angel, Morgan and Fernando, Shaymaa. Deep "Thank you" to my friend Shagor who stood next to me all the way, for his efficient chemistry advices, jokes, funny

and lovely spirit and the confidence he gave me. My thanks to my friend and best “intern” Kajetan who inspired me a lot with his motivation, for the joyful time we spend together in preparing cryptophanes and of course for the chemistry songs he used to write.

“Thank you” for my best friends Batoul, Riva, Sarah, Hadi, Sarah, Zahraa and Haydar for their unconditional support and for their positive vibes. Thanks all for being always next to me.

Finally, I would like to thank my parents, for their unlimited love, who strive a lot for us to achieve our dreams, especially my father who believed in me, gave me all the freedom and supported me emotionally and financially to reach what I am today. Thanks for the cutest sisters Israa and Maysaa and my brother Firas, and specifically for my soulmate Soha, for being always caring, for your unlimited wise advices and for sharing the hardest and the happiest moments, without you I would have really felt homesick.

Table of Content

List of Abbreviations and Symbols

@: represents the complexation of the guest in the host

α: optical rotation angle

EtOAc: ethyl acetate

Ac: acetate

AC: absolute configuration

APTRA: aminophenol triacetic acid

BAIB: bis(acetoxy)iodo]benzene

9-BBN: 9-Borabicyclo(3.3.1)nonane

B/B_0: magnetic field

CB: cucurbiturils

CTB: cyclotribenzylene

CTG: cyclotriguaïcylene

CEST: chemical exchange saturation transfer

DNA: deoxyribonucleic acid

DIPEA: di-isopropyl ethylamine

DMF: dimethylformaide

DHP: dihydropyran

DNP: dynamic nuclear polarization

DMSO: dimethyl sulfoxide

δ: chemical shift

ΔH: enthalpy change

ΔS: entropy change

ΔG: Gibbs free energy change

d: doublet

ee: enantiomeric excess

ECD: electronic circular dichroism

EDCI: N-ethylcarbodiimide

E: electrophile

equiv.: equivalents

ε: absorbtivity

HRMS: high resolution mass spectrometry

HSQC: heteronuclear single quantum coherence spectroscopy

HPLC: high performance liquid chromatography

HOBt: hydroxybenzotriazole

HP: hyperpolarized

ITC: isothermal calorimetric titration

IUPAC: international union of pure and applied chemistry

IR: infrared

J: coupling constant

k: Boltzmann constant

K: association constant

λ: wavelength

MRI: magnetic resonance imaging

Me: methyl

M_0: magnetization vector

m: multiplet

NMR: nuclear magnetic resonance

NOE: nuclear Overhauser effect

μ: electric dipole moment

OH: hydroxyl

PEG: polyethylene glycol

PPTS: pyridinium para-toluene sulfonate

ppm: part per million

ROA: raman optical activity

R: rotational strength

rac: racemic

SOR: specific optical rotation

SEOP: spin exchange optical pumping

S_N: nucleophilic substitution

T_1: longitudinal relaxation time

T_2: transverse relaxation time

THF: tetrahydrofuran

THP: tetrahydropyran

TLC: thin layer chromatography

TEMPO: (2,2,6,6-tetramethylpiperidin-1-yl)oxyl

TBTQ: tribenzotriquinacenes

VCD: vibrational circular dichroism

V: volume

UV: ultra violet

Résumé de la Thèse:

Les cryptophanes constituent une classe de composés macrocycliques uniques caractérisée par la présence d'une cavité lipophile dont la taille peut varier selon la nature du cryptophane. En solution, cette cavité est susceptible d'accueillir divers substrats comme de petites molécules ou des atomes (ions, gaz rare) dont les propriétés physiques s'en trouvent alors modifiées. Depuis la première description de ces composés en 1981 par André Collet, les cryptophanes ont connu un regain d'intérêt au début des années 2000 avec la mise en évidence de la complexation du xénon par des cryptophanes de petites tailles. Cette découverte a depuis été exploitée par plusieurs équipes internationales pour préparer des bio-sondes moléculaires pouvant présenter un intérêt en imagerie de résonance magnétique nucléaire (IRM) du xénon hyperpolarisé. Au contraire des autres techniques IRM développées jusqu'ici, l'IRM du xénon hyperpolarisé des complexes xénon-cryptophane repose sur une technique de détection basée sur le déplacement chimique. Les complexes xénon-cryptophane présentent ainsi une signature spécifique qui peut être facilement identifiée et exploitée pour produire une image IRM. La très grande sensibilité de la technique combinée aux propriétés exceptionnelles des complexes xénon-cryptophanes rendent cette approche extrêmement intéressante pour concevoir de nouveaux traceurs pour l'imagerie RMN du xénon hyperpolarisé.

Ce travail nécessite toutefois de développer en amont de nouveaux cryptophanes présentant toutes les caractéristiques requises pour une utilisation optimale en milieu physiologique. La mise en œuvre de composés présentant une bonne solubilité est par exemple cruciale pour éviter les phénomènes d'agrégation pouvant se produire dans les milieux aqueux. Le greffage sélectif d'une tête de reconnaissance présentant une activité biologique prédéfinie constitue également un verrou important qu'il faut prendre en compte. Au cours de ces 20 dernières années des résultats importants ont été rapportés dans la littérature et ont permis de démontrer l'intérêt de ces systèmes supramoléculaires pour l'imagerie RMN. Cependant, les systèmes développés jusqu'ici n'ont pas permis de résoudre de manière satisfaisante les deux points soulevés ci-dessus.

Ce travail de thèse a pour objectif de développer de nouveaux cryptophanes hydrosolubles possédant une fonction organique unique permettant d'accrocher une tête de reconnaissance. Pour cela, un cryptophane de type [223] possédant une fonction réactive a été modifiée de façon à introduire de manière sélective une fonction acide carboxylique sur la chaîne dioxypropylene. Cette approche originale permet de tirer profit des six autres fonctions localisées sur les cycles aromatiques pour introduire des groupements hydrosolubles à une autre étape de la synthèse. Nous avons ainsi pour la première fois été capable de préparer de nouvelles plateformes organiques de type cryptophanes répondant à ce cahier des charges strict. L'intérêt de cette nouvelle approche réside également dans la très grande flexibilité de nos systèmes organiques puisqu'ils peuvent être très rapidement utilisés par d'autres pour y introduire de nouvelles fonctionnalités. Pour mettre en avant notre stratégie de synthèse nous avons développé un cryptophane capable de détecter les ions zinc et nickel en milieu physiologique. Les avantages et les inconvénients liés à notre approche sont discutés en détail dans ce mémoire.

La deuxième partie de ce mémoire est consacrée à l'étude des propriétés chiroptiques de cryptophanes donnant lieu à un phénomène d'auto-encapsulation lequel dépend de la nature du solvant. C'est la première fois que cet effet est observé avec ces composés macrocycliques. Pour mettre en évidence ce phénomène plusieurs techniques comme la spectroscopie RMN et Infrarouge (IR) ou encore les techniques chiroptiques de dichroïsme circulaire électronique (ECD) et vibrationnel (VCD) ont été utilisées. Celles-ci révèlent des modifications importantes en fonction de la nature et la taille du solvant. Cependant, une étude réalisée sur plusieurs composés montre clairement que seules les techniques RMN et IR permettent de mettre en évidence ce phénomène d'auto-encapsulation. Cet effet original apparaît donc comme un autre moyen pour ces composés macrocycliques de combler leur cavité sans faire intervenir d'autres changements conformationnels plus énergétiques.

General Introduction

General Introduction

Cryptophanes are container-like molecular structures that have the ability to encapsulate various substrates in their lipophilic cavity. This structure, which is elegantly tailored, has offered different lessons in supramolecular chemistry especially in host-guest interactions. The high affinity of cryptophanes to xenon has been smartly exploited to design ^{129}Xe-NMR/MRI sensors. Unlike the usual proton-based MRI tracers, ^{129}Xe-cryptophane combination allows accessing smart MRI biosensors that are characterized by their fast response and high sensitivity. Since 2001, a large number of hyperpolarized ^{129}Xe-cryptophane biosensors has been reported for the detection of various physical and biological targets like pH, temperature, enzymatic activity and ionic analytes. The synthesis of these molecular structures remains challenging and this thesis is dedicated to develop a new strategy aimed at facilitating the elaboration of these cryptophanes based biosensors.

The first part of this manuscript describes the synthesis of cryptophane platforms for biosensing applications. In the introductory chapter of this part, we gave a general view on cryptophane derivatives and their main features. Additionally, we delivered a non-exhaustive description of the new imaging and hyperpolarization techniques and the biosensors reported in literature. In a second chapter, we focused our attention on the synthesis and development of new cryptophane-[223] platforms, characterized by their improved water solubility and easy functionalization via the two available reactive sites. The sensors elaborated from these new cages were studied by hyperpolarized ^{129}Xe NMR spectroscopy and ITC experiments and the results are reported in the third chapter.

A second part of this manuscript is dedicated to the synthesis and the characterization of cryptophane-[223] derivatives subjected to self-encapsulation. An introductory chapter of this part describes the synthesis of enantiopure cryptophanes and their characterization by different

chiroptical tools. In the second chapter, we reported the main results that evidence the self-encapsulation phenomenon and the corresponding chiroptical variations induced by it for a series of cryptophane-[223] derivatives.

At the end of each part of this manuscript, we reported the detailed experimental procedures leading to the new derivatives and their corresponding characterizations. An additional part gathers the main compounds and their corresponding numbers in the text. This part is added to facilitate the reading of the thesis. The references are all gathered at the end of the manuscript.

Part I: Development of New Cryptophane-[223] Platforms for ^{129}Xenon Based Biosensing Applications

Chapter 1: Bibliography

Introduction

The knowledge in biological systems' chemistry is inevitably inspiring.[1] Inspirited by natural processes, supramolecular chemistry or "the chemistry beyond the molecule" has emerged, as the study of the structure and function of intermolecular assemblies among molecules driven by weak non-covalent interactions.[2] Supramolecular chemistry has served, to a great extent in a better understanding of biological processes, which are vastly governed by non-covalent bonds like hydrogen bonding, Van der Waals interactions, solvophobic effect and coulombic interactions.[3] From protein folding, enzyme-substrate assembly, genetic information storage, transcription, to the most complicated cells interaction, highly selective and delicate cascade of events takes place, starting from the selective recognition of a receptor or a "host" to a substrate or a "guest".[4,5,6] This recognition is based on complementarity, the strength and kind of interactions and the extent of preorganization of the non-complexed species before the binding event.[7] Exploiting this knowledge, Pedersen in 1967[8], Lehn and Sauvage in 1969[9] and Cram in 1973[10] have developed new families of structurally ion-selective complexes, establishing by this the foundations of the field. Greater complexity has been added to this field by introducing photo or electro-responsive motifs, making dynamic molecular assemblies, Figure 1.[11]

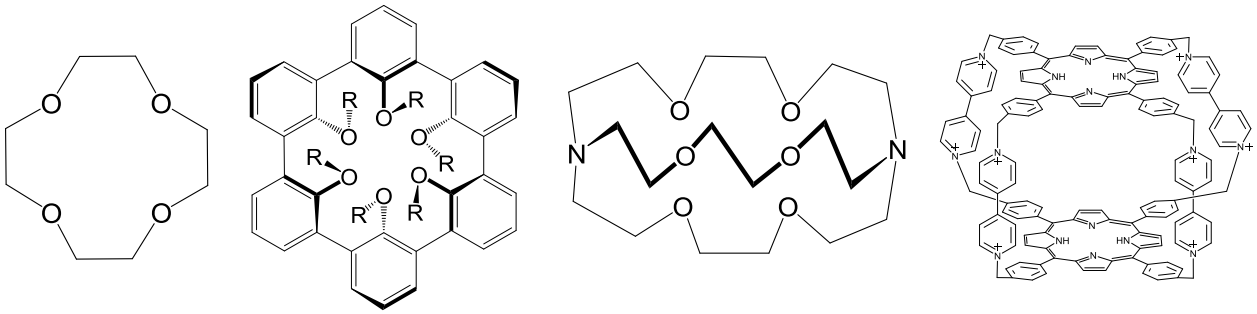

Figure 1: earliest receptor crown ether by Pedersen, Cram's spherand, Lehn's macrobicylic cryptands and Stoddart's modern containers.

Among the vast majority of supramolecular designs, molecular containers possessing hollow, concave hydrophobic surfaces have gained special attention. Mimicking enzyme's hydrophobic pocket, these containers can selectively recognize smaller convex molecules based on the size, shape and nature of the inner surface.[12,13] The residency time of such complexes is strongly dependent on the host's structure. For example, molecules with rigid enclosed spheres can permanently encapsulate guests and these are referred to as carcerands.[14,15] Other structures possess dynamic portals[16] allowing the exchange of the contained molecule with the bulk such as cavitands, deep cavitands,[17] cryptophanes,[18] hemicarcerands,[19] cyclodextrins,[20] hemicryptophanes,[21] and calixarenes,[22] Figure 2. Once the complex formed, a change in the guest behavior is expected, due to the change in the surrounding environment. These include physical, mainly magnetic properties, which are well characterized by NMR spectroscopy, conformational and catalytic properties.[12] This effect is especially important because it paves the way for many applications such as catalysis, stabilization of highly reactive intermediates, sensors, nano-scale molecular reactors and separation agents.[23, 24 ,21]

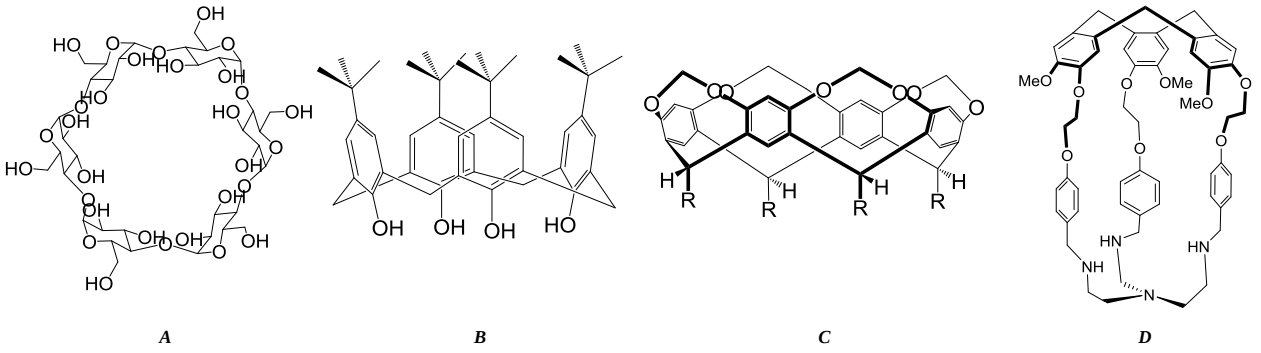

Figure 2: examples of cavity-containing macrocycles like cyclodextrins **A**, calixarenes **B**, cavitand **C** and hemicryptophane **D**.

The elegantly elaborated cryptophanes constitute a family of the earliest molecular containers with a hydrophobic cavity, Figure 3. Reported by André Collet in 1981, cryptophanes are initially

made up of two C_3-symmetric cyclotribenzylene CTB units connected by three modifiable bridges. The first cryptophane synthesized was the cryptophane-A, which is still very useful nowadays to prepare new cryptophane derivatives. This cryptophane was initially constructed to bind lipophilic molecules like halogenomethanes and isobutanes constituting by this, the first family of molecular containers to isolate lipophilic guests from the bulk.[18] Remarkably, enantioenriched cryptophanes were the first molecular hosts to isolate and discriminate between the two enantiomers of CHFClBr, one of the smallest chiral molecules. For a long period of time, cryptophanes have been mainly framed in fundamental research, where the study of their complexes has served to understand molecular recognition. Since 2001, these molecules have gained a lot of attention in xenon based sensing applications. The remarkable structural features of cryptophanes, from chirality, tunable cavity size and solubility have been heavily exploited to finely tune properties to applications. In this chapter a detailed description of cryptophanes' structure, symmetry, conformations, synthesis, complexes and applications will be discussed.

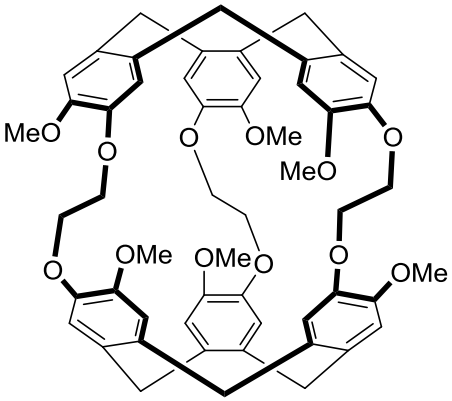

Cryptophane-A

Figure 3: structure of cryptophane-[222] $(OMe)_6$ or the so-called cryptophane-A, under the IUPAC name: 3,22-(Epoxyethanoxy)-6,9:25,28-dietheno-7,36:17,26-dimethano 14,18:33,37 dimetheno18H,37 Hdibenzo[j,na1].

1. Cryptophanes: General Features

1.1. Structure and Nomenclature:

Cryptophanes are constructed from two C_3-symmetric CTB units, connected by three bridges whose length and nature can be varied. Numerous cryptophane derivatives have been prepared so far and the readers can refer to different reviews made by Collet, Brotin, Dutasta and Holman to appreciate the large diversity of cryptophane derivatives, which have been prepared to date.[25, 26, 27] To talk about the CTB units, they have been synthesized since 1915 but correctly described in 1965.[28] These units are synthesized from three consecutive Friedel-Crafts alkylations of electron rich 3-4-disubstituted benzyl alcohols, which adopt a crown-shaped conformation. Depending on its substituents, CTB units can have an achiral C_{3v}-symmetry if the substituents on the CTB rims, R_x and R_y are identical or a chiral C_3 or C_1-symmetry if they are different, Figure 4.[29] The two enantiomers of the chiral CTB units possess helical chirality, hence they can adopt an *M* or *P* helicity, which can interconvert at high temperature as will be seen later. CTB, by themselves, have been utilized for many applications, including binding of neutral molecules like fullerene, cations and anions and form liquid crystals.[30,31,32] To talk about the cryptophanes' bridges, they can vary in nature and length from alkyl, alkenyl, aryl or alkynyl chains.[33,34,35] The CTB and the bridges, combined, can determine the properties of the resulting cage like cavity size, solubility, chirality and their affinities to the guests.

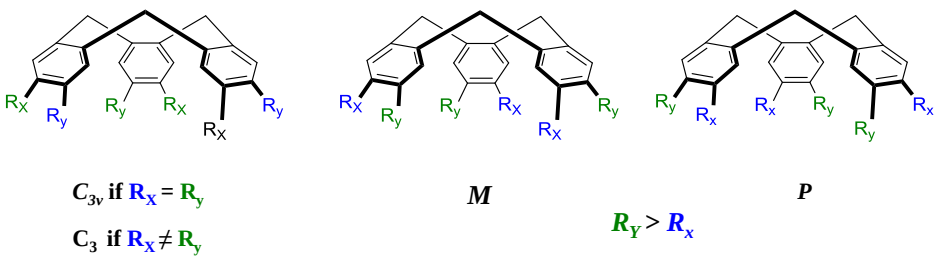

Figure 4: CTB unit symmetry and helical chirality.

The IUPAC nomenclature of cryptophanes is not adopted due to its complexity and length, Figure 3. Since the first reported cage, simpler names were given by A. Collet to different cages like A, B, C, E, etc... For example, cryptophane-A was the first cage prepared by Collet and co-workers. This cage possesses three ethylenedioxy linkers and six methoxy groups on the two CTB units. Cryptophane-B, however is the *syn*-isomer of cryptophane-A, which is recently reported by Brotin et al.[36] These simplified names reflect neither the structure nor the time at which the cages were synthesized. Henceforth, a more generalized naming system is adopted. This system is based on indicating the length of the linkers and the nature of substituents on the CTB caps whenever possible. For example cryptophane-A becomes [222] $(OMe)_6$. For the moment no concrete naming system is adopted and each research group tends to name cryptophanes on their own way.

1.2. Cryptophane Symmetry:

Molecular symmetry of cryptophanes is one of the key features to be studied to better understand their mode of complexation and interactions with the guest. Inherited from the chirality of CTB caps and the arrangement of the substituents around the linkers, cryptophanes exist in two different diastereomers, the *syn* and the *anti*. This modification can have a huge impact on the binding properties of these derivatives, Figure 5.

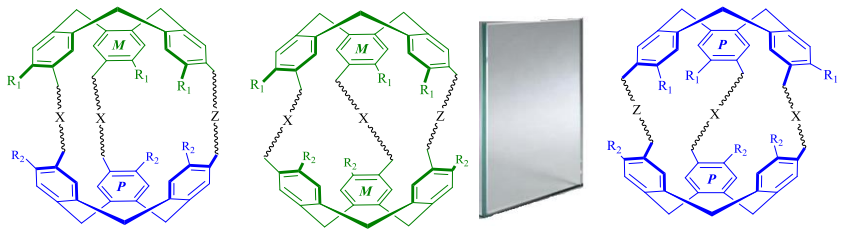

Figure 5: possible cryptophanes' configurations.

Compared to *syn*-isomer, *anti*-cryptophane is more flexible and has better binding properties. The *anti*-diastereomer forms when two CTB with the same absolute configuration are connected (*MM* or *PP*). This derivative is always chiral whatever the nature of the substituents or the linkers are, like cryptophane-A with D_3 symmetry. The *syn* isomer is formed when the two CTB connected have opposite handedness (*MP*). This isomer is achiral, provided that the substituents and the linkers are identical (R_1=R_2 and X=Z), like cryptophane-B with C_{3h} symmetry, else it will be chiral like cryptophane-D (*syn*-Cryptophane-[222] $(OMe)_3$) with C_3 symmetry. Table 1 provides the details of the point group and the chirality of the two diastereomers depending on the nature of the substituents and the linkers.[26]

Configuration	Substituents and linkers	Symmetry	Chirality
Syn	R1=R2, X=Z [36,37]	C_{3h}	Achiral
	R1=R2, X≠Z	*Cs*	Achiral
	R1≠R2, X=Z[29]	C_3	Chiral
	R1≠R2, X≠Z	C_1	Chiral
Anti	R1=R2, X=Z[37]	D_3	Chiral
	R1=R2, X≠Z[38]	C_2	Chiral
	R1≠R2, X=Z[39,40]	C_3	Chiral
	R1≠R2, X≠Z[41]	C_1	Chiral

Table 1: summary of cryptophanes' symmetry and chirality.

1.3. Conformation:

The CTB bowls of cryptophanes can adopt two different conformations, a stable "crown" as proved by X-ray structure and a less stable "saddle" shaped conformation (disfavored by 13-16 kJ/mol). The formation of the "crown" conformer is usually evidenced by ^{1}H NMR spectroscopy, which shows distinct signals for the two diastereotopic protons of the methylene bridge (axial and equatorial protons). The latter pseudo-rotating "saddle" conformer is an intermediate in the inter-conversion of the two "crown" conformational isomers (*M* and *P*) obtained at higher temperature (at 100 °C, the interconversion takes place in few minutes), Figure 6. It is specifically formed by an inward flipping of the CTB methylene bridge. The lack of stability of the latter compared to "crown" conformation is due to the repulsion of the two hydrogens on the methylene bridge.[42,43] The two conformations show distinct NMR signals and they can be easily identified.

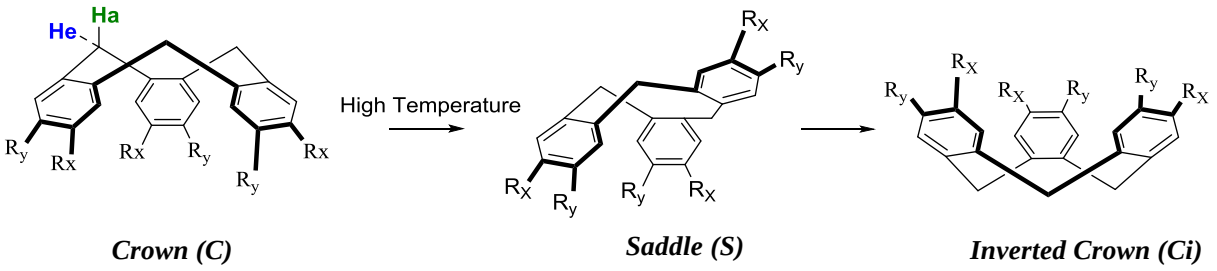

Figure 6: inter-conversion between CTB crown conformers passing by a relatively non-stable saddle conformer.

Similar to CTB, tribenzotriquinacenes (TBTQ) are a family of three mutually fused indanes, developed by D. Kuck and coworkers.[44,45] These molecules are similar to CTB in symmetry and shape but differ in conformational rigidity. TBTQ are usually more rigid than CTB thanks to the bridge fusing the three methylene groups. With their original structure and rigidity, these molecules are usually hard to obtain in C_3-symmetry. Racemic mixture of TBTQ trialdehydes has

been also used to construct cryptophanes by dynamic covalent assembly with enantiopure (1*S*,2*S*)-diamino-cyclohexane. This strategy led to the formation of three diastereomeric mixtures of multiple Schiff's bases and their corresponding hydrolysis gave rise to the enantiopure *M* and *P*-TBTQ, Figure 7.[46]

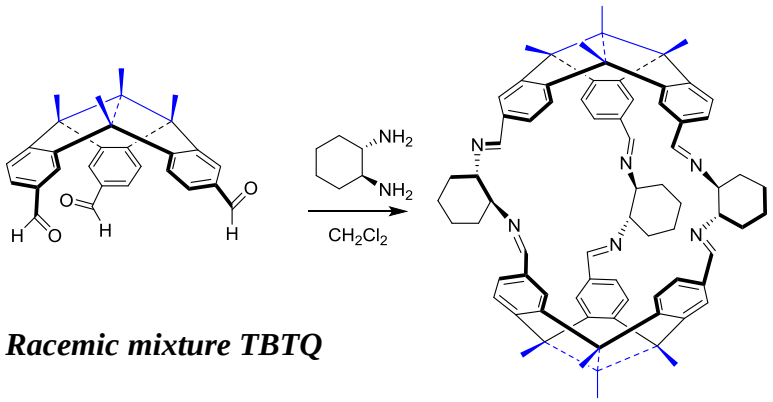

Figure 7: structure of a TBTQ derivative and the cryptophane derived by dynamic covalent assembly.

Cryptophanes derived from CTB, however show some flexibility and undergo a similar type of conformational conversion to that of the CTB caps. These forms are the following, out-out (*CC*), in-out (*CCi*), saddle-out (*CS*) and in-in (*CiCi*) conformers, Figure 8. It is noteworthy that the presence of several conformers can complicate the characterization of the cryptophane derivatives.

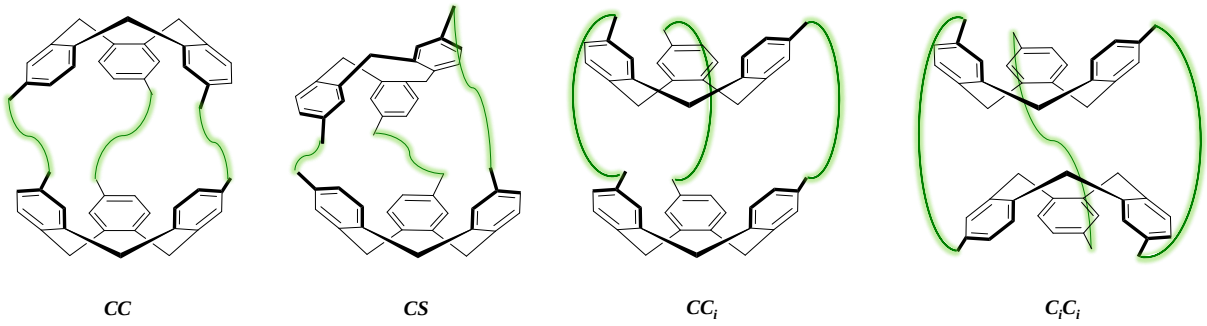

Figure 8: possible conformers of cryptophanes.

The (*CS*) conformer or the so-called imploded form possesses a unique ^{1}H NMR signature compared to the (*CC*) conformer.[47,48,49] This form was initially observed in cryptophanes with long flexible linkers or in the presence of a solvent that does not fill the cavity. [50] Surprisingly, smaller cryptophane cages (i.e. cryptophane-[222] derivatives) are also capable to implode like cryptophane-[222] $(OCH_2CO_2H)_6$. The imploded form can readily be formed upon heating or storing the compounds for a long time in the solid state. For example, the imploded form of m-xylyl-bridged cryptophane was obtained at high temperature (210 °C). Purification of this form offered a clean detailed ^{1}H NMR and single crystals were also analyzed assuring the (*CS)* conformation, Figure 9.[47]

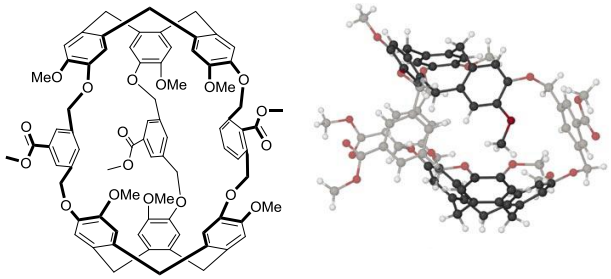

Figure 9: m-xylyl bridged cryptophane capable of forming imploded form on the left. Imploded form of the cryptophane as determined by the single-crystal structure on the right.

Recently, we have discovered a new type of conformational isomer with cryptophane-[223] bearing a substituent on the central propylenedioxy linker. This conformation corresponds to the position of the central substituent that can be inside or outside the cavity, which is referred to as "self-encapsulation". This new conformational change represents an easy way for cryptophanes to fill their cavity with low energetic cost. The process is solvent dependent and will be thoroughly discussed in the second part of this thesis.

1.4. Cryptophane Complexes:

As mentioned previously, cryptophanes possess a lipophilic cavity suitable to accommodate different guest molecules. Being a container molecule, cryptophanes' binding process is governed by constrictive binding property for the in-out exchange of the guest, Figure 10. Cryptophanes binding portals are the linkers and its cavity is defined by the three dimensional arranged six aromatic rings. Cryptophanes' constrictive binding is based on "sliding door" mechanism, that is the optimization of the cryptophanes' portals by squeezing or expansion to accommodate the corresponding guest.[16] This mechanism involves conformational changes of its flexible linkers. In cryptophanes, the stability of the guest@cryptophane complex is governed by several factors, mainly the volume compatibility (very large or very small guests do not fit properly based on ratio of coefficient packing $V_{guest}/ V_{cryptophane} = 0.55$)[51], size and shape of the guest (globularly shaped guests) and electronic effect (highly polarizable atoms like xenon) and of course the symmetry of the cage itself, which greatly affects the binding properties.[27]

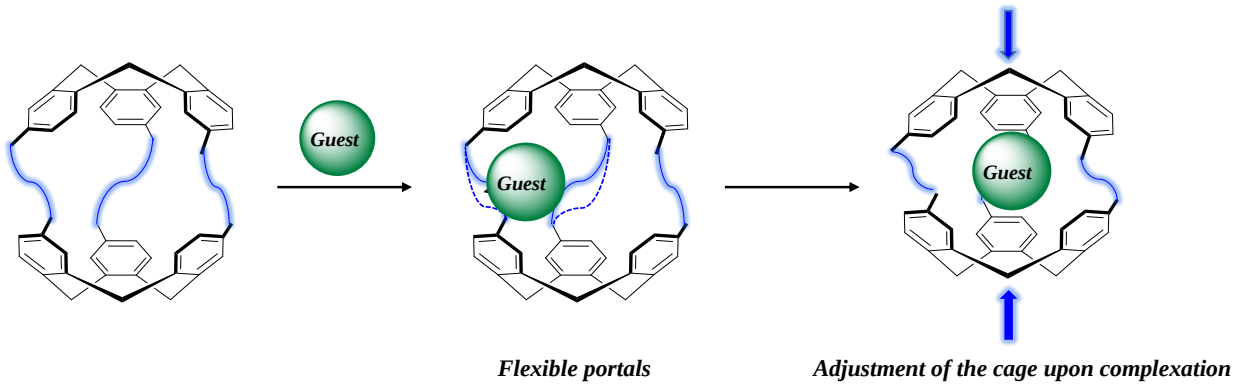

Figure 10: constrictive binding of guests by sliding the portals (linkers), followed by the adjustment of the cavity size.

Complexation studies are investigated in both organic and aqueous media depending on the cage solubility and the guest of interest. ^{1}H NMR spectroscopy serves as a leading tool to study such interactions, showing a high shielding of the encapsulated guest by the effect of the cage's ring

current. Isothermal calorimetric titration (ITC) appears as another useful method to measure accurately the association constant in water or in organic solvents. In addition, this method gives access to thermodynamic parameters of complexation (ΔH°, ΔS° and ΔG°). Thus ITC is a very important analytical tool to understand how the binding process between a cryptophane and a guest molecule takes place. Brotin and co-workers have used intensively this method to determine the association constant between water-soluble cryptophanes and cationic species. Below is a representative ITC plot for the titration of cryptophane-[222] $(OH)_5$ dissolved in LiOH (0.1M) and Tl(OAc) performed at 298K. This titration reveals the strong association constant (K_a = 2.39 10^9 M^{-1}) of Tl^+ by this cryptophane derivative, Figure 11.[52]

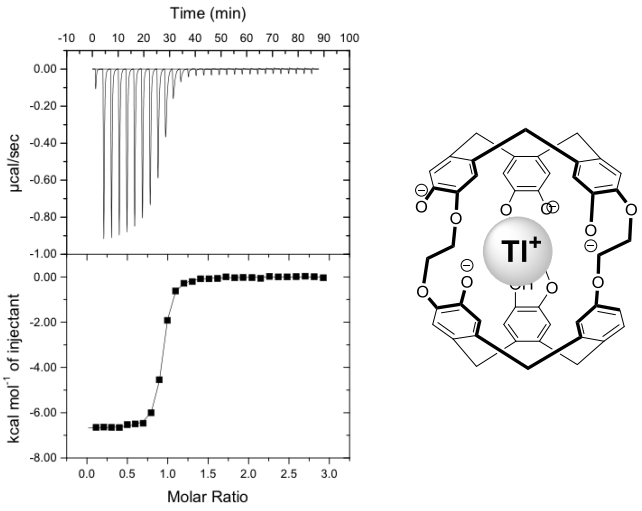

Figure 11: representative plot of the raw ITC data for the titration of cryptophane-[222] $(OH)_5$ (29.9 µM) with Tl^+ (401 µM) in competition with Rb^+ (299 µM).

In the coming sections, we will describe the different types of guests encapsulated by cryptophanes in solution.

1.4.1. Encapsulation of Neutral Species:

Cryptophanes are well known for their interesting ability to encapsulate neutral molecules like $CHCl_3$, CH_2Cl_2, isobutane, CHFClBr, CHFClI, epoxides, and gases like methane and xenon.[53,54,55,29,56,57] These complexation studies are done in solution. 1,1,2,2-tetrachloroethane appears as the solvent of choice because it is too big to enter the cavity of the smallest cryptophanes (cryptophane-[111], cryptophane-A, cryptophane-C). Thus it does not act as a competitor with the guest studied. Other non-competing solvents might also be employed like bis(trichlromethyl)ketone that was used by Crams and coworkers.[58] Recent studies show that 1,1,2,2-tetrachloroethane can partially enter the cavity of cryptophane-E and larger cryptophanes.[48] What is quite interesting in these complexes is the ability of cryptophanes to scavenge lipophilic guests in organic solvents, without having a hydrophobic effect. Another remarkable feature is that cryptophanes differentiate guests based on little volume changes. For example, cryptophane-E has a higher affinity to $CHCl_3$ compared to $CHCl_2Br$.[59]

1.4.2. Enantioselective Binding of Guests:

Enantioselective binding of chiral guests is also possible with cryptophanes. Unfortunately, the number of examples reported in the literature is rare because enantiopure cryptophanes are hard to obtain and the number of small chiral guests that can enter their cavity is limited and difficult to obtain in their enantiopure form. This enantioselective binding was first demonstrated by distinguishing the two enantiomers of CHFClBr by ^{1}H NMR spectroscopy using cryptophane-C ([222] $(OMe)_6$). The difference in binding constants between the two diastereomeric complexes affects the orientation adopted by the guest inside the cavity and its magnetic properties, which will be readily detected by ^{1}H NMR spectroscopy. Enantioselective complexation of *R*-methyl oxirane was also realized in water by enantiopure *PP*-cryptophane-[222] $(OH)_5$ with a free

energy difference 1.7 kJ/mol compared to the less stable *S*-methyl oxirane@*PP*-cryptophane, Figure 12. Recently, the complexation of additional oxiranes by the same cryptophane derivative was also tested and studied by ^{1}H NMR and electronic circular dichroism spectroscopy, ECD. Most interestingly, 2,2′-bioxirane, which has two chiral centers shows three diastereomers in the presence of enantiopure cryptophane. These diastereoisomers are readily distinguished by ^{1}H NMR spectroscopy.[60,61]

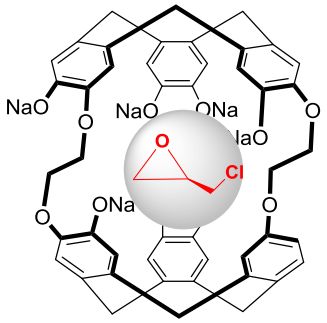

Figure 12: enantioselective encapsulation of (*R*)-epichlohydrin cryptophane by *MM*-cryptophane-[222] $(OH)_5$.

1.4.3. Encapsulation of Cationic Species:

Cryptophane cages are also suitable for cation complexation. The encapsulation of organic (ammonium) cations has been thoroughly studied in the past. However, complexation of metallic cation is more recent. Remarkably, the binding of alkali cations (rubidium, cesium) occurs in water, a strong competing solvent, and under basic conditions in order to solubilize the cryptophane derivative. As revealed by titration experiments, this work has shown that thallium (Tl^{+}) (caution: very toxic) is very well recognized under these conditions. More recently, some measurements have also been obtained at pH close to 7, with new cryptophane derivatives. In cation complexation, the presence of phenol groups seems mandatory to observe an efficient binding and the replacement of these groups by carboxylic acid moieties results in a lack of

complexation. For instance, cryptophane hexa-carboxylate does not bind cationic species such as cesium or thallium cations under the same conditions.[62,63,64,65,66,67]

1.4.4. Encapsulation of Anionic species:

The electron rich cavity of cryptophanes renders anion complexation impossible. Coordination of the aromatic rings with electron withdrawing transition metals from their outer rims makes cryptophane's cavity poor in electrons, thus suitable for anion complexation. This has been smartly demonstrated by Holman and co-workers that reported a water soluble cryptophane-[333] $(OMe)_6$ cage with six $[Cp^*Ru]^+$ moieties. Encapsulation of $[CF_3SO_3]^-$, $[SbF_6]^-$ and $[PF_6]^-$ was then achieved using this cage and they were stabilized by π-anion interactions, Figure 13.[68]

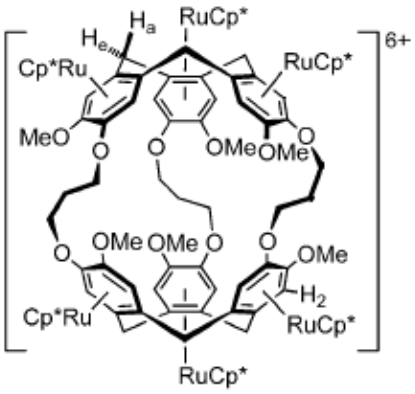

Figure 13: structure of water soluble cryptophane [333] $(OMe)_6$ $[Cp^*Ru]Cl_6$. [68]

2. Synthesis of Cryptophanes

The construction of cryptophane cages has been achieved in three different ways, the simplest *direct method*, the *template method* and the *coupling method*, all starting from the vanillic alcohol building block. These methods mainly differ in the way of creating and/or connecting the two CTB units.[27] Each method has its own advantages and inconveniences and we will give one or two examples per each.

2.1. Direct Method or Two-Step Cryptophane Synthesis:

The *direct method* consists of the trimerization of properly bridged and substituted vanillic alcohol dimers. With six consecutive Friedel-Crafts alkylations under acidic conditions (usually formic acid works very well), the *direct method* provides cryptophanes in low yields and it gives a lot of side-product (mainly polymerized byproducts). The reaction is controlled by the diffusion, so it is not possible to use diluted conditions to decrease the formation of the byproducts. This strategy allows the access of exclusively D_3 and C_{3h} symmetrical cages, and it is more suitable for the construction of intermediate size cages (bridge size < 6) as the increase in the bridge length drops the yield to the favor of the intramolecular condensation.[37,69] The approach has been used by chemists to obtain cryptophanes rapidly for complexation studies but it is less used to obtain sophisticated functionalized cages. An example is given with the synthesis of cryptophane-E, which has been obtained with a relatively high yield of 20%, Figure 14. In the case of cryptophane-A, the same approach gives rise to this derivative with an extremely low yield (1-2%).

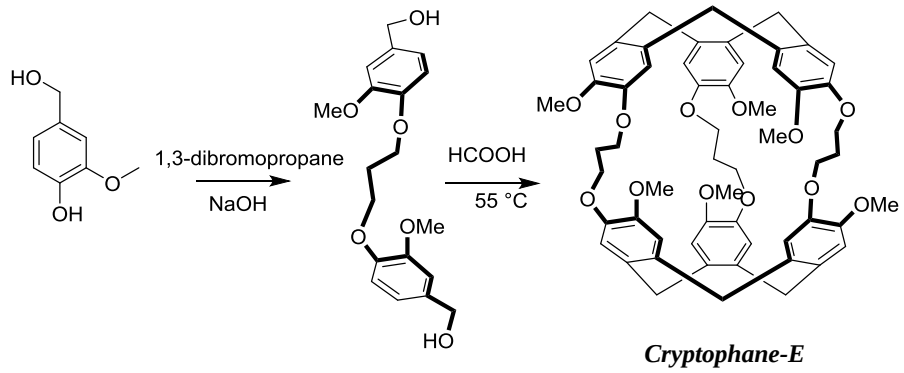

Figure 14: synthesis of cryptophane-E starting from vanillic alcohol by the *direct method* where it is obtained in 20% yield.

2.2. Template Method:

The *template method* is the earliest and by far the most employed approach to prepare cryptophane derivatives, because it allows the access to a wide range of cages of different symmetry and functionalization.[18] It is also the most appropriate method to obtain fair quantities of cryptophanes. In this method a CTB unit is first constructed, then elaborated by the attachment of three bridges with peripheral benzyl alcohols to form the so-called "template". The cyclization of the second CTB is usually carried under diluted acidic conditions usually 10^{-3} M in pure formic acid or in equal mixture of formic acid/$CHCl_3$. Other conditions have been used to conduct the second intramolecular cyclization like perchloric acid/methanol mixture, and scandium triflate/ acetonitrile mixture. The latter provides a milder condition and makes purification easier.[70] The main advantage of this method compared to the *direct method* is that it is not diffusion controlled, this indicates that more diluted conditions can be used, thus decreasing the polymeric side-products. With this strategy, accessible synthesis of C_1-symmetric cages with different bridges and substituents is achieved. A wide range of *syn* and *anti*-configurations are constructed. The diastereoselectivity of the cyclization is dependent on many conditions like substituents and linker's length, which are usually hard to control and predict. For example, it was believed that cryptophanes with an odd number of carbons on the linker tend to give *syn*-configurations, whereas, even ones give *anti*-configurations. Opposite to this claim, nona- and dodecamethoxy-[222] cryptophanes, give rise to *anti* and *syn* configurations, although they have even number of carbons on the linkers.[71] As an illustration of the higher yields obtained with *template method* compared to the *direct method*, we can talk about cryptophane-A, which is obtained in a higher yields (80%) compared to 1-2% yield, Figure 15.

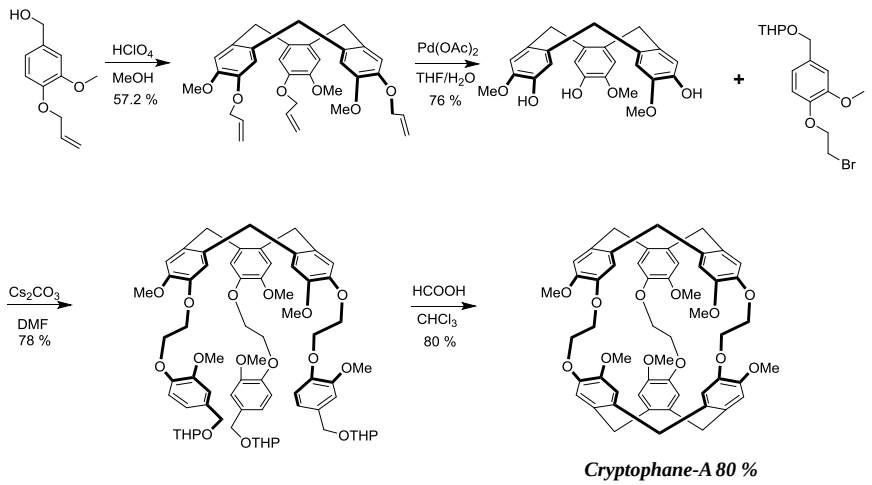

Figure 15: synthesis of cryptophane-A by the *template method* with 80% yield.

2.3. Coupling Method:

As its name implies, the method relies on the coupling of two properly functionalized CTB units. Unlike the first two methods, in the coupling approach no need to use acidic conditions. *Coupling method* was first utilized by Cram and coworkers in 1991 to couple a bis-alkyne-bridged CTB by cupric oxidative coupling.[58] This method was later employed to synthesize other cryptophanes like the cryptophane-[111] by Brotin, Dutasta and co-workers, Figure 16,[55] and cryptophane-[000] by Hardie and co-workers.[54] Asymmetric cryptophanes-[221] and [112] by Rousseau and co-workers[72] and aryl-bridged cryptophane by Holman and co-workers[73] have also been prepared in low yields by using a similar approach.

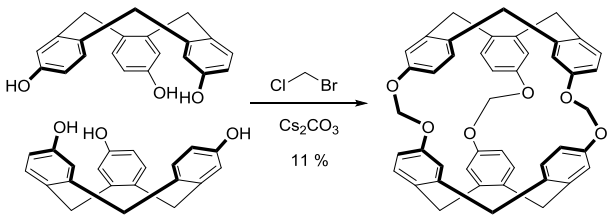

Figure 16: synthesis of cryptophane-[111] by *coupling method*.

2.4. Functionalization and Solubilization of Cryptophanes:

As many other symmetrical lipophilic supermolecules, the main synthetic challenge relies on the selective functionalization and solubilization of the core. These two different aspects are very important for the design of xenon-biosensor, as it will be seen later. Added functionalities can eventually be used to introduce a sensing unit, water solubilizing groups, a chiral moiety to optically resolve cryptophanes enantiomers or an anchoring arm to attach them to nanoparticles. These functionalities can be introduced either before or after the cage cyclization. Herein, a detailed description of the functionalization strategies is addressed.

Readily formed cryptophanes can be modified by substituting the existing functionalities, mostly methoxy groups, with other ones via alkylation, acetylation or dehydroxylation. Since 1987, André Collet reported an efficient selective procedure to remove the six methoxy groups on cryptophane-A core, using lithium diphenylphosphide producing a water soluble cage with six phenols. Since then, Brotin and co-workers have reported an improved approach. The six phenol moieties are then replaced by other functionalities like acetates or methyl esters, Figure 17. The latter are then hydrolyzed to give six carboxylic acid groups providing a water soluble cage up to pH = 5.[74,34] Other cages of different linker size were also functionalized by this way offering water soluble cryptophanes.[67]

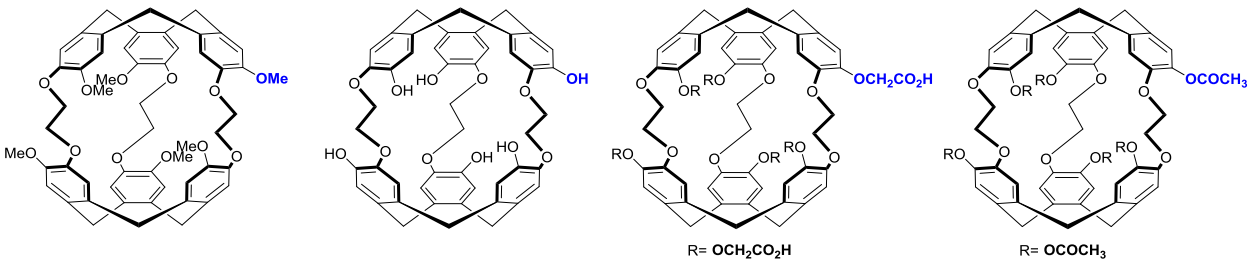

Hexa-methoxy derivative *Water soluble hexa-phenol* *Water soluble hexa-acid* *Hexa-acetate derivative*

Figure 17: functionalization of cryptophanes after a demethylation step either by alkylation or acylation reactions.

The *template method* is the method of choice to synthesize asymmetric cages with different linkers' length and substituents. This method is widely employed to construct different cryptophanes families like mono, tri and dually functionalized cages. In this strategy, a suitably decorated linker or linkers are grafted on the CTB followed by the formation of the second CTB cap.

To talk about the mono functionalized cryptophanes, Brotin and co-workers were able to successfully synthesize mono-allyl protected cryptophane-A derivative, Figure 18. Exploiting the *template method*, a single ethylenedioxy arm possessing an allyl protected benzyl alcohol was introduced to a doubly alkylated CTB, cyclization under acidic conditions yielded the corresponding product, which was further utilized to construct a wide range of symmetric, asymmetric and dimeric cages.[75,76,77,78]

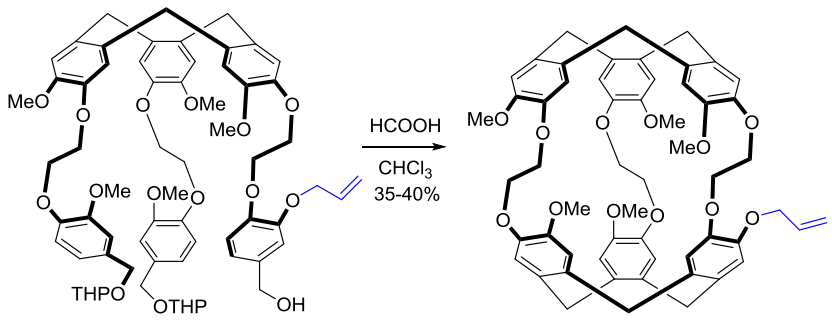

Figure 18: synthesis of mono-allyl protected cryptophane-A from its corresponding template.

Using the same strategy, Dmochowski and co-workers reported the synthesis of mono-propargylic cryptophane-A derivative, which was then functionalized by copper catalyzed cycloaddition.[79] By the same group, successful allyl, benzyl or propargyl tri-functionalized-[222] cages were described using scandium triflate or perchloric acid/methanol for the cyclization step.[70,80] Equally, Rousseau and co-workers described a water soluble tri-functionalizable cage

with three polyethylene glycol groups (PEG) and three propargyl groups on the second CTB, which proved their reactivity for Huisgen cycloaddition.[81] Schröder and co-workers also reported a dually dendronized cage with enhanced water solubility, Figure 19.[82,83] In the latter case, it is worth mentioning that the corresponding di-acidic derivative has never been described. According to our knowledge in cryptophane synthesis, we believe that the two acidic moieties are grafted on the same CTB units, and that the structure of the dendrimer substituted cage is not correct.

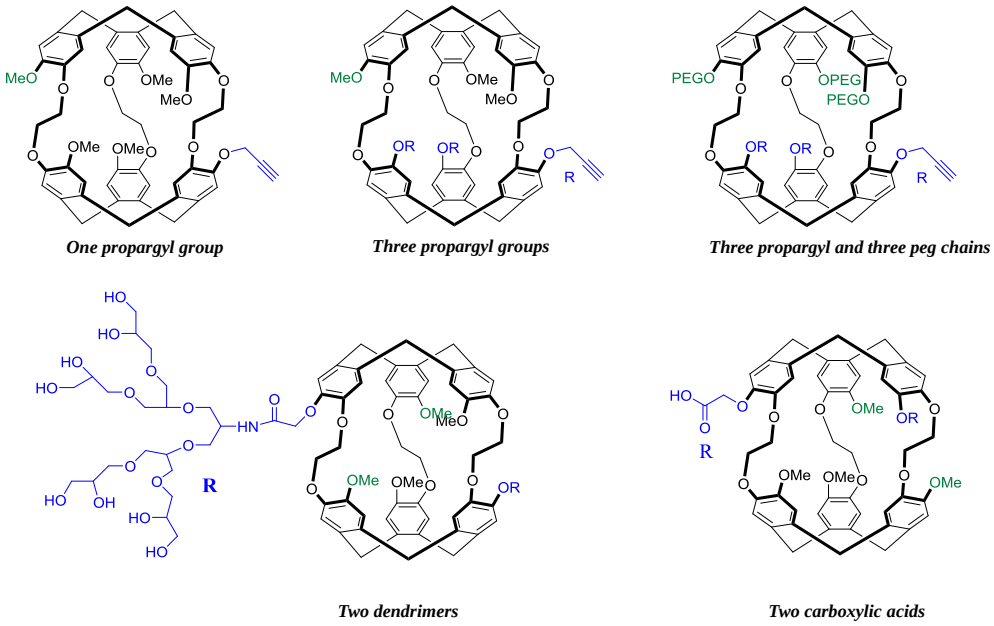

Figure 19: access of multiply functionalized cryptophane by *template method*.

Apart from cryptophane-A platform, Brotin and co-workers reported a dually functionalized cryptophane-[223] core using the *template method*, bearing a central hydroxy group on the propylenedioxy arm and six methoxy groups on the CTB rims. Demethylation of this cage with lithium diphenylphosphide (1 M) provided the cryptophane hexa-phenol with central secondary alcohol, which is soluble in water under basic conditions and has a high affinity to metal cations

like cesium and thallium. The obtained phenol groups were either acetylated or alkylated by methyl bromoacetates. Hydrolysis of methyl esters provided a water-soluble cage with six carboxylic acid moieties and a central hydroxyl group, Figure 20. Further functionalizations were made on the central secondary alcohol like mesylation and alkylation as will be detailed in the second chapter.[41]

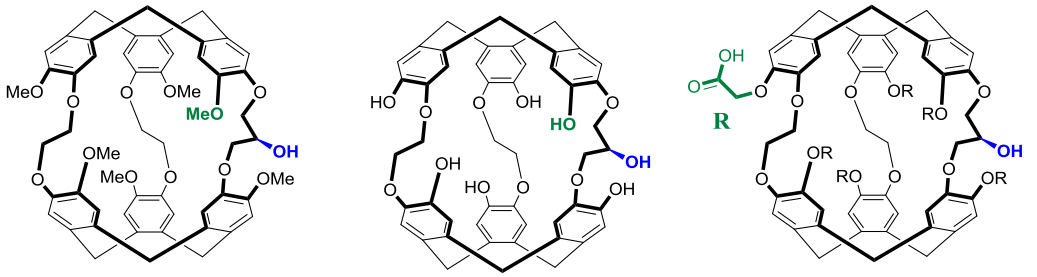

Dually functionalized cage ***Water soluble hexa-phenol*** ***Water soluble hexa-carboxylic acid***

Figure 20: family of dually-functionalized cryptophane cages bearing a central hydroxyl group and six modifiable groups on the CTB rims.

Introducing water-solubilizing substituent is even more complicated with other cryptophanes such as cryptophane-[111] skeleton since this compound is devoid of substituents. Indeed, in absence of any existing functionality on cryptophane-[111] core,[55] new methods have been developed to render it water soluble and functionalizable. Cryptophane-[111] core was first solubilized in water by the metalation of the arene rings with six $[Cp^*Ru]^+$ moieties.[84] Introduction of a single substituent was also possible by introducing iodine or bromine followed by palladium catalyzed coupling reactions.[85,86,87] Metal-free water soluble cryptophane-[111] was also synthesized by Rousseau and co-workers, by an amide coupling of the mono-carboxylic acid derivative with a single tri-sulfonated linker, Figure 21.

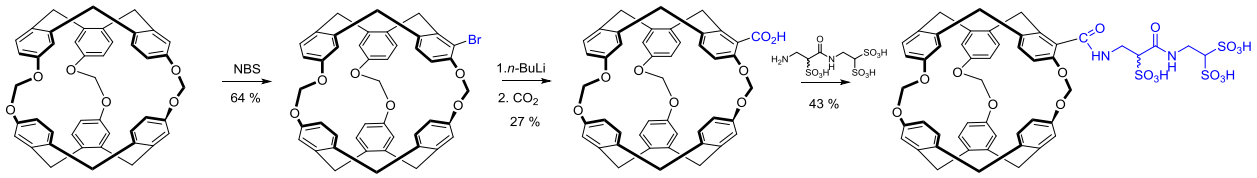

Figure 21: example on mono-functionalization of cryptophane-[111] by water-solubilizing group.

3. Xenon-cryptophane Properties and Applications

Xenon is an inert noble gas discovered by Ramsay and Morris Travers in 1898 and obtained by fractional distillation of the liquid air.[88] The biocompatibility of the gas has been demonstrated in 1951, by Stewart C. Cullen who showed its anesthetic effect.[89] Xenon is a doping agent that enhances athletic performance and it has been forbidden since 2015 by the World Anti-Doping Agency (WADA).[90,91,92] Among the eight naturally occurring isotopes, only ^{129}Xe and ^{131}Xe are stable with natural abundance of 26.5% and 21.1% and nuclear spins of 1/2 and 3/2, respectively, making them NMR active. ^{129}Xe is the most used isotope thanks to its higher abundance, simple NMR signature and the possibility to be hyperpolarized, which will be seen later. Bearing 54 electrons and a volume of 42 Å^3, xenon electronic cloud is highly polarizable, and it interacts strongly with the surrounding environment via London dispersion forces and hydrophobic interactions. This high polarizability is reflected by the large chemical shift range (about 300 ppm in water for non-covalently bound xenon) indicating also the large sensitivity of the gas to its surrounding environment.[93] Apart from sensitivity, high polarizability renders the gas lipophilic and this may explain its anesthetic behavior.[89] Ostwald solubility or the ratio of the volume of gas absorbed to the volume of the absorbing liquid at the same pressure and temperature is given in table 2, which shows a moderate and high solubility of the gas in aqueous and organic media, respectively. For example the solubility of the gas in fat tissues (1.3) is almost 10 times higher than that in blood (0.14).[94]

Liquid	Ostwald Solubility
Hexane	4.8
Oil	1.9
Fat Tissue	1.3
DMSO	0.66
Water	0.11
Blood	0.14
Plasma	0.1
Saline	0.09

Table 2: solubility of xenon in different media.

In addition to the high sensitivity, wide range solubility and chemical inertness, long relaxation time is another important property to be added to the list. Unlike proton relaxation mechanisms, xenon relaxation times are affected by intrinsic and extrinsic parameters (transient and persistent Xe-Xe van der Waals dimer relaxations as the intrinsic factors (spin-rotation); atomic diffusion through gradients of the magnetic field and interaction with the cell wall relaxations as the extrinsic factors (dipole relaxation)). These relaxation processes contribute differently if xenon is in the solid, liquid or gas phase. For liquid state, relaxations are mostly decreased by wall and solvent interactions and the presence of oxygen or any paramagnetic species drastically decrease the relaxation times T_1 and T_2 of xenon.[95]

The simplest way to introduce xenon into the body is by inhalation.[96] Thanks to this, real-time high-resolution lung imaging was achieved, which is usually hard to attain by the conventional MRI, due to low proton density. This is currently a hot research topic that may offer new imaging utilities for medical applications.[97,98] Some ^{129}Xe MRI brain experiments have been also realized

in rodents. Intravenous and arterial introduction of the gas allows a specified organs imaging.[99,100] All these experiments are promising and suggest that xenon can be used as an exogenous tracer for biomedical studies.

As mentioned previously, the characteristic volume of xenon (42 $Å^3$) allows its encapsulation in different hosts of matching cavity volume. In 1998, Bartik et al. reported the first ^{129}Xenon@Cryptophane-A inclusion complex in 1,1,2,2-tetrachloroethane-d_2. The binding constant is impressively high, of about 4000 M^{-1} even higher than that of chloroform and dichloromethane in 1,1,2,2-tetrachloroethane-d_2. The ^{129}Xe@Cryptophane complex is stabilized by London dispersion forces between the polarizable atom and electron rich aromatic rings. Over the past two decades, a wide variety of cages has been synthesized for this purpose, most interestingly, the cryptophane-[111] cage synthesized by Brotin and Dutasta, showing the highest binding constant of xenon of about 10000 M^{-1} in 1,1,2,2-tetrachloroethane-d_2 due to the perfect volume compatibility. Since then, cryptophane cages have been intensively used for xenon encapsulation in organic and aqueous media. Moreover, cryptophanes are not the only hosts for xenon encapsulation in solution, where several other molecular hosts capable of xenon complexing have been reported in the literature.

3.1. Different Hosts for ^{129}Xe Inclusion:

α-cyclodextrins are cyclic oligosaccharides that possess a relatively apolar internal cavity of volume in the order of 140 $Å^3$. This large cavity size makes the ^{129}Xe association constant very weak (K_a = 22.9 M^{-1}) in water and the in-out exchange is relatively fast. The formation of xenon@cyclodextrin complex in that case was proved by proton–xenon heteronuclear NOE experiments.[101] Recent study investigated a cyclodextrin based pseudo-rotaxane, where the large cavity was threaded with a disubstituted alkyl chain, to decrease its volume, hence slowed the in-

out exchange rates.[102] Thiacalix[4]arene also showed weak binding constants (K_a = 13.6 M^{-1}) to xenon, with a concentration dependent chemical shift variations.[103] Ternary complexes of pillar[5]arene derivative, an organic guest and xenon were also studied, showing a variation in the xenon chemical shift upon adding the organic guest like hexane.[104] Better association properties were recorded with cucurbit[n]urils CB, which are composed of n glycoluril units and have a hydrophobic cavity accessible through two identical portals surrounded by polar carbonyl groups. Specifically, water-soluble CB* [6] derivative has a high xenon binding constant in water of 3000 M^{-1} obtained by ITC. The appearance of two signals for the free (190 ppm) and encapsulated xenon (97 ppm) indicates a slow exchange between the bound and unbound species at the NMR time scale. It is worth mentioning that in CB xenon's in-out exchange rate can be modulated by adding cations that interact with the polar carbonyl groups, hindering by this the kinetics of exchange, Figure 22.[105,106,107,108] The first in-*vivo* imaging for the detection ^{129}Xe@CB [6] in water was also performed, where it was possible to localize the cage in brain, heart, kidneys, liver and aorta. [109]

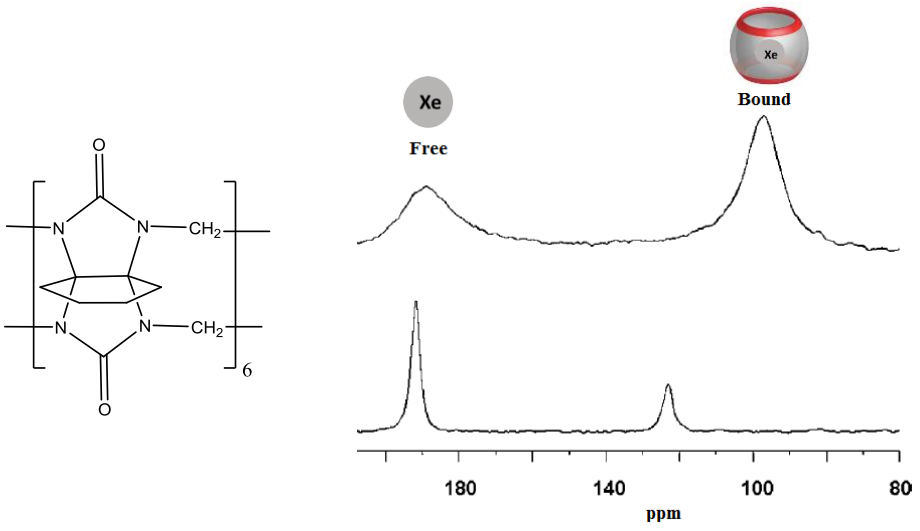

Figure 22: ^{129}Xenon NMR spectra of xenon in the presence of CB* [6] in pure water (above) and aqueous Na_2SO_4 solution at 298 K.

3.2. ^{129}Xenon@Cryptophane Complexes:

Compared to the previously discussed molecules, cryptophane appears as the host of choice for xenon encapsulation due to many different reasons.[110] Along with the high binding constants, slow exchange at the NMR time-scale and relatively optimized in-out kinetics, the possibility to functionalize cryptophanes is a significant property to be added on the list. With this property, successful grafting of water solubilizing or sensing units is made possible. In addition, the latter allows a perfect tuning of xenon complexation properties like chemical shifts, binding constant, and kinetics. For the moment, cryptophanes are the most investigated hosts in this domain, where a notable number of cages have been developed with various cavity size, substituents and applications. Each of these cages has different binding affinity and chemical shift depending on their structures and this will be detailed in the next paragraphs.

3.2.1. ^{129}Xenon@Cryptophane Binding Constants:

One factor affecting xenon binding affinity is the cavity volume. In organic media, usually 1,1,2,2-tetrachloethane, smaller cryptophanes like cryptophane-[111] and [222] $(OMe)_6$ (A), with a cavity volumes of about 81 and 95 $Å^3$ respectively, tend to have high binding constants, of 10000 M^{-1} and 3900 M^{-1}, respectively.[55,110] Larger cages showed a lower binding constant as expected, like cryptophanes [223] $(OMe)_6$, [233] $(OMe)_6$ and [333] $(OMe)_6$ (E), with binding constants of about 2800, 800 and 10 M^{-1} respectively.[111] This trend confines with the packing coefficient of the guest to host volumes described earlier that must be 0.55. For example in cryptophane-[111] and cryptophane-A, these coefficients are equal to 0.49 and 0.6, respectively, which are more or less optimal for these complexations. In aqueous media, however, higher binding constants are usually observed due to the hydrophobic effect of the lipophilic cavity. The interaction in aqueous media is entropically favored, where water molecules filling possibly the

hydrophobic cavity tend to leave to be replaced by the lipophilic gas. For example, cryptophane-[111] $(RuCp^*)_6Cl_6$ exhibits a binding constant of about 29000 M^{-1}.[84] Cryptophanes functionalized with hexa-carboxylic groups like cryptophane-A hexa-acid (K_a~6800 M^{-1}), [223] $(OCH_2CO_2H)_6$ (K_a~2200 M^{-1}), [233] $(OCH_2CO_2H)_6$ (K_a~2200 M^{-1}) and finally cryptophane-E $(OCH_2CO_2H)_6$ (K_a~1000 M^{-1}) show higher binding constants compared to their congeners in 1,1,2,2-tetrachloroethane, but still following the same decreasing trend in terms of increasing cavity volume.[50] Tri-functionalized water-soluble cages, based on cryptophane-A derivative, were also described to effectively bind xenon showing incomparable high binding constants up to K_a~ 42000 M^{-1}, Figure 23. It is worth mentioning that these values are obtained by ITC and not by xenon NMR spectroscopy, making the comparison between the previously mentioned values difficult.[80,112,113]

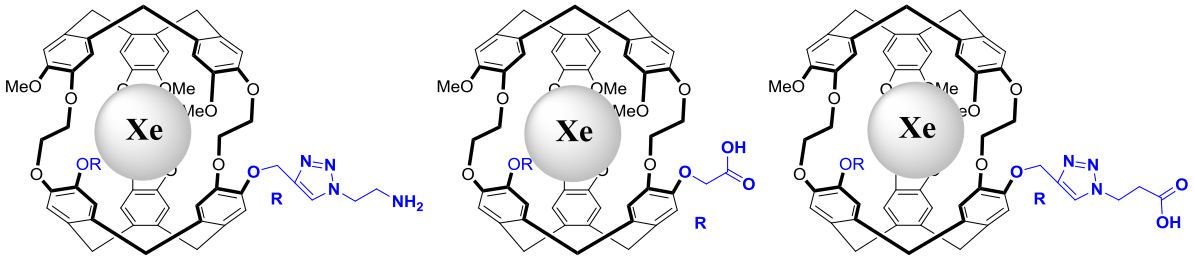

Figure 23: structure of water-soluble tri-functionalized cryptophanes cages bearing different functionalities displaying different xenon binding constants.

Substituents on the cryptophanes rims, also affect the values of binding constants as illustrated in the previous example. A clearer effect can be seen with the tri-functionalized cryptophanes [111] shown in Figure 24, where adding three methoxy or three bromine atoms drops the binding constants to K_a~10 M^{-1}, this can be directly explained by the packing coefficient, which is approximately equal to 0.79 larger than the one described for the non-functionalized

cryptophane-[111] cages. It seems that these substituents hinder xenon binding by preventing the cage to adopt a *syn* periplanar expanded conformation.[114] Up to now, rim functionalization is only limited to oxygen derived substituents. However, adding new original functions or different heteroatoms like sulfur or nitrogen is quite complicated. Thus the trend predicted of binding constants is restricted to what have been synthesized.

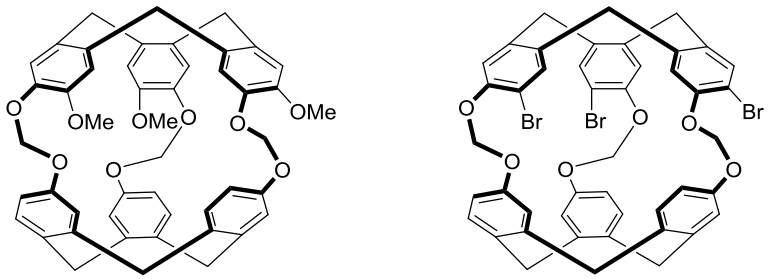

Figure 24: structure of tri-functionalized cryptophane-[111] derivatives.

3.2.2. ^{129}Xe@Cryptophane Chemical shift:

Xenon polarizability is clearly reflected by the ultimate sensitivity of its surrounding environment, which has been illustrated in different examples. For instance, in an original example, a series of deuterated cryptophanes were prepared and their ^{129}Xe complexes were studied. The ^{129}Xe NMR spectroscopy revealed that the encapsulation of xenon in completely deuterated cryptophane-A derivative leads to an upfield shielding of its signal by 1.19 ppm compared to the one non-deuterated cage. This example manifests the extraordinary sensitivity of this element to discriminate between the non-deuterated and deuterated cryptophane cages.[115] In addition, a mixture of diastereomers may split a xenon signal into two, each corresponds to a different isomer.[116,117] Variations in solvent, temperature, pressure, pH or structure of the host induce a detectable change in ^{129}Xe chemical shift. Pines and co-workers have demonstrated the use of ^{129}Xe@cryptophane-[222] derivative for MRI thermometry. Upon temperature change, the

chemical shift of the encapsulated ^{129}Xe increases linearly with a rate of 0.1 to 0.3 ppm/K. This change is a result of increase in both, the cryptophane's conformational flexibility and the accessibility of xenon to new cryptophane's regions. The temperature variations were successfully mapped by MRI, facilitating the detection of temperature changes up to 0.1 °C.

To talk about the effect of cavity volume on xenon's chemical shift, a series of cryptophanes [222], [223], [233], [333] bearing identical substituents ($(OMe)_6$ or $(CH_2CO_2H)_6$), have been studied in 1,1,2,2-tetrachloethane-d_2 or water. The study showed a subsequent decrease in the chemical shifts by almost 10 ppm from smallest to largest cages. Although this trend seems to be directly linked to cavity volume, in reality it is likely to be a consequence of many different parameters like cage's shielding effect and most importantly the conformation adopted by the linkers upon xenon encapsulation.[111]

In general, for cryptophanes-[222] type molecules, the chemical shift varies from 62-78 ppm in both aqueous and organic media. Contrary to the formerly mentioned trend, the smallest cryptophane-[111] has a chemical shift of 31 ppm in 1,1,2,2-tetrachloroethane-d_2. In this cage, possible modulation of the chemical shifts in cryptophane-[111] is achieved by grafting electron donating or withdrawing groups of different sizes and orientations on the cage rims. For instance, Xe@tri-methoxy or Xe@tri-bromo functionalized cages show chemical shifts of 39 and 80 ppm, respectively. [114] Additionally, going from electron-poor hexa-boronic acid cryptophane to the electron-rich hexa-hydroxy cage by oxidation triggers a shielding in chemical shifts by almost 62 ppm.[118] This fact is also impressively illustrated in water soluble cryptophane-[111] $(RuCp^*)_6Cl_6$. In this innovative example, the chemical shift of the water soluble cage is completely reversed and it appears at 301 ppm, downfield shifted by about 277 ppm compared to the organic version appearing at 31 ppm.[84] These examples show that even a small structural change of the

cryptophane skeleton induces large chemical shift variations of the ^{129}Xe signal. This effect is mainly a consequence of the ring current modification that takes place upon these changes. In turn the modification in ring current modifies the magnetic properties of the xenon nucleus, Figure 25.

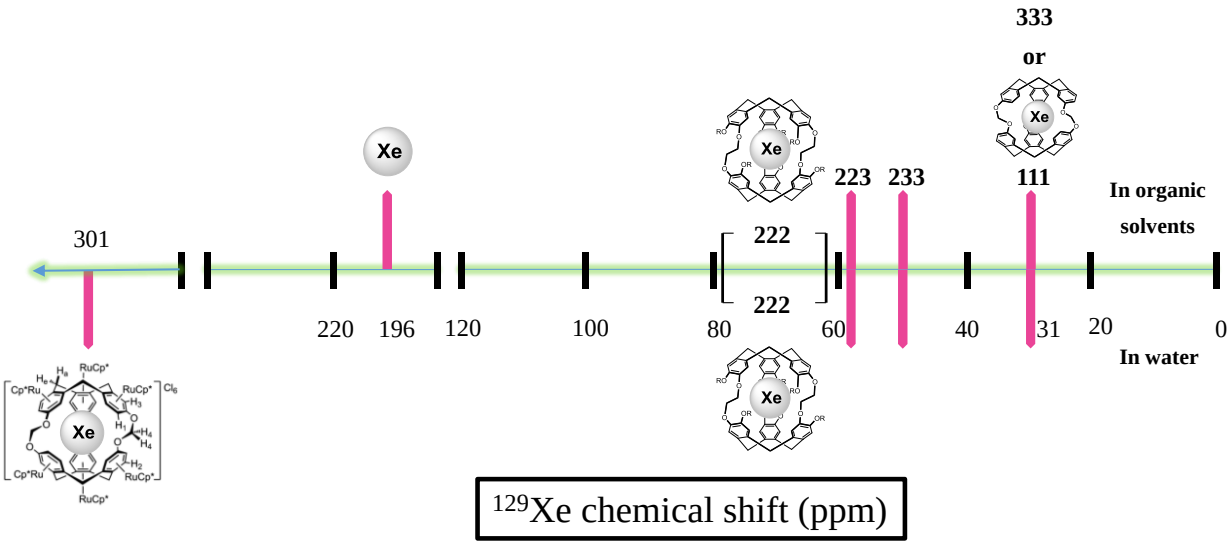

Figure 25: schematic presentation of ^{129}Xe@cryptophanes chemical shifts in water and in organic media.

4. Xe@Cryptophane Biosensors for NMR and MRI Applications

Combining the exceptional properties of cryptophanes (encapsulation and modulation of chemical structure) and xenon (magnetic properties and hyperpolarization) paves the way to develop a new class of ultrasensitive non-invasive molecular MRI tracers. The principle of these NMR biosensors relies on varying the resonance frequency of the encapsulated xenon, compared to the bulk, which can be exploited to monitor changes at the molecular level. This concept has been first demonstrated in 2001 by Pines and co-workers, where they described the first ^{129}Xe@Cryptophane biosensor for avidin in-*vitro* detection. A cryptophane-[222] monoacid, functionalized with a water solubilizing linker consisting of amino-acid chain, and a biotinylated

tail was specifically prepared for this purpose. Upon biotin-avidin complexation, a change in the cage environment i.e. rotational and vibrational motions is excellently translated by a hyperpolarized ^{129}Xe chemical shift variation. In this example, an unambiguous assignment of free, caged and caged xenon recognizing the protein was done, showing a downfield shift by about 2.3 ppm upon avidin complexation, Figure 26.[119] Later on, a detailed description of the obtained signals was performed, showing the sensitivity of the caged xenon to different diastereomers present in solution.[116] Several versions of this biosensor bearing linkers of variable flexibility and length were synthesized, in an attempt to optimize its design to get better responsiveness (structure **a** in figure 37).[120]

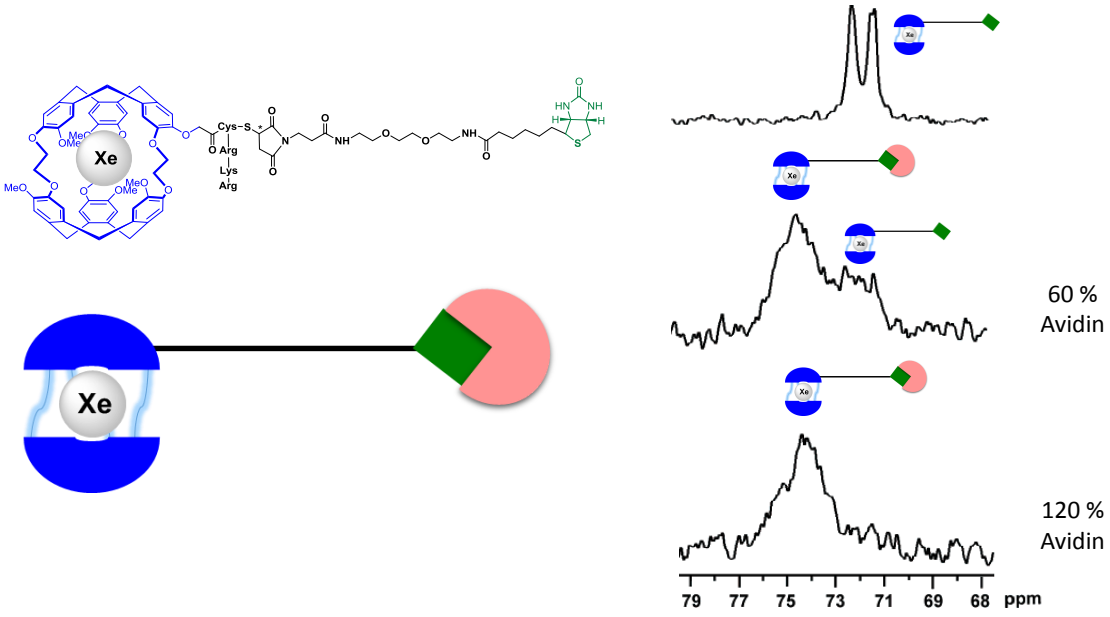

Figure 26: structure of the first Xenon@Cryptophane based sensor and the corresponding HP xenon spectrum, showing at around 70 ppm the signals of cryptophane-encapsulated species. Upon avidin addition, a shift of about 2.3 ppm is observed with a decrease in the intensity of xenon encapsulated in functionalized cage.

The important sensitivity gain delivered in this example is due to the use of hyperpolarized (HP) ^{129}Xe compared to the much less sensitive thermally polarized gas. Hyperpolarization is defined as a transient imbalance in the nuclear spin repartition between energy levels, which initially

follows the Boltzmann distribution.[77] Perturbing Boltzmann populations of nuclear spins will increase the polarization consequently increasing the global magnetization. Typically, this will enhance the signal by four to five times orders in magnitude depending on strength of the magnetic field B_0. Hyperpolarization is achievable by different methods like Brute force, dynamic nuclear polarization (DNP) but Spin Exchange Optical Pumping (SEOP) remains the most convenient and rapid method to produce small amount of hyperpolarized ^{129}Xe, Figure 27.[121] Nevertheless this technique is not common in laboratories and it requires specific skills to design and operate this kind of apparatus. For this reason our team established an old collaboration with Dr. Patrick Berthault and his co-workers in CEA, (Paris, Saclay), who are specialized in the production of (HP) ^{129}Xe by SEOP using the apparatus shown in Figure 27. In addition this group has succeeded to use (HP) ^{129}Xe as an MRI tracer and developed new NMR sequences and protocols for efficient sensors detection.

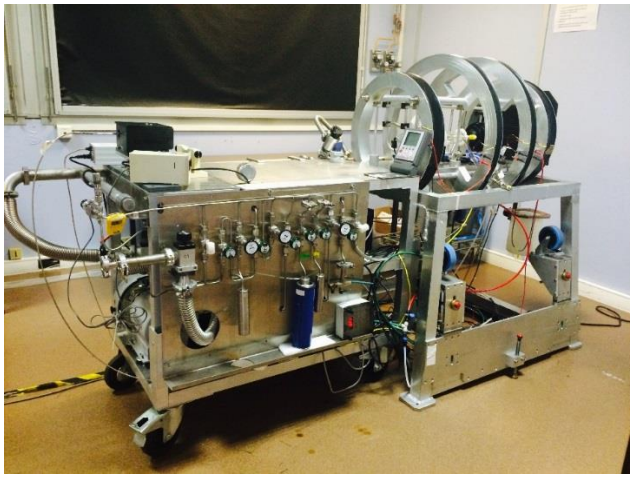

Figure 27: equipment for production of hyperpolarizing xenon gas of Berthault group at CEA Paris.

Technically speaking, SEOP is a two-step process polarization. The first step involves the polarization of electronic spins of the gaseous alkali metal (Rubidium), followed by a transfer of this polarization to the nuclear spins of the noble gas by Fermi-contact interactions. Usually,

another gas (nitrogen) is added to the cell to favor this process and to quench the fluorescence of the rubidium atoms. In the first step, the presence of a magnetic field renders the magnetic moments (m_g= +/- *1/2*) of both the ground ($^2S_{1/2}$) and excited states ($^2P_{1/2}$) non-degenerate (different in energy). Circularly polarized laser tuned at the D_1 transition of Rb, i.e. at 794.7 nm, is applied leading to the excitation of spin population from ground state (m_g = - *1/2*) to the excited state (m_g = + *1/2*). In other words, the angular momentum of the photon is transferred to the electron of the rubidium atom. The relaxation however takes place by the accumulation of spin population in the (m_g = + *1/2*) state rather than (m_g = - *1/2*) of the ground state thus leading to electronic spins hyperpolarization of the rubidium atoms. In the second step, the electronically polarized Rb steam collides with the noble gas (^{129}Xe) leading to a spin exchange consequently forming a nuclear spin polarized ^{129}Xe, Figure 28. Hyperpolarized, ^{129}Xe can be stored at low temperature (77 K) in the solid state in a magnetic field of 0.1 T, where it is possible to maintain its polarization for a long time depending on the storage conditions.[122,123] Great care has to be taken to avoid the gas depolarization by using for example special cells coated with silane- or siloxane coatings.

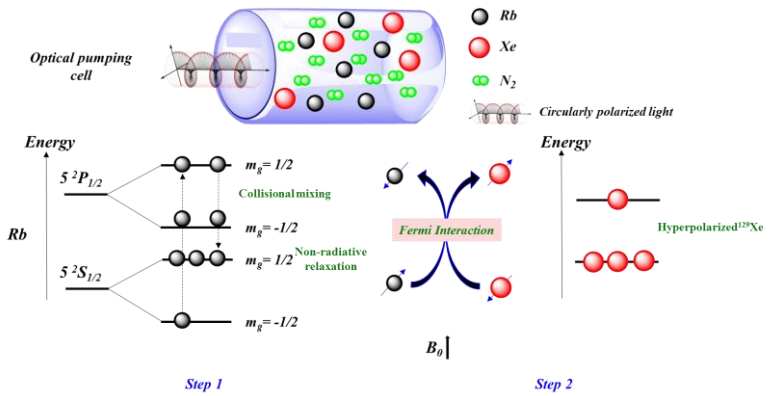

Figure 28: SEOP cell is irradiated by circularly polarized laser light that can be absorbed by the Rb atoms. The first step involves a photon absorption resulting in selective population depletion from one Rb ground electronic state leading to its hyperpolarization. In the second step, gas-phase collisions allow spin order to be transferred from the Rb atom electrons to the noble gas nuclei by Fermi contact hyperfine interactions, thus hyperpolarizing the noble gas.

Over the last ten years, many efforts have been made to detect very low concentrations of xenon-complexes. For example, Pines and co-workers have shown that hyper-CEST (Chemical Exchange Saturation Transfer) experiments can be used to gain more sensitivity.[124] This technique relies on the indirect detection of the biosensor, which are usually present in micromolar concentrations via observing the variations at the bulk level, which is present in millimolar concentrations.[125] In this experiment, caged xenon is first irradiated by a saturation pulse to depolarize it. The depolarized caged nucleus is then exchanged with the bulk by another (HP) one. Upon its encapsulation, (HP) ^{129}Xe will be depolarized and exchanged again. The process is repeated many times leading to the accumulation of depolarized ^{129}Xe in the bulk, which in turn decreases the intensity of free ^{129}Xe, (on-resonance spectrum in Figure 29). Observing the difference between on/off resonance spectra allows the signal enhancement by three times order in magnitude consequently decreasing the detection threshold to picomolar range, Figure 29.

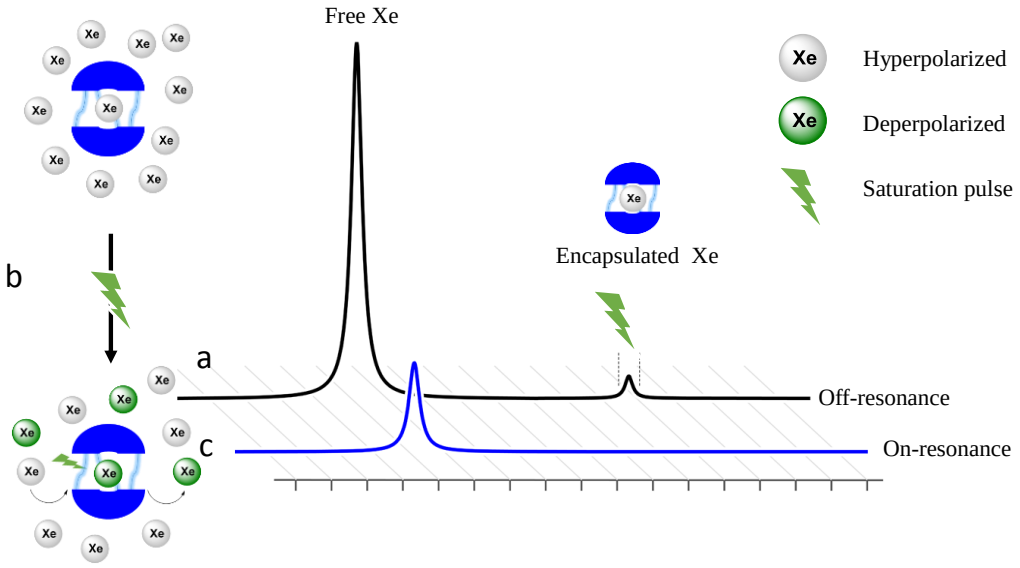

Figure 29: hyper-CEST detection scheme for encapsulated ^{129}Xe a) the initial spectrum obtained after a second of acquisition without selective irradiation b) selective radio frequency depolarization of the encapsulated ^{129}Xe resulting in its depolarization and the accumulation of depolarized gas in the bulk c) the resulting spectrum from selective "on resonance" saturation of the encapsulated ^{129}Xe showing a drop in its intensity.

This technique is currently used to record magnetic resonance images of some (HP) ^{129}Xe tracers. Some of these tracers will be discussed in the next section.

4.1. ^{129}Xe@Cryptophane Sensors:

With the increasing number of Xenon@Cryptophane sensors, one can distinguish between two types, smart or density based sensors.[77] In the former, an interaction with the biological target either generates or shifts the existing ^{129}Xe signal, in the latter, a variation in signal intensity as a function of local environment is observed. In the next paragraphs, we will present briefly an overview of some xenon-based sensors. The biosensors will be arranged based on the contribution of different groups working in the field and the sensors derived from cryptophane-A will be referred to as cryptophane-[222] derivatives.

4.1.1. Pines and Co-workers:

The first milestone example described by Pines and coworkers established the basics of this field, and opened the gate for further developments at structural and technical levels. In parallel to the synthesis of biosensors, Pines and co-workers have developed new NMR techniques to enhance the (HP) ^{129}Xe NMR sensitivity or to spatially map it. For example, spectrally resolved magnetic resonance images of a biotinylated sensor, Figure 30, were achieved. Cages were first immobilized on an avidin bearing surface thanks to the strong affinity between avidin and biotin ($K_a = 10^{15}$ M^{-1}). Then, a current flow of (HP) ^{129}Xe saturated water was passed through the sample. Thanks to the high chemical shift difference among the xenon pool and the cryptophane-biotin complex, a successful detection of the bound xenon with almost zero background noise was performed, Figure 30.[126]

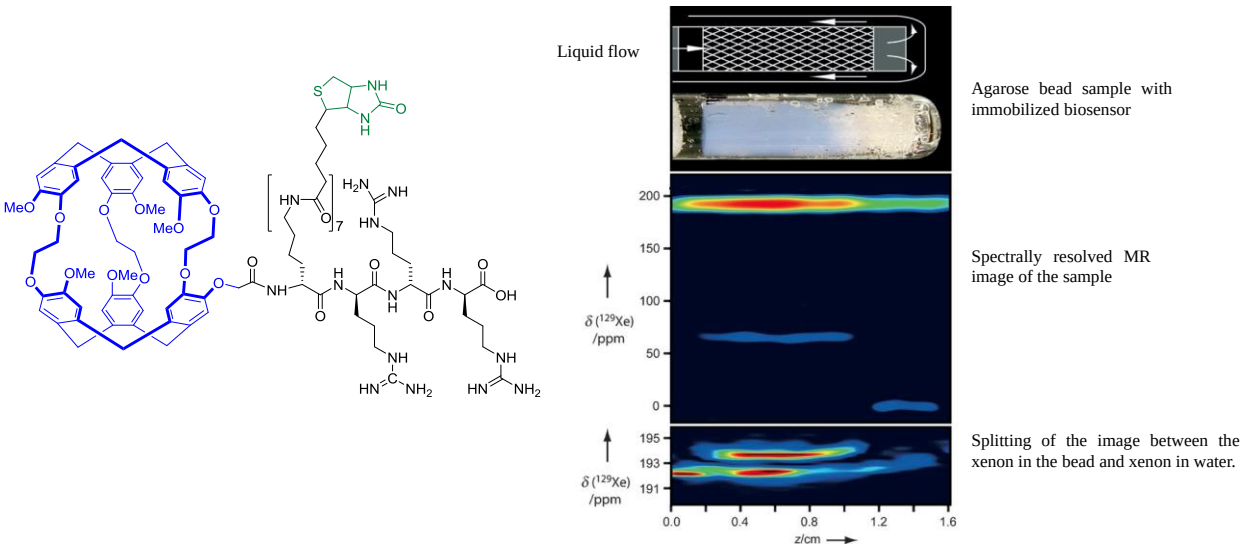

Figure 30: structure of the water soluble biotinylated biosensor immobilized on avidin bearing agarose beads. On the right are the spectrally resolved xenon-based MR images of the agarose bead. [126]

As previously illustrated, (HP) ^{129}Xe is sufficiently sensitive to distinguish between diastereomeric mixtures of cryptophanes. To avoid this problem, the group proposed a new approach based on simply constructing supramolecular assemblies of cryptophane-[222] monoacid and amine-bearing dendrimers. These assemblies are stabilized by acid-base and hydrophobic interactions. A single assembly bears more than one cryptophane cage, which in turn leads to an amplification of the (HP) ^{129}Xe signal intensity.[127] In another example, the group utilized a mono-acid cryptophane-[222] derivative (structure **b** in figure 37) and attached it to a viral capsid. With almost hundred twenty-five cages grafted on the capsid surface, enhancement of sensitivity to picomolar (0.7 pM) level has been realized.[128] In another example, the grafting of several cryptophane-[222] derivatives (structure **c** in figure 37) to EGPR-targeted bacteriophages for cancerous cell detection was also done. The detection of these cancerous cells was performed with high specificity. This was successfully demonstrated by using in-*cellulo* ^{129}Xe NMR spectroscopy assisted with hyper-CEST experiments. Fluorescence imaging also assured the

specific cell-surface binding with minimal cell internalization of the targeted bacteriophage with cancerous cells.[129]

4.1.2. Berthault and Co-workers:

Among the different contributions of this group in the field, we chose here to discuss only some major examples. Similar to Pines, Berthault group selected to work with cryptophane-[222] monoacid cage and functionalized it with short DNA strand (structure **d** in figure 37). It is noteworthy that in this example an enantiopure cryptophane derivative was used for the design of the final molecule. Detection of the hybridization of this strand with its complementary sequence was made possible via simple (HP) ^{129}Xe signal and a moderate downfield shift by 0.5 ppm was observed at low concentration (10 µM). At higher concentration, the authors observed micelle formation, which in turn resulted in the appearance of multiple signals. Interestingly, introducing a non-complementary sequence did not change the initial chemical shift. This type of experiments is rather complicated by ^{1}H NMR especially at low concentrations.[130]

In 2011, the same group reported the first internalization (endocytosis) of a cryptophane sensor to a cell, by grafting cryptophane cages to the transferrin protein (a cell penetrating peptide). A dual detection by ^{129}Xe NMR and fluorescence imaging assured the internalization. Unfortunately, the hydrophobic nature of the cage led to non-specific interactions with cell membranes, which were also revealed by ^{129}Xe NMR, Figure 31.[131] These results highlighted the hydrophobicity of cryptophanes and suggested that a modification of the cage's solubility has to be considered. The problem can be solved for instance by introducing water-solubilizing substituents on the cryptophane skeleton, which is crucial to ensure a good solubility in physiological media for in-*vivo* ^{129}Xe MRI experiments.

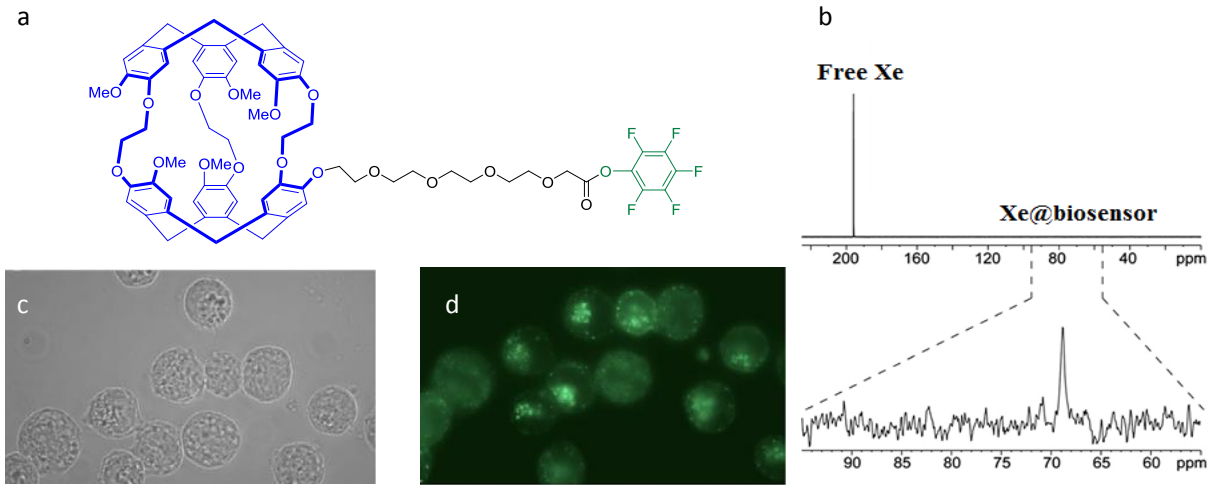

Figure 31: a) structure of the cryptophane derivative, b) hyperpolarized xenon spectrum of xenon trapped in transferrin linked cages obtained in one scan, and the sub-spectrum was obtained by accumulation of 256 selective excitations with a repetition time of 122 ms after c) microscopic image of the cells incubated with the biosensor d) fluorescence imaging assuring the presence of the biosensor in the studied cells.[131]

To avoid the solubility problems, the consortium formed by groups of P. Berthault, T. Brotin and B. Rousseau turned their attention towards new cryptophane derivatives showing higher solubility in water at neutral pH. Thus, they replaced the initial cryptophane-[222] derivative by the more soluble cryptophane-[222] hexacarboxylate. From this molecule several biosensors have been prepared.

A bimodal biosensor incorporating a cryptophane-[222] hexacarboxylate and a biarsenical compound CrAsH for fluorescent detection of peptides was also prepared (structure **e** in figure 37) by this group. Upon binding with an optimized tailored peptide sequence, the CrAsH probe enhanced significantly its fluorescence properties. The tracer also displayed a modified ^{129}Xe NMR chemical shift that can reach 9.2 ppm.[132,133]

The same group showed that the couple xenon-cryptophane complex could be used as a pH sensor. Two examples have been reported with a modified cryptophane-[222] derivatives bearing respectively three and six carboxylic acid moieties. In these examples, a change of the pH of the

bulk resulted in a change of the encapsulated xenon chemical shift. For instance, with the cryptophane-[222] hexacarboxylate, a modification of the pH from 3.5 to 10.8 resulted in an upfield shift of ^{129}Xe NMR signal by about 4 ppm.[134] In a second novel approach for pH sensing, the group employed two pH-sensitive cryptophane-[222] derivatives bearing respectively three and six carboxylic acid moieties. In this example, the pH is accessed by measuring the difference in chemical shifts between the two cages ($\Delta\delta_{AB}$) upon pH variation. This approach is rather more convenient and accurate than observing the difference in chemical shifts between the free (HP) ^{129}Xe and encapsulated one, because the latter can be affected by several parameters like the nature of a buffer, temperature or the presence of ions in solution, Figure 32.[40]

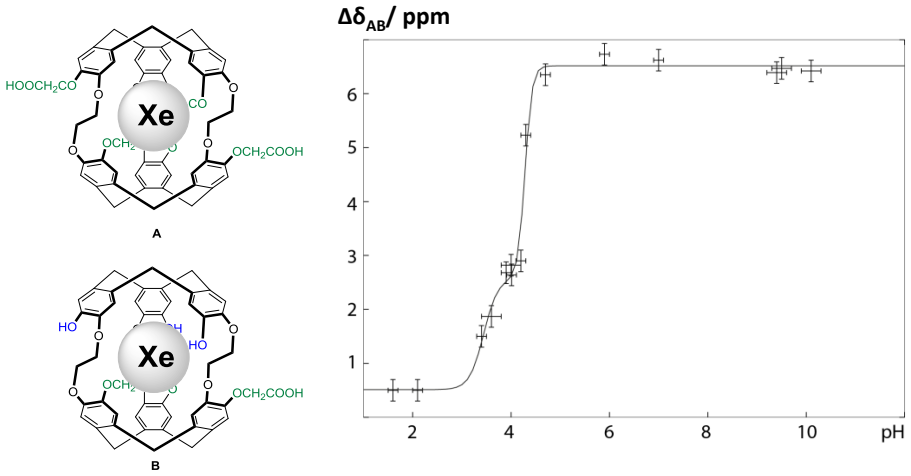

Figure 32: structure of pH-sensitive cryptophanes **A** and **B** and the corresponding plot of chemical shift difference of **A** and **B** as a function of pH. [40]

This strategy can be used to map the pH in tissues but it requires chemical modification of the cage's structure by replacing carboxylic acid by other groups, which are responsive at physiological pH.

A smart biosensor made of NTA group grafted on an enantiopure cryptophane-[222] hexa-carboxylate derivative for zinc detection has been specifically prepared. The use of enantiopure

cage avoids the multiplication of the bound (HP) ^{129}Xe signal since the NTA group contains a stereogenic center, leading to the formation of two diastereomers in solution. Upon binding with zinc, the ^{129}Xe signal downfield shifts by 1.2 ppm. The depolarization of this signal by specific irradiation allowed to obtain an MR image and to detect low concentration of zinc in the nanomolar range (30 nM). Interestingly, the concept of *multiplexing experiments* has been nicely exemplified by introducing different cations (Cd^{2+}, Zn^{2+}, Pb^{2+}) into the solution. The (HP) ^{129}Xe spectrum, revealed for each cation, a specific signature. This example shows that it is possible to detect several analytes at very low concentrations in a very short time (within seconds) with only one xenon-carrier, Figure 33.[135,136]

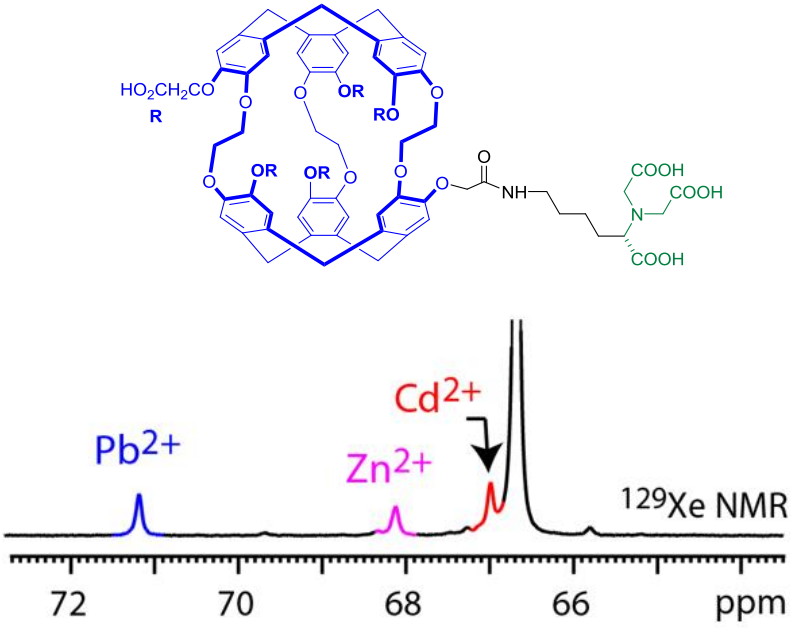

Figure 33: structure of NTA-substituted cryptophane-A hexa-acid, and the corresponding HP 129-xenon NMR spectrum upon different metal cations chelation.[135,136]

4.1.3. Dmochowski and Co-workers:

In a first attempt to study cryptophane internalization and cytotoxicity, Dmochowski and coworkers bioconjugated modified cryptophane-[222] derivative (structure **f** in figure 37) with three cationic peptides, $(D\text{-}Arg)_9$, TAT and $(RGD)_4$ by [3+2] cycloaddition. The first two versions are not specific, whereas the third biosensor targets cancer cells overexpressing $\alpha_v\beta_3$ integrin receptor. The three cryptophanes showed a little cytotoxicity on a concentration suitable for (HP) ^{129}Xe NMR. Cell internalization was monitored by fluorescence imaging, but no (HP) ^{129}Xe NMR was performed at that time.[137] Starting from the same cryptophane derivative and using the same strategy, a folate-targeted biosensor (structure **g** in figure 37) was also prepared. The sensor bears water solubilizing peptide chain, Cy3 fluorophore and a folate interacting unit. Confocal microscopy and (HP) ^{129}Xe NMR spectroscopy proved the endocytosis of the sensor selectively by folate membrane receptors.[138]

Protein targeted cryptophanes were also developed. Using the same strategy ([3+2] cycloaddition), the tri-propargyl cryptophane-[222] derivative (structure **h** in figure 37) was functionalized with three *p*-benzenesulfonamide, varying in linker's length. These biosensors target human carbonic anhydrase protein and they distinguished between the two isozymes of carbonic anhydrase with a chemical shift difference of about 4.3 ppm.[139,140]

Calcium-activated calmodulin-targeted cryptophane off-on biosensor was also developed using a similar strategy. In the absence of activated calmodulin, an intramolecular interaction between the cryptophane-[222] derivative and its corresponding peptide chain prevents xenon binding, which is revealed by the absence of the characteristic ^{129}Xe@Cryptophane signal. In contrast, adding the activated protein restores the ability of the cage to bind xenon, hence displaying a characteristic signal by (HP) ^{129}Xe NMR.[141]

Concerning ^{129}Xe@Cryptophane complexes sensitivity to their physical environment, Dmochowski and coworkers developed another smart pH sensor for cell labeling. This cage bears a pH sensitive peptide chain that undergoes conformational change upon going from pH = 5.5 to pH = 7.5. The peptide adopts a functional conformation at acidic pH, capable of acid cell labeling, whereas it loses its penetration activity upon neutralization. These conformational variations were successfully studied by tryptophan fluorescence, electronic circular dichroism and xenon NMR spectroscopies. In this example, hyper-CEST proved a high sensitivity of the sensor up to picomolar concentrations. Most importantly, the interaction of acidic cell with this biosensor showed a record breaking chemical shift of about 13.4 ppm relative to the non-bound form at neutral pH, Figure 34.[142]

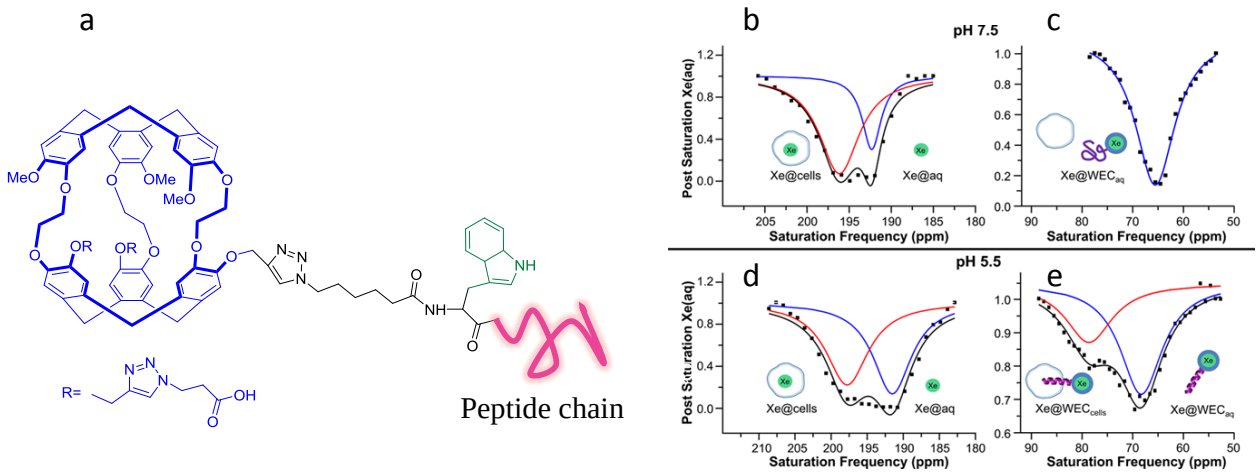

Figure 34: a) structure of the biosensor, hyper-CEST ^{129}Xe NMR spectra at **pH 7.5** b) Xe@cells, red trace (196.3 ppm); Xe@aq, blue trace (192.3 ppm); (c) Xe@sensor (65.0 ppm) and at **pH 5.5**; (d) Xe@cells, red trace (198.0 ppm); Xe@aq, blue trace (192.0 ppm); (e) Xe@sensor-cells, red trace (78.4 ppm) and Xe@sensor, blue trace (68.0 ppm). Sums are shown as solid black lines. Figure adapted from reference 142.

4.1.4. Schröder and Co-workers:

Schröder and his team have significantly contributed in this field. We will present below some interesting examples dealing with the design and synthesis of new biosensors dedicated for instance for membrane interactions studies and bimodal sensors for in-*cellulo* MRI.

Taking the advantage of cryptophane's lipophilic nature, a detailed study on bimodal cryptophane-[222] derivative partitioning between different liposomal vesicles has been conducted. In this study, two new cryptophane-[222] derivatives functionalized with fluorescent probes (for example structure **j** in figure 37) were prepared. The partition and interactions of these conjugates between different lipid bilayers were assessed both by fluorescence imaging and ^{129}Xe NMR assisted hyper-CEST experiments. The two complementary techniques served to give a clear image about the interaction modes, indicating a different response of the cages in different lipid layers.[143] Two other cages, of bimodal cryptophane-[222] derivatives bearing fluorescent probes and anchoring units were also developed.[144] Using these new constructs, they were able to perform a simultaneous detection of these sensors by (HP) ^{129}Xe NMR and fluorescence in cells. Thanks to ^{129}Xe hyper-CEST experiments, the detection of this biosensor at concentrations as low as 15 µM was made possible, Figure 35.[145]

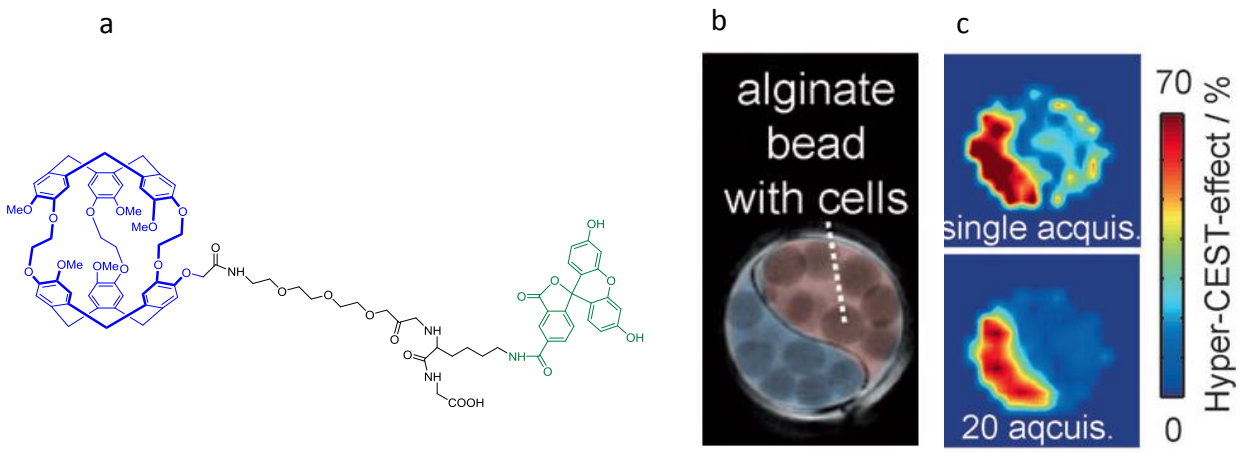

Figure 35: structure of the biosensor bearing a fluorophore, b) ^{1}H MRI of the two compartment phantom housing cells encapsulated within alginate beads. Blue compartment is filled with CrA-FAM labeled cells and the red one is incubated with unlabeled cells. c) Localization of the two compartments by a single CEST-acquisition (2 min) compared to the more sensitive accumulations of 20 CEST-acquisitions.[145]

Using the same technique, this group was able to nicely target metabolically labeled glycans (glycopolymers species) located at the cell membranes and cannot be easily reached with conventional ^{1}H MRI. The strategy is based on an immediate attachment of the biosensor on the labeled glycan surface via a covalent bond (structure **k** in figure 37). Particularly, the glycans were labeled by an azide-bearing synthetic sugar, which is then incorporated as an azide-functionalized sialic acid at the terminal of the glycans. Taking the advantage of this terminal azide function, the group engineered an alkyne bearing cryptophane-[222] cage. This cage was allowed to react with the azide function by a copper catalyzed "click" reaction. By this, a successful multimodal (fluorescent probe and (HP) ^{129}Xe sensor) labeling of the cell was achieved. Fluorescence imaging was employed to assess the efficiency of the binding. Then, (HP) ^{129}Xe NMR experiments were also conducted to image these labeled cells.[146]

4.1.5. Xin Zhou and Co-workers:

Development of cryptophane-[222] derivatives for biothiol detection was achieved in organic media. A mono-functionalized cryptophane-[222] bearing an acrylate moiety aimed to react with biothiols derivatives such as cysteine, homocysteine, or glutathione has been prepared. Interestingly, the reaction between the two molecules by 1-4 addition resulted in a change of the ^{129}Xe NMR chemical shift approximatively by 1.5 ppm (structures **m** and **n** in figure 37).[147,148] In another example, Zhou and co-workers described the synthesis of a cryptophane for detection of H_2S (structure **o** in figure 37) in organic solution. In this example, the cage was also decorated with azido-bearing weakly fluorescent molecule. Upon H_2S addition, immediate reduction of the azido group to an aniline takes place leading to fluorescence enhancement combined with a change in (HP) ^{129}Xe NMR chemical shift.[149]

In a third example, this group also reported the synthesis of cryptophane dimer for mercury detection. As exemplified in Figure 36, the two cryptophane-[222] derivatives are connected by a dipyrrolylquinoxaline linker. Upon addition of mercuric cations into the solution, a conformational change of the whole structure occurs from an open clamp to a closed one. This change brings the two cages closer to each other, which in turn affects the ^{129}Xe chemical shift, Figure 36.[150]

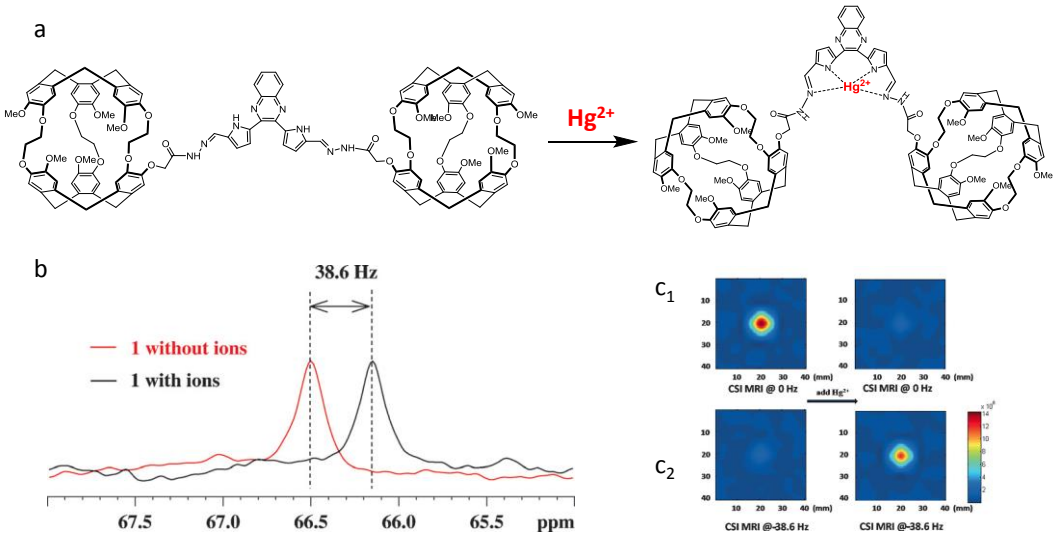

Figure 36: a) structure of the cryptophane dimer and the conformational change observed upon mercury cation addition, b) HP 129-xenon NMR spectrum with and without the metal ion c) chemical shift image (CSI MRI) of sensor c_1) with, and c_2) without the addition of cation.

It is worth mentioning that the above mentioned summary does not fully cover all examples described in literature. We tried only to select the most relevant examples of each group without going into exhaustive details. Some other groups also contributed in this field like Freund and co-worker who described the interaction between cryptophane-[222] derivative bearing a specific peptide ligand with the major histocompatibility complexes protein (structure **i** in figure 37).[151] Meersmann and co-workers also described a new sensing strategy based on the modulation of (HP) ^{129}Xe relaxation times by grafting a gadolinium (III)-DOTA unit on the cryptophane-[222] monoacid core. This sensor could be turned off by performing a selective reaction to remove the gadolinium (III) from DOTA unit thus increasing the (HP) ^{129}Xe relaxation times.[152]

Chapter 1: Bibliography

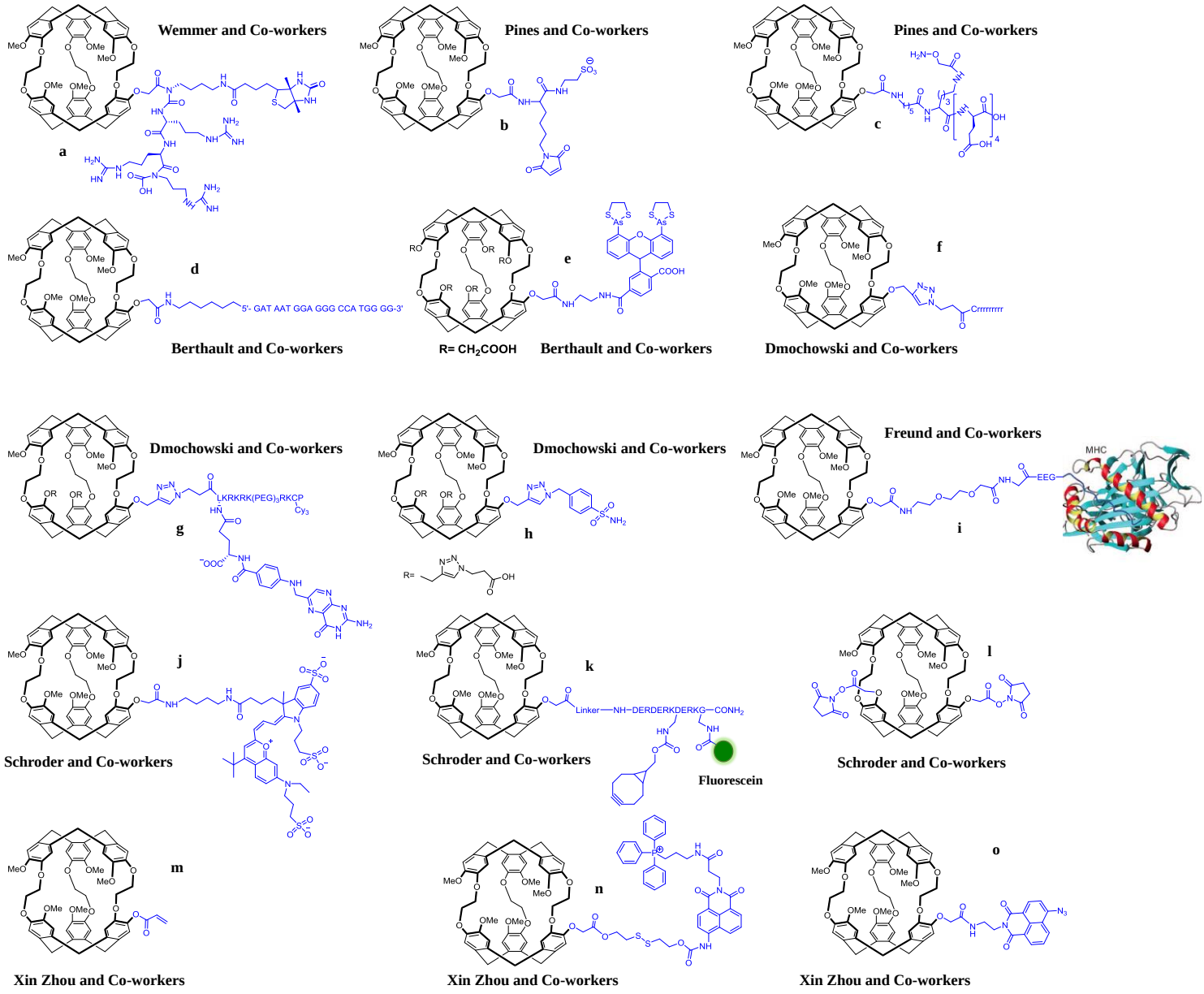

Figure 37: structures of some biosensors developed by different groups.

4.2. Physical and Structural Requirements to Construct Efficient Sensors:

After discussing the advances reached in xenon-based MRI applications, especially at the technical level, we can resume the different requirements needed to obtain a suitable (HP) ^{129}Xe based biosensors. One of these requirements is the selective binding of xenon compared to other guests in physiological media. Fast in-out exchange of xenon is another important feature to be considered since it allows a continuous replacement of the caged xenon with a hyperpolarized one from the bulk. The latter is crucial for the detection of xenon-sensor at low concentration by using the hyper-CEST technique. This sequence will enhance the sensitivity by several orders of magnitude. A slow exchange at the NMR-scale is also required to clearly distinguish among the different species in solution (free xenon, caged xenon and caged xenon recognizing a biological target). Long T_1 relaxation is also crucial to be able to manipulate xenon without losing polarization (i.e. transfer of the hyperpolarized gas, mixing and measurement). The xenon carrier itself has to be water soluble to avoid self-aggregation or interaction with cells membrane. In addition it must be prepared in fair quantities and easily modified in order to introduce a sensing unit. Finally, the carrier has to be non-toxic and its bio-distribution has to be assessed prior in-*vivo* MRI experiments. These two requirements can only be evaluated at the end of the synthesis.[77]

5. Objectives

Cryptophane derivatives have been heavily used to build xenon biosensors because they meet most of the requirements listed above. As seen previously, the overwhelming majority of designed biosensors use a cryptophane-[222] core, where the tethering unit or units are usually grafted on the aromatic core of the cage. Two main types of these cores are used, the cryptophanol-[222] and the cryptophane-[222] hexacarboxylate derived from cryptophane-A. The

former cage is mono-functionalizable via the only available hydroxyl group and thus no symmetry problem is encountered and the platform can be prepared in gram scale. However, with five methoxy groups, the cage suffers from limited water solubility and it tends either to aggregate or to interact with the cell membranes. Cryptophane-[222] hexacarboxylate shows a higher water solubility, but the cage is D_3-symmetric thus its mono-functionalization and purification is tough because statistical mixture of byproducts are inevitably obtained. Other cryptophane-[222] cages are sometimes used but they also suffer from similar problems.

In this regard, development of a new platform bearing two orthogonal reactive functions could be seen as a solution of the formerly mentioned problems. Hence, in addition to the six identical functions on the aromatic core, a chemical function can be introduced on the cryptophane backbone. This allows the grafting of a tethering unit and hydrophilic groups selectively and separately.

Cryptophane-[223] core appears to be the optimal cage of choice for such a design. Structurally speaking, the cage possesses two ethylenedioxy and a propylenedioxy arms, where the latter can be selectively functionalized, and six identical functionalities at the aromatic rims, Figure 38. Xenon complexation by cryptophane-[223] has already been assessed in water and this carrier offers convenient characteristics (in-out exchange, binding constants…) suitable for xenon-based sensing applications.

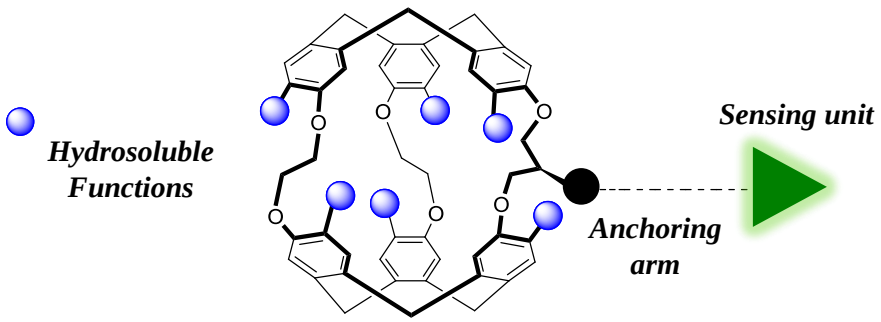

Figure 38: possible dual functionalization of cryptophane-[223] cages.

In 2015, our group has successfully reported a first generation of cryptophane-[223]-type molecules, which proved satisfying water solubility at neutral pH and suitable xenon complexation properties. Our results have revealed, however, that these molecules showed little reactivity towards introducing a sensing unit as it will be detailed in the next chapter.

In this thesis, a developed version of mono-functionalized cryptophane-[223] with enhanced reactivity has been prepared and their xenon complexation properties have been also assessed. To demonstrate the originality of our approach, we have grafted on this skeleton several sensing units. The detailed synthetic pathways leading to these platforms, along with their successful functionalization will be described in the following chapter. (HP) ^{129}Xenon NMR studies of the obtained sensors will be also investigated in chapter 3. The advantages and disadvantages of our strategy will be then discussed in details.

Chapter 2: A New Generation of Dually Functionalized Cryptophanes [223]: Synthesis and Functionalization

1. 1st Generation of Dually Functionalized Cryptophane-[223] Derivative

In this chapter, before describing in details our synthetic work, we wish to present an overview of the first generation of cryptophane-[223] cages bearing two orthogonal functionalities synthesized by Dr. Laure-Lise Chapellet et al. We will also discuss the main advantages and disadvantages of this strategy.[41]

Anti-cryptophane-[223] derivative (C_2-symmetry) possesses a unique propylenedioxy arm, where a central anchoring unit can be added. This allows us to keep the six hydroxyl groups untouched to introduce other substituents. The addition of functionality at the center of the propylenedioxy arm decreases the molecular symmetry (C_1-symmetry). However, it is important to note that no additional stereocenter is created upon this structural change since the two CTB units possess the same absolute configuration (*MM* or *PP*). This won't be the case for *syn*-cryptophane-[223] type molecules, where the two CTB units possess different descriptors (*MP*/*PM*). Consequently, introduction of a new functionality at this position does not complicate the synthesis of such constructs since no diastereomeric mixtures are obtained.

Chapellet et al. described the first generation of bi-functionalized [223] cages. These cages were decorated with a secondary alcohol grafted on the central carbon of the propylenedioxy arm and six carboxylic acid moieties on the CTB rims, Figure 39. This platform was successfully obtained in eight steps starting from the commercially available vanillic alcohol **1**.

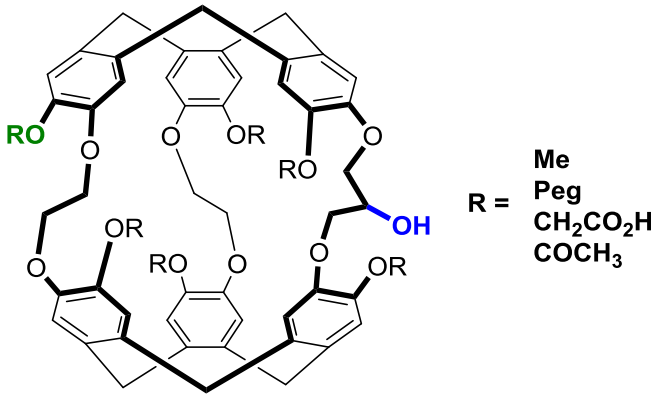

1st generation of dually functionalized cages

Figure 39: structure of a dually functionalized cryptophane-[223] derivative bearing a central secondary alcohol on the propylenedioxy linker.

A CTB unit, **5** functionalized with two ethylenedioxy substituted vanillic alcohols was allowed to react via an S_N2 type reaction with 3-methoxy-4-(oxiran-2-ylmethoxy)phenylmethanol **6** prepared in two steps from vanillic alcohol **1**. The second ring closing reaction was then performed under two different conditions. The first cyclization condition of compound **7** employs a Lewis acid, scandium triflate, $Sc(OTf)_3$, without protection of the central hydroxyl group and the benzyl alcohol, hence decreasing the number of required steps. Applying these conditions led to the formation of the desired *anti*-cryptophane **8** in a moderate yield (23%). The second strategy required the protection of both the benzyl alcohols as THP, compound **9**, and the central alcohol by an allyl function, compound **10**, followed by the cyclization in formic acid/ chloroform mixture (50 /50) to offer the protected cage **11** in a higher yield (44%). Although this strategy requires more steps, it facilitates the purification of cryptophane precursors by increasing their lipophilicity. The protection as an OTHP acetal gives rise to multiple diastereomers thus complicating the precursors **9** and **10** characterization, Figure 40. It is noteworthy that the separation of these stereoisomers is not necessary as the second cyclisation offers only one cage as two enantiomers.

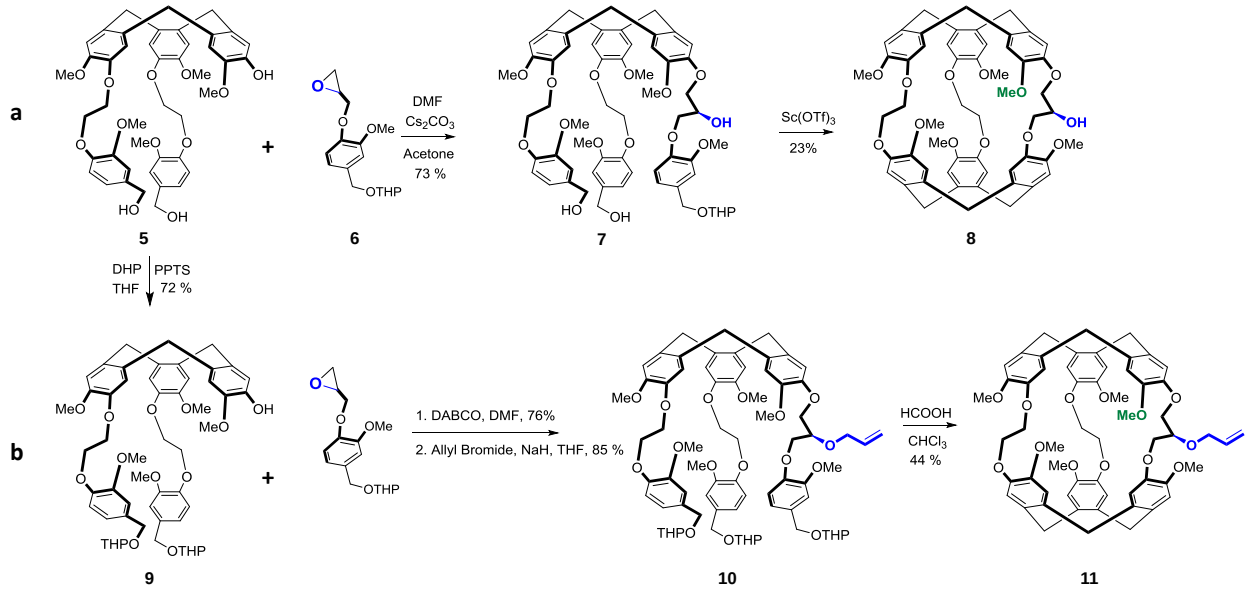

Figure 40: a) scandium triflate catalyzed cyclization versus b) formic acid catalyzed cyclization to obtain the dually functionalized cage.

With this platform in hands, the gate was opened to produce a complete generation of dually functionalized cages. For example, demethylation of the six methoxy groups of compound **8** provided the hexa-phenol cage with central secondary alcohol **12**. This cage is soluble in LiOH (0.1 M), and it showed high affinity towards thallium and cesium cations with respective binding constants of 10^9 and 10^8 M^{-1} at 298 K, respectively, Figure 41.[64]

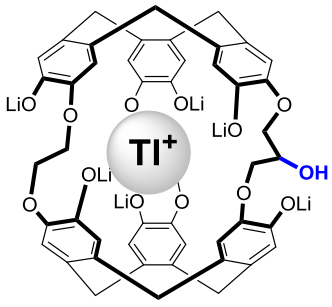

Figure 41: structure of water soluble hexa-phenol for Tl cation complexation.

Introduction of six water-solubilizing substituents (carboxylic acid precursors or six PEG groups) was done under smooth conditions by selective alkylation of the six phenols on the CTB rims of compound **12** offering compounds **13** and **14**. The hydrolysis of the **13** to the corresponding hexa-carboxylic acid cage was also performed. These conditions leave the secondary alcohol function unreacted, Figure 42. These cages show acceptable solubility at neutral pH at moderate concentrations.

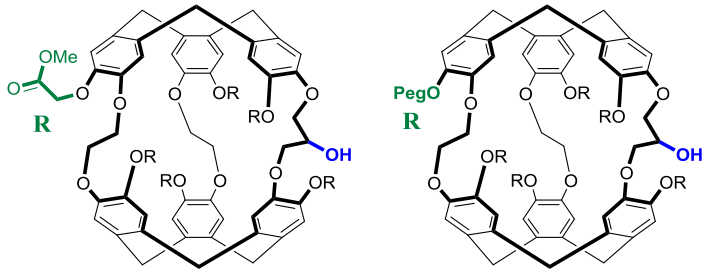

13 **14**

Figure 42: structure of water-soluble or pre-water soluble dually functionalized cages, bearing either six methyl ester groups **13** or six PEG groups on the aromatic rims, **14**.

To test the reactivity of the central hydroxyl group on compound **13**, it was first converted into an electrophile via mesylation reaction to give compound **15** and then allowed to react with different nucleophiles like sodium azide and ethanethiolate. These experiments have shown that there was no possibility to perform any nucleophilic substitution at this position due to steric hindrance. Under different reaction conditions (thermal or microwave assisted reactions), we observed that the mesylated derivative was either recovered as an imploded form or it was hydrolyzed to the initial alcohol, compound **13**. In addition, attempts to exploit the nucleophilicity of the hydroxyl group, in the presence of six ester functionalities also failed due to selectivity issues. Strong bases were always needed to deprotonate the hydroxyl group. This in turn led to the deprotonation of the α-protons of the ester groups leading to the formation of side-products, Figure 43.

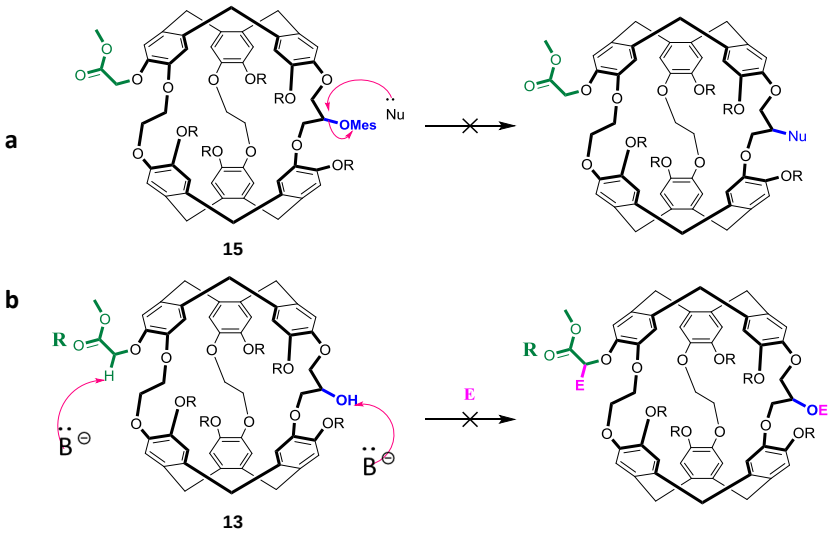

Figure 43: illustration of failed trials to alkylate cryptophane **13**.

Oxidation of the secondary alcohol in compound **13** to the corresponding ketone was also achieved by using Dess martin periodinane reagent in dichloromethane to give cryptophane **16**. The yield obtained is modest (34%) and an optimization is required to get the cage in decent amounts. This functionality can be exploited in performing imine condensation or Wittig type reactions to graft a spacer and a sensing unit, Figure 44.

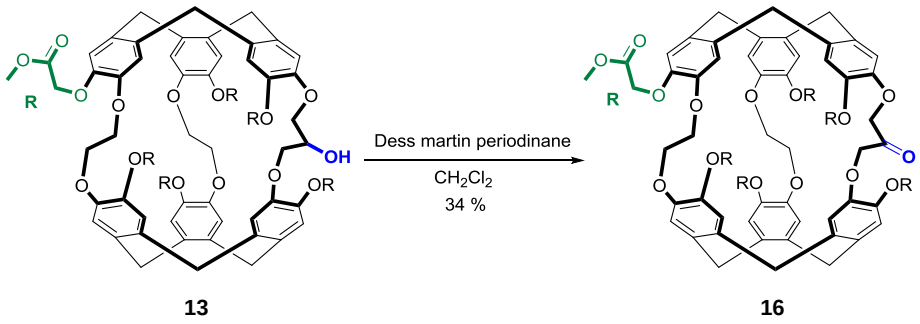

Figure 44: oxidation of the secondary alcohol of cryptophane **13** into a ketone.

The ^{129}Xe NMR spectra of the water-soluble cages displayed two peaks for free and encapsulated xenon indicating a slow exchange at NMR time scale. A fast in-out exchange dynamics of xenon

was also observed suitable for hyper-CEST technique to detect the cages at low concentrations. This interesting work established the bases of a new design for dually functionalized cages, solving by this the symmetry and water solubility problems. The main disadvantage, however, is the little reactivity of the central secondary alcohol. The limited reactivity prevents the possibility to easily elaborate biosensors and an optimization of the cryptophane skeleton is required.

In this manuscript, we present a second developed generation of dually functionalized cryptophane-[223] derivatives. In this work, a simple replacement of the secondary alcohol by a primary one enlarged the scope of reactivity of this cage towards nucleophilic substitution, electrophilic activation and oxidation, Figure 45. Successful grafting of different sensing units as well as water solubilizing groups was also possible proving by this that our cages possess all the specificities needed to build-up xenon biosensors. In the next sections, we describe the synthetic strategy leading to these derivatives. It is worth mentioning that a part of this work has been recently published in the *Journal of Organic Chemistry*. Baydoun et al, *JOC*, **2019**, DOI: 10.1021/acs.joc.9b01093.

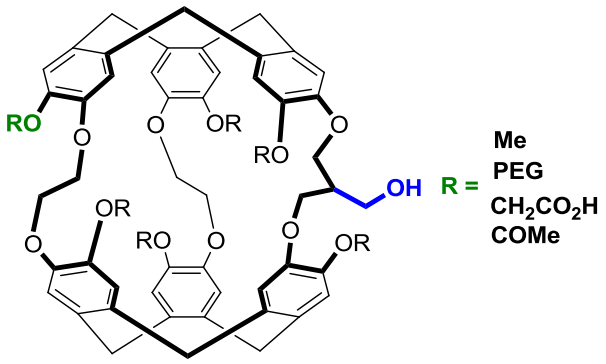

2nd generation of dually functionalized cages

Figure 45: structure of the second generation of bi-functionalized cages.

2. Retrosynthetic Analysis of Modified Cryptophane-[223] Derivatives

The targeted cryptophane-[223] derivatives presented in this manuscript are asymmetric with two types of linkers: two ethylenedioxy and one functionalized propylenedioxy arms. *Template method* is employed, because it allows a selective introduction of different linkers having various length and substituents.

Basically, compound **27** shown in Figure 46 can be obtained after either performing a chemical transformation to an existing properly functionalized cryptophane or directly by cyclizing a precursor molecule containing a primary alcohol.

Three routes can be envisioned to obtain compound **27**, routes **I**, **II** and **III**. The retrosynthetic analyses of these strategies are shown in Figure 46 and Figure 47. We decided to detail only the successful strategy (synthetic route **I**) in this manuscript.

In route **I**, compound **27** can be obtained by performing a hydroboration-oxidation step on the terminal alkene of cryptophane **26**. This crucial step assures a regioselective insertion of the hydroxyl group on the terminal position. Cryptophane **26** itself is a result of classical cyclization of the tri-substituted template **25** by three consecutive Friedel-Crafts alkylations. In turn, the latter can be obtained after a double alkylation of a mono-substituted derivative **23** by compound **24** whose synthesis has already been reported.[153] The mono-alkylated synthon **23** is a result of an alkylation between **4**[154] and an alkenyl substituted vanillic alcohol **22**. Compound **22** can be easily prepared by reacting vanillic alcohol **1** with 3-chloro-2-chloromethyl-1-propene **19**.

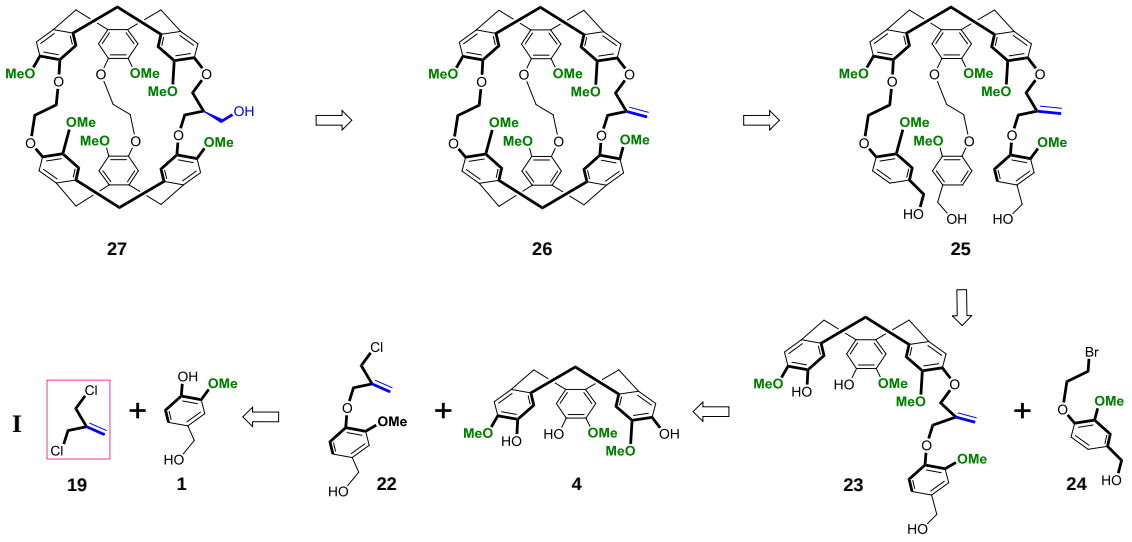

Figure 46: retrosynthetic analysis strategy **I** leading to *anti*-cryptophane **27**.

The two other envisioned synthetic routes (strategies **II** and **III)** employ more or less the same steps discussed in route **I,** namely cyclization and alkylation, but differ in the origin of the primary alcohol. In route **II** for example, the hydroxyl group on the cryptophane **27** is a result of a reduction of the methyl ester group. Route **III**, however, represents the simplest way since it requires less synthetic steps. In this route the primary alcohol function is introduced at the very beginning of the synthesis. It is worth mentioning that all the chiral synthons shown in Figure 46 have been isolated as racemic mixtures. In addition, most of these synthetic steps involve different protection at a certain stage of the synthesis.

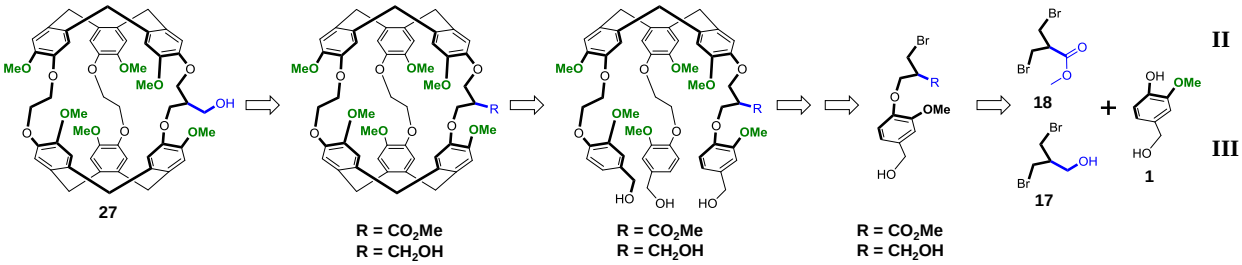

Figure 47: retrosynthetic routes **II** and **III**.

3. Synthesis of Cryptophane 27

A modified *template method* has been used to prepare cryptophane **27**. First, a CTB cap is synthesized, followed by its elaboration with properly functionalized benzyl alcohols and finally their cyclization to offer the cage of interest.

The CTB cap, **4** was synthesized in three linear steps, based on a known procedure starting from the commercially available 4-(hydroxymethyl)-2-methoxyphenol **1**.[25] Vanillic alcohol **1** was first protected by a reaction with allyl bromide under basic conditions (potassium carbonate) to give the allyl protected **2** in 75%. This protection step is necessary because the cyclisation of unprotected vanillic alcohol produces side-products in large quantities.[153] Compound **2** was then cyclized under acidic conditions using perchloric acid/methanol by performing simultaneously three Friedel-Crafts alkylations to offer the tri-allyl CTB **3** in a moderate yield (57%). The latter was then de-protected by using palladium acetate, triphenylphosphine and trimethylamine in THF/water mixture to offer CTB **4** in 79% yield, Figure 48.

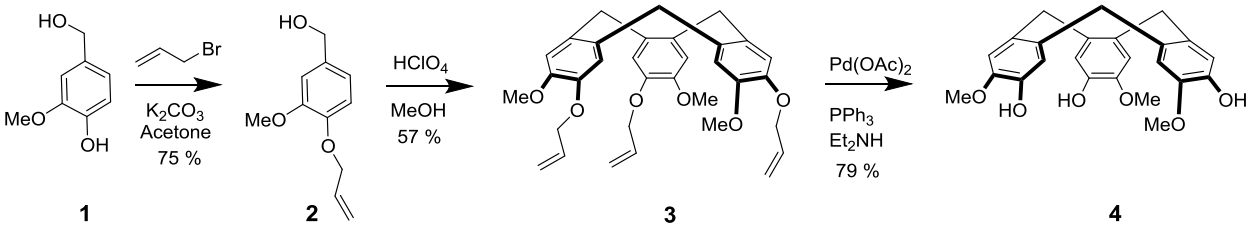

Figure 48: synthesis of the first CTB **4** cap.

The second important step involves the synthesis of the substituted vanillic alcohol arm bearing either the primary alcohol or its precursors. The simplest thing to be tried was to introduce a primary alcohol unit, 3-bromo-2-bromomethyl-1-propanol, **17**, on the vanillic alcohol **1** by an alkylation step under basic conditions (potassium carbonate). Attempts to make compound **20**

failed, producing a lot of side-products that could not be easily identified by NMR spectroscopy or mass spectrometry. The second possibility was to alkylate the vanillic alcohol **1** by an ester substituted group (3-bromo-2-bromomethyl-1-methyl propanoate) **18**. This can be eventually reduced to the corresponding alcohol derivative **20**. Based on this, the same reaction conditions were used and they gave rise to the desired alkylated compound followed by an elimination reaction to offer the byproduct **21**. Finally, the use 3-chloro-2-chloromethyl-1-propene, **19**, in excess provided the desired product, **22** in a decent yield (65%), Figure 49.

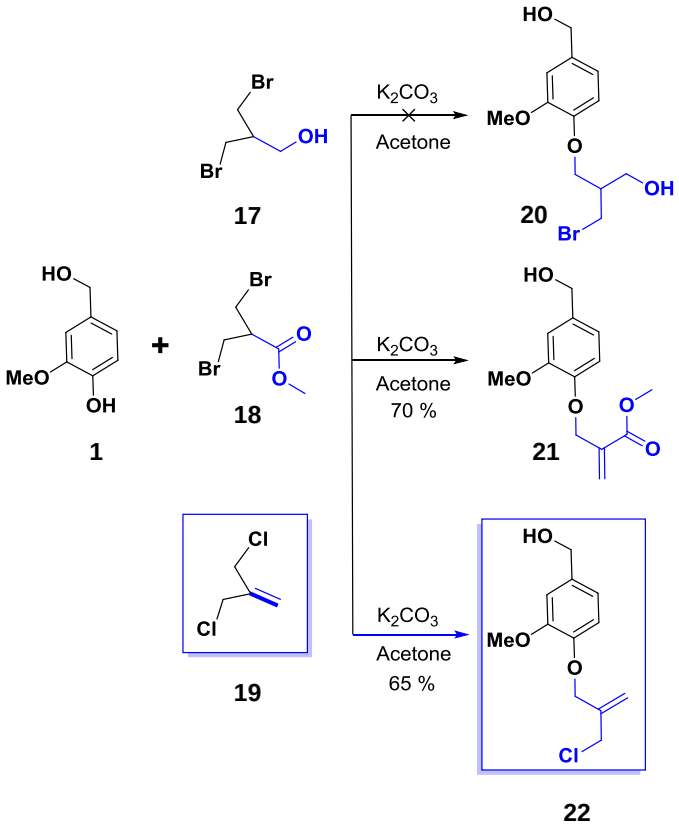

Figure 49: tried strategies for adding the primary alcohol moiety or its precursors.

Having synthesized these two parts, it is time now to assemble them by an alkylation step in DMF under smooth basic conditions. In this step, a statistical mixture of three products is unavoidable thus leading to the formation of the desired compound in a moderate yield. Herein,

protection of the benzyl alcohol is not necessary to assure a good separation of the three main products. The desired product **23** was isolated as a racemic mixture in 40% yield, Figure 50.

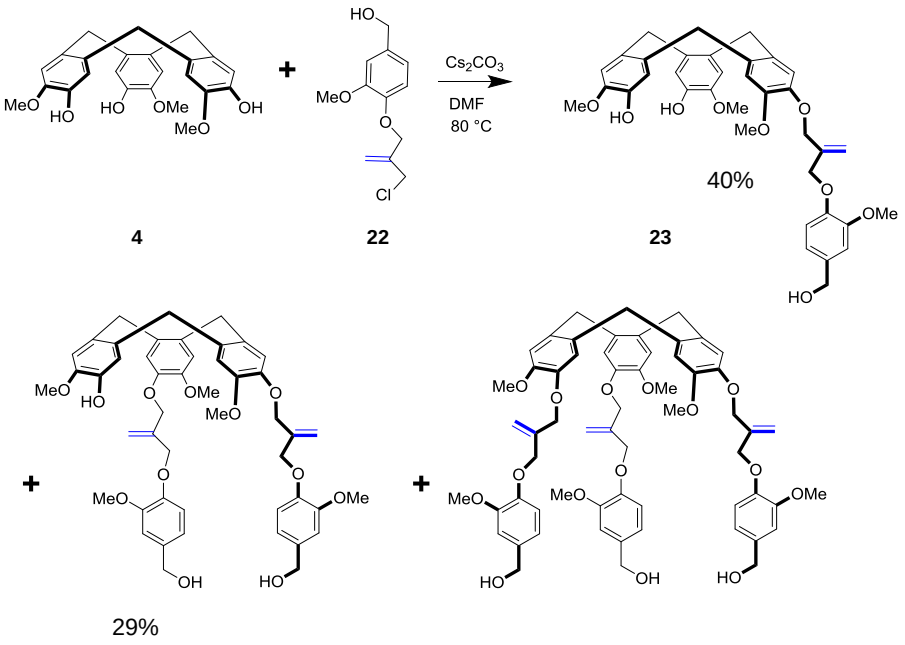

Figure 50: scheme showing the synthesis of **23** in racemic form and the corresponding byproducts.

Double alkylation of the mono-alkylated compound **23** by the two ethylenedioxy arms **24** was also performed under basic condition using cesium carbonate in DMF to offer the desired product **25** in 84% yield. The two arms have to be protected in the form of OTHP acetal to decrease the polarity of the cryptophane precursor and facilitate its separation on silica gel, Figure 51. Unfortunately, addition of THP groups produces several diastereomeric compounds that cannot be separated by column chromatography and it complicates the interpretation of the ^{1}H NMR spectra. Nevertheless, some characteristic protons signals can be clearly identified. For instance, the ^{1}H NMR spectrum of compound **25** shows fifteen protons in the aromatic regions ranging between 6.65 and 7.00 ppm and two protons characteristic of the alkene group at 5.3 ppm. In

addition, six axial and equatorial protons of the CTB are displayed between 3.4 and 4.6 ppm respectively.

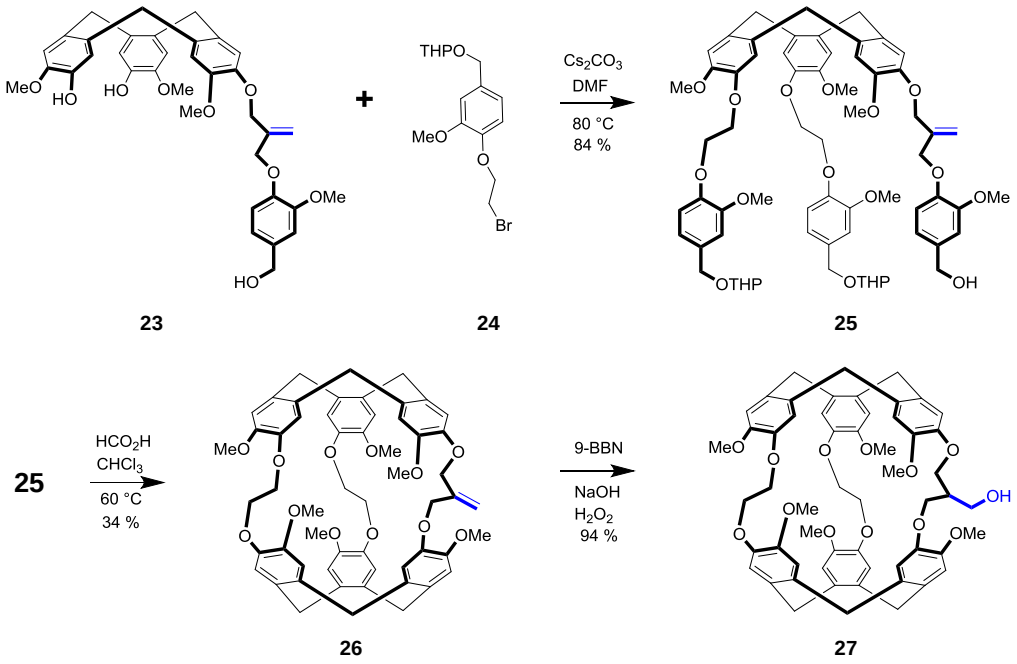

Figure 51: synthesis of cryptophane **26** by cyclization using formic acid and the hydroboration-oxidation step to introduce the primary alcohol derivative **27**.

The formed tri-alkylated template **25** was successfully cyclized under diluted concentrations (10^{-3} M) in a mixture of formic acid and chloroform (50/50: v/v) at 60 °C for about 6 hours. This reaction involves rapid deprotection of the OTHP groups and it allows three Friedel-Crafts alkylations affording the desired *anti*-cryptophane **26** in 34% yield. At this stage, the *anti*-configuration has been adopted based on previous results obtained with cryptophane-[223] derivatives.[64] As usual, this cryptophane is obtained as a racemic mixture and it has a C_2-symmetry. This symmetry is clearly revealed by ^{1}H NMR spectrum that displays only six singlets in the aromatic region between 6.6 and 6.7 ppm corresponding to twelve protons. In addition, the two alkenyl protons are shown at 5.58 ppm and appear as a singlet. Finally, the six methoxy groups grafted on the cryptophane skeleton are revealed as three sets of singlet, Figure 52. At this

stage, we can take advantage of the presence of the double bond to perform subsequent reactions like metathesis or addition reactions for instance.

It is noteworthy that employing an alkene function during the synthetic pathway saves a lot of protection steps, which would be required if we used a more reactive primary alcohol function instead. For instance, we can assume that the latter function will be surely dehydrated under the acidic conditions used for the cyclization step.

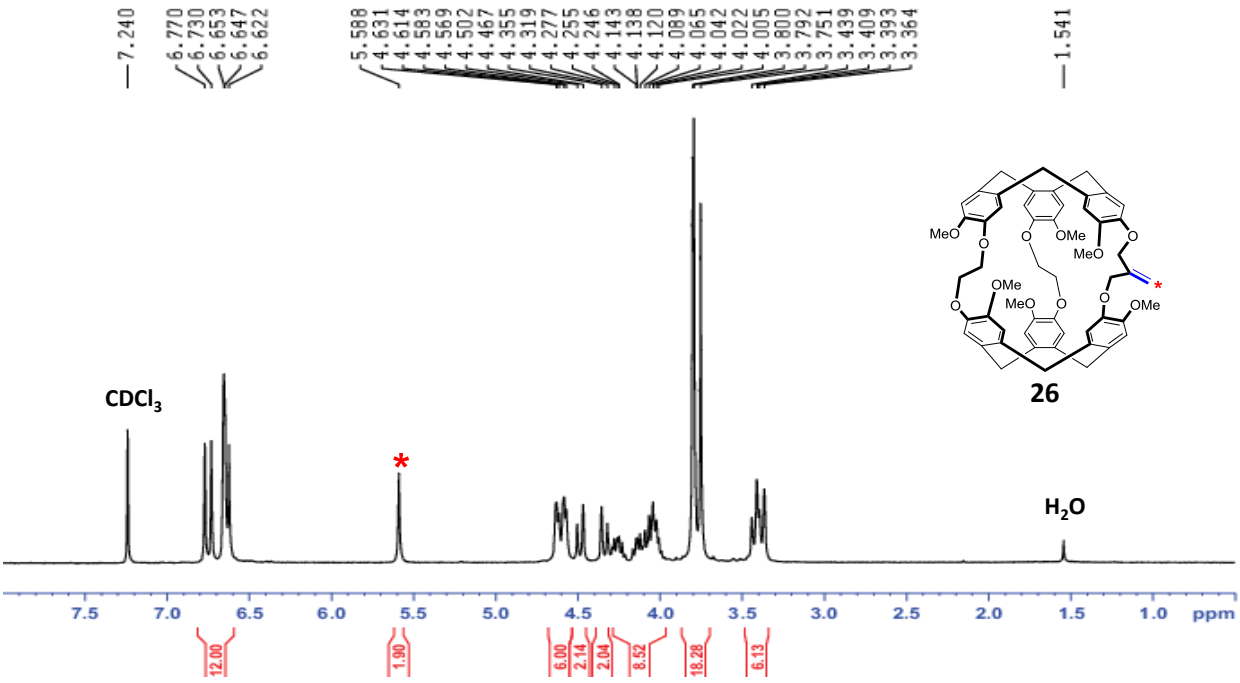

Figure 52: ^{1}H NMR spectrum of cryptophane **26** illustrating the C_2-symmetry.

To introduce a primary alcohol on the alkene arm of cryptophane **26** several reactions can be imagined but a hydroboration-oxidation step seems to us the best way to afford the desired product **27**. To do so, we have used 9-BBN (0.5 M in THF), NaOH (3 M) and H_2O_2 in a mixture of THF and CH_2Cl_2 (80/20). Based on the analysis of the crude product, the reaction gave rise to exclusively cryptophane **27** and the second regioisomer was not detected. Purification of the

compound afforded cryptophane **27** in an excellent yield (94%). The low solubility of starting material led us to change the usual conditions. Thus, such type of boron-based oxidation is carried only in THF, where it acts as both a solvent and a boron stabilizing ligand. In our case, using these conditions resulted in a decrease of the reaction yield (56%). Addition of CH_2Cl_2 was thus mandatory to completely dissolve the starting material and to drive the reaction to completion. Other peroxide-based conditions (Oxone) were also tried to perform the oxidation of the double bond. Unfortunately, these conditions led to a complete decomposition of the starting material. It is noteworthy that oxidation of the double bond led to a decrease of the molecular symmetry. Thus, *anti*-compound **27** has a C_1-symmetry and it was isolated as a racemic compound. The proton NMR spectrum of the cage also reflects the lowering of the symmetry since the aromatic protons now appear as twelve singlets. The proton signal corresponding to the alkene group is no longer present and it is replaced by a new downfield shifted signal at 2.4 ppm that corresponds to the β hydroxyl proton (shown in **red** in Figure 54). Fortunately, we succeeded to obtain X-ray quality crystal of compound **27** from a chloroform/ethanol mixture and to get its X-ray structure. An ORTEP representation allowed us to assure the *anti*-configuration as assumed before. The cavity volume of the host was estimated to be 108 $Å^3$ with an electron count of 30, which is compatible with the presence of an ethanol molecule, Figure 53.

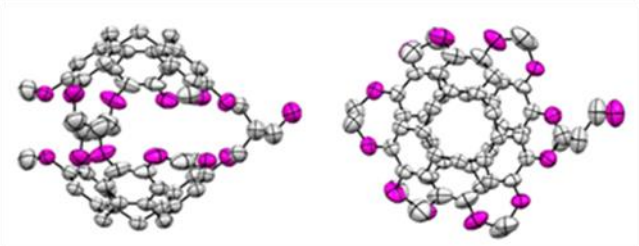

Figure 53: ORTEP representation of compound **27.** Two different views are shown. Hydrogen atoms have been removed for clarity. The cavity is filled with an ethanol molecule (not shown). The displacement ellipsoids were plotted at 30% probability level.

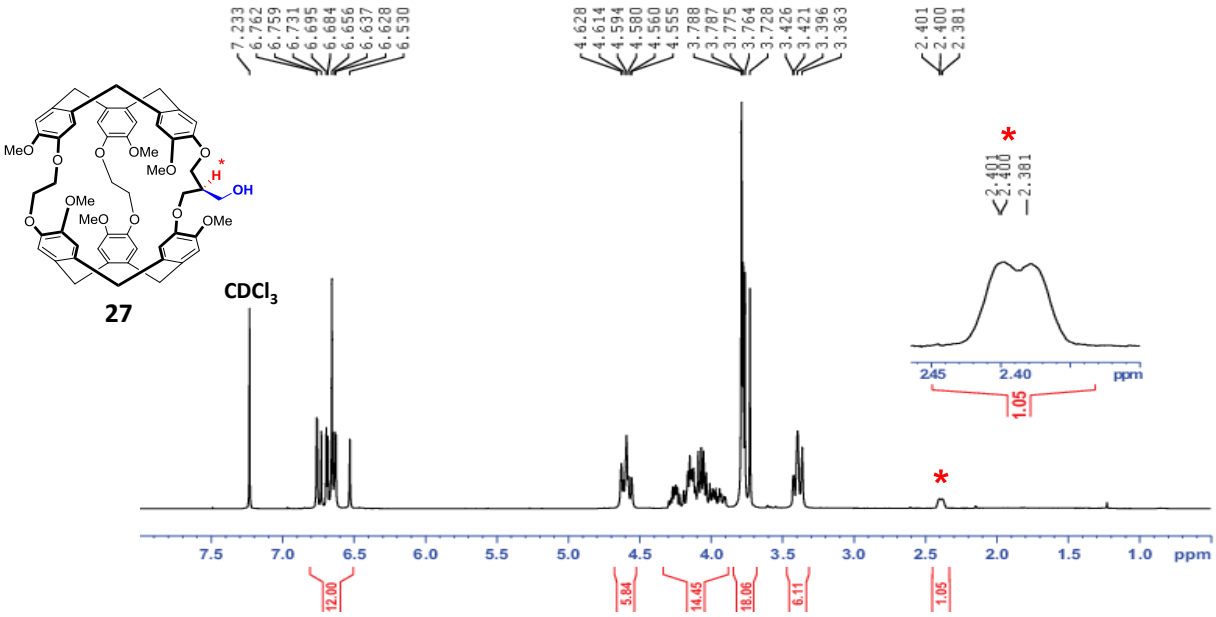

Figure 54: ^{1}H NMR spectrum of compound **27** reflecting the C_1-symmetry and zoomed is the central proton on the propylenedioxy arm (shown in red for illustration).

4. Reactivity of the Primary Alcohol on Cryptophane 27

Attachment of a primary alcohol on the middle of the propylenedioxy arm offers new routes for further functionalizations. For example, we can imagine converting the hydroxyl group into a nucleophile under basic conditions. It might be also transformed into an electrophile by performing a mesylation reaction for instance. Finally, we can perform an oxidation reaction to convert the alcohol group into an aldehyde or a carboxylic acid. These different functionalizations are needed to introduce a spacer that will carry the sensing arm.

4.1. Electrophilic Activation and Nucleophilic Substitution of the Primary Alcohol:

To invert the reactivity of the primary alcohol to an electrophile, it is necessary to convert it into a good leaving group. This can be achieved by the reaction of the alcohol function of compound **27** with mesyl-chloride or tosyl-chloride for instance. Surprisingly, the transformation

of the primary alcohol to the corresponding tosylate group via a reaction with p-toluenesulfonyl chloride in pyridine failed and the starting material was recovered. This lack of reactivity is probably due to the bulkiness of the tosylate group. Using excess of the less bulky methanesulfonyl chloride in a pyridine/dichloromethane at 60 °C afforded the expected mesylated compound **28** in a good yield (82%), Figure 55. For this compound, the ^{1}H NMR spectrum shows a deshielding of the β hydroxyl proton by about 0.4 ppm with respect to the starting material. In addition, a singlet integrating for three protons at 3.07 ppm corresponding to the methyl group of the mesylate is also clearly visible on the spectrum.

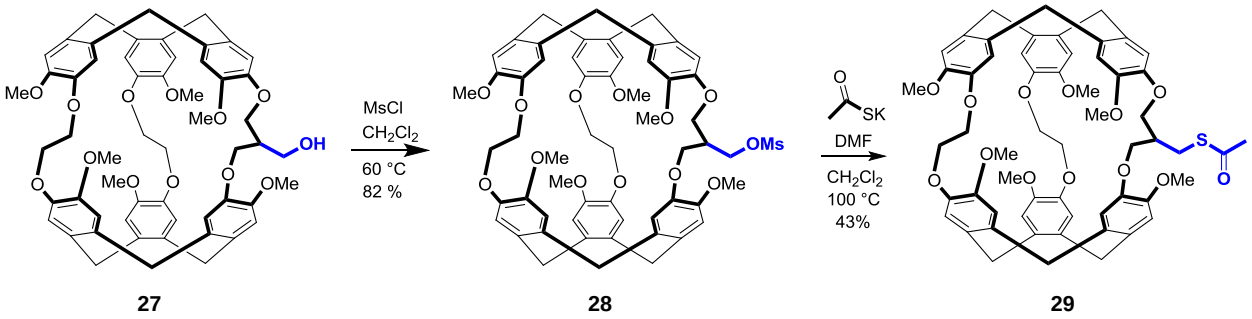

Figure 55: mesylation of cryptophane **27** followed by nucleophilic substitution by potassium thio-acetate to form cryptophane **29**.

With the mesylated cryptophane **28** in hands, many different reactions can be envisaged. For instance, a reaction with sodium thio-acetate in DMF/CH_2Cl_2 mixture afforded the protected thiol derivative **29** in a moderate yield (43%). This example offers the first nucleophilic substitution reaction performed on an electrophilic cryptophane-[223] derivative. The formation of the cage was evidenced by ^{1}H NMR spectrum that shows the disappearance of the methyl group corresponding to the mesylate group (3.07 ppm). Instead, this signal was replaced by another singlet appearing at 2.37 ppm and that stands for the methyl group of the thio-acetate moiety. The potential hydrolysis of this cage gives rise to the thiol-substituted derivative. This might have

many promising applications as a peroxide sensor or as a precursor to build-up new cryptophane derivatives.

Interestingly, this reaction did not afford only new cryptophane derivatives, but also it demonstrated the higher accessibility and electrophilic reactivity of the cage compared to its secondary alcohol congener. The thorough investigations performed on this derivative revealed some interesting features (self-encapsulation phenomena) that will be discussed in more details in the second part.

4.2. Oxidation of Cryptophane 27:

Beside the successful electrophilic activation of the cage, oxidation of the primary alcohol to the corresponding aldehyde and carboxylic acid appears a promising approach to attach new functionalities by a wide range of reactions like Wittig type reactions, reductive imination, aldolic condensation or amide coupling reactions.

The partial oxidation of the primary alcohol **27** to the aldehyde **30** was performed using Dess-Martin periodinane in freshly distilled CH_2Cl_2 at room temperature. It is worth mentioning that the use of freshly distilled CH_2Cl_2 is mandatory to render the reaction complete, Figure 56. Other conditions were also tried like BAIB/ TEMPO reagents in CH_2Cl_2 at room temperature offered exactly the same results.[155] The ^{1}H NMR spectrum of the crude aldehyde **30** shows a complete conversion of the alcohol, which is revealed by the appearance of the characteristic aldehyde peak at 9.92 ppm. A deshielding of the β hydroxyl proton by about 1 ppm (3.22 ppm) is also observed. Other impurities corresponding to Dess Martin monoiodinane byproduct are detected on this spectrum. Unfortunately, attempts to purify the obtained product by column chromatography on silica gel led to transformation of this derivative. ^{1}H NMR spectrum showing

two additional signals between 4.0 to 5.0 ppm confirms the transformation of this derivative. This might be explained by the formation of the enol tautomer but the integration does not assure this assumption. A partial decomposition of the compound can be also envisaged to explain these results.

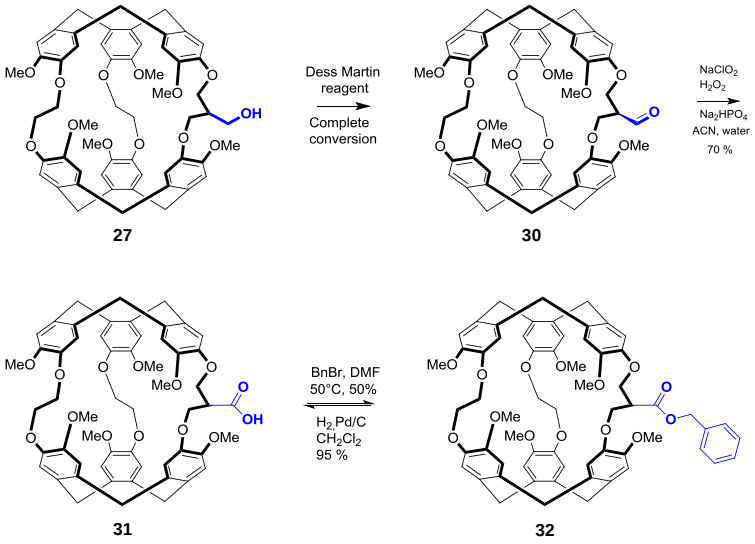

Figure 56: oxidation of cryptophane **27** into an aldehyde **30** and then to the carboxylic acid derivative **31**.

Thus to avoid this problem, the aldehyde derivative was immediately used in the next oxidation step without further purification. The second oxidation to carboxylic acid **31** was carried using sodium chlorite in acetonitrile/water mixture at room temperature to offer the desired product **31** in a good yield (70%).[156] This cage was stable enough and it was purified by two different methods, either by precipitation from chloroform/diethyl ether mixture or by column chromatography on silica gel. In the latter case, the acid derivative was converted into the corresponding benzyl ester **32** that is more easily purified by chromatography. This step was followed by a hydrogenolysis reaction with a palladium catalyst in a dichloromethane/methanol mixture to give rise to the acid derivative **31** in an excellent yield (95%). However, the first purification method was preferred and it offers the compound in a higher yield (70%), Figure 56.

Direct oxidation of the primary alcohol **27** to the carboxylic acid **31** using trichloro-cyanuric acid failed showing a complete decomposition of the starting materials.[157]

The above described derivatives constitute new family of functionalizable cryptophane-[223] type cages, which will be further elaborated by other chemical transformations.

5. Synthesis of Water-Soluble Platforms for Xenon-Based Sensors

The introduction of water-solubilizing substituent is another key transformation that has to be considered. Interestingly, our cryptophane skeleton possesses several functionalities that can be selectively modified to introduce these substituents. The following paragraph is dedicated to the different strategies used to introduce the water solubilizing groups.

5.1. Demethylation Reaction:

Prior to the introduction of water-solubilizing groups on the cryptophane rims, a demethylation step of the six available methoxy groups is required. Demethylation of these groups using lithium diphenylphosphide (1 M) is well established on this type of molecular host. The synthesis of lithium diphenylphosphide was described by E. Vejeds[158] and used by A. Collet to produce cryptophane-[222] $(OH)_6$ and optimized by Brotin and co-workers. This method is selective for methyl ether deprotection, due to the steric hindrance of diphenylphosphide, and it leaves unreacted the three bridges. Even though this reagent can be kept for weeks in a fridge, we recommend using freshly prepared solution of lithium diphenylphosphide to obtain reliable results.

Introducing water solubilizing precursors at the very beginning of the synthesis can be done by demethylation of the methoxy groups of compound **26**, Figure 57. Attempts to perform this reaction with freshly prepared $LiPPh_2$, at 60 °C in THF produced the expected demethylated

product but it showed also the disappearance of the NMR signal corresponding to the double bond. The appearance of several byproducts indicates the decomposition of the starting material under these conditions.

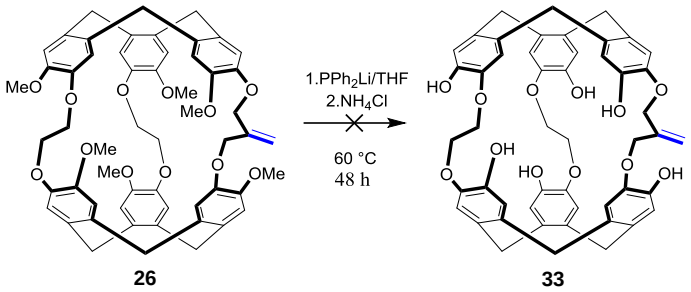

Figure 57: attempts to demethylate cryptophane **26** to form cryptophane **33**.

We switched to another strategy, which is the demethylation of cryptophane **27** bearing a primary alcohol function followed by a selective alkylation step. Our previous experience with cryptophane **12** revealed that secondary alcohol was reactive towards the phenol alkylation reaction when methyl bromoacetate is used as an electrophile. As our alcohol **27** is less hindered and even less basic than that in cryptophane **12**, a protection step is hence necessary to selectively functionalize the six phenols. As mentioned previously, the demethylation step is performed under basic conditions and an acidic workup is usually needed to recover the demethylated product. Keeping this information in mind, we must choose an acid and base tolerant protecting group. Based on our knowledge, we believe that a tetrahydropyranyl group would be a good candidate to resist both basic and mild acidic conditions. So we first protected the cage **27** as an acetal under mild acidic conditions using PPTS/DHP reagents. Compound **34** was thus obtained in a good yield (75%), Figure 58. Adding a new stereocenter on the cage led to the formation of a mixture of diastereomers, which are not separable by column chromatography but they can be easily distinguished by ^{13}C NMR spectroscopy.

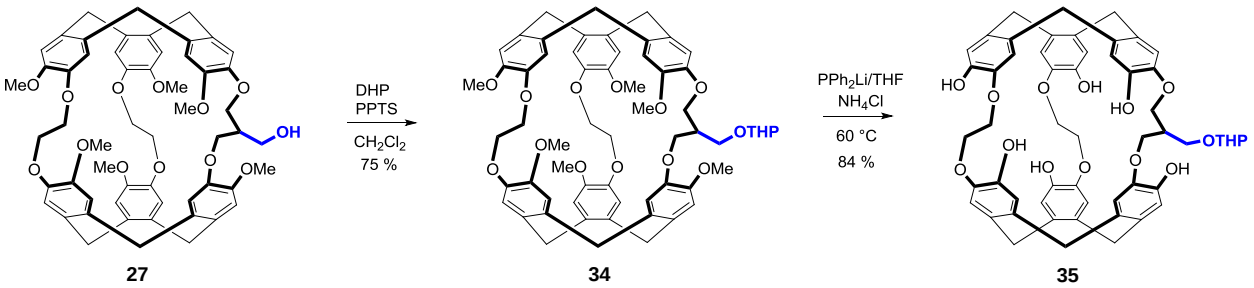

Figure 58: protection of cryptophane **27** by a THP group followed by a demethylation step to form cryptophane **35**.

Compound **34** was then subjected to a demethylation step in a freshly prepared $LiPPh_2$ (1 M) solution in THF at 60 °C for 48 hours. A long reaction time was used to insure that all the methoxy groups are removed. The reaction was then treated at 0°C using mild acidic (ammonium chloride; pH ~ 5.0) conditions to keep the THP group intact. Although highly polar, we were able to purify the cage **35** on silica gel using a mixture of DMF/acetone as an eluent. This offered the pure compound **35** in a good yield (84%), Figure 58. The ^{1}H NMR of this dual functionalized cage in DMSO-d_6, displays several signals corresponding to the hydroxyl groups of the two diastereomers and twelve overlapped protons in the aromatic regions. The axial and equatorial protons give a more complicated pattern and they cannot be resolved. Again, the ^{1}H NMR spectrum shows a splitting of certain signals because of the presence of the two couple of diastereomers, Figure 59.

This dually functionalized compound **35** is a leading chemical platform to construct xenon-based biosensors. The six available phenols can be functionalized selectively with different water solubilizing groups keeping the primary alcohol intact. Then the latter can be selectively deprotected and transformed at a later stage in the synthesis.

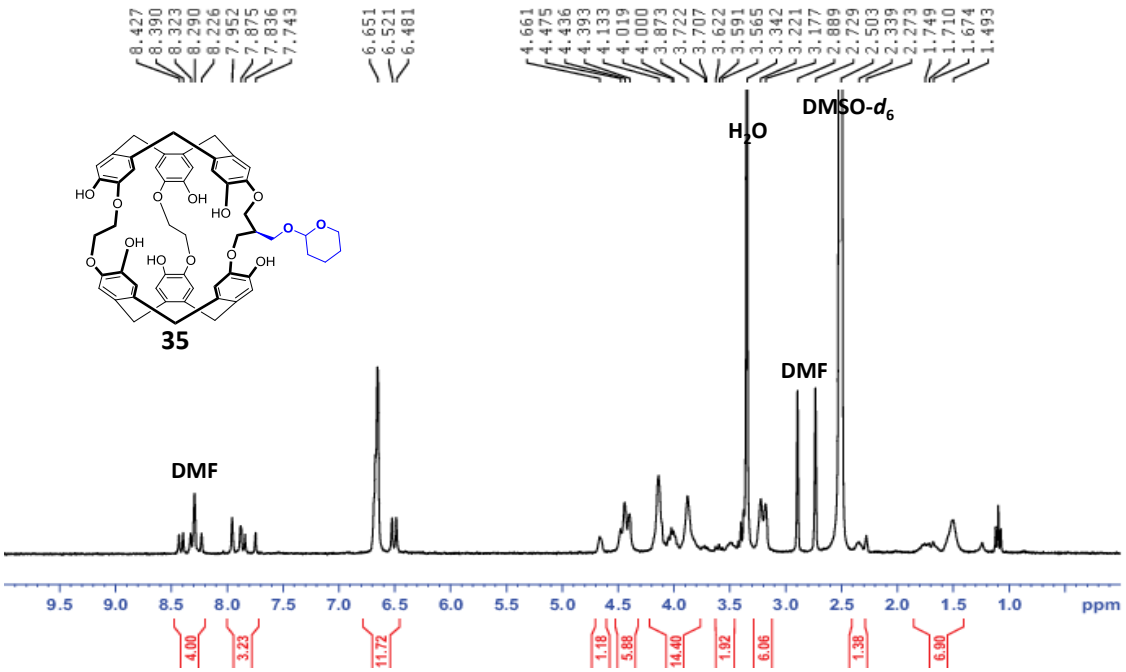

Figure 59: ^{1}H NMR spectrum of cryptophane **35** in 400 MHz spectrometer.

5.2. Introducing Water-Soluble Groups:

Cryptophane rims can be decorated with different solubilizing functions like carboxylic acid derivatives, polyethylene glycol (PEG) or sulfonyl groups. In our case, we focused on grafting selectively six ester groups on the cryptophane **35** rims as precursors to six carboxylic acid functions.

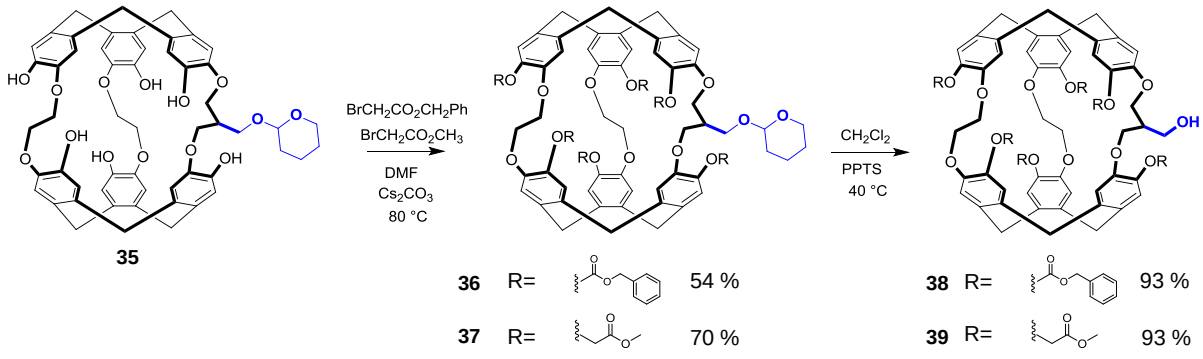

Figure 60: alkylation of compound **35** followed by a deprotection step to form compounds **38** and **39**.

We chose to introduce two types of ester group, methyl or benzyl esters to access the carboxylic acid derivative by hydrolysis under basic condition or hydrogenolysis with a palladium catalyst. These cryptophanes can be obtained by performing an S_N2-type reaction on an appropriate alkylating reagent. To do so, the cage was dissolved in DMF in presence of cesium carbonate. Then alkylation with methyl or benzyl bromoacetate afforded the expected derivatives **36** and **37** in 54% and 70% yields, respectively. These two precursors were also isolated as diastereomeric mixtures but their purification was tedious owing to their high lipophilicity. It is worth mentioning that unlike cryptophane **37**, benzyl protected cryptophane **36** tends to implode easily as ascertained by its ^{1}H NMR spectrum. This imploded form seems to be reversed back to its initial (*CC*) conformer after the OTHP deprotection. Consequently, the unprotected cage **38** was obtained in an excellent yield (93%). The inversion to the initial (*CC*) conformer is mostly due to the used reaction conditions (CH_2Cl_2 at 40 °C). Under these conditions, the cage will be surely filled back with dichloromethane thus restoring the initial conformation. Same conditions were used to obtain the unprotected derivative **39** and it was also obtained in almost quantitative yield (93%), Figure 60.

Successful selective grafting of water-solubilizing precursors on the compound **35** afforded us two new platforms, **38** and **39** for ^{129}Xe-based biosensing applications. These two derivatives can be either used immediately to graft a sensing unit or can be subjected to subsequent reactions.

5.3. Chemical Transformations of Cryptophanes 38 and 39:

One of the strategies used to functionalize the primary alcohol of methyl protected cage **39**, was to simply alkylate it under basic conditions. In this reaction two main requirements have to be considered, the reaction temperature and the used base. In order to avoid implosion of the cryptophane skeleton, a relatively low reaction temperature has to be employed (between 25 and

40 °C). Additionally, mild bases have to be used because strong ones will deprotonate the α-ester protons leading to the formation of many side-products.

We chose to introduce a protected carboxylic acid arm via the alkylation of the hydroxyl group by benzyl bromoacetate to form derivative **40**, Figure 61. Taken the above considerations into account, we chose either potassium tert-butoxide or DBU as bases due to their bulky structure and matching pK_a. In both cases, the cage was dissolved in DMF in the presence of the base, and then the alkylating agent was added at room temperature. None of these conditions worked, and these reactions resulted in the formation of many side-products.

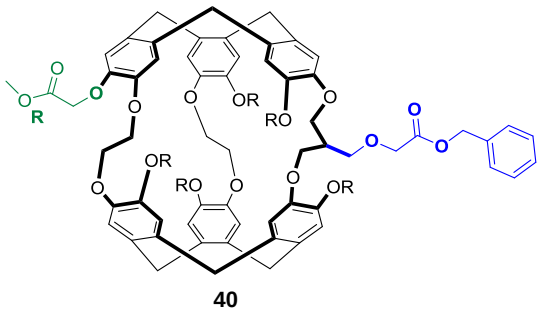

40

Figure 61: structure of compound **40**.

These conditions triggered us to use another strategy, which is the oxidation of the primary alcohol. The readily established oxidation conditions used to oxidize cryptophane **26**, were also employed here. So the benzyl or methyl esters derivatives, **38** and **39** were first oxidized to aldehydes by Dess Martin periodinane in dry CH_2Cl_2 to offer cryptophanes **41** and **42**. The ^1H NMR spectra of these cages show a complete conversion of the starting material, which were used in the next step without prior purification. The obtained aldehydes were subjected to a second oxidation step to form the corresponding acid using sodium chlorite, in an acetonitrile/water mixture at room temperature. The lipophilicity of the cages allowed us to

purify them by column chromatography to offer the corresponding pure benzyl and methyl ester derivatives **43** and **44** in 70 and 78% over two steps, respectively, Figure 62.

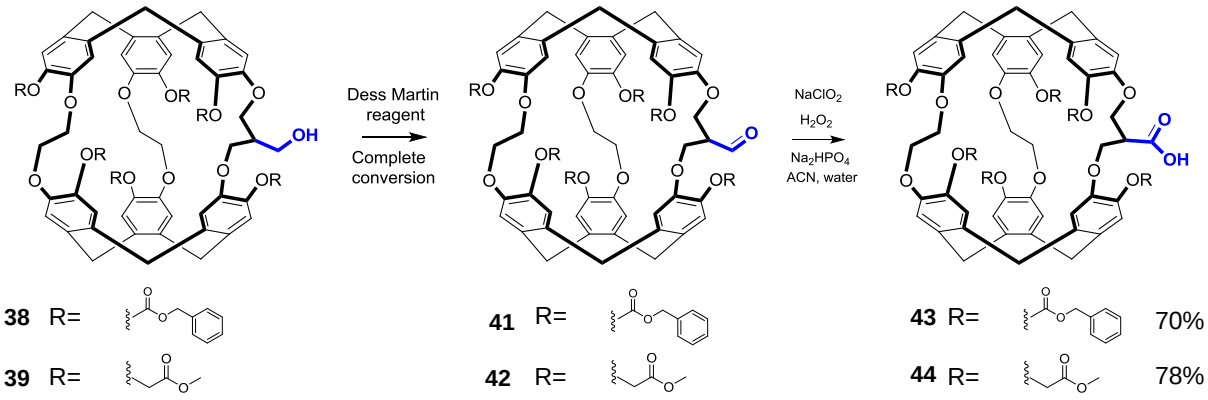

Figure 62: oxidation of compounds **38** and **39** to the aldehyde and the corresponding acids **43** and **44**.

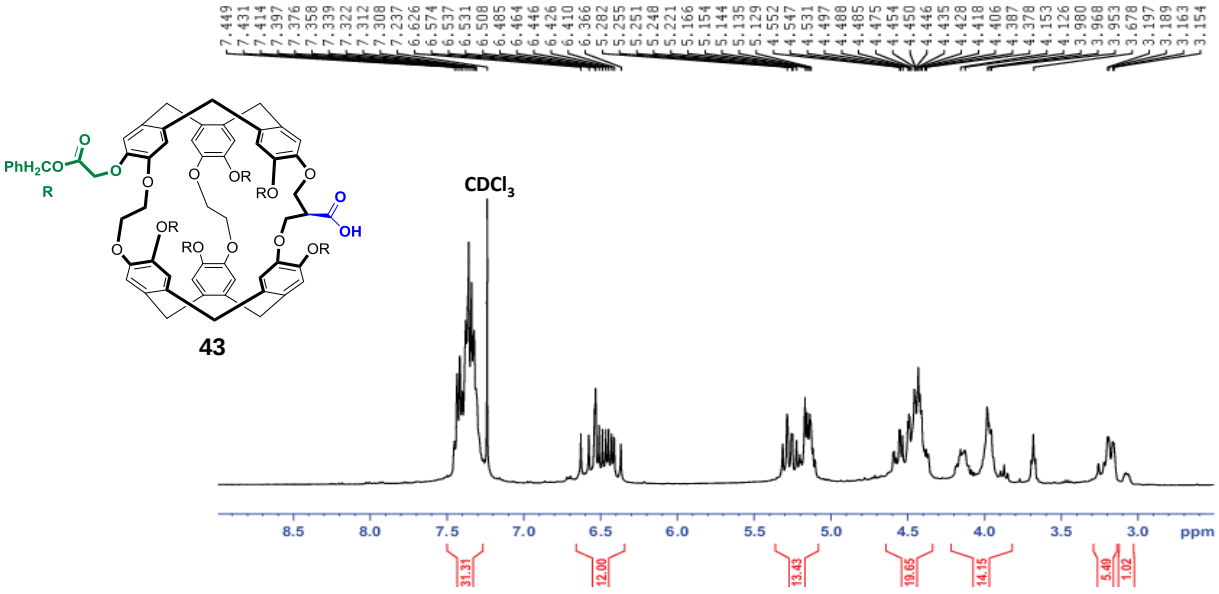

Figure 63: ^{1}H NMR spectrum of compound **43** in $CDCl_3$ in 400 MHz spectrometer.

The proton spectrum of the benzyl ester protected cage **43** is displayed above, showing overlapped signals of thirty protons corresponding to the benzyl protecting groups, twelve signals ranging between 6.2 to 6.36 ppm corresponding to the aromatic protons of two CTB and interestingly a deshielded signal of the β carboxylic acid proton located at 3.15 ppm, Figure 63.

These two formerly presented cryptophane-[223] derivatives set up a new family of dually functionalizable platforms. These platforms can be immediately used for building different xenon-carriers for MRI applications. The synthesis of these compounds constitutes a very important result as it considerably simplifies the introduction of the sensing unit. It is noteworthy that this could not be achieved with the water-soluble cryptophane hexa-carboxylate. In addition, the presence of a carboxylic acid function at the cage's propylenedioxy linker is of special interest because it is widely used in biochemistry to elaborate sensors via amide coupling reactions. The cleavage of the six other ester groups can also afford very easily the corresponding water-soluble sensors.

6. Functionalization of Cryptophane-[223] Derivatives by Sensing Units

In the first chapter we presented a wide range of ^{129}Xe-based biosensors, which are mostly derived from cryptophane-[222] monoacid. The attachment of the sensing unit to this cryptophane core is usually achieved by an amide coupling. In our case, we used the same approach to link different amine or aniline-bearing sensing units to cryptophane derivatives **43** and **44**. This step is followed by the cleavage of the protecting groups to offer the water soluble cryptophane-[223] molecular sensors. In the next paragraphs, we will present the different sensing units grafted to the cryptophane-[223] cores and the problems encountered during the synthesis, Figure 64.

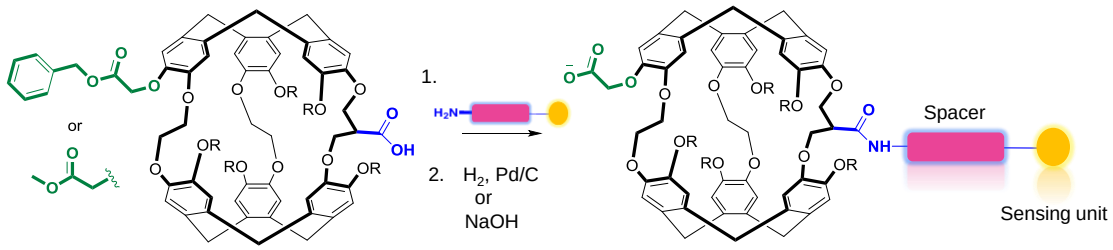

Figure 64: schematic presentation showing the possible functionalization of compound **43** and **44** by an amide coupling reaction.

6.1.Hydroxamic Acid Functionalized Water-Soluble Cryptophane-[223]:

Hydroxamic acids are a family of organic compounds of molecular structure $R_CC(O)N(R_N)OH$ (R_C = alkyl/aryl; R_N = alkyl/aryl or H), Figure 65. These compounds were first described by H. Lossen in 1869, where he reported the synthesis of oxalohydroxamic acid from diethyl oxalate and hydroxylamine.[159] Hydroxamic acids are weak acids that undergo two consecutive deprotonations of the first (N-OH) proton to give the hydroxamato group and a second deprotonation (NH-O) to offer the hydroximato function. The pK_a of the first deprotonation ranges between 8.5 and 9.4 in aqueous media.[160] Hydroxamic acids are characterized by their ability to chelate a wide range of transition metals. The chelating ability is readily exploited by nature, in which they exist in many bacteria as the so-called siderophore for coordinating dissolved iron-(III). These iron-(III)-siderophore complexes are recognized by cell-surface proteins, which transport them to the cytoplasm where they release their iron-(III) content. Additionally, they act as inhibitors for Ni (II) urease and Zn (II)-containing metalloproteins like matrix metalloprotease (MMP), which are involved in cancerous cell proliferation.[161,162]

Hydroxamic acids coordinate transition metals via the two oxygen atoms as proved by X-ray crystal structures. In contrast, coordination of transition metals via an oxygen-nitrogen coordination mode has never been reported so far, at least for the primary hydroxamic acid derivatives.

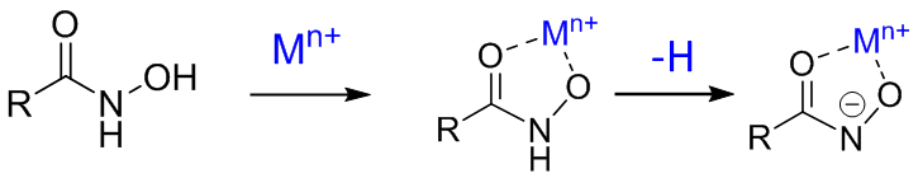

Figure 65: structure of hydroxamic acid function and its corresponding (O, O) chelation modes.

As established in literature, hydroxamic acids chelates effectively the late transition metals like copper, nickel and zinc with comparable binding constants in the order of 10^5 M^{-1}. This triggered us to connect this simple chemical function to our dually functionalized cage and study its interaction with different cations.[160]

The link between hydroxamic acid and cryptophane **43** was achieved via an amide coupling reaction. Herein, the source of our hydroxamic acid function is the commercially available O-benzyl hydroxylamine.

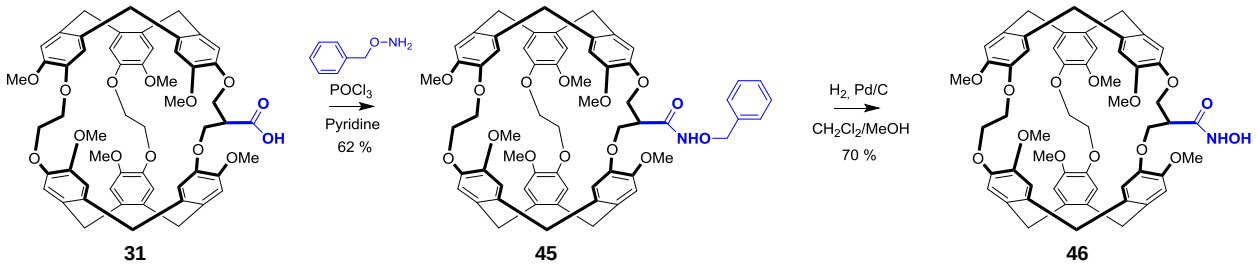

Figure 66: synthesis of compound **46** bearing a hydroxamic acid function.

In order to assess the feasibility of the reaction we first tried the amide coupling on cryptophane **31**. The coupling reaction between this cage and the O-benzyl hydroxyl amine was performed in pyridine using phosphorous oxychloride as a coupling reagent, Figure 66.[163] Under these conditions the carboxylic acid is first converted to the acyl chloride and then reacted with the amine function. This reaction offered the coupled compound **45** in 62% yield. The ^{1}H NMR spectrum of this compound shows a characteristic deshielded proton of the amide group at 9.7 ppm. Interestingly the diastereotopic protons of the benzyl group appear as an AB system at 4.9 ppm. Finally, the latter derivative was deprotected at room temperature using a hydrogenolysis reaction under classical conditions (H_2, Pd/C (10%), CH_2Cl_2/MeOH mixture). These conditions afforded the compound **46** in a good yield (70%).

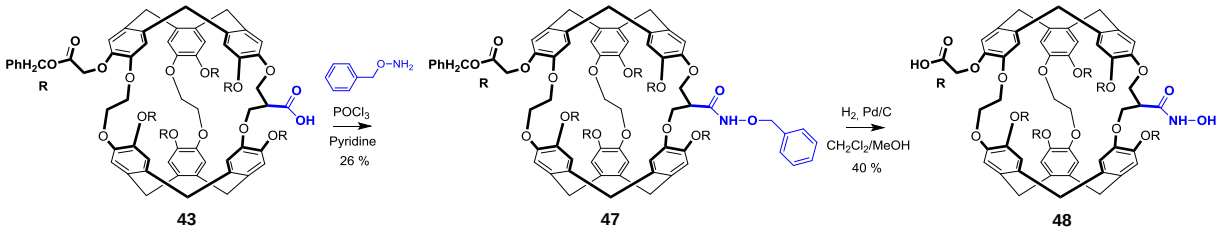

Figure 67: synthesis of water-soluble cryptophane-[223] **48** bearing a central hydroxamic acid function.

These results prompted us to extend our work to compound **43**. Compound **43** was preferred because the seven benzyl groups can be removed in a single hydrogenolysis step. The coupling reaction between O-benzyl hydroxylamine and compound **43** offered compound **47** in a low yield (26%). The low yield can be explained in part by the difficulties encountered during the purification of this derivative. The latter compound was then deprotected by hydrogenolysis. This deprotection step was monitored by TLC. Although the TLC shows a full conversion of the protected cage, compound **48** was only isolated in 40% yield, Figure 67. This might be due to the difficulties to extract this compound. Compared to the starting material, the ^{1}H NMR spectrum of **48** displays in DMSO-d_6 a deshielded set aromatic protons ranging between 6.6 and 7.0 ppm. In addition, a characteristic signal of the proton of the hydroxamic acid function is observed at 9.6 ppm. It is worth mentioning that this derivative is soluble in water at a pH ranging between 4 and 14.

Compound **48** clearly demonstrate the interest of our approach. Indeed, this compound represents the first dually functionalizable cryptophane-[223] sensor, showing acceptable solubility at neutral pH. Compound **48** has been prepared in twelve steps from CTB **4**. Even though this synthesis looks tedious this platform can be designed in a relatively short period of time (1-2 months) in fair quantities. Our approach allows us to bring solutions to the symmetry and solubility problems encountered with other cryptophanes.

6.2.Cryptophane-[223] Bearing an APTRA Derivative:

APTRA or (o-aminophenol-N,N,O-triacetic acid) ligand has been first reported by London and coworkers in 1988. It was initially used to detect cytosolic magnesium and it was connected to an aromatic fluorinated reporter. Unexpectedly, this unit showed a higher affinity to calcium compared to magnesium, where its detection limit is in mM range whereas that of the calcium is in the µM range. Several MRI and fluorescent probes were developed based on a chelating APTRA ligand. Development of more sensitive reporters capable to detect calcium in pico-molar range can be achieved by designing a new (HP) ^{129}Xe@cryptophane derivative functionalized with an APTRA function.[164,165,166,167]

Our targeted APTRA derivative **52** is functionalized with an aniline moiety to anchor it to the cryptophane-[223] derivative via an amide bond, Figure 68. This unit was synthesized in three linear steps starting from a commercially available 2-amino phenol **49** based on a slightly modified known experimental procedures.[168,169] It starts with the alkylation of the **49** with methyl bromoacetate using DIPEA as a base to afford compound **50** in a moderate yield (60%). Nitration of compound **50** in a mixture of nitric and acetic acid afforded compound **51** in 80% yield. The last step involved a hydrogenation step using catalytic amount of palladium on charcoal. This reaction gave rise to APTRA derivative **52** in a good yield (90%).

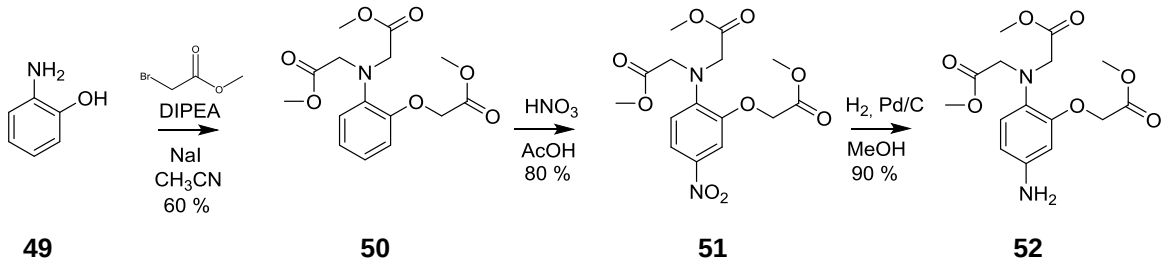

Figure 68: synthesis of the APTRA unit **52**.

Here again, the reaction was performed on the organic version **31** to ensure its viability. Coupling of the APTRA derivative **52** with the compound **31** was performed in pyridine and phosphorous oxychloride. This reaction offered compound **53** in low yield (22%) due to partial decomposition of the APTRA moiety, Figure 69.

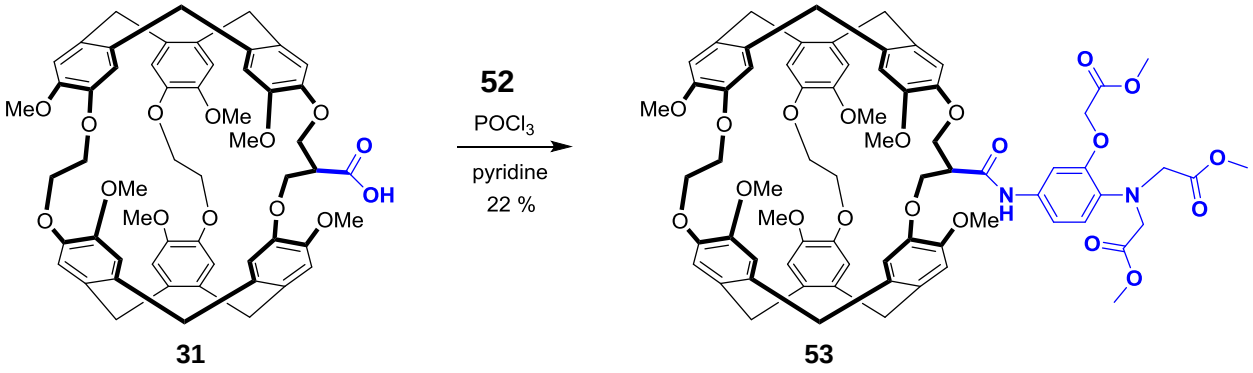

Figure 69: synthesis of organic version of cryptophane-[223] **53** bearing an APTRA derivative.

We then extended this reaction to the pre-water soluble version **44**. We chose this compound because it has the same protecting groups as derivative **52**. The linkage between the two units was also performed by an amide coupling reaction using phosphorous oxychloride and pyridine to give the product **54** as a white solid in 30% yield, Figure 70. The ^{1}H NMR spectrum of this pre-water soluble precursor **54** displays a characteristic signal at 9.07 ppm corresponding to the amide proton and three additional signals in the aromatic region that belong to the APTRA core. For the hydrolysis step, several conditions were tried to simultaneously remove the nine methyl groups and all use different hydroxide salts like LiOH, NaOH and KOH as summarized in Table 3. The solvent used for this step was either a mixture of THF/water or with methanol. The starting material was first dissolved in THF then the metal hydroxide solution was added at zero °C then to 25 °C and monitored by TLC. All the tried reactions revealed the disappearance of starting material within only 10 minutes, except for the first entry, where it was left over night at

40 °C. After that, the crude was extracted with CH_2Cl_2 and then acidified using HCl in ice to offer a white powder. This was then checked by ^1H NMR to reveal either partially hydrolyzed (LiOH) or decomposed byproducts (NaOH) and this was confirmed by HRMS. A last trial with 18 equiv. of KOH (0.3 M) provided the targeted product **55** in about 70% yield. The formation of this product was confirmed by HRMS.

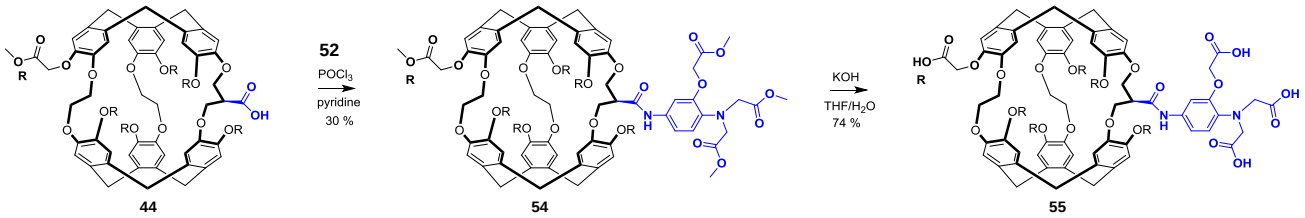

Figure 70: synthesis of water soluble cryptophane **55** functionalized by an APTRA derivative.

It seems that there is a very narrow window between the hydrolysis and decomposition of this compound, where a careful tuning of the chosen base and its equivalence must be done to avoid these problems. Unfortunately, the hydrolyzed compound **55** shows also some light sensitivity issues where it turns brownish when exposed to light. This prevented us from studying its (HP) ^{129}Xe encapsulation properties because they may give misleading results.

Hydroxide salt	Equivalence	Concentration M	Temperature °C	Solvent	Results
LiOH	10	0.01	0 to 40	THF/Water	Partial hydrolysis
LiOH	27	0.01	0 to 25	THF/Water/MeOH	Partial hydrolysis
NaOH	50	2.5	0 to 25	THF/Water	Decomposed
NaOH	27	0.01	0 to 25	THF/Water	Decomposed
KOH	18	0.3	0 to 25	THF/Water	Product 74%

Table 3: different trials to hydrolyze compound **54** to the water soluble cryptophane **55**.

6.3. Biotin Functionalized Cryptophane-[223] Cage:

To further illustrate the feasibility of our approach, we turned our attention towards the bio-conjugation of cryptophane-[223] by a biotin arm for avidin detection. This was chosen because of the high binding constant, which is estimated to be in the range of $K = 10^{15}$ M^{-1}. Our biotin source is the commercially available biotin-PEG2-amine, which will be linked to the cryptophane-[223] core by amide coupling reaction, Figure 71.[119]

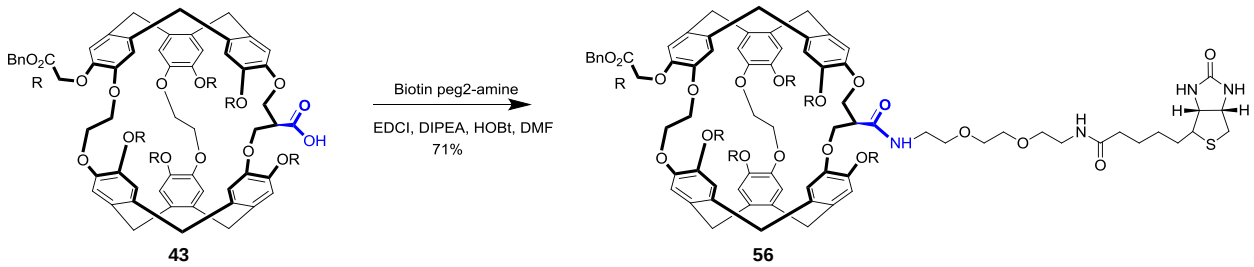

Figure 71: synthesis of compound **56** by an amide coupling reaction of cryptophane **43** and biotin-PEG 2- amine.

To link these two parts, we simply used the well-established amide coupling conditions i.e. phosphorous oxychloride/ pyridine. Unfortunately the reaction did not work and the cryptophane was recovered at the end of the synthesis. The usual coupling conditions using EDCI/HOBt in the presence of DIPEA in DMF for 16 hours gave better results and provided compound **56** as a white powder in 71% yield. The purification of this compound is quite tedious due to its high polarity. The ^{1}H NMR spectrum of **56** shows a clear signature of the biotin arm in the up field region as also demonstrated by the ^{13}C NMR and the HRMS, Figure 72.

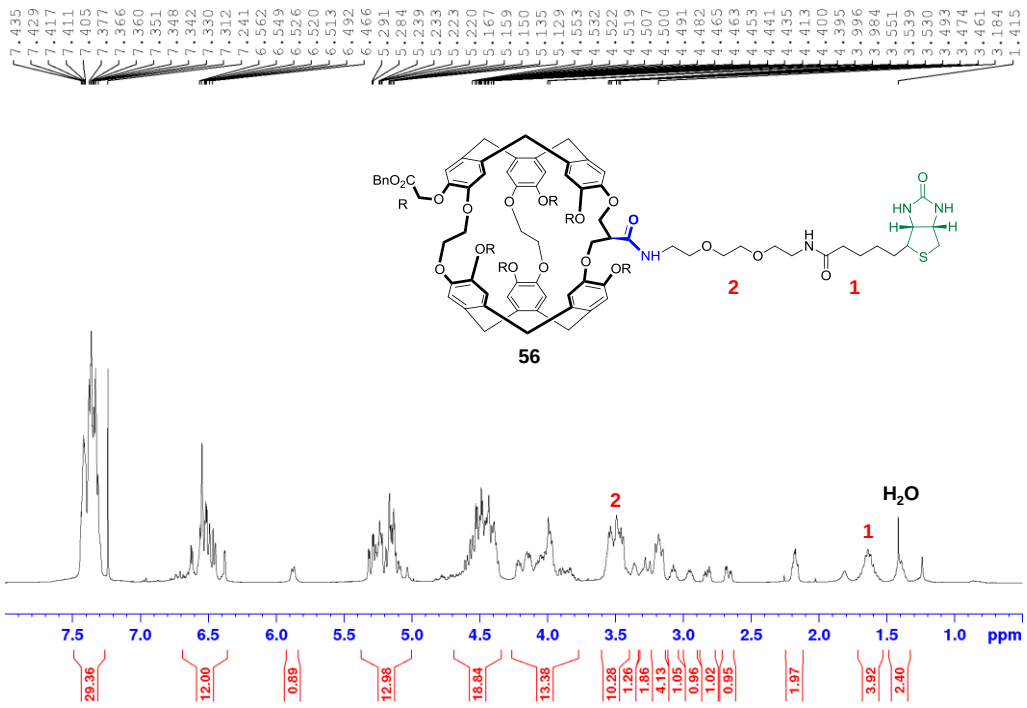

Figure 72: ^{1}H NMR of compound **56** in $CDCl_3$ in 400 MHz spectrometer.

The production of the water-soluble sensor **57** necessitates an additional hydrogenolysis step. Hydrogenolysis using the classical conditions (H_2, Pd/C in a CH_2Cl_2/MeOH mixture) revealed the appearance of a benzyl protected new byproduct. The lack of benzyl deprotection might be due to the sulfur atom, which poisons the catalyst. We switched then to the hydrolysis condition using 18 equiv. of KOH (0.3 M) in THF/water mixture for 30 minutes, and this time the product

57 was successfully obtained after an extraction and acidification step. The ^{1}H NMR spectrum of this derivative shows the full disappearance of the six benzyl groups but the compound is still not pure. The formation of compound **57** was also confirmed by HRMS and xenon NMR experiments. Further work has to be done to optimize this step, Figure 73.

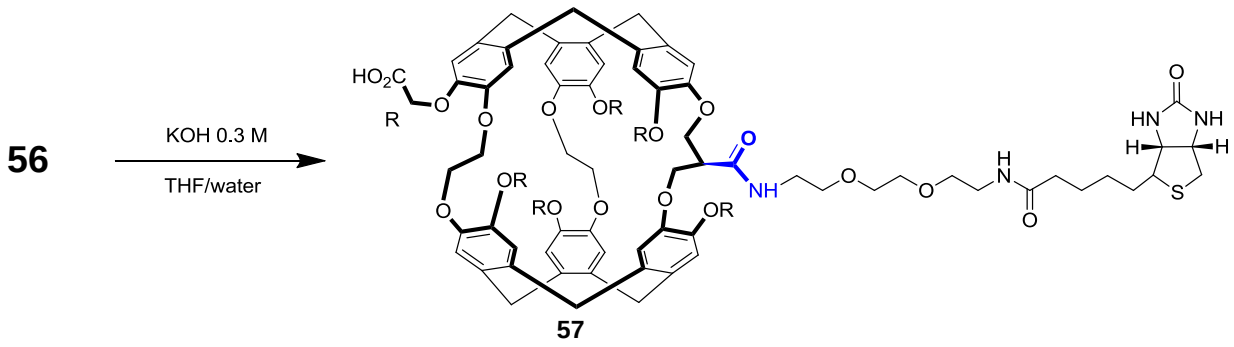

Figure 73: synthesis of water soluble cryptophane **57**.

The success of this reaction clearly shows that it is possible to enlarge the scope of reactivity with our platforms. Further experiments will be necessary in the future to improve the grafting of the sensing arm.

Chapter 3: Hyperpolarized ^{129}Xe NMR Spectroscopy and ITC Experiments of the ^{129}Xe@Cryptophane-[223] Sensors

From a structural point of view, we have been able to construct water-soluble selectively functionalizable cryptophanes, solving by this the solubility and symmetry problems encountered when using other cages. To test if our platforms attain the requirements for the targeted sensing applications, we have studied the (HP) ^{129}Xe NMR spectroscopy of these cages in collaboration with Dr. Patrick Berthault at the Laboratoire de Structure et Dynamique par Résonance Magnétique (LSDRM) at CEA in Saclay, France. The production of the (HP) ^{129}Xe is achieved by a batch mode SEOP, with a polarization ranging between 15 to 20%. The hyperpolarized ^{129}Xe NMR experiments were performed at 11.7 T. In addition to this, isothermal titration calorimetry (ITC) experiments were also conducted to assure the interactions of our sensors with the targeted analytes.

1. Characterization of Cryptophane 48 Bearing a Hydroxamic Acid Group

Cryptophane derivative **48** is water-soluble over a large range of pH. Two experimental campaigns were launched to see the effect of metals chelation and pH variation by (HP) ^{129}Xe spectroscopy and ITC.

1.1. Effect of pH:

To ascertain the ability of cryptophane **48** to bind xenon, a simple (HP) ^{129}Xe NMR was done in D_2O at 298 K. This spectrum shows two peaks corresponding to the free xenon in solution at 196 ppm and the caged xenon at 55 ppm, Figure 74. Indeed the latter signal is upfield shifted compared the free xenon due to cryptophane's shielding effect of the six aromatic rings surrounding the encapsulated xenon. The appearance of two signals indicates a slow in-out exchange dynamics of xenon. This behavior has already been observed with cryptophane-[223] type derivatives that show also specific signal for the ^{129}Xe@Cryptophane-[223] between 50 and 60 ppm.

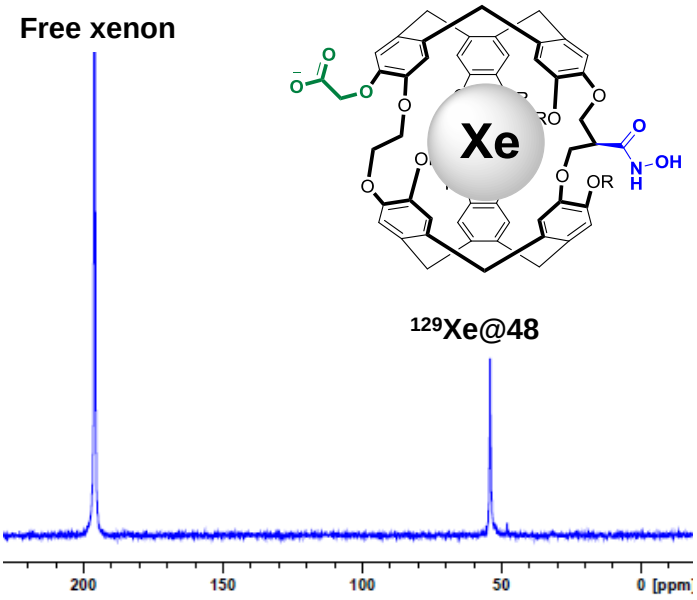

Figure 74: one-scan (HP) ^{129}Xe NMR spectrum of compound **48** in D_2O recorded at 25 °C.

In the first chapter, we presented the remarkable ability of (HP) ^{129}Xe@cryptophane complexes to sense the slight variations in the pH.[38,134] We specifically discussed two cages, the cryptophane hexacarboxylate and the cryptophane tri-carboxylate, each bearing different ionizable groups. Having seven ionizable groups on cryptophane **48** derivative triggered us to investigate the effect of pH change and eventually compare it to the previously reported results.

For this purpose the (HP) ^{129}Xe NMR spectra of compound **48** (0.2 mM) was studied at three different pH values (pH= 3.3, 8.2 and 9.9) in D_2O at 298 K. The spectra at each pH show two NMR signals. One signal corresponding to xenon dissolved in the bulk at 196 ppm and the upfield shifted signal of the caged one, Figure 75. At pH 9.9, 8.2 and 3.3 the encapsulated xenon peaks are located at 58.4 (green), 59.4 (red) and 61.3 ppm (blue), respectively, Figure 75. Between pH values of 9.9 and 8.2 not much variation in the encapsulated xenon signal is observed (1 ppm) although the pKa value of the hydroxamic acid group is reported to be in this range.[160] This result indicates that the ionization of the hydroxamic acid function grafted on the

propylenedioxy arm is not "felt" by the encapsulated xenon. This result seems to be very surprising and disappointing because the hydroxamic function is very close to center of the cage. Consequently, we assumed that the close proximity between this function and the encapsulated xenon would result in a greater effect. The lack of sensitivity can be, in part, explained by the localization of the sensing unit. In contrast to the other examples reported in the literature, this sensing unit is located on the linker. Consequently it won't affect the ring current of the CTB units as in the case of other biosensors developed so far.

The drop of the pH to acidic conditions (pH = 3.3) resulted a greater chemical shift variation by about 3 ppm. This variation is due to the change of ionization state of the carboxylic acid groups grafted on the CTB rims, which in turn modifies the ring current of the benzene rings. Similar effect was previously observed with cryptophane-[222] hexacarboxylate, where the change in the pH values from 3.5 to 10.8 resulted in a downfield shift by nearly 4 ppm.[134] The greater variation observed in case of cryptophane-[222] hexacarboxylate compared to our cryptophane-[223] derivative can be explained by the smaller cavity size of this compound.

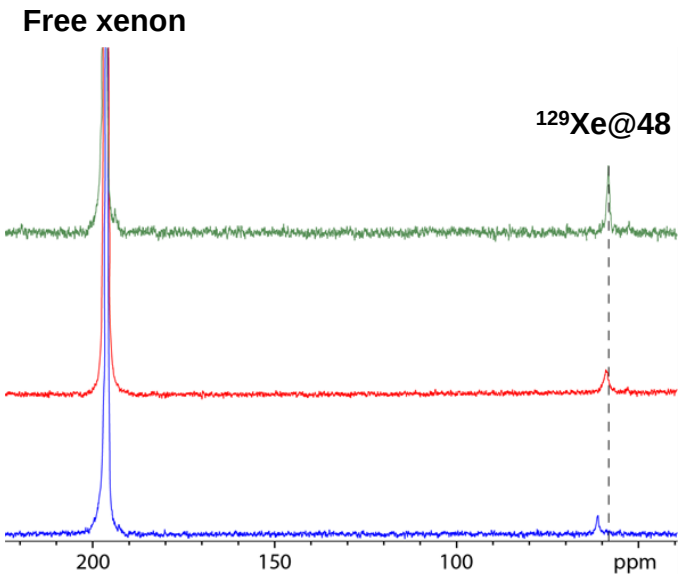

Figure 75: one-scan ^{129}Xe NMR spectra recorded at 298 K of compound **48** (0.2 mM) in D_2O at pH = 9.9 (green), pH = 8.9 (red) and pH = 3.3 (blue).

1.2. Zinc and Nickel Complexation by ITC and (HP) ^{129}Xe Spectroscopy:

Grafting a hydroxamic acid function on the cage's **48** arm allowed us to study the chelation of different metal cations like zinc and nickel. To assure that our probe chelates these cations we used ITC experiments. This technique allows us to access not only the binding constants but also the thermodynamic parameters of the complexation (ΔG°, ΔH°, ΔS°). To avoid misleading results it was necessary to conduct these experiments in presence of a buffer. Indeed, in absence of buffer, the addition of a small amount of cationic species changes the pH of the solution and in turn it affects the parameter of complexation. It took a while for us to optimize the experimental conditions due to solubility issues of the metal salt. For instance, $ZnCl_2$ was not soluble neither in HEPES, phosphate buffer nor MOPS. It is noteworthy that a cloudy solution was obtained in all cases even though some articles reported these conditions.[170] Fortunately, we found that 2-amino-2-hydroxymethyl-1,3-propanediol (TRIS) (20 mM, pH = 7.5) could be used to dissolve zinc chloride.

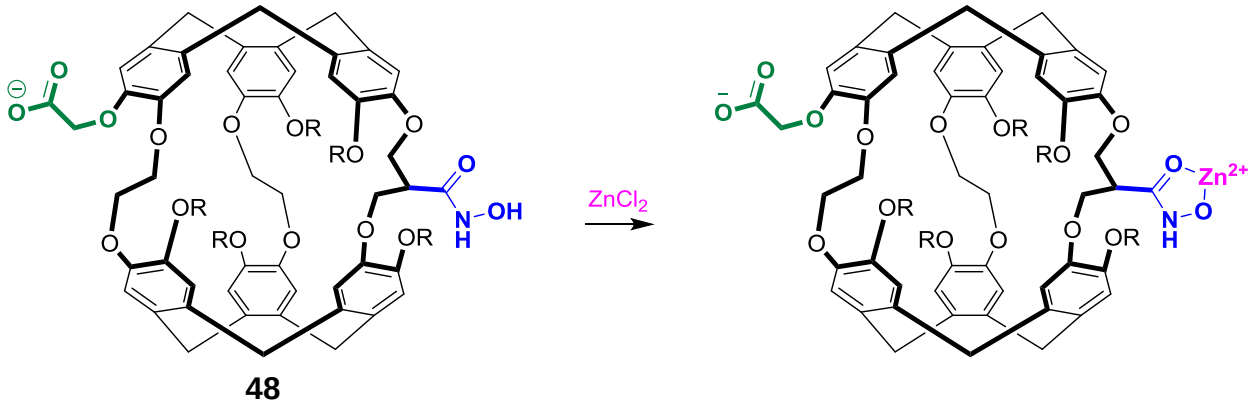

48

Figure 76: chelation of zinc cation by compound **48**.

The titration of cryptophane **48** (0.08 mM) with $ZnCl_2$ (1mM) in 20 mM of TRIS buffer at pH = 7.5 has shown an effective complexation of the zinc cation by the hydroxamic acid function, Figure 76. Our measurements are compatible to 1:1 complex. This binding process is exothermic and the following thermodynamic parameters have been measured $\Delta H° = -4.3 \pm 0.08$ kcalmol^{-1} and $K_a = 4.4 \pm 0.22 \times 10^4$ M^{-1} obtained at 298 K. This leads to a calculated positive $T\Delta S° \sim 0.63$ kcal mol^{-1}K^{-1} and $\Delta G° = -6.3$ kcal mol^{-1}, Figure 77. Similar results are obtained upon titration of our cage with $NiCl_2$. Assuming a 1:1 complex, the obtained thermodynamic parameters are the following $K_a = 3.64 \pm 0.14 \times 10^4$ M^{-1}; $\Delta H° = -5.75 \pm 0.10$ kcal mol^{-1} leading to a free enthalpy of complexation $\Delta G°$ and entropy of complexation $T\Delta S°$ of - 5.6 kcal mol^{-1} and 0.15 kcal mol^{-1} K^{-1}, respectively. It is worth mentioning that these thermodynamic parameters are a resultant of different processes taking place in addition to the metal chelation, like the dehydration of the metal ion, the metal-induced deprotonation of the hydroxamic acid function, and finally their interactions with the buffer.

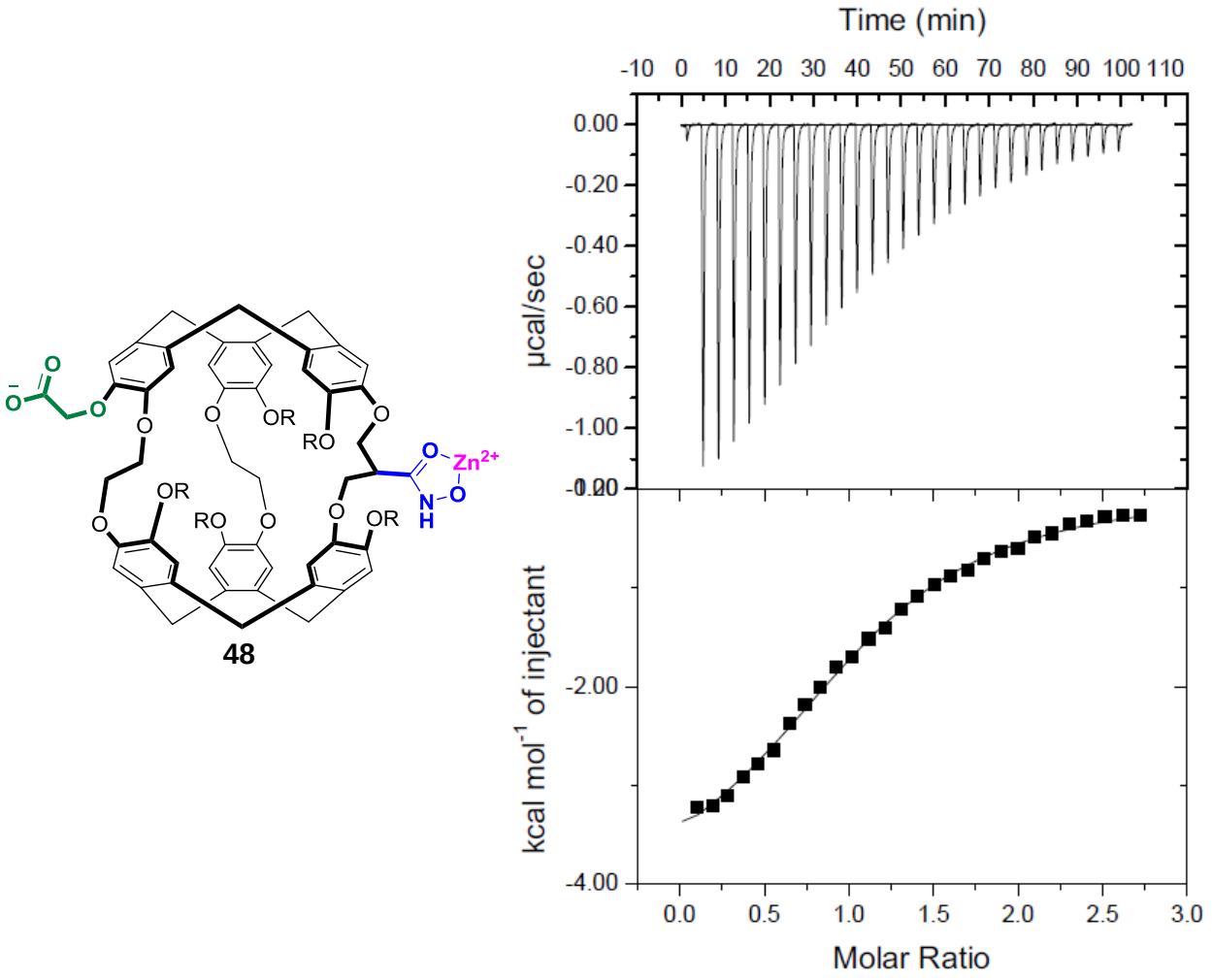

Figure 77: representative plot of the raw ITC data for the titration of **48** with Zn^{2+}. Titrations were carried out at 298 K in TRIS buffer (20 mM, pH = 7.6) with **48** (0.08 mM) in the sample cell and 1mM of Zn^{2+} in the syringe.

Additional titration experiment in TRIS (20 mM pH = 7.5) was conducted with cryptophane-[222] hexacarboxylate (0.08 mM) and $ZnCl_2$ (1 Mm) to study the effect of the six carboxylate groups on such a complexation, Figure 78. The obtained enthalpogram shows very little endothermic interaction between the zinc cation and the carboxylated cage. Thus, it can be concluded that the effect observed in Figure 77 results only from the interaction of the hydroxamic acid arm with the zinc cation.

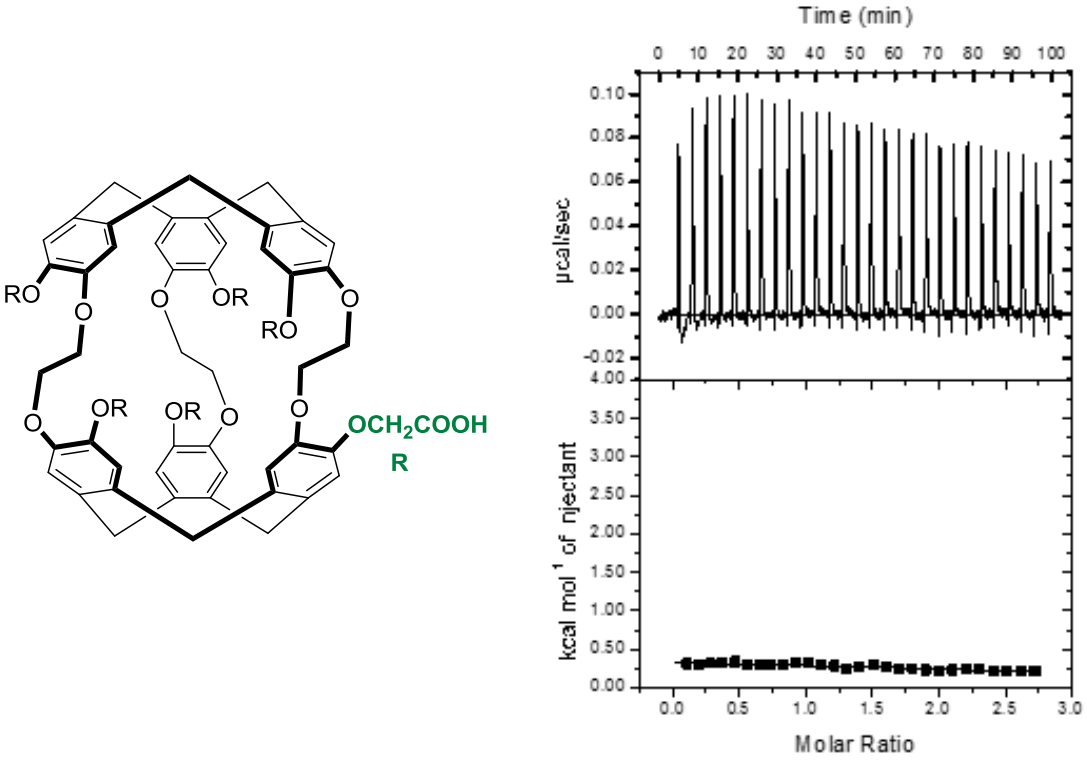

Figure 78: representative plot of the raw ITC data for the titration of **cryptophane-[222] hexa-acid** with Zn^{2+}. Titrations were carried out at 298 K in TRIS buffer (20 mM, pH = 7.6) with **cryptophane** (0.08 mM) in the sample cell and 1mM of Zn^{2+} in the syringe.

Metals-hydroxamic acid complexation has been exhaustively studied in literature and our results are in accordance with what has been reported. For example, the binding constant (K_a = 3.64 ± 0.14× 10^4 M^{-1}) of Ni^{2+} cation with cryptophane **48** is of the same order as the one obtained with benzohydroxamic acid chelator reported by Harty and co-workers.[171] In the latter example, the authors reported a two-site sequential binding of consecutive binding constants (K_1 = 1.5×10^4 M^{-1} and K_2 = 850 M^{-1}) corresponding to formation of 1:2 complex. Similarly, zinc binding by our cryptophane chelator reveals a moderate binding constant (K_a = 4.4 ± 0.22×10^4 M^{-1}) lower than that reported with acetohydroxamic acid (K_a = 2.8×10^5 M^{-1}). In another study, the Zn^{2+}-acetohydroxamic acid complexation reveals the formation of a 1:2 complex of respective binding constants K = 4.3×10^9 M^{-1} and K = 1.5×10^4 M^{-1}. These results indicate that the binding

mechanism and strength is strongly dependent on the experimental conditions and the structure of hydroxamic acids.[172,173] The fact that we obtain a 1:1 complex rather than a 1:2 one can be explained by the molecular size of the cages used. Thus, the steric hindrance prevents two cages to be in close proximity.

After confirming the chelating ability of our cage, we have investigated the complexation process by (HP) ^{129}Xe NMR spectroscopy. These studies were performed in the same experimental conditions as the one used for the titration experiments: TRIS buffer (20 mM, pH = 7.5). Here again, the successive addition of zinc cation solution from 1 to 5 equiv. did not induce significant change of the (HP) ^{129}Xe@cryptophane⊂Zn^{2+} complex. Although the zinc cation is very close to portals of the cryptophane's skeleton, only little spectral modifications are observed. This result is a bit disappointing compared to the previously reported biosensor with cryptophane-[222] derivative bearing an NTA arm, Figure 33. The localization of this sensing unit makes a great difference since as previously mentioned; it affects more significantly the ring current of the benzene ring. In turn, it induces larger magnetic modifications on the encapsulated xenon. This result approves also the little change in xenon signal at pH between 8.2 and 9.9.

The little sensitivity of xenon NMR at this position can also be exemplified by studying the cryptophane **34** bearing a THP group. Cage **34** exists as a mixture of two diastereomers but xenon NMR spectroscopy was unable to distinguish two signals corresponding to each of them. This result also contrasts with the reported examples of cryptophane derivatives bearing a mixture of diastereomers. However, it assures our hypothesis concerning the position of the sensing units.[116,117]

2. Complexation Studies of Cryptophane 57 Bearing a Biotin Derivative

After proving that our platforms cannot serve as smart xenon biosensors due to the position of the sensing unit, we wanted to test its ability as density based sensor instead. This requires the grafting of a sensing unit that has a high affinity to the targeted moiety. For this reason, we chose the classical biotin-avidin complex due to the high binding constant reported ($K_a = 10^{15}\ M^{-1}$). The hyperpolarized ^{129}Xe NMR experiments of compound **57** revealed two peaks, one corresponds to the free xenon in solution, resonating at 196 ppm and another sharp signal at 52 ppm corresponding to the encapsulated xenon in the cavity of **57**. The sharp signal obtained for Xe@**57** gives an indication about the purity of our compound because assessing this parameter by conventional spectroscopic techniques was hard. We used only HRMS to assure the formation of our compound. Upon avidin addition, broadening of the initial signal is observed with a shift by about 5 ppm (57.5 ppm). It is worth mentioning that the complex precipitates partially under the used experimental conditions, so an optimization of these conditions is required. Nevertheless, this chemical shift change and broadening have already been observed with the first example of xenon cryptophane biosensor reported by Pines and co-workers. Interestingly, unlike Pines example which shows four signals corresponding to the two cryptophanes diastereomers, only one sharp signal is obtained in our case, thus facilitating the analysis, Figure 79.

These promising results assure that our platforms can still be used as MRI tracers, if conjugated with biological probes that have a very high affinity to the targeted units.

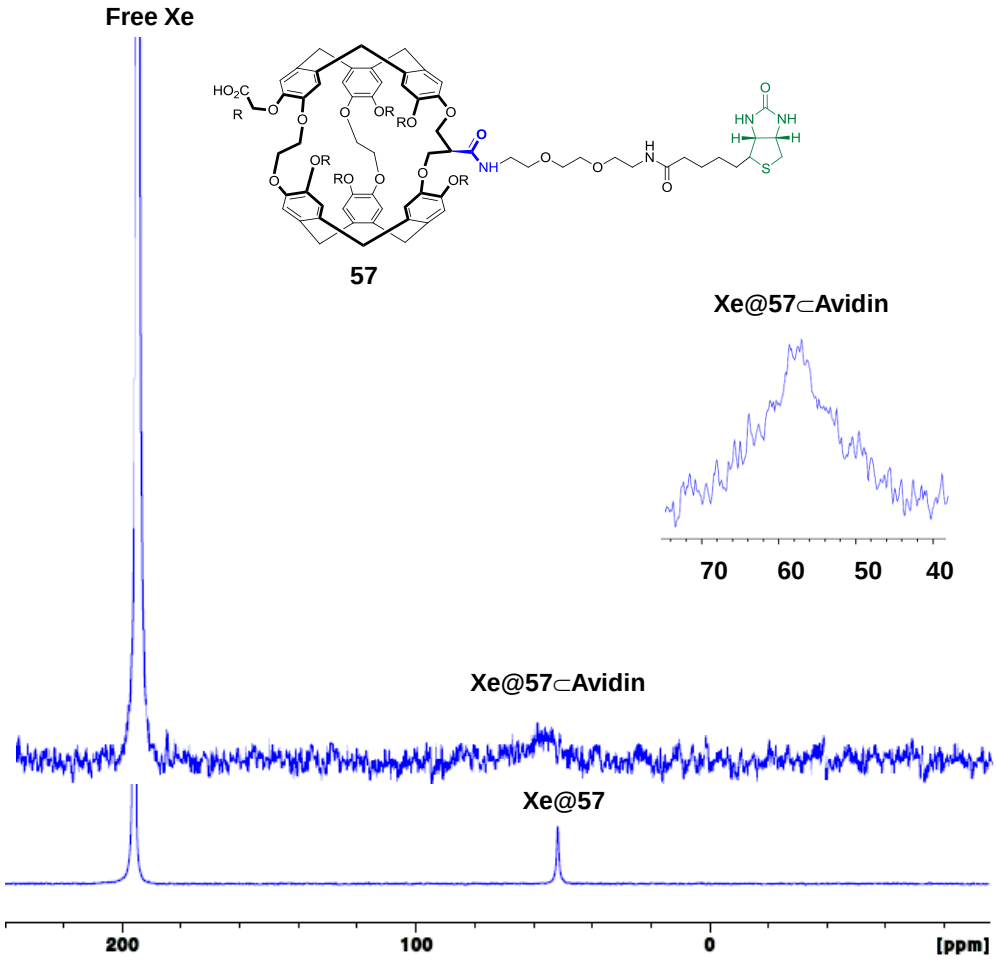

Figure 79: one-scan ^{129}Xe NMR spectra recorded at 298 K of compound **57** (0.9 mM) in PBS buffer with 10% D_2O at pH = 6.4, and upon of one equiv. of avidin (0.2 mM) at pH = 7.4.

Conclusion of Part I

Conclusion of Part I

In this part of the manuscript, we have successfully described the leading strategy towards new cryptophane-[223] derivatives functionalized by a primary alcohol. This function exhibits a greater reactivity towards electrophilic activation and nucleophilic substitution compared to the secondary alcohol in the first generation of cryptophane-[223] derivatives. Thanks to the various chemical transformations, we were able to elaborate two real platforms (cryptophanes **43** and **44**) bearing six ester groups and a unique carboxylic acid arm. The presence of a carboxylic acid moiety at the propylenedioxy bridge allows the selective grafting of a spacer and a sensing arm. To prove the versatility of our cages, we grafted different sensing units like hydroxamic acid for metal chelation, APTRA derivative for calcium detection and finally a biotin arm for avidin binding. This was followed by a hydrolysis or hydrogenolysis step to produce the water soluble sensors. With these platforms, we were able to solve the two main problems encountered with cryptophanes namely the symmetry and water solubility. To study the responsiveness of our platforms, we investigated cryptophane **48** bearing a hydroxamic acid unit for metal chelation. The ability of this cage to bind metals has been confirmed by ITC experiments. The (HP) ^{129}Xe NMR spectroscopy of this cage showed a little sensitivity upon metal chelation. These discouraging results can be explained mainly by the position of the sensing arm. Being at the center of the propylenedioxy arm, the sensing unit has less probability to change the benzene ring currents. This in turn induces fewer changes in the magnetic field around the encapsulated cage. The fact that compound **48** is poorly responsive by ^{129}Xe NMR, does not prevent its employment as an MRI tracer but this novel strategy does not seem appropriate to design "smart" biosensors as previously defined. However, this study allowed us to assure the importance of the sensing arm position to get "smart" biosensors and we were able to find discrete solutions for this synthetic challenge.

Experimental Part

EXPERIMENTAL DETAILS:

Organic Synthesis:

Mass spectra (HRMS) were performed by the Centre de Spectrométrie de Masse, University of Lyon. Analyses were performed with a hybrid quadrupole-time of flight mass spectrometer, microToF QII equipped with an Electrospray ion source. Data Analysis® 4.0 was used for instrument control, data collection, and data treatment. HRMS analyses were performed in full scan MS with a mass range from 50 to 2000 Da at an acquisition rate of 1 Hz. Transfer parameters were: RF Funnel 1, 200 V; RF Funnel 2, 200 V; hexapole, 50 V; transfer time, 70 µs and PrePulse storage time, 1 µs before each acquisition batch, external calibration of the instrument was performed with a sodium formate clusters solution. ^{1}H and ^{13}C NMR spectra were recorded at 400 and 100.6 MHz, respectively. Chemical shifts are referenced to Me_4Si (^{1}H, ^{13}C). Column chromatographic separations were carried out over Merck silica gel 60 (0.040-0.063 mm). Analytical thin layer chromatography (TLC) was performed on MERCK silica gel TLC plates F-254. The solvents were distilled prior to use: DMF and CH_2Cl_2 from CaH_2, THF from Na/benzophenone and pyridine from KOH.

ITC Experiments:

Isothermal titration calorimetry (ITC) experiments were performed at 298 K. In a standard experiment, the host solution (0.08 mM) in TRIS (20 mM, pH = 7.5) was placed into the calorimeter cell (1,4 mL) and 28 successive aliquots (10 µL) of guest solution (10 times more concentrated, 1mM) were added via a computer-automated injector at 3 min intervals. Heat changes were recorded after each addition. Heats of dilution were measured by a blank experiment (in absence of host) under the same conditions and they were subtracted from the

titration data prior to curve fitting. The first injection was discarded from each data set to remove the effect of guest diffusion across the syringe tip during the equilibration process. Titrations curves were fitted with the one binding site model using origin software.

Production of hyperpolarized xenon:

Hyperpolarized xenon was produced in the batch mode via SEOP (Spin Exchange Optical Pumping) using a home-built setup. Rubidium is used as the alkali metal, and five minutes suffice to produce five milliliters of xenon at a polarization ranging from 15 to 20%. Frozen hyperpolarized xenon immersed in a bath of liquid nitrogen and subjected to a magnetic field of 0.3 T provided by a solenoid is transported near the NMR magnet. There it is sublimated in the fringe field of the magnet and transferred thanks to a vacuum line to the NMR tube. A hollow spinner enabled us to condense it in the upper part of the NMR tube (screw capped Wilmad PP-528) without cooling the solution. The hyperpolarized ^{129}Xe NMR experiments were performed at 11.7 T (^{129}Xe resonance frequency 138.35 MHz) using a 5mm-broadband inverse probe head.

Crystallography:

A suitable crystal of Cryptophane **27** was selected and mounted on a Gemini kappa-geometry diffractometer (Agilent Technologies UK Ltd) equipped with an Atlas CCD detector and using Cu radiation (λ= 1.5418 Å). Intensities were collected at 150 K by means of the CrysAlisPro software. Reflection indexing, unit-cell parameters refinement, Lorentz-polarization correction, peak integration and background determination were carried out with the CrysAlisPro software. An analytical absorption correction was applied using the modeled faces of the crystals. The resulting set of hkl was used for structure solution and refinement. The structures were solved by direct methods with SIR97 and the least-square refinement on F2 was achieved with the

CRYSTALS software. All non-hydrogen atoms were refined anisotropically. The hydrogen atoms were all located in a difference map, but those attached to carbon atoms were repositioned geometrically. The H atoms were initially refined with soft restraints on the bond lengths and angles to regularize their geometry (C---H in the range 0.93--0.98 Å, O--H = 0.82 Å) and Uiso(H) (in the range 1.2-1.5 times Ueq of the parent atom), after which the positions were refined with riding constraints. Residual electronic density inside and in between the cryptophane cages was located but could not be modelled. The contribution of the disordered solvent molecules was removed using the SQUEEZE algorithm. The volume of the cryptophane cage was calculated to be 108 $Å^3$ using the VOID algorithm within the PLATON software. CCDC 1900550 contains the supplementary crystallographic data for cryptophane **27**. These data can be obtained free of charge from the Cambridge Crystallographic data Centre via www.ccdc.cam.ac.uk/data request/cif.

Synthesized compounds:

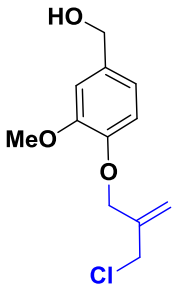

22

Compound 22: 3-chloro-2-chloromethyl-1-propene or **19** (4.49 ml, 64.8 mmol, 2 equiv.) was added under argon to a mixture of K_2CO_3 (4.48 g, 32.4 mmol, 1 equiv.) and vanillic alcohol **1** (5 g, 32.4 mmol, 1 equiv.) in acetone (60 mL). The reaction mixture was heated for 16 hours at 80 °C under an argon atmosphere. Then, the solvent was evaporated under reduced pressure. The solid residue was then dissolved in ethyl acetate (200 mL). The organic layer was washed three times with 0.1 M NaOH solution and finally washed with water. The organic layer was dried over Na_2SO_4 and the solvent was evaporated under reduced pressure. The crude was then subjected to column chromatography on silica gel (CH_2Cl_2/AcOEt: 80/20). After evaporating the solvents, compound **22** was collected as a white solid (5.1g, 65%). Mp: 60 °C.

^{1}H NMR (400 MHz, $CDCl_3$, 25 °C): δ (ppm) 6.91-6.83 (m, 3H), 5.34 (m, 2H), 4.65 (s, 2H), 4.58 (d, J = 5.8 Hz, 2H), 4.18 (s, 2H), 3.84 (s, 3H), 1.65 (t, J = 5.8 Hz, 1H).

^{13}C {^{1}H} NMR (100.6 MHz, $CDCl_3$, 25 °C): δ (ppm) 149.8, 147.4, 140.7, 134.5, 119.3, 117.5, 114.2, 111.06, 69.4, 65.2, 55.9, 45.08

HRMS (ESI): m/z $[M+Na]^+$ calcd. for $C_{12}H_{15}NaClO_3$ 265.0607 found 265.0602.

Experimental Part

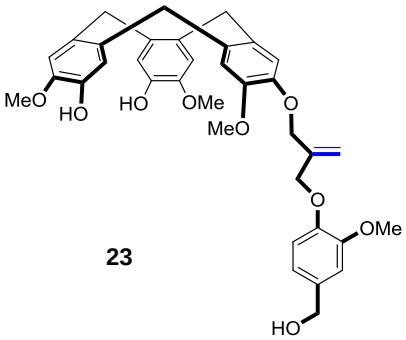

23

Compound 23: Derivative **22** (2.0 g, 8.2 mmol, 1 equiv.) was added under an argon atmosphere to a stirred mixture of Cs_2CO_3 (5.4 g, 16.4 mmol, 2 equiv.) and cyclotriguiacylene **4** (3.5 g, 8.6 mmol, 1 equiv.) in DMF (120 mL). The mixture was heated up to 80°C for 16 hours under an argon atmosphere. Then, the dark-brown mixture was poured in water (200 mL) and extracted 5 times with ethyl acetate (800 mL). The combined organic layer was then washed 5 times with water (500 mL) and dried over Na_2SO_4. Evaporation of the solvent under reduced pressure left an oily residue, which was purified on silica gel (AcOEt/petroleum ether: 90/10). Evaporation of the fractions gave rise to compound **23** (2 g, 40%) as a glassy product.

^{1}H NMR (400 MHz, $CDCl_3$, 25 °C): δ (ppm) 6.92 (s, 1H), 6.87 (s, 1H), 6.84 (s, 1H), 6.79 (s, 1H), 6.77 (s, 1H), 6.73 (s, 1H), 6.69 (s, 1H), 6.67 (s, 1H), 6.58 (m, 1H), 5.40 (s, 1H), 5.37 (s, 1H), 5.29 (m, 2H), 4.71 (s, 3H), 4.67-4.62 (m, 4H), 4.52 (m, 2H), 3.84 (s, 3H), 3.79 (s, 3H), 3.71 (s, 3H), 3.65 (s, 3H), 3.52-3.46 (m, 3H), 1.54 (m, 1H).

^{13}C {^{1}H} NMR (100.6 MHz, $CDCl_3$, 25 °C): δ (ppm) (100.6 MHz, $CDCl_3$) 149.3, 147.8, 147.1, 146.1, 144.9, 144.8, 143.7, 143.6, 140.2, 133.8, 132.1 (2C), 131.9, 131.5, 130.9, 118.96, 115.6, 115.2, 115.0, 114.8, 113.3, 113.2, 112.0, 111.8, 110.5, 69.6, 69.4, 64.9, 55.75, 55.7, 55.5, 55.3, 36-35.9 (3C).

HRMS (ESI): *m/z* $[M+Na]^+$ calcd. for $C_{36}H_{38}NaO_9$ 637.2413 found 637.2408.

Experimental Part

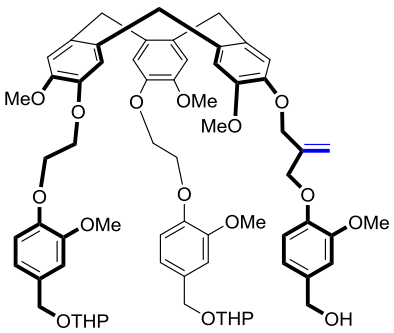

25

Compound 25: 2-((4-(2-bromoethoxy)-3-methoxybenzyl)-oxy)tetrahydro-2H-pyran **24** (4.106 g, 11 mmol, 2 equiv.) was added under an argon atmosphere to a stirring mixture of Cs_2CO_3 (7.69 g, 23 mmol, 2 equiv.) and CTB **23** (3.65 g, 5.94 mmol, 1 equiv.) in DMF (140 mL). The reaction mixture was heated to 80°C for 16 hours under an argon atmosphere. Then, the yellowish mixture was poured in water (200 mL) and ethyl acetate (200 mL). The aqueous layer was extracted 5 times with ethyl acetate (500 mL). The combined organic layer was then washed 5 times with water (500 mL) and dried over Na_2SO_4. The solvent was removed under reduced pressure to leave a glassy solid, which was purified on silica gel (AcOEt/petroleum ether: 90/10) to give rise to compound **25** (5.63 g, 84%) as a white glassy solid.

^{1}H NMR (400 MHz, $CDCl_3$, 25 °C): δ (ppm) 7.01-6.65 (15s, 15H), 5.30 (s, 1H), 5.29 (s, 1H), 4.73-4.63 (m, 10H), 4.53 (m, 2H), 4.43-4.32 (m, 8H), 3.90 (m, 2H), 3.86 (2s, 6H), 3.74-3.71 (3s, 9H), 3.61 (s, 3H), 3.48-3.53 (m, 5H), 1.85-1.59 (m, 12H).

^{13}C {^{1}H} NMR (100.6 MHz, $CDCl_3$, 25 °C): δ (ppm) 149.8, 149.7 (2C), 148.6, 148.5, 148.3, 147.6 (2C), 147.5, 146.9 (2C), 146.8, 147.5, 140.6, 134.5, 133.1 (2C), 132.5, 131.9 (2C), 131.8 (3C), 120.5 (3C), 119.2, 117.0, 116.9, 116.1, 115.1, 113.8-114.3 (8C), 112.1 (2C), 111.0, 97.7 (3C), 70.1, 69.9, 68.6 (2C), 68.4, 67.93, 65.1, 62.2 (2C), 55.7-56.2 (6C), 36.3 (2C), 30.5 (2C), 25.4 (2C), 19.4 (2C).

HRMS (ESI): *m/z* $[M+Na]^+$ calcd. for $C_{66}H_{78}NaO_{17}$ 1165.5136 found 1165.5131.

Experimental Part

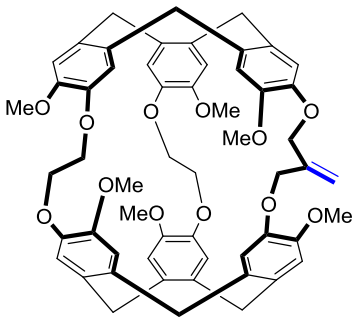

26

Cryptophane 26: CTB **25** (0.70 g, 0.62 mmol) was dissolved in a mixture of chloroform (300 ml) and formic acid (300 ml). The solution was then stirred for 6 hours at 55 - 60 °C. The solvent was then evaporated under reduced pressure to leave a yellow residue. It was then purified by column chromatography on silica gel (CH_2Cl_2/Acetone: gradient 97/3 up to 95/5). The white solid was then crystallized in a mixture of CH_2Cl_2 and ethanol. The crystals were collected on a fritted glass and washed with diethyl ether. Compound **26** (0.19 g, 34%) was obtained as a white solid.

^{1}H NMR (400 MHz, $CDCl_3$, 25 °C): δ (ppm) 6.77 (s, 2H), 6.72 (s, 2H), 6.65 (s, 2H), 6.655 (s, 2H), 6.64 (s, 2H), 6.62 (s, 2H), 5.58 (s, 2H), 4.63-4.56 (m, 6H), 4.46 (d, *J*=10.7 Hz, 2H), 4.35 (d, *J*=10.7 Hz, 2H), 4.29-4.09 (m, 8H), 3.80 (s, 6 H), 3.79 (s, 6H), 3.75 (s, 6H), 3.43-3.36 (m, 6H).

^{13}C {^{1}H} NMR (100.6 MHz, $CDCl_3$, 25 °C): δ (ppm) 149.5 (2C), 149.4 (2C), 147.7 (2C), 147.3(2C), 146.6 (2C), 146.4 (2C), 140.0 (1C), 133.8 (4C), 132.2 (2C), 131.9 (2C), 131.3 (2C), 130.6 (2C), 120.7, 120.4 (2C), 120.3 (2C), 113.9 (2C), 113.3 (2C), 113.2 (2C), 112.2 (2C), 69.6 (2C), 68.9 (2C), 68.8 (2C), 56.1 (2C), 55.5 (2C), 55.4 (2C), 36.4 (2C), 36.08 (2C), 36.04 (2C).

HRMS (ESI): *m/z* $[M+Na]^+$ calcd. for $C_{56}H_{56}NaO_{12}$ 943.3669 found 943.3664.

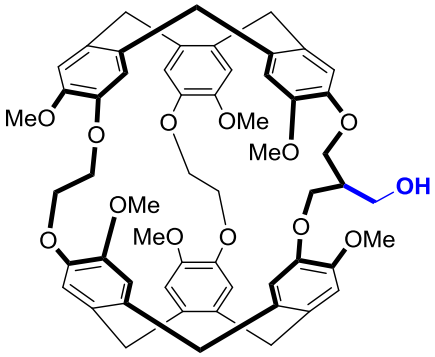

27

Cryptophane 27: Derivative **26** (0.28 g, 0.304 mmol) was dissolved in a mixture of THF (20 mL) and CH_2Cl_2 (5 mL) under an argon atmosphere. Then, 9-BBN (1.81 mL, 0.5M, 0.9 mmol, 3 equiv.) was added dropwise at 0 °C. The solution was stirred at 50 °C for 5 hours. The mixture was then quenched at 0 °C by a dropwise addition of a NaOH solution (0.56 mL, 3M) and then by addition of H_2O_2 (1.7 mL, 15%). The reaction was stirred overnight at room temperature for 16 hours. Then, the reaction was quenched by a dropwise addition of 20 ml of $Na_2S_2O_3$ solution at 0 °C. The reaction mixture was poured in CH_2Cl_2 (50 ml) and the aqueous layer was washed 5 times with CH_2Cl_2 (each time 50 ml). The combined organic layers were dried over Na_2SO_4 and the solvent was evaporated under reduced pressure. The residue was subjected to column chromatography using silica gel (CH_2Cl_2/acetone: gradient 90/10 up to 80/20). Compound **27** (0.27 g, 94%) was then isolated as a white solid and washed on a frit with diethyl ether.

^{1}H NMR (400 MHz, $CDCl_3$, 25 °C): δ 6.79-6.61 (m, 10 H), 6.51 (s, 2H), 4.62-4.53 (m, 6H), 4.25-3.93 (m, 14 H), 3.87-3.77 (4s, 12 H), 3.74 (s, 3H), 3.71 (s, 3H), 3.43-3.34 (m, 6H), 2.40 (m, 1H).

^{13}C {^{1}H} NMR (100.6 MHz, $CDCl_3$, 25 °C): δ (ppm) 149.6, 149.5 (2C), 149.4, 147.5, 147.4, 147.3, 146.7, 146.6 (2C), 146.63, 146.3, 134 (2C), 133.8 (2C), 132.5, 132.3, 132.1, 131.5, 131.3, 131.1, 130.8, 130.6, 120.5, 120.4, 120.2, 120.0, 114.3, 114.2, 113.6, 113.2, 112.7, 112.3, 112.1, 111.8, 69.8, 69.5, 68.9, 68.7, 68.5, 67.0, 64.3, 56.3 (2C), 55.5 (2C), 55.4, 55.3, 40.2, 36.4 (2C), 36.1 (3C), 36.

HRMS (ESI): *m/z* $[M+Na]^+$ calcd. for $C_{56}H_{58}NaO_{13}$ 961.3775 found 961.3770.

Experimental Part

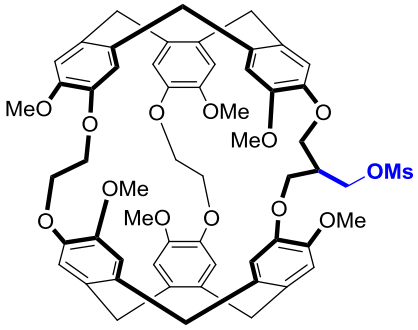

28

Cryptophane 28: Excess of methanesulfonyl chloride (1.3 mL, 16.8 mmol) was added at 0 °C to a mixture of cryptophane **27** (0.5 g, 0.53 mmol), CH_2Cl_2 (25 mL) and pyridine (2.3 mL, 28.5 mmol). The mixture was stirred for 16 hours at 70 °C before the addition of methanol (25 mL) at room temperature. The solvents were evaporated and the resulting solid dissolved in CH_2Cl_2 (100 mL). The organic layer was washed twice with water (50 mL) and brine (50 mL), dried over Na_2SO_4 and evaporated. Silica gel chromatography (CH_2Cl_2/acetone: gradient 95/5 up to 90/10) afforded pure cryptophane **28** (0.42 g, 82%) as a white solid.

^{1}H NMR (400 MHz, $CDCl_3$, 25 °C): δ (ppm) 6.83-6.62 (m, 10H), 6.56 (s, 2H), 4.76-4.70 (m, 6H), 4.56-4.48 (m, 2H), 4.34-4.21 (m, 2H), 3.92-3.22 (m, 10H), 3.88 –3.74 (6s, 18H), 3.49-3.33 (m, 6H), 3.07 (s, 3H), 2.84-2.68 (m, 1H).

^{13}C {^{1}H} NMR (100.6 MHz, $CDCl_3$, 25 °C): δ (ppm) 149.6 (2C), 149.5, 148.0, 147.8, 146.9, 146.8 (2C), 146.7 (2C), 146.5 (2C), 134.1, 134.0, 133.9 (2C), 132.4 (3C), 132.2, 131.6 (2C), 130.9, 130.8, 120.5, 120.4 (2C), 120.3, 114.2 (2C), 113.8, 113.6, 113.3, 112.8, 112.6, 69.7, 69.1, 69.0, 67.8, 64.9, 64.0, 56.4, 55.8 (2C), 55.7 (2C), 55.6 (2C), 53.6, 39.7, 37.1 (2C), 36.5 (2C), 36.3, 36.2, 31.1.

HRMS (ESI): *m/z* $[M+Na]^+$ calcd. for $C_{57}H_{60}NaO_{15}S$ 1039.3550 found 1039.3545

Experimental Part

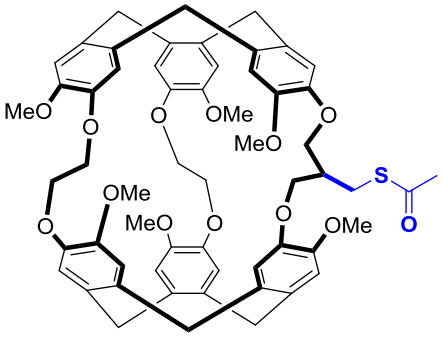

29

Cryptophane 29: A mixture of cryptophane **28** (0.15 g, 0.150 mmol, 1 equiv.), potassium thioacetate (0.1 g, 0.85 mmol, 5 equiv.), DMF (2 mL) and CH_2Cl_2 (0.5 mL) was stirred for 3 days at 100 °C before the addition of CH_2Cl_2 (20 mL) and water (20 mL) at room temperature. The aqueous layer was extracted by CH_2Cl_2 (3 × 20 mL). The combined organic layers were washed by water (4 × 20 mL), NaCl (20 mL), dried over Na_2SO_4 and evaporated. Silica gel chromatography (CH_2Cl_2/acetone: 94/6) and washing over a fritted glass with diethyl ether afforded pure cryptophane **29** (0.065 g, 43%) as a white solid.

^{1}H NMR (400 MHz, $CDCl_3$, 25 °C): δ (ppm) 6.85–6.62 (m, 10H), 6.54 (s, 2H), 4.75 – 4.50 (m, 6H), 4.37- 4.20 (m, 3H), 4.19- 3.91 (m, 8H), 3.88–3.73 (6s, 18H), 3.51–3.33 (m, 6H), 3.31–3.10 (m, 1H), 3.21–3.10 (m, 1H), 2.59 –2.44 (m, 1H), 2.37 (s, 3H).

^{13}C {^{1}H} NMR (100.6 MHz, $CDCl_3$, 25 °C): δ (ppm) 195.7, 149.6 (2C), 149.5 (2C), 147.6, 147.1, 146.9, 146.8, 146.7 (2C), 134.2, 134.1, 134.0, 133.9, 132.6, 132.5, 148.0, 131.7 (2C), 131.6 (2C), 130.7 (2C), 120.5 (2C), 120.7, 120.4, 114.4 (2C), 113.8, 113.7, 112.6, 112.5, 112.4, 69.8 (2C), 69.5, 69.1, 69.0, 66.4, 65.4, δ 64.8, 56.4 (2C), 56.0, 55.8, 55.7, 55.6, 40.3, 36.6 (2C), 36.2 (2C), 36.1 (2C), 30.7, 27.9.

HRMS (ESI): *m/z* $[M+Na]^+$ calcd. for $C_{58}H_{60}NaO_{13}S$ 1019.3652 found 1019.3647

Experimental Part

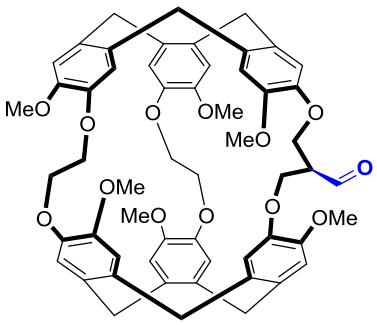

30

Compound 30: Compound **27** (0.26 g, 0.20 mmol, 1 equiv.) was introduced and dissolved in freshly distilled CH_2Cl_2 (26 ml). Excess of Dess martin periodonane (15% wt solution in CH_2Cl_2 2.6 ml) was then added. The reaction mixture was stirred under argon for 16 hours at room temperature. The next day crude was filtered on a fritted glass and the filtrate was collected and evaporated under reduced pressure. The resulting crude was crystalized from chloroform diethyl ether to give beige precipitate that were collected on a fritted glass and washed with ether. **The produced product was used directly in the next step without further purification on silica because of its sensitivity.**

HRMS (ESI, $[M+Na]^+$) calcd. for $C_{56}H_{56}O_{13}$ 959.37 found 959.35.

Experimental Part

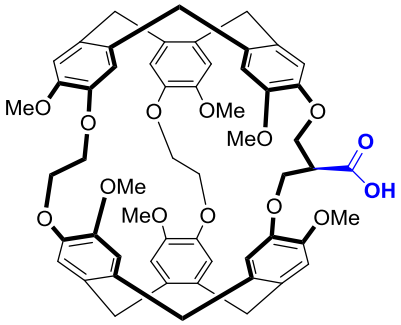

31

Compound 31: cryptophane **32** (0.1 g, 0.1 mmol, 1 equiv.) was introduced and dissolved in acetonitrile (3 ml) and water (0.3ml). Then sodium chlorite (0.019 g in 0.2 ml H_2O, 0.212, 2 equiv.) was added along with sodium phosphate monobasic (0.0031g in 0.01 ml H_2O, 0.0212, 0.2 equiv.) and then hydrogen peroxide (0.102 ml). The mixture was kept for 16 hours and then quenched with sodium thiosulfate (0.2 ml) at 0 °C. The solvent was then evaporated under reduced pressure and the resulting crude was crystalized from $CHCl_3$ and diethyl ether to give white precipitate. These precipitate were filtered on a fritted glass and washed with ether to give the compound **31** (0.07 g) as pure white product in 70% yield.

Compound 31: compound **32** (0.07 g, 0.067 mmol) was dissolved in a mixture of CH_2Cl_2/MeOH (4ml/2ml) along with catalytic amounts Pd/C (10% by weight). The mixture was kept under hydrogen for 16 hours at room temperature. The obtained crude was then filtered on celite followed by the evaporation of solvent, to afford compound **31** as a white solid (0.059 g, 95%).

^{1}H NMR (400 MHz, $CDCl_3$, 25 °C): δ (ppm) 6.77-6.57 (12s, 12 H), 4.63- 4.55 (m, 6 H), 4.38- 4 (m, 12 H), 3.8-3.75 (6s, 18 H), 3.43-3.36 (m, 6 H), 3.3 (m, 1H).

^{13}C {^{1}H} NMR (100.6 MHz, $CDCl_3$, 25 °C): δ (ppm) 172.7, 149.59, 149.54, 149.47, 149.41, 147.9, 147.7, 146.76, 146.73, 146.67, 146.64, 146.5, 146.3, 134.0, 133.8, 133.7 (2C), 132.6, 132.4, 132.2, 132.1, 131.5, 131.4, 131.1, 131.0, 120.2 (3C), 120.1, 114.1 (3C, 113.6 (2C), 113.5 (2C) 112.6, 69.6, 69.5, 68.8 (2C), 65.2, 64.8, 56.3 (2C), 55.8, 55.6, 55.5 (2C), 45.3, 36.4 (2C), 36.15 (4C).

HRMS (ESI, $[M+Na]^+$) calcd. for $C_{56}H_{56}NaO_{14}$ 975.3567 found 975.3562.

Experimental Part

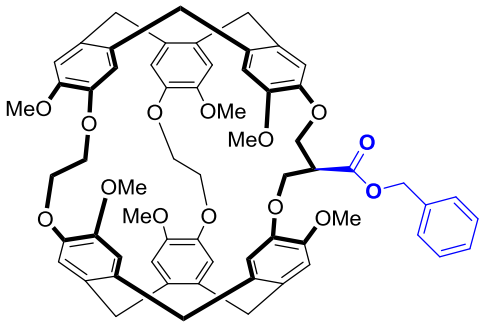

32

Compound 32: Potassium carbonate (0.07g, 0.506 mmol, 2.5 equiv.) was added along with compound **31** (0.19g, 0.2 mmol, 1 equiv.) and dissolved in DMF (2.5 ml) for 10 minutes. After that benzyl bromide (0.046 ml, 0.38 mmol, 2 equiv.) was added and the mixture was heated for 16 hours at 50 °C. After 16 hours the crude was washed five times with ethyl acetate and the produced organic layer was washed 5 times with water. The resulting organic layer was dried over Na_2SO_4 and then filtered. The solvent was evaporated under reduced pressure then the crude was subjected to column chromatography using SiO_2 (CH_2Cl_2/ acetone: 90/10) to give it as pure white product (0.1 g, 50%).

^{1}H NMR (400 MHz, $CDCl_3$, 25 °C): δ (ppm) 7.36- 7.29 (m, 5 H), 6.67-6.53 (12 s, 12H), 5.32-5.27 (d, J=12.5 Hz, 1H), 5.2-5.16 (d, J=12.5 Hz, 1H), 4.62-4.55 (m, 6H), 4.4-3.9 (m, 12 H), 3.79-3.69 (6s, 18 H), 3.43 -3.35 (m, 6H), 3.31 (m, 1H).

^{13}C {^{1}H} NMR (100.6 MHz, $CDCl_3$, 25 °C): δ (ppm) 170.6, 149.5, 149.49 (2C), 149.4, 148.0, 147.6, 147.0, 146.8, 146.7 (2C), 146.6 (2C), 135.9, 134.0, 133.9 (2C), 133.4, 132.37, 132.3, 132.0, 131.8, 131.4, 131.3, 130.87, 130.8, 128.5 (2C), 128.1, 127.8 (2C), 120.4 (3C), 120.2, 114.1, 114.0, 113.94, 113.61, 113.16 (2C), 113.09, 112.49, 69.67, 69.61, 68.95 (2C), 66.61, 64.79, 64.25, 56.28 (2C), 56.07, 55.56 (2C), 55.5, 46.02, 36.42 (2C), 36.12 (2C), 36.03 (2C).

HRMS (ESI): *m/z* $[M+Na]^+$ calcd. for $C_{63}H_{62}NaO_{14}$ 1065.4037 found 1065.4032.

Experimental Part

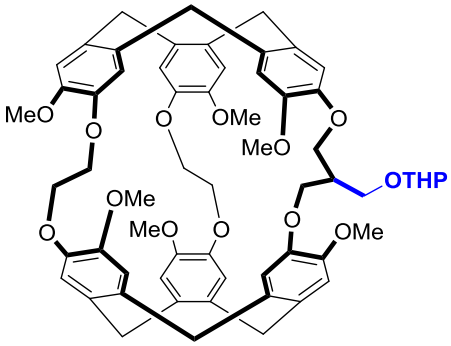

34

Cryptophane 34: A solution of PPTS (0.12 g, 0.47 mmol) in CH_2Cl_2 (1 mL) was added to a solution of **27** (0.3 g, 0.31 mmol) and 3,4-dihydropyran (0.1 mL, 1.09 mmol) in THF (8 mL). The solution was heated up to 60 °C for 48 hours. Then, the solvent was evaporated under reduced pressure. The oily residue was subjected to column chromatography on silica gel (CH_2Cl_2/acetone: 90/10) to give rise to compound **34** as a mixture of two diastereomers in the form of white solid (0.23 g, 75%) was collected on a fritted glass and washed with diethyl ether.

^{1}H NMR (400 MHz, $CDCl_3$, 25 °C): δ (ppm) 6.76-6.55 (12s, 12H), 4.69 (m, 1H), 4.60-4.55 (m, 6H), 4.20-3.97 (13H), 3.88 (m, 2H), 3.78 (3s, 9H), 3.76-3.74 (3s, 9H), 3.59 (m, 1H), 3.38-3.35 (m, 6H), 2.60 (m, 1H), 1.82-1.50 (m, 6H).

^{13}C {^{1}H} NMR (100.6 MHz, $CDCl_3$, 25 °C): δ (ppm) 149.4 (3C), 147.9, 147.6, 147.4, 147.3, 147.2, 146.8, 146.7, 146.5 (2C), 134.0, 133.95, 133.9, 133.8, 132.4 (2C), 131.4 (4C), 130.6 (2C), 120.5 (4C), 114 (2C), 113.7, 113.5, 113.0, 112.8, 112.4 (2C), 112.3, 98.4, 69.7, 69.0, 65.5, 65.4, 64.7, 62.6, 61.8, 56.2, 55.8, 55.6 (2C), 55.5, 55.4, 40.5, 36.4 (2C), 36.0 (4C), 30.7, 25.5, 19.71, 19.2.

HRMS (ESI): *m/z* $[M+Na]^+$calcd. for $C_{61}H_{66}NaO_{14}$ 1045.4350 found 1045.4344.

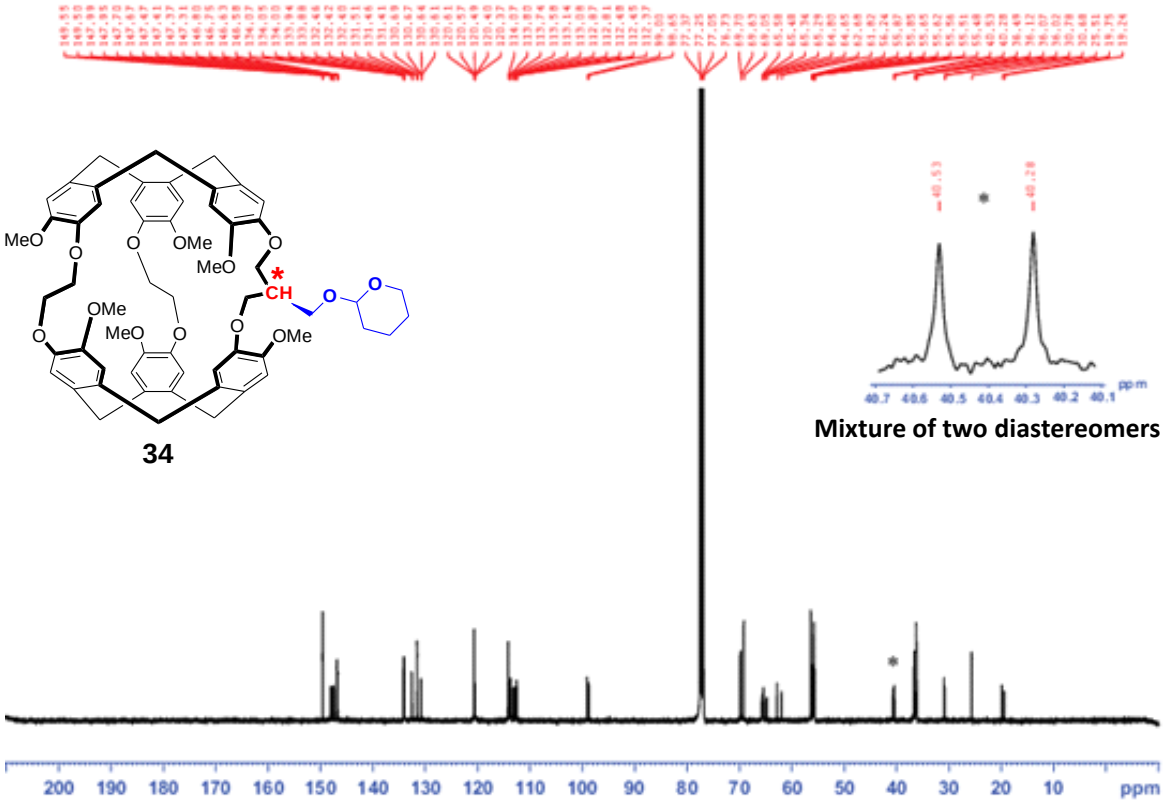

Figure 80: ^{13}C NMR of cryptophane **34** composed of a mixture of diastereomers in $CDCl_3$.

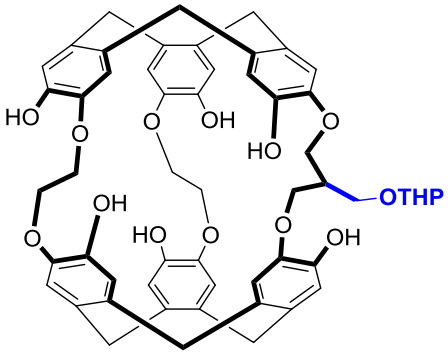

35

Cryptophane 35: (4 mL, 4.1 mmol, 20 equiv.) of lithium diphenylphosphide (1 M) was added to a solution of **34** (0.21 g, 0.21 mmol) in THF (3 mL) under an argon atmosphere. The red solution was heated up to 60 °C for 48 hours. Then, the mixture was poured in 20 mL of water and then extracted 5 times with CH_2Cl_2. The aqueous solution was acidified at 0 °C with an ammonium chloride solution (10 mL, pH ~ 5). The resulting precipitate was collected on a fritted glass and washed with water. The dried solid was then washed several times with diethyl ether to give a beige solid. The solid was then purified on column chromatography (silica gel, acetone/DMF: 96/4) to give clean compound **35** as a mixture of two diastereomer (0.16 g, 84%).

^{1}H NMR (400 MHz, DMSO *d*$_6$, 25 °C): δ (ppm) 8.42-8.22 (6s, 3 H), 7.95-7.74 (6s, 3H), 6.65-6.48 (m, 12H), 4.66 (m, 1H), 4.47-4.39 (m, 6H), 4.13-3.87 (m, 13H), 3.72 (m, 1H), 3.34 (m, 2H), 3.22-3.17 (m, 6H), 2.33 (m, 1H), 1.67-1.49 (m, 6H).

^{13}C {^{1}H} NMR (100.6 MHz, $CDCl_3$, 25 °C): δ (ppm) 146.8, 146.7, 146.3, 146.2, 146, 145.9, 145.6, 145.4, 145.06, 145.0, 144.8, 144.7, 134.3, 134.1, 134.0, 133.9, 132.9, 132.8, 131.4, 131.2, 130.9, 130.8, 129.7, 129.6, 120.5, 120.3, 119.3 (2C), 118.7, 118.5, 118.02 (2C), 117.4, 116.9, 115.6, 115.5, 98.9, 69, 68.7 (2C), 67.6, 66.5, 65.9, 62.2, 35.6 (2C), 35.2 (4C), 30.8, 25.5, 19.8, 19.7.

HRMS (ESI): *m/z* $[M+Na]^+$ calcd. for $C_{55}H_{54}O_{14}Na$ for 961.3411 found 961.3405.

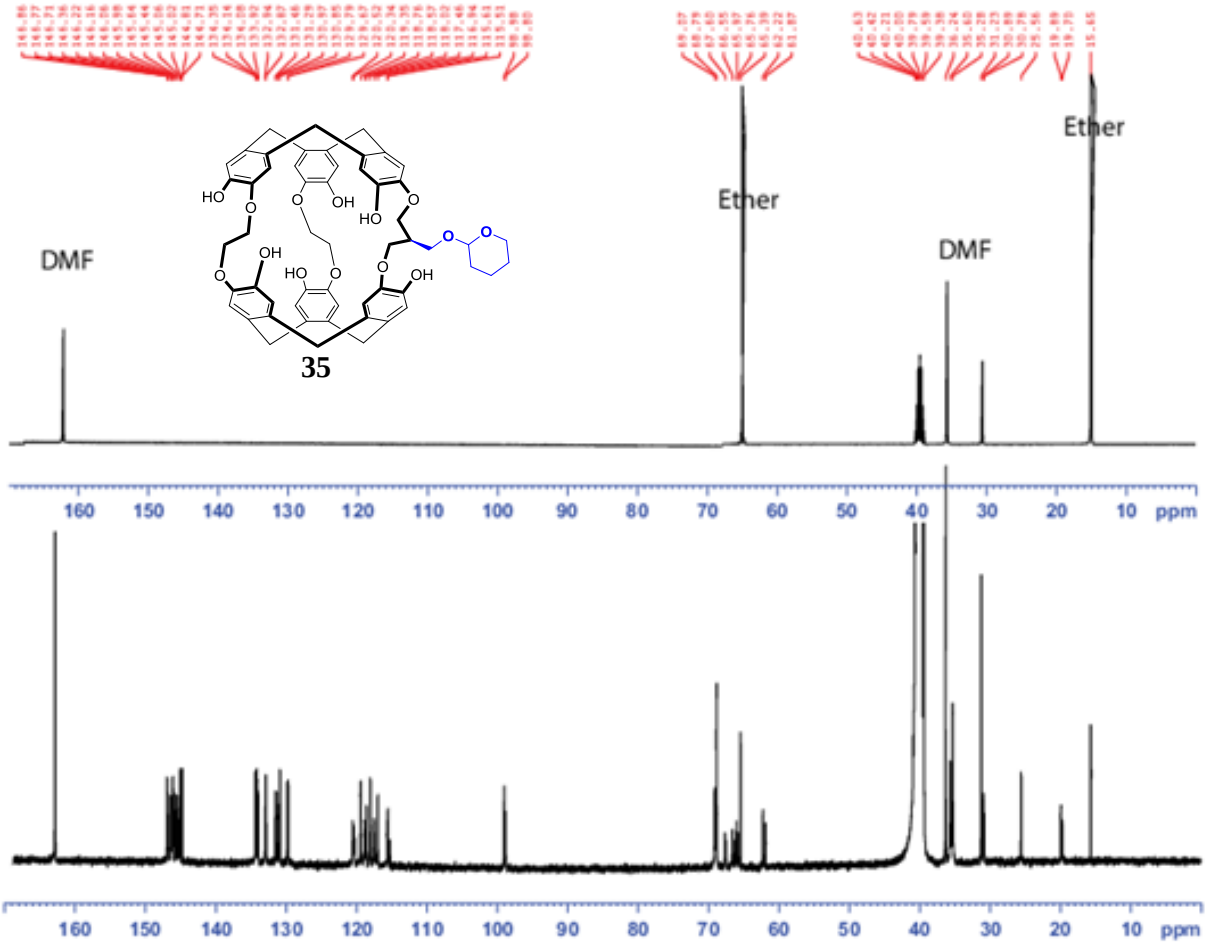

Figure 81: ^{13}C NMR spectrum of compound **35** in DMSO-d_6 in 400 MHz spectrometer.

Experimental Part

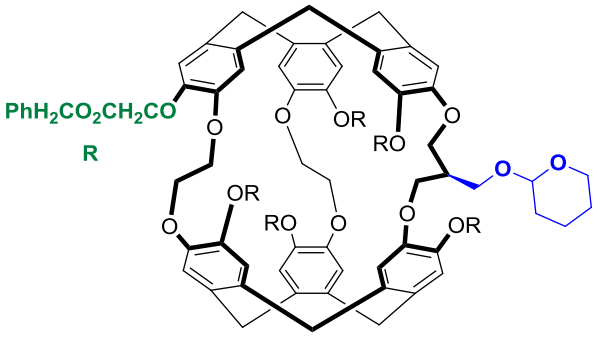

36

Compound 36: Benzyl bromoacetate (0.88 mL, 5.5 mmol, 12 equiv.) was added under an argon atmosphere to a solution of compound **35** (0.44 g, 0.46 mmol, 1 equiv.) and Cs_2CO_3 (1.83 g, 5.5 mmol, 12 equiv.) in DMF (8 mL). The mixture was heated for 16 hours at 60 °C under argon. The mixture was poured in water and then extracted 5 times with AcOEt. The combined organic layers were then washed 5 times with water, dried over Na_2SO_4. Filtration and evaporation of the solvent under reduced pressure gave an oily residue, which was subjected to column chromatography on silica gel ($CHCl_3$/acetone: 95/5). Compound **36** was collected as viscous oil (0.43 g, 54%) as a mixture of two diastereomers. This compound was used without further purification for the next step.

^{1}H NMR (300 MHz, $CDCl_3$, 25 °C): δ (ppm) 7.15-7.01 (m, 30 H), 6.42-5.99 (12s, 12H), 5.00-4.8 (m, 12 H), 4.36-4.07 (m, 18 H), 3.88- 3.49 (m, 13 H), 2.87- 2.82 (m, 6H), 1.98 (m, 1H), 1.45 (m, 6H).

HRMS (ESI, $[M+Na]^+$) calcd. for $C_{109}H_{102}NaO_{26}$ 1849.6557 found 1849.6552.

Experimental Part

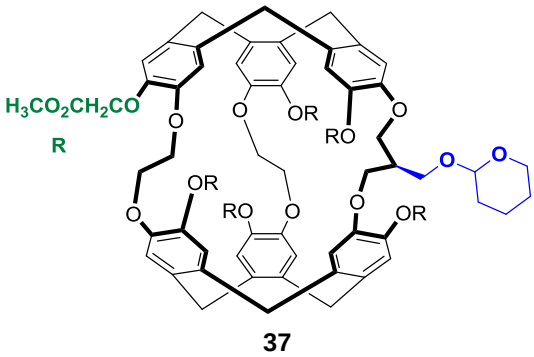

37

Compound 37: Methyl bromoacetate (0.2 mL, 2.28 mmol, 24 equiv.) was added under an argon atmosphere to a mixture of cryptophane **35** (0.09 g, 0.095 mmol, 1 equiv.) and Cs_2CO_3 (0.37 g, 1.13 mmol, 12 equiv.) in DMF (3 mL) and CH_2Cl_2 (1 mL). The mixture was heated up to 50 °C for 16 hours under argon. Then, the mixture was poured in water and extracted 5 times with AcOEt. The combined organic layers were then washed 5 times with water and dried over Na_2SO_4. Evaporation of the solvent gave rise to an oily residue, which was subjected to column chromatography on silica gel ($CHCl_3$/acetone: gradient 90/10 to 85/15). Compound **37** was isolated as a white solid as a mixture of two diastereomers (0.090 g, 70%) and used without further purification for the next step.

^{1}H NMR (400 MHz, $CDCl_3$, 25 °C): δ (ppm) 6.86-6.68 (10 H, 10s), 6.55-6.53 (2H, 2s), 4.68-4.48 (18 H, m), 4.44-3.75 (35 H, m), 3.35-3.34 (6H, m), 2.51 (1H, m), 1.83 (m, 6 H).

HRMS (ESI): *m/z* $[M+Na]^+$ calcd. for $C_{73}H_{78}NaO_{26}$ 1393.4679 found 1393.4673.

Experimental Part

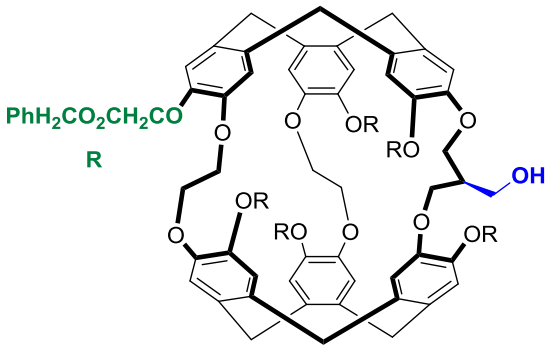

38

Compound 38: PPTS (0.3 g, 1.3 mmol, 5 equiv.) in methanol (2 mL) was added in one portion to cryptophane **36** (0.47 g, 0.25 mmol) in CH_2Cl_2 (6 mL). The solution was heated to 40 °C for 48 hours. Then, the solvents were evaporated under reduced pressure and the residue was purified on silica gel (CH_2Cl_2/acetone: 96/4). Compound **38** (0.4 g, 93%) was obtained as white glassy solid.

^{1}H NMR (400 MHz, $CDCl_3$, 25 °C): δ (ppm) 7.42-7.30 (m, 30H), 6.58-6.39 (12s, 12H), 5.31-5.00 (m, 12H), 4.60-4.36 (m, 18 H), 4.18-3.83 (m, 14H), 3.26-3.05 (m, 6 H), 3.02 (m, 1 H).

^{13}C {^{1}H} NMR (100.6 MHz, $CDCl_3$, 25 °C): δ (ppm) 169.5, 169.3, 169.2 (2C), 169, 168.8, 148.4, 147.9, 147.6, 147.5 (2C), 147.4, 147.2 (4C), 146.0 (3C), 135.6 (2C), 135.5, 135.4 (3C), 134.7, 134.3, 133.8, 133.5, 133.4, 133.37, 133.2 (2C), 132.9, 132.0, 131.6, 131.3, 128.5-128.8 (30 C), 121.1, 120.7, 120.6, 119.7, 119.4, 119.2, 119.1, 118.8, 118.1, 115.5, 113.5, 113.1, 69.7, 69.1, 68.8, 68.6, 68.1, 68.0, 67.9, 67.9, 67.8, 67.7, 67.2, 67 (2C), 66.9 (2C), 66.8, 66.7, 66.6, 66.3, 63.4, 41.1, 36.2, 35.9, 35.7 (3C).

HRMS (ESI): *m/z* $[M+Na]^+$ calcd. for $C_{104}H_{94}NaO_{25}$ 1765.5981 found 1765.5976.

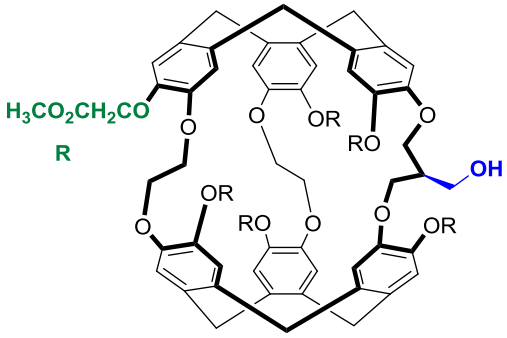

39

Compound 39: PPTS (0.050 g, 0.2 mmol) in methanol (3 mL) was added under an argon atmosphere to a solution of **37** (0.17 g, 0.12 mmol) in CH_2Cl_2 (5 mL). The solution was stirred under argon at 40 °C. The solvents were evaporated under reduced pressure and the oily residue was subjected to column chromatography on silica gel (CH_2Cl_2/acetone: 80/20). After evaporating the solvents, compound **39** (0.14 g, 93%) was collected on a fritted glass as a white solid and was washed with a small volume of diethyl ether.

^{1}H NMR (400 MHz, $CDCl_3$, 25 °C): δ (ppm) 6.82-6.55 (12s, 12 H), 4.66-4.46 (m, 18 H), 4.34-3.78 (m, 32 H), 3.40-3.34 (m, 6H), 2.29 (m, 1H).

^{13}C {^{1}H} NMR (100.6 MHz, $CDCl_3$, 25 °C): δ (ppm) 170.0, 169.8, 169.7 (2C), 169.6, 169.2, 148.3, 147.9, 147.6 (3C), 147.4, 147.2, 147.1 (2C), 147.0, 145.9 (2C), 134.9, 134.8, 134.4, 133.8, 133.5, 133.48, 133.3, 133.2, 133.1, 132.9, 131.8, 131.7, 121.0, 120.8, 120.3, 119.7, 119.3, 119.2, 118.9, 118.4, 118.1, 114.7, 113.5, 113.1, 69.6, 69.2, 68.8 (2C), 68.6, 68.3, 67.7 (2C), 67.5, 67.3, 67.0, 66.5, 66.3, 51.8-52.1 (6C), 41.0, 35.7-36.2 (6C).

HRMS (ESI): *m/z* $[M+Na]^+$ calcd. for $C_{68}H_{70}NaO_{25}$ 1309.4103 found 1309.4098.

Experimental Part

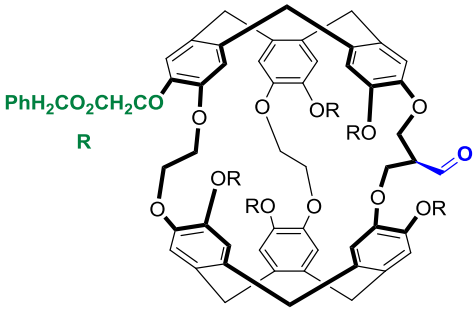

41

Compound 41: Excess of Dess martin periodinate reagent (15% wt solution in CH_2Cl_2, 0.9 mL; 0.37 mmol) was added at room temperature to a solution of **38** (0.1 g, 0.057 mmol) in freshly distilled CH_2Cl_2 (13 mL). The solution was stirred at room temperature for 16 hours. Then, the solution was filtered on a fritted glass. The filtrate solution was collected and the solvent was removed under reduced pressure to leave a solid residue. Dissolution in a minimum of CH_2Cl_2 and precipitation with diethyl ether gave rise to compound **41** as white solid. This compound decomposes on silica gel. Thus, **41** was used **without further purification** for the next step. An HRMS spectrum allows us to ascertain the structure of **41**.

HRMS (ESI): *m/z* $[M+Na]^+$ calcd. for $C_{104}H_{92}NaO_{25}$ 1763.5825 found 1763.5819.

Experimental Part

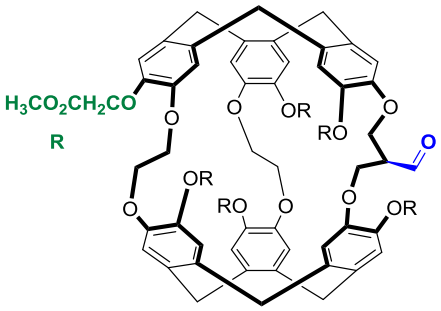

42

Compound 42: Excess of Dess martin periodinate (15% wt solution in CH_2Cl_2) reagent (0.4 mL; 0.16 mmol) was added at room temperature to a solution of **39** (0.15 g, 0.11 mmol) in freshly distilled CH_2Cl_2 (4 mL). The solution was stirred at room temperature for 16 hours under an argon atmosphere. Then, the solution was filtered on a fritted glass. The filtrate solution was collected and the solvent was removed under reduced pressure to leave a solid residue. Dissolution in a minimum of CH_2Cl_2 and precipitation with diethyl ether gives rise to compound **42** as white solid. This compound also decomposes on silica gel. Thus, compound **42** was **used without further purification** for the next step. An HRMS spectrum allows us to ascertain the structure of **42**.

HRMS (ESI): *m/z* $[M+Na]^+$ calcd. for $C_{68}H_{68}NaO_{25}$ 1307.3947 found 1307.3942.

Experimental Part

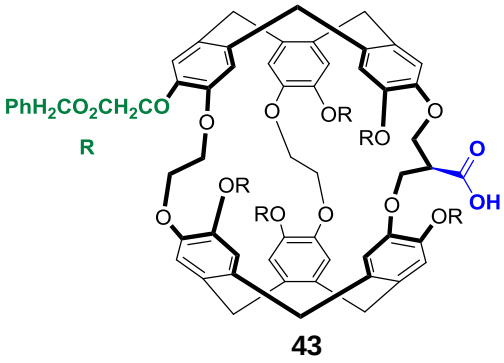

43

Compound 43: Sodium chlorite (0.01 g in 0.1 ml water, 0.16 mmol, 3 equiv.) was added along with sodium monobasic phosphate (99.45 µg in 0.01 ml water, 0.0083 mmol) and H_2O_2 (1.59 µl) to a solution of compound **41** (0.1 g, 0.06 mmol, 1 equiv.), CH_3CN (1.5 mL), H_2O (0.15 mL) under an argon atmosphere at room temperature. The, solution was stirred for 16 hours at room temperature and the solvent was removed under reduced pressure. The resulting residue was subjected to column chromatography on silica gel (CH_2Cl_2/acetone: 75/25). After evaporation of the solvents, compound **43** (0.07 g, 70 %) was collected as white solid.

^{1}H NMR (400 MHz, $CDCl_3$, 25 °C): δ (ppm) 7.44-7.30 (m, 30H), 6.62-6.36 (12s, 12H), 5.31-5.09 (s, 12H), 4.55-4.37 (m, 18 H), 4.15-3.95 (m, 12H), 3.19-3.15 (m, 6H), 3.07 (m, 1H).

^{13}C {^{1}H} NMR (100.6 MHz, $CDCl_3$, 25 °C): δ (ppm) 172.5, 169.6, 169.4, 169.3, 169.2 (2C), 169.1, 147.8, 147.7 (2C), 147.6 (2C), 147.4 (2C), 147.3, 147.2 (2C), 146.2, 145.9, 135.2,-135.5 (6C), 134.4 (2C), 133.6 (2C), 133.3, 133.2 (2C), 133.1 (2C), 133.0, 132.4, 132.0, 128.6-128.8 (30C), 120.9 (2C), 120.6, 120.27 (2C), 119.1 (2C), 118.8, 118.3, 117.5, 114.5, 114.2, 69.4, 69.3, 68.8 (2C), 68.1, 68.0, 67.9 (2C), 67.2 (2C), 67.0-66.9 (6C), 64.8 (2C), 62.8, 45.6, 36.1 (2C), 35.7 (4C).

HRMS (ESI): *m/z* $[M+Na]^+$ calcd. for $C_{104}H_{92}NaO_{26}$ 1779.5774 found 1779.5769.

Experimental Part

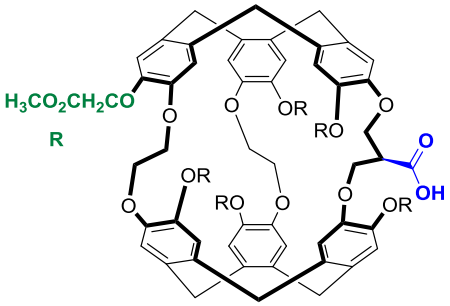

44

Compound 44: Sodium chlorite (0.035 g in 0.35 mL water, 0.38 mmol, 2 equiv.) was added along with sodium monobasic phosphate (0.01g in 0.017 mL water, 0.07 mmol) and H_2O_2 (0.53 mL) to a solution of compound **42** (0.25 g, 0.19 mmol, 1 equiv.), CH_3CN (5.3 mL), H_2O (0.15 mL) under an argon atmosphere at room temperature. The, solution was stirred for 16 hours at room temperature and then quenched with sodium thiosulfate (2 mL) at 0°C. The solvent was then removed under reduced pressure. Then, the crude was recrystallized from CH_2Cl_2 and diethyl ether to give a white precipitate. Filtration on a frit allows us to collected compound **44** (0.19 g, 78%) as a white solid. This solid was washed several times with diethyl ether and dried in air.

^{1}H NMR (400 MHz, $CDCl_3$, 25 °C): δ (ppm) 6.81-6.60 (12s, 12 H), 4.66-4.42 (m, 18 H), 4.38-4.13 (m, 12 H), 3.83-3.76 (6s, 18 H), 3.39-3.36 (m, 6 H), 3.24 (m, 1H).

^{13}C {^{1}H} NMR (100.6 MHz, $CDCl_3$, 25 °C): δ (ppm) 172.6, 170, 169.9 (4C), 169.8, 147.8, 147.7, 147.7 (2C), 147.6, 147.5 (2C), 147.4, 147.3 (2C), 146.4, 146.2, 134.5 (2C), 133.7, 133.6, 133.5, 133.4 (4C), 133.3, 133.2, 132.9, 132.3, 121.0 (2C), 120.1 (2C), 119.7, 119.3 (2C), 118.2 (2C), 117.4, 115.4, 115.0, 69.5 (2C), 68.8 (2C), 67.7 (2C), 67.6 (2C), 67.2, 67.0, 65.6, 65.2, 52.0-52.2 (6C), 45.9, 36.3 (3C), 35.9 (3C).

HRMS (ESI): *m/z* $[M+H]^+$ calcd. for $C_{68}H_{69}O_{26}$ 1301.4077 found 1301.4072.

Experimental Part

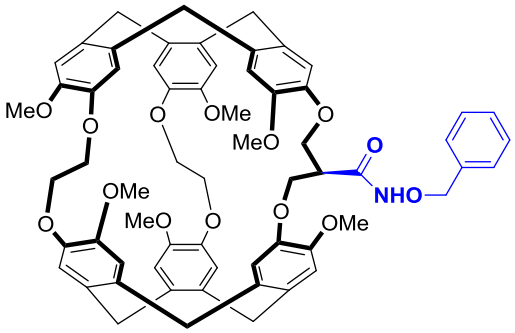

45

Compound 45: Cryptophane **31** was introduced (0.13 g, 0.13 mmol, 1 equiv.) and then dissolved in freshly distilled pyridine (2ml). Then O-benzyl hydroxylamine (excess, 0.04 ml) was added and the solution was brought to -15 °C. $POCl_3$ (excess, 0.05 ml) was introduced drop wisely and the solution was stirred for 30 minutes at -15 °C then for 5 hours at room temperature. The obtained yellowish solution was poured cautiously in ice/water/$NaHCO_3$ at 0 °C in which a lot of precipitates were obtained. The solution was filtered then extracted 5 times with CH_2Cl_2 and the solvent was evaporated under reduced pressure. The obtained crude was purified on silica (CH_2Cl_2/Acetone: 90/10) to afford the product as white powder which was further washed with diethyl ether (0.09 g, 62%).

^{1}H NMR (400 MHz, $CDCl_3$, 25 °C): δ (ppm) 9.70 (s, 1H), 7.42-7.3 (m, 5H), 6.74-6.55 (12s, 12H), 4.96-4.91 (d, j=, 11.5 Hz, 1H), 4.91-4.94 (d, j=11.5, 1H), 4.62-4.55 (m, 6H), 4.26-3.82 (m, 12H), 3.79-3.67 (6s, 18H), 3.4-3.36 (m, 6H), 3.09 (m, 1H).

^{13}C {^{1}H} NMR (100.6 MHz, $CDCl_3$, 25 °C): δ (ppm) 169.7, 149.6, 149.5, 149.4, 149.3, 148.1, 147.86, 146.8, 146.7, 146.6 (2C), 145.4, 135.6, 134.0, 133.9, 133.7, 133.6, 133.2, 132.4, 132.0 (2C), 131.5, 131.48, 131.4, 130.9, 129.2 (2C), 128.6, 128.4 (2C), 120.3 (2C), 120.1, 119.9, 114.7, 114.4, 114.2 (2C), 113.7, 113.5, 112.9, 112.5, 77.2, 69.7, 69.4, 68.9, 68.7, 66.6, 64.5, 56.3, 56.3, 55.69, 55.61, 55.5, 55.4, 46.1, 36.4, 36.1 (4 C).

HRMS (ESI): *m/z* $[M+H]^+$ calcd. for $C_{63}H_{63}NaNO_{14}$ 1080.4146 found 1080.4140.

Experimental Part

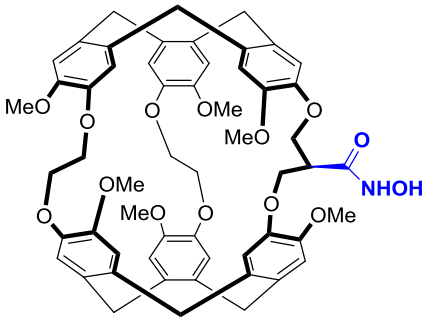

46

Compound 46: The protected cryptophane **45** (0.07 g, 0.066 mmol) was introduced along with catalytic amount of Pd/C (10% by weight) and then dissolved in CH_2Cl_2/ Methanol mixture. The solution was purged first with Argon then with hydrogen and placed under hydrogen atmosphere for 24 hours. The produced solution was filtered on cellite and washed with CH_2Cl_2 for several times. It is important to mention that the product was slightly colored (reddish). Following this, the solvent was evaporated under reduced pressure and the obtained solid was washed with diethyl ether to offer pure product **46** (0.02 g 30%).

^{1}H NMR (400 MHz, $CDCl_3$, 25 °C): δ (ppm) 10.21 (s, 1H), 6.76-6.6 (12s, 12H), 4.56-4.53 (m, 6H), 4.24- 3.92 (m, 12H), 3.83-3.74 (6s, 18H), 3.41-3.37 (m, 6H), 3.2 (m, 1H).

HRMS (ESI): *m/z* $[M+H]^+$ calcd. for $C_{56}H_{57}NNaO_{14}$ 990.3676 found 990.3671.

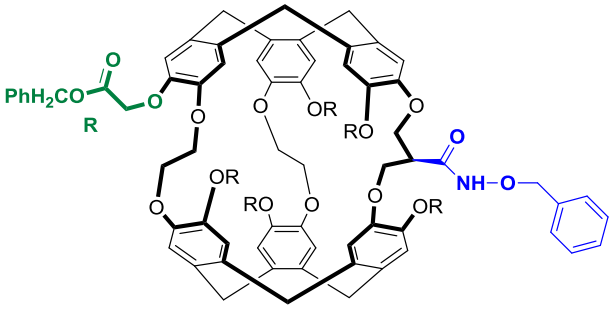

47

Compound 47: Excess of $POCl_3$ (0.013 mmol) was slowly added at -15 °C to a solution of **43** (0.14 g, 0.08 mmol, 1 equiv.) and O-benzyl hydroxylamine (0.020 mL) in pyridine (3 mL). The solution was stirred for 30 minutes at this temperature hours and then stirred for further 5 hours at room temperature. The solution was quenched by addition of a mixture of ice/water/$NaHCO_3$ at 0 °C**.** The obtained mixture was washed 5 times with CH_2Cl_2. Then the combined organic layers were dried over Na_2SO_4. The solution was filtered and the solvent was removed under pressure to leave a residue. Purification on silica gel (CH_2Cl_2/acetone: 95/5) gave rise to compound **47** (0.04 g; 26%) as a white solid. This solid was collected on a fritted glass and washed several times with diethyl ether.

^{1}H NMR (400 MHz, $CDCl_3$, 25 °C): δ (ppm) 9.63 (s, 1H), 7.43-7.26 (m, 35H), 6.59-6.26 (12s, 12H), 5.35-4.94 (m, 14H), 4.65-4.34 (m, 18H), 4.05-3.68 (m, 12H), 3.27-3.19 (m, 6H), 2.89 (m, 1H).

^{13}C {^{1}H} NMR (100.6 MHz, $CDCl_3$, 25 °C): δ (ppm) 169.5, 169.4, 169.3, 169.2, 169.1, 168.7, 168.6, 147.9, 147.7, 147.6, 147.66, 147.5, 147.3 (2C), 147.2 (2C), 146.5, 146.4, 146.3, 135.3-135.7 (6C), 134.6, 134.2, 133.7, 133.6, 133.4 (2C), 133.3, 133.2, 133.1 (2C), 132.6, 132.1, 129.5-129.5 (35C), 121.0, 120.7, 120.0, 119.6, 119.5, 119.1, 118.8, 118 (2C), 115.5 (3C), 115.2, 78.1, 69.7, 69.1, 68.7, 68.4, 68.1, 67.9, 67.8 (2C), 67.3, 66.8-66.9 (6C), 66.5, 66.0, 64.7, 47.3, 36.0, 35.9, 35.7 (4C).

HRMS (ESI): *m/z* $[M+Na]^+$ calcd. for $C_{111}H_{99}NNaO_{26}$ 1884.6353 found 1884.6347.

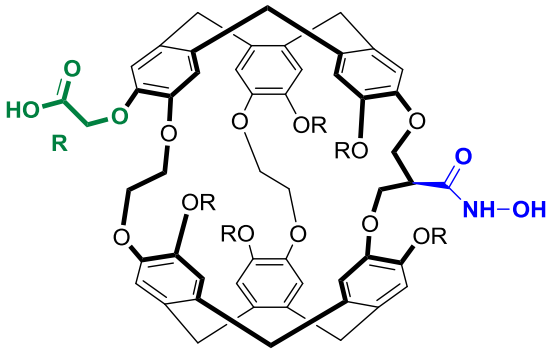

48

Compound 48: Hydrogen gas was bubbled into a solution of cryptophane **47** (0.057 g, 0.03 mmol) and Pd/C (10%) (0.05 g) in a mixture of CH_2Cl_2 (2 mL) and methanol (1 mL). The solution was kept under hydrogen atmosphere for two nights at room temperature. Then, the mixture was filtered on cellite and washed CH_2Cl_2 and methanol. The solvents were evaporated under reduced pressure to leave a residue. It was then dissolved in aqueous NaOH (0.3 M) and the aqueous layer was washed 3 times whit CH_2Cl_2. Acidification with few drops of conc. HCl at 0 °C gave rise to a precipitate which was collected on a fritted glass and washed several times with diethyl ether. Compound **48** (0.015 g, 40%) was obtained as a white solid.

^{1}H NMR (400 MHz, $CDCl_3$, 25 °C): δ (ppm) 9.69 (s, 1H), 6.94-6.69 (12s, 12H), 4.79-4.29 (m, 30 H), 3.98-3.84 (m, 7H).

^{13}C {^{1}H} NMR (100.6 MHz, $CDCl_3$, 25 °C): δ (ppm) 171.5, 170.4 (3C), 170.1, 170.0, 168.3, 148.5, 148.2, 147.5, 147.4, 146.3 (2C), 146.2, 146.1, 146.0, 145.9, 145.4, 144.8, 134.9, 133.8, 133.7, 132.9, 132.8 (3C), 132.7, 132.6, 132.3, 132.2, 132.0, 123.9, 120.2, 118.8 (2C), 118.6, 118.4, 117.8, 117.4, 117.1, 115.7 (2C), 115.3, 68.9, 68.2, 67.9 (2C), 67.8, 67.2, 66.9, 66.8, 66.0, 65.6, 65.4, 65.1, 43.3, 35.4-35.0 (6C).

HRMS (ESI): *m/z* $[M+Na]^+$ calcd. for $C_{62}H_{57}NNaO_{26}$ 1254.3066 found 1254.3061.

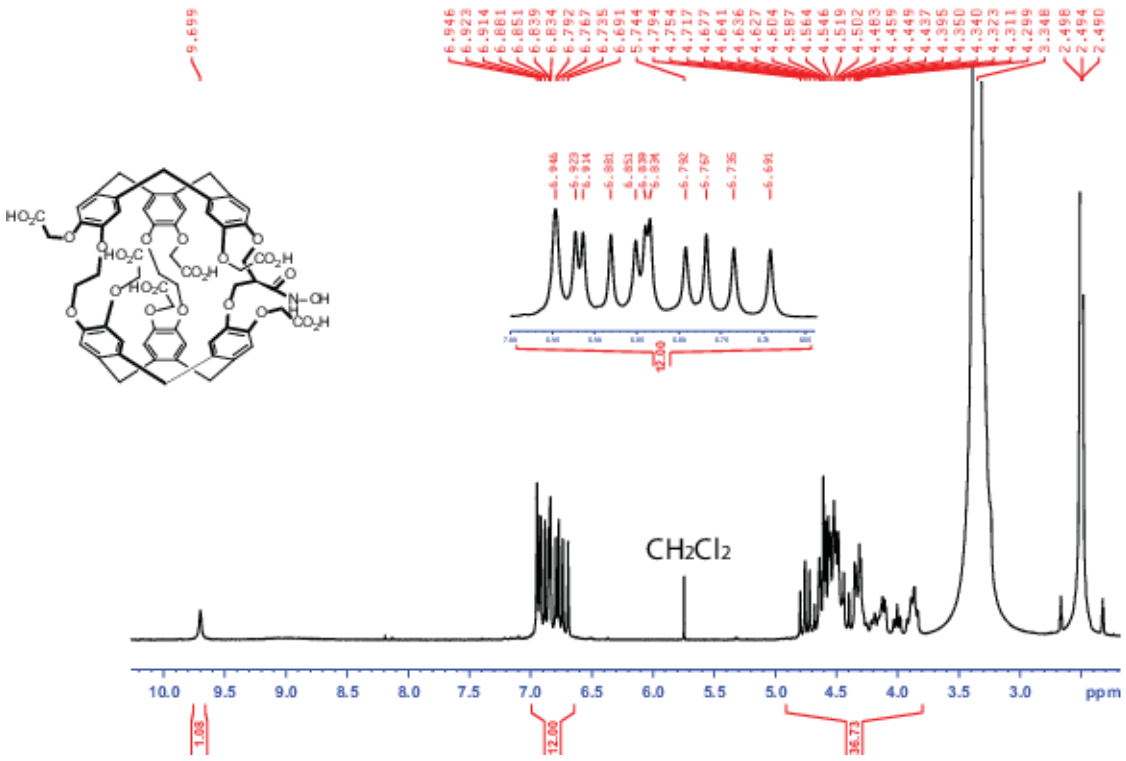

Figure 82: ^{1}H NMR spectrum in DMSO-d_6 of compound **48**.

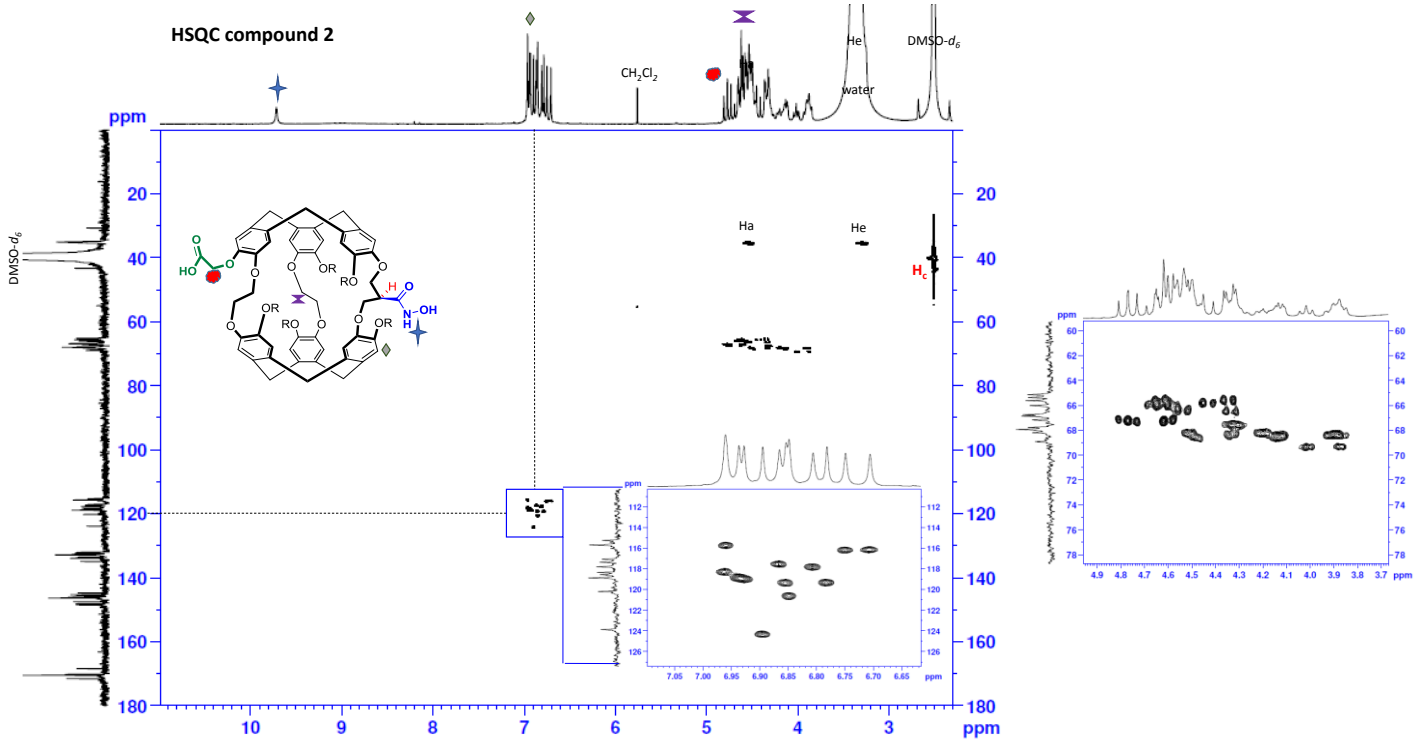

Figure 83: HSQC of compound **48** in DMSO-d_6 in a 400 MHz spectrometer. Zoomed is the aromatic region corresponding to twelve proton and their corresponding carbons.

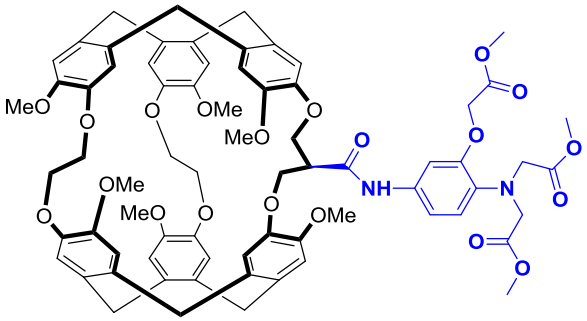

53

Compound 53: Cryptophane **31** (0.035 g, 0.036 mmol, 1 equiv.) was first introduced and dissolved in freshly distilled pyridine (1ml). Then the aniline **52** (0.0148 g, 0.0435 mmol, 1.2 equiv.) was added and the mixture was brought to -15 °C. After that $POCl_3$ (1.1equiv., 4.03 µl, 0.043 mmol) drop wisely and then stirred at -15 °C for 30 minutes then at room temperature for 5 hours. The obtained solution was quenched by introducing it in $H_2O/NaHCO_3$/ Ice at 0 °C. After that the crude was extracted 5 times with CH_2Cl_2 and then dried (note a lot of precipitate are obtained) over Na_2SO_4. The solvent was evaporated under reduced pressure and the crude was subjected to column chromatography using SiO_2 ($CHCl_3$/Acetone: 70/30) to give **53** as the white product with (0.01 g, 22%).

^{1}H NMR (400 MHz, $CDCl_3$, 25 °C): δ (ppm) 9.30 (s, 1H), 7.52 (d, 1H), 6.93 (m, 2H), 6.78-6.56 (12s, 12H), 4.7-4.56 (m, 8H), 4.97-3.97 (m, 16 H), 3.84-3.69 (9s, 27 H), 3.46-3.37 (m, 6 H), 3.25 (m, 1H).

^{13}C {^{1}H} NMR (100.6 MHz, $CDCl_3$, 25 °C): δ (ppm) 171.6 (2C), 169.2, 168.8, 150.0, 149.6, 149.5 (2C), 149.3, 147.9, 147.8, 146.88, 146.8, 146.7 (2C), 146.6, 145.5, 135.7, 134.0, 133.9 (2C), 133.8, 133.7, 133.1, 132.28, 132.24, 132.1, 131.6, 131.5, 131.0, 130.9, 120.6 (3C), 120.6, 120.2, 114.21 (2C), 113.9, 113.8, 113.7, 113.6, 113.5, 112.8, 112.5, 107.6, 69.7, 69.4, 68.9, 68.8, 66.0, 65.9, 65.8, 64.5, 56.3, 56.2, 52.8, 55.7, 55.6, 55.5, 53.6, 52.1, 51.7 (2C), 48.4, 36.4, 36.3, 36.1 (4C).

HRMS (ESI): *m/z* $[M+H^+]^+$ calcd. for $C_{71}H_{74}N_2O_{20}$ 1274.4834 found 1275.4908

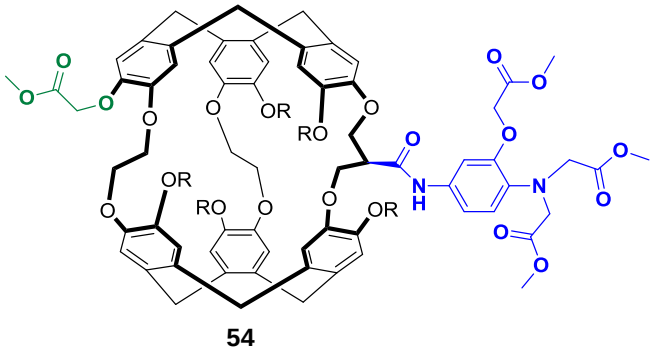

54

Compound 54: Compound **44** (0.13 g, 0.09 mmol, 1 equiv.) was introduced and then dissolved in freshly distilled pyridine (1 mL). Then compound **52** was added (0.033 g, 0.09 mmol, 1equiv.). The mixture was stirred at -15 °C, then $POCl_3$ (0.010 mL, 0.1 mmol, 1.2 equiv.) was added drop wisely and the mixture turned red upon addition. The solution was stirred for 30 minutes at -15 °C then stirred for 5 hours at room temperature where it turned orange. The solution was then poured carefully on a mixture of ice/water/$NaHCO_3$. The obtained solution was extracted 5 times with CH_2Cl_2, then dried over Na_2SO_4, filtered and the solvent was evaporated under reduced pressure. The brownish crude was subjected to column chromatography using silica gel ($CHCl_3$/ Acetone: 65:35) the desired product as white powder (0.05 g, 30%).

^{1}H NMR (400 MHz, $CDCl_3$, 25 °C): δ (ppm) 9.07 (s, 1H), 7.44 (m, 1H), 7.04 (m, 1H), 6.84 (m, 1H), 6.82-6.52 (12s, 12H), 4.69-4.45 (m, 20 H), 4.26-4.15 (m, 18 H), 3.84-3.64 (9s, 27H), 3.46-3.34 (m, 6H), 3.12 (m, 1H).

^{13}C {^{1}H} NMR (100.6 MHz, $CDCl_3$, 25 °C): δ (ppm) 171.6 (2C), 170, 169.9, 169.89, 169.8 (2C), 169.5, 169.3, 169.2, 149.8, 147.9, 147.8, 147.7 (3C), 147.5, 147.44, 147.41, 147.2, 147.0, 146.6 (2C), 135.6, 134.9, 134.4, 133.9, 133.6, 133.57, 133.5 (2C), 133.4 (3C), 133.1 (2C), 132.3, 132.2, 121.1, 120.6, 120.4, 120.2, 119.7, 119.4, 118.9, 118.5, 118.0, 116.3, 115.7, 115.4, 1114.0, 107.6, 69.9,69.21, 68.7, 68.5, 67.9, 67.6, 67.5, 67.4, 67.2, 67.8, 66.0 (2C), 53.6 (2C), 52.1, 52.09, 52.05 (2C), 52.026 (2C), 51.9, 51.7 (2C), 49.1, 36.2 (3C), 35.9 (3C).

HRMS (ESI): *m/z* $[M+Na]^+$ calcd. for $C_{83}H_{86}N_2NaO_{32}$ 1645.5061 found 1645.5056.

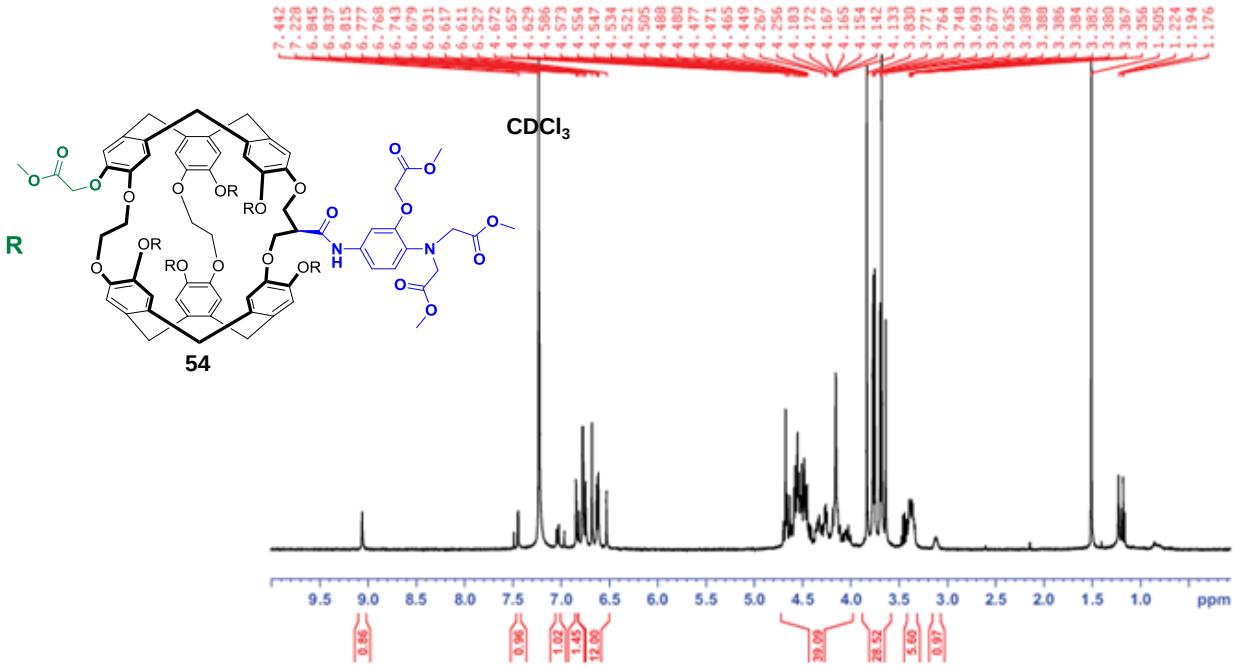

Figure 84: ^{1}H NMR spectrum of compound **54** in $CDCl_3$ in a 400 MHz spectrometer.

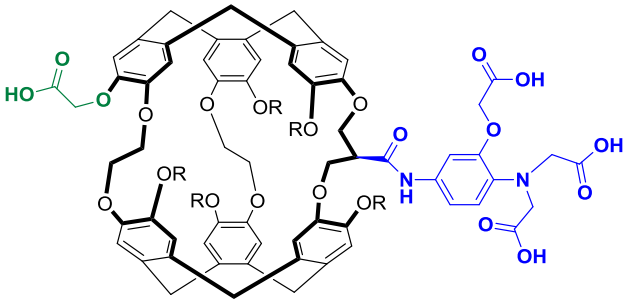

55

Compound 55: Compound **54** (0.03 g, 0.0184 mmol, 1 equiv.) was dissolved in THF (1.18 ml) and then (0.3 M) KOH solution (1.1 ml, 18 equiv.) was added drop wisely at 0 °C. The reaction was stirred for 30 minutes at room temperature. The solvent was evaporated under reduced pressure and then the crude was dissolved in a minimum amount of water. The obtained aqueous layer was washed twice with CH_2Cl_2. The resulting aqueous layer was acidified at 0°C with concentrated HCl solution. The obtained precipitate was collected on a fritted glass and then washed with ether to give compound **55** (0.02 g, ~74%) as a white compound. The compound showed high sensitivity to light and heat and it structure is confirmed by HRMS.

HRMS (ESI): *m/z* $[M+Na]^+$ calcd. for $C_{74}H_{68}N_2NaO_{32}$ 1519.3652 found 1519.3647.

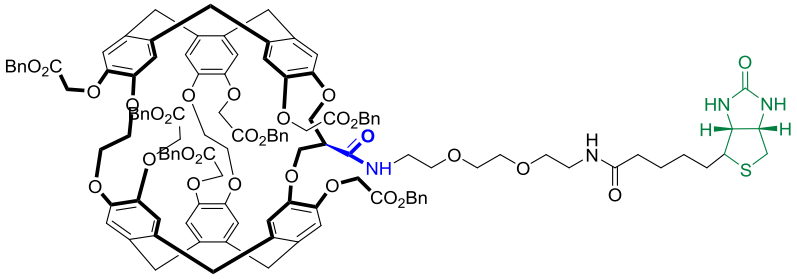

56

Compound 56: To a solution of **43** (0.07 g, 0.039 mmol, 1equiv.) dissolved in DMF (1.5 ml) was added EDCI.HCl (0.01 g, 0.055 mmol, 1.4 equiv.), HOBt (0.015 g, 0.11 mmol, 0.28 equiv.) and DIPEA (0.11 mmol, 0.02 ml, 3 equiv.) and stirred for 10 minutes. Then Biotin peg 2-amine (0.014 g, 0.039 mmol, 1 equiv.) dissolved in DMF (0.5 ml) was added and the mixture is stirred for 16 hours. The reaction mixture was extracted 5 times with CH_2Cl_2 and the resulting organic layer was washed 5 times with brine. The solvent was removed under reduced pressure and the resulting crude was subjected to column chromatography on silica gel (CH_2Cl_2/MeOH: 95/5). Compound **56** (0.06 g, 71%) was obtained as white solid.

^{1}H NMR (400 MHz, $CDCl_3$, 25 °C): δ (ppm) 7.3-7.2 (m, 30H), 6.6-6.3 (12s, 12H), 5.8 (bd s, 1H), 5.3-5 (m, 12 H), 4.5-4.3 (m, 19H), 4.2-3.7 (m, 13 H), 3.47-3.4 (m, 10H), 3.1-3.3 (m, 7H), 3.01 (m, 1H), 2.9 (m, 1H), 2.8 (m, 1H), 2.6 (m, 1H), 2.1 (m, 2H), 1.6 (m, 4H), 1.44 (m, 2H).

^{13}C {^{1}H} NMR (100.6 MHz, $CDCl_3$, 25 °C): δ (ppm) 173.2, 171.1, 169.6, 169.7 (5C), 163.4, 148, 147.6, 147.4 (3C), 147.2 (4C), 147, 146.4, 135.3 (6C), 134.4, 134.1, 133.5, 133.4 (21C), 133.2 (2C), 133 (2C), 133.7, 132.6, 131.8, 128.6 (30C), 120.8, 120.5, 120.2, 119.7, 119.3, 118.9, 118.6, 118.2, 117.9, 117.5, 115.5, 114.7, 70.1, 69.9, 69.7 (2C), 69.5, 69, 68.6, 68.4, 67.9, 67.8, 67.7, 67.4, 67.2 (4C), 66.8 (3C), 667.7 (3C), 66.3, 65.56, 61.5, 60, 55.2, 47.6, 40.3, 39, 35.9 (2C), 35.7(2C), 35.63 (2C), 30.2, 27.8 (2C), 25.3.

HRMS (ESI): *m/z* $[M+2Na]^{2+}$ calcd. for $C_{120}H_{120}Na_2N_4O_{29}S$ 1079.3777 found 1079.3772.

Experimental Part

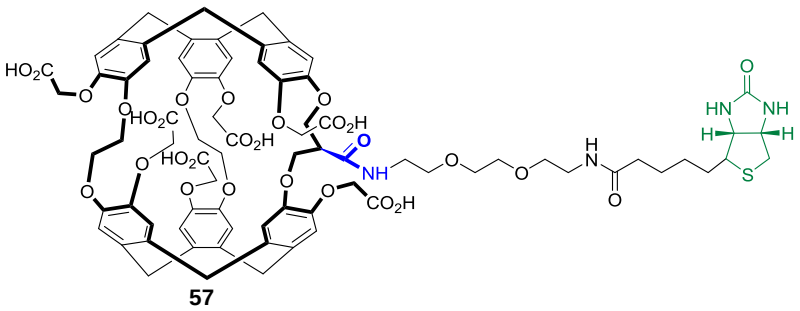

57

Compound 57: Compound **56** (0.06 g, 0.028 mmol, 1 equiv.) was dissolved in THF (1.6 ml) and then (0.3M) KOH solution (1.6 ml, 18 equiv.) was added drop wisely at 0 °C. The reaction was stirred for 30 minutes at room temperature. The solvent was evaporated under reduced pressure and then the crude was dissolved in a minimum amount of water. The obtained aqueous layer was washed twice with CH_2Cl_2. The resulting aqueous layer was acidified at 0 °C with diluted HCl solution. The obtained precipitate was collected on a fritted glass and then washed with ether to give compound **57** as a white compound. Optimization of purification is necessary to be done. The formation of **57** is confirmed by mass spectrometry and the mass found for this derivative is 1572.4942.

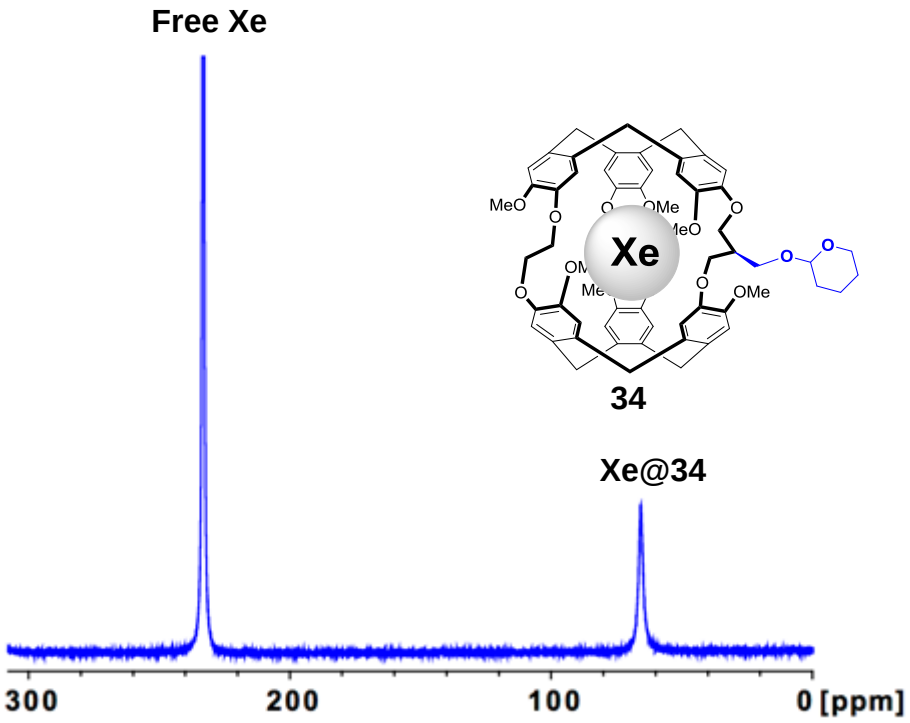

Figure 85: hyperpolarized ^{129}Xe NMR spectrum of compound **34** recorded at 298 K in $C_2D_2Cl_4$-d_2.

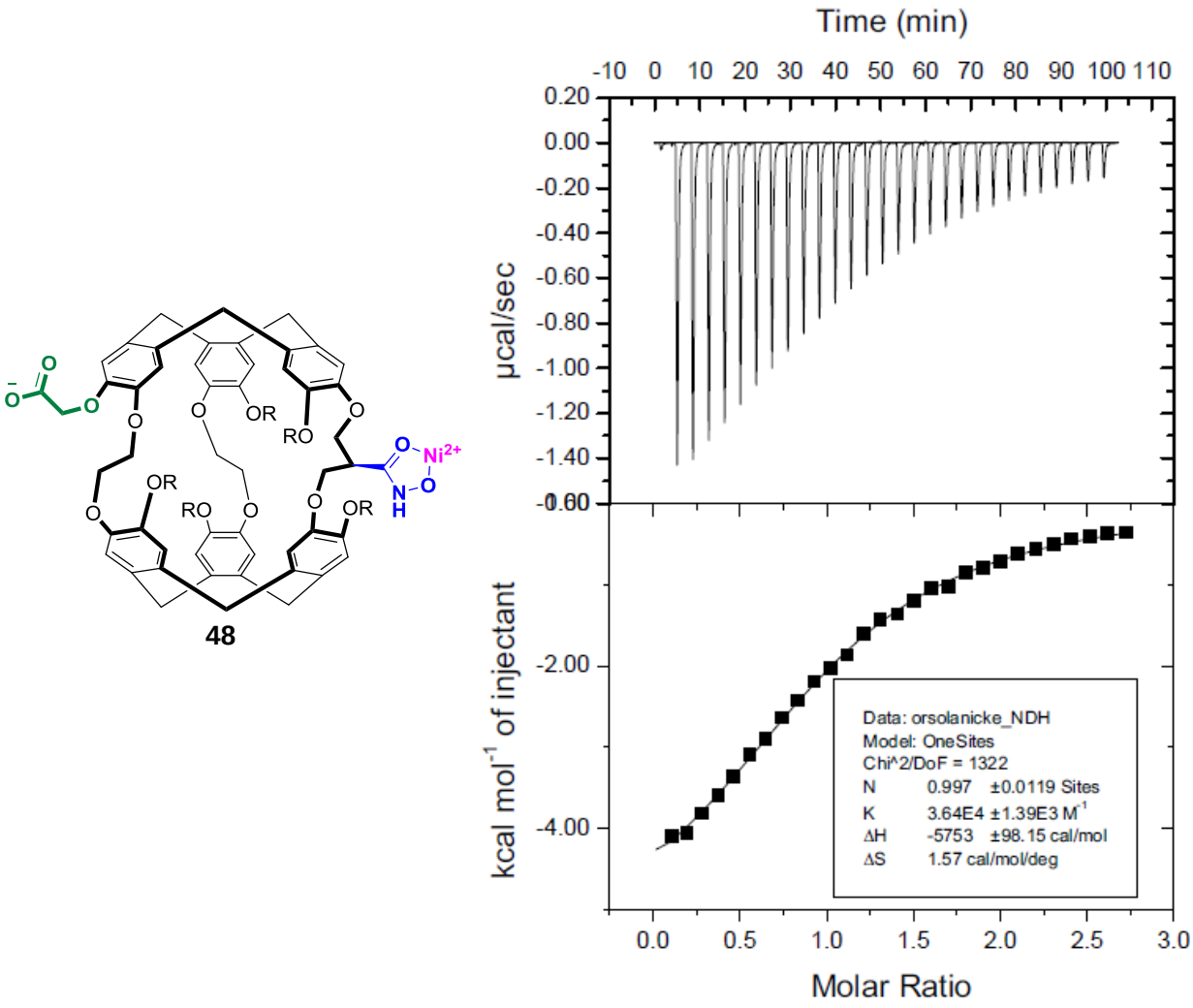

Figure 86: Calorimetric titration of compound **48** in H_2O/TRIS (20 mM; pH = 7.6). The solution host (c = 0.08 mM) was placed into the calorimeter cell (1.4 mL) and 28 successive aliquots (10 µL) of Ni^{2+} solution (c = 1.0 mM) were added at 3 min intervals.

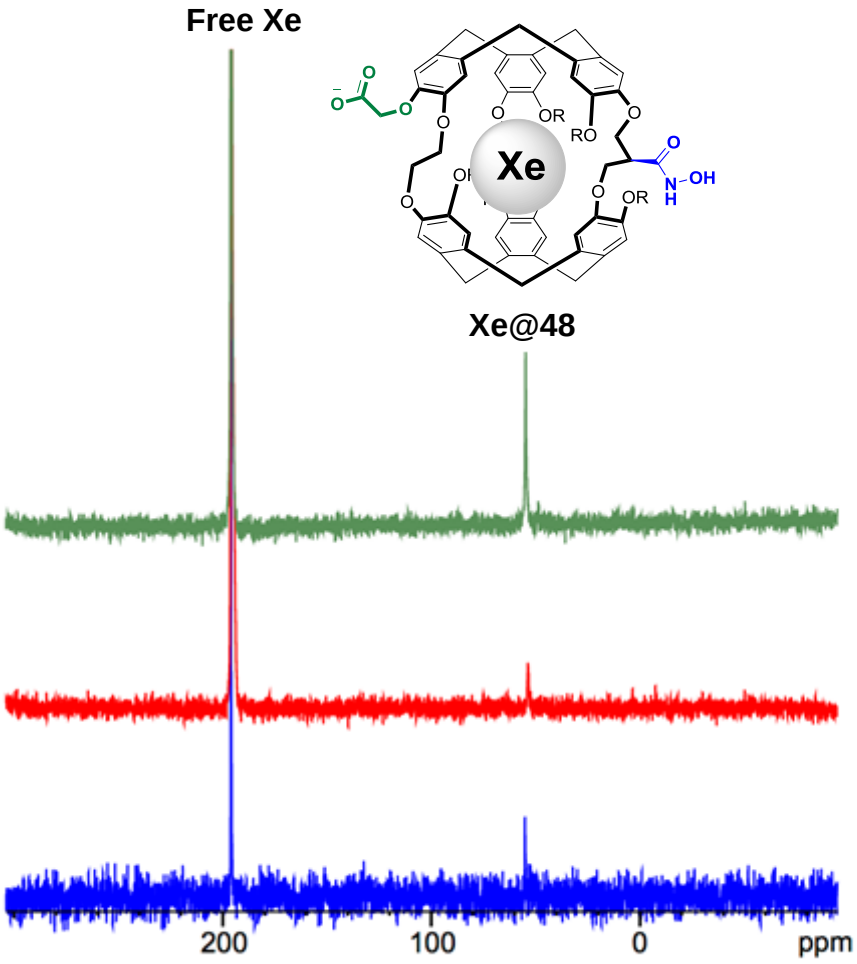

Figure 87: Hyperpolarized 129-xenon spectra of compound **48** in TRIS buffer (20 mM, pH = 7.5) at 25 °C a) in absence of Zn^{2+} (green spectrum). b) in presence of 1.0 equiv. of Zn^{2+} (blue spectrum). c) in presence of 5.0 equiv. of Zn^{2+}.

Part II: Chiroptical Properties of Cryptophane-[223] Subjected to Self-Encapsulation Phenomena

Chapter 1: Bibliography

Chapter 1: Bibliography

In the introductory chapter of the first part, we presented the main features of cryptophane derivatives. Among these features, we are particularly interested in investigating the symmetry and the inherent chirality of cryptophanes. Cryptophanes symmetry has an obvious impact on their complexation properties. Depending on the adopted configuration, i.e. *syn* or *anti*, cryptophanes can be chiral or achiral (see chapter I). For example, the *syn* derivative is achiral provided that the two CTB units and the three linkers are identical. Otherwise these *syn*-cryptophanes exhibit an inherently chiral structure. On the other hand, the *anti*-derivatives are always chiral regardless the nature of substituents and the linkers. Thus, many different chiral cryptophane derivatives can be prepared and each derivative is expected to exhibit characteristic chiroptical properties.

The chiroptical properties of enantiopure cryptophanes can be exploited to study the cryptophane itself (determination of the absolute configuration, molecular conformation in solution or in the solid state). More importantly, these chiroptical properties can be also used to study their interactions with chiral or achiral guests. Nowadays, chemists possess in hands a lot of chiroptical techniques to investigate these molecules and their complexes. For instance, the determination of the specific optical rotation can be achieved via optical rotation dispersion (ORD) or polarimetric measurement. Electronic and vibrational circular dichroism spectroscopies (ECD, VCD) are additional tools to characterize these molecules. These two techniques are complementary and they possess their own advantages and disadvantages. Recently, Raman Optical Activity (ROA) has emerged as another useful technique to gain information about the absolute configuration of organic molecules such as cryptophanes and their complexes. X-ray crystallography is another tool that can be used to characterize compounds in the solid state providing information about the absolute configuration of these molecules.

Chapter 1: Bibliography

In the following sections, we will provide a brief overview describing different examples of some reported chiral cryptophanes. We will mainly discuss the different approaches used to synthesize enantiopure cryptophane derivatives. Finally, we will describe the chiroptical properties of these cages and their complexes, which have been investigated by the different spectroscopic techniques mentioned above.

1. Examples on Chiral Cryptophanes

To start with the chiral cryptophanes, it is worth first to discuss the *anti*-cryptophane derivatives, which are numerous, compared to the chiral *syn*-cryptophanes. The first reported cryptophane cage is the *anti*-cryptophane-A **58**,[18] which possesses a D_3-symmetry. This particular arrangement results from a stereospecific replication of the parental CTB unit symmetry. With this example, a clear illustration of the inherent chirality was delivered. Apart from this example, other D_3-cryptophane derivatives were also described such as *anti*-cryptophane-E, which possesses three propylenedioxy linkers and six methoxy groups. So generally, *anti*-cryptophane derivatives bearing the same CTB substituents and linkers possess a D_3-symmetry.

A decrease of the molecular symmetry from D_3 to C_3 is obtained when one of the two CTB units carry three different substituents. For example, substituting the three methoxy groups of cryptophane-A by three hydrogen atoms on one CTB unit results the *anti*-cryptophane-C, **59**.[29] Other C_3-symmetrical cages were also recently reported based on the cryptophane-A skeleton, like cryptophane-[222] $(OCH_2CO_2H)_3$ $(OH)_3$.[174] Further decrease in cryptophanes molecular symmetry from D_3 to C_2 is achieved by changing one of the three linkers but keeping the same CTB substituents. For example, *anti*-cryptophanes-[223] **60**, [233] **61** or [224] **62** $(OMe)_6$ are all chiral with C_2-symmetry.[111] The crystal structure of compound *PP*-**60** assures its *anti*-configuration, Figure 88.

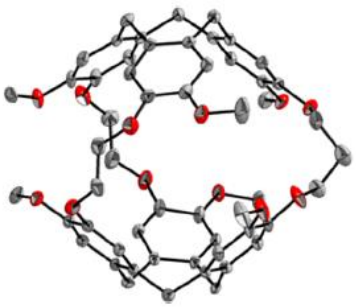

Figure 88: crystal structure of *PP*-**60**.

In the first chapter of this manuscript, we also reported a chiral C_2-cage with a [223] skeleton bearing a central alkenyl moiety on the propylenedioxy arm, compound **26**.[38] C_1-symmetrical cryptophanes are also numerous and they are obtained if cryptophanes possess different linkers or substituents. Cryptophane-[222] monoacid **63**, which is widely used for xenon-based biosensing applications has a C_1-symmtery is one example, Figure 89.[75] It is noteworthy that all the cryptophanes described in the second chapter of the first part possess C_1 symmetry except compound **26**.

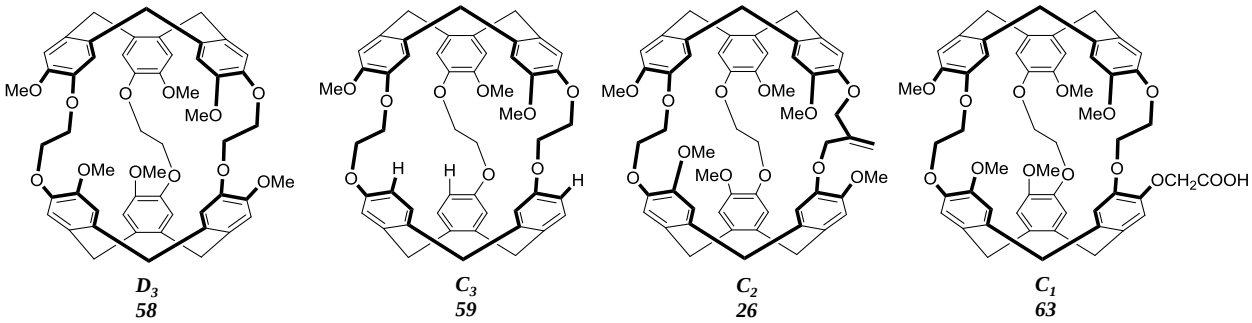

Figure 89: symmetry of some *anti*-cryptophane derivatives.

Syn-derivatives are less numerous but they constitute another interesting class of chiral cryptophanes. The first described chiral *syn*-cryptophane is cryptophane-D **64**, the diastereomer of cryptophane-C, **59** described above. Similar to compound **59**, this derivative has a C_3-symmetry. Other cages that bear the same symmetry are the thio-containing cryptophane **65** and the nona-methoxy cryptophane-[222], **66** derivatives shown in Figure 90.[175,176]

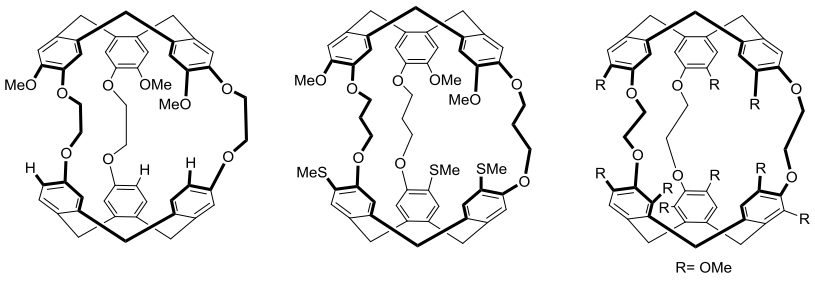

C_3 ***64*** ***C_3*** ***65*** ***C_3*** ***66***

Figure 90: chiral *syn*-cryptophane derivatives.

2. Synthesis of Enantiopure Cryptophane Derivatives

Chiral cryptophane derivatives are usually obtained as a racemic mixture. Therefore, the study of their chiral properties requires the separation of the two enantiomers. Several approaches can be tested to separate these enantiomers. For instance, asymmetric synthesis of these derivatives starting from enantiopure starting materials is one of the readily used approaches. The separation of the two enantiomers via the formation of a diastereomeric mixture can also be employed. Then, the diastereomers can be separated by different techniques such as column chromatography or crystallization. Finally, HPLC using a chiral stationary phase can be used to obtain these enantiopure molecules. All these techniques possess their own advantages and drawbacks as will be discussed in the following sections.

2.1. Enantiomerically Enriched Cryptophanes by Asymmetric Synthesis:

Enantiopure CTB units have been prepared to synthesize enantiomerically enriched cryptophanes with high ee. Collet and co-workers have used extensively this approach to prepare enantiopure cryptophane derivatives with D_3 or C_3-symmetry. This approach appears as an easy way to access these enantiopure molecules. Unfortunately, great care in the choice of the experimental conditions has to be considered since the CTB unit tends to easily racemize above

room temperature. Thus, under the experimental conditions required to perform the second ring closing reaction, a partial racemization is inevitable. Consequently, this approach only allows getting enantiomerically enriched cryptophane derivatives with a moderate to high ee (65 – 95%). Enantiopure CTB units, themselves can be synthesized from the trimerization of the properly functionalized enantiopure starting materials bearing a chiral auxiliary. This trimerization step results in the formation of two diastereomeric CTB units, which can be readily separated on silica gel. Recovery of the desired enantiopure CTB is then achieved by applying multistep reactions. For example, Collet and co-workers reported the synthesis of the two enantiopure cyclotriguaïcylene (CTG) (*M* and *P*), **72** units using α-bromo-propanoic acid as the chiral auxiliary.[177] The first step involved the cyclization of the optically pure vanillic alcohol derivative **67**, in $HClO_4$ (65%). This step afforded a diastereomeric mixture of the two CTB units, compounds **68**. An additional esterification step using diazomethane allowed the access of the two separated diastereomers, **69**. These two diastereomers were subjected to subsequent reactions to give the desired enantiopure CTG, **72,** Figure 91.

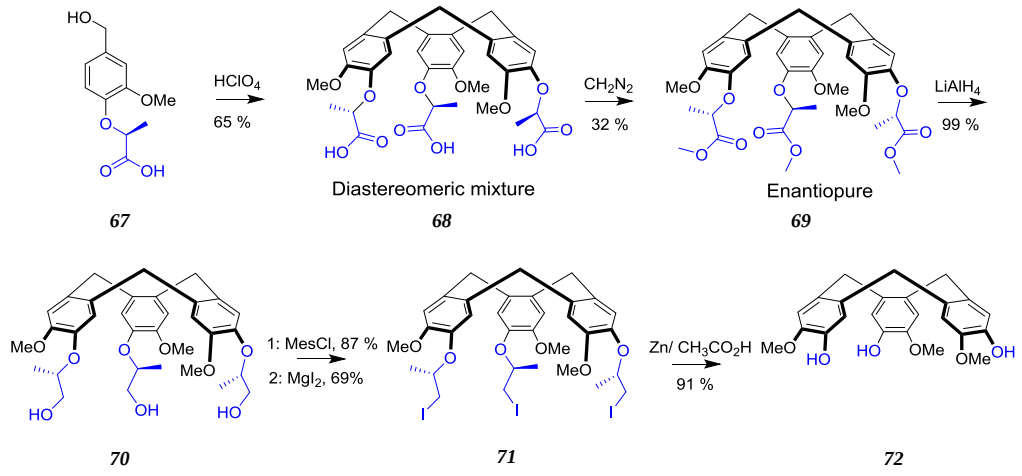

Figure 91: synthesis of enantiopure **72** from optically pure vanillic alcohol derivative **67**.

The second strategy overlies on reacting a readily trimerized CTB with a chiral auxiliary to form two diastereomers, which are separated by chromatography. For example, chiral auxiliaries like Ɠ-camphanic acid or *R*-(+)-2-phenoxypropanoic acids were employed and they were mildly removed after the separation.[178,154]

Exploiting the resolved CTB units, enantiomerically enriched cryptophanes were synthesized, like the cryptophane-A, **58**. The synthesis of *PP*-**58** starts with the preparation of the *M*-CTG, **72** followed by a substitution reaction to give the *P*-CTB template. Unlike the parental CTG units, cryptophanes are resistant to racemization at high temperature. Other enantiomerically enriched cryptophane derivatives with D_3-symmetry were also reported, like cryptophane-E or cryptophane derivatives bearing unsaturated linkers like compounds **73**, **74** and **75** shown in Figure 92.[18, 33, 34]

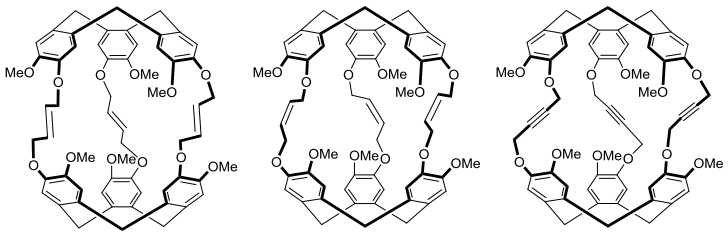

Figure 92: structure of enantiomerically enriched *MM-anti*-cryptophane derivatives having D_3-symmetry.

Enantiopure cryptophane-C, **59** was specifically synthesized to encapsulate enantiomerically enriched chlorofluorobromomethane, one of the simplest chiral compounds. Collet and co-workers reported the synthesis of this enantiopure cage by using a strategy similar to that reported for cryptophane-A. Thus, the enantiopure *M*-(+)-CTB $(OH)_3$, compound **76** was alkylated with substituted vanillic alcohol derivative **77** to give the desired *M*-template **78**. Cyclisation at 95 °C offered both the *syn-MP*-**64**, and *anti-MM*-**59** in 5% and 20%, respectively. These two diastereomers were easily separated by column chromatography, Figure 93.

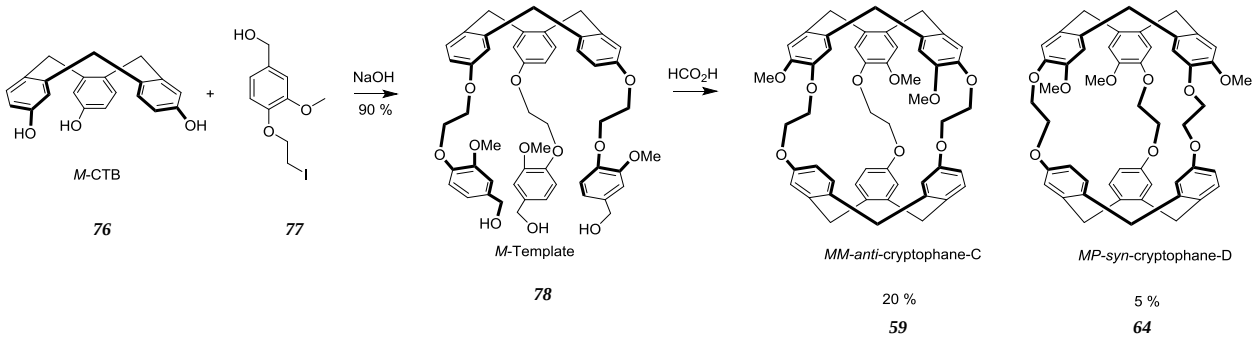

Figure 93: synthesis of enantioenriched **59** and **64**.

Recently, Crassous and co-workers have used this strategy to synthesize enantiomerically enriched thio-substituted cryptophanes **79**, Figure 94. These compounds have been obtained from the corresponding functionalized enantiopure CTB units. It is noteworthy that in this case, the second ring closing reaction gives rise to a significant racemization since the two *MM* and *PP* cryptophane enantiomers were obtained in an ee 81.6 and 65.6 %, respectively. This cryptophane was later used to determine the ee of enantioenriched chlorofluoroiodomethane derivative. The recognition process was studied by ^{19}F and ^{1}H NMR spectroscopy.[179,180]

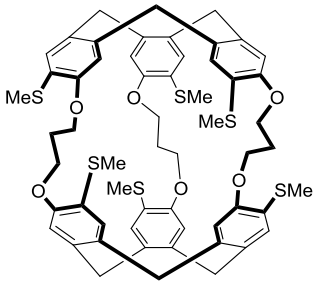

Figure 94: structure of the enantioenriched compound **79**.

It is worth to mention that the resolved cryptophanes obtained by enantioenriched CTB units have an ee between 65 and 99%. It is important to be aware for the unavoidable racemization of the enantiopure CTB units, which constitutes the main disadvantage of this method.

Unlike the CTB units, tribenzotriquinacenes or the so-called TBTQ possess a more rigid skeleton. Although structurally similar, TBTQ are resistant to temperature-induced racemization practiced by the CTB units. This difference is due to the additional methyl bridge fusing the three methylene bridges together. Resolving the two enantiomers of TBTQ derivatives can be achieved by several strategies. One strategy reported is based on breaking their C_{3v}-symmetry by mono-functionalizing one or the three arene rings leading to either a C_1 or C_3 symmetrical molecule, respectively. These inherently chiral molecules can eventually be used to build chiral self-assemblies. For example, the TBTQ derivative **80** bearing one functionalized aromatic ring was optically resolved using (*R*)-BINOL. The two obtained diastereomers (**81** is one of them) were separated by column chromatography in 34% and 33% yields. The saponification of these esters allows the recovery of the enantiopure TBTQ, **80** with 97% and 95%, Figure 95. The chiroptical properties of these two derivatives were studied by polarimetry and ECD spectroscopy.[45]

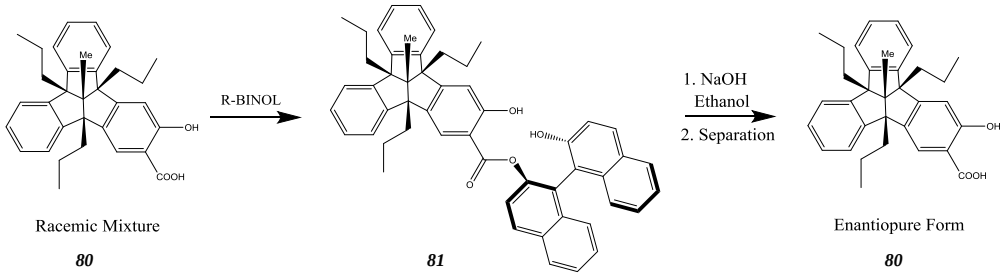

Figure 95: diastereoselective optical resolution of TBTQ derivative using *R*-BINOL.

Stereoselective and enantioselective synthesis of TBTQ was also achieved by employing bio-catalysis. Starting from four isomers of alcohol functionalized TBTQ **82**, one pair of

diastereomers (*M*,*R*) and (*P*,*R*) was selectively acylated using commercially available *Candida Antarctica lipase* to give two diastereomeric ester derivatives **83**. These compounds were then easily separated by column chromatography with a total yield of 48%. Enantioselective hydrolysis of the esters using *lipase PS* afforded the *P*-TBTQ derivative whereas using *Candida Antarctica lipase* the *M*-derivative was selectively hydrolyzed, Figure 96.[181]

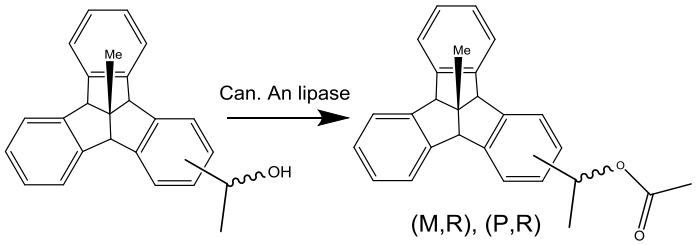

82 ***83***

Figure 96: bio-catalyzed stereoselective optical resolution of TBTQ.

In the first chapter, we have also described another method to obtain these compounds in their enantiopure form. Based on a previous work reported by Warmuth and co-workers, Kuck and co-workers synthesized a TBTQ based cryptophane by thermodynamic dynamic resolution approach. Thus, reacting racemic TBTQ trialdehydes with (*S*,*S*)-diaminocyclohexane offered three couples of cryptophane diastereomers (*P*,*P*,*S*,*S*,*S*) (*M*,*M*,*S*,*S*,*S*) (*P*,*M*,*S*,*S*,*S*) in 29%, 40% and 25% yields, respectively. These diastereomers were separated by chromatography and then hydrolyzed to give enantiopure TBTQ building blocks. Some derivatives of these molecules were used to build enantiomerically self-sorted nanotubes indicating their versatility to construct highly organized systems.[46] Therefore, these compounds offer many interesting possibilities to design enantiopure cages. However, their synthesis and functionalization are tedious; hence these compounds cannot be easily used in their enantiopure form to design MRI tracers for ^{129}Xe NMR applications.

2.2. Synthesis of Cryptophanes by Dynamic Resolution:

Using a thermodynamic dynamic resolution approach, Warmuth and co-workers have reported the resolution of CTB derivative **84** with high ee. The imination of a racemic mixture of CTB derivative functionalized by three aldehydes with two equivalents of (*R*,*R*)-diaminocyclohexane, **85** offered a unique (*P*,*P*,*R*,*R*,*R*)-cryptophane enantiomer **86** in an excellent 92% yield. In fact, the high reaction temperature and thermodynamic sink of the obtained cryptophane enantiomer were the main reasons behind this complete inversion. The hydrolysis of compound **86** in a mixture of trifluoroactetic acid and water gave the enantiopure (*P*)-**84** in 92% with a high ee (99%), Figure 97.[182]

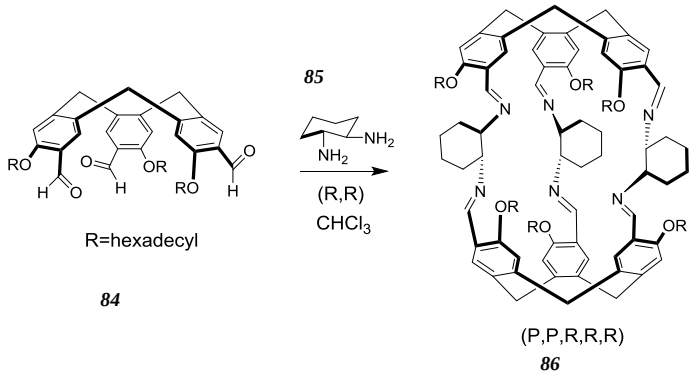

Figure 97: synthesis of (*P*,*P*,*R*,*R*,*R*)-cryptophane.

2.3. Enantiopure Cryptophanes by Separation of Diastereomers:

Synthesis of enantiopure cryptophane derivatives can also be achieved by reacting a cryptophane in its racemic form with a chiral auxiliary. This in turn leads to the formation of a diastereomeric mixture that can be separated by different techniques. Brotin and co-workers reported this approach in 2003, where they successfully obtained the two enantiomers of cryptophanol-A, **87**. In this synthesis, the only available hydroxyl group on the cryptophane-[222] skeleton was allowed to react with (1*S*)-(-)-camphanic acid chloride **88** leading to two

diastereomeric compound **89**. Thanks to the large difference in solubility between these two compounds, the separation of these diastereomers was made possible by crystallization from hot toluene. This allowed to collect the first diastereomer in approximatively 15% yield (ee=98-100%). The second enantiomerically enriched diastereomer was collected and then hydrolyzed under basic conditions. Reacting this compound with (1*R*)-camphanic acid chloride and applying the same procedure allowed to get the second diastereomer in 10% yield and ee = 98%-100%. Cleavage of the chiral auxiliary offered enantiopure cryptophanol-A, **87**, Figure 98.[183,78]

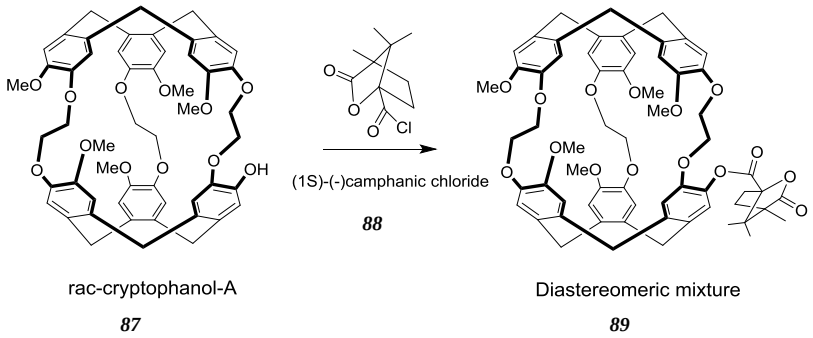

Figure 98: resolving cryptophanol-A by forming diastereomers with camphanic acyl chloride.

The enantiopure compound **87** was subjected to various chemical transformations to give new enantiopure cryptophanes. The interest of this approach lies on the fact that no racemization takes place compared to the CTB based method. Thus, new enantiopure cryptophanes with different symmetry can be easily obtained by this way, whatever the experimental conditions (high temperature, solvents…). As an example, we can report the synthesis of some other enantiopure cages starting from *PP* and *MM*-cryptophanol-A. For example, enantiopure cryptophane-A was prepared from enantiopure cryptophanol-A. The latter was then demethylated with excess of $LiPPh_2$ to give the enantiopure hexa-hydroxyl cryptophane, **90**, with an excellent yield.

Subsequent alkylation and hydrolysis allowed the formation of an enantiopure cryptophane with six carboxylic acid functions.[184,185]

Following the same approach, Dmochowski and co-workers synthesized enantiopure trisubstituted cryptophane-A derivatives. Racemic mixture of tri-hydroxyl cryptophane-A, **91** was resolved by esterification with (*S*)-Mosher's acid, **92** to give two diastereomeric compounds **93**, which were separated by column chromatography. The overall yield was 70% with 35% yield per each compound, Figure 99. The enantiomeric purity w

as assessed by ECD. The chiral auxiliary was then removed by hydrolysis under basic conditions without any loss of optical activity. Further functionalization of the two isomers resulted new cryptophanes of various applications.[186]

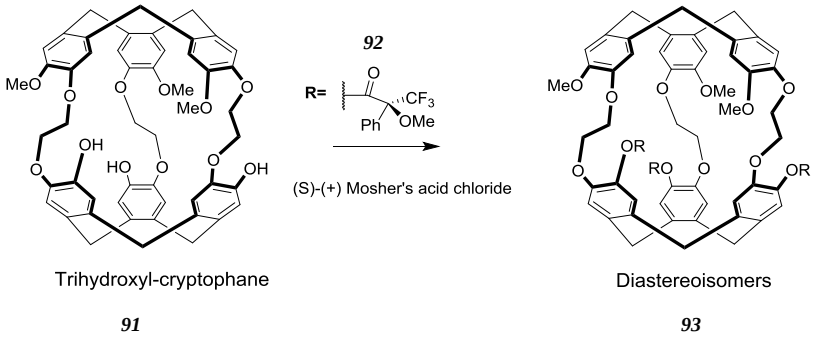

Figure 99: resolving tri-hydroxy cryptophane-[222] by Mosher's acyl chloride.

Although this strategy offers the cryptophane derivatives in excellent enantiomeric excess compared to the CTB-based method, this approach requires more synthetic steps and optimization of the separation step for each diastereomer.

2.4. Resolving Cryptophanes by HPLC:

Resolving cryptophanes by HPLC has gained a great attention in the last few years since this approach does not necessarily require chemical transformations. The method solely lies on using

a suitable chiral stationary phase to separate the two enantiomers. The main inconvenience of this technique is its limitation to small-scale separation due to the high cost of semi-preparative columns, sensitivity and large volumes of mobile phase. This method also requires optimization of the separation conditions that can be difficult in some cases. Solubility issues of the racemic material have also to be taken into consideration.

Collet and co-workers in 1989 reported the first use of HPLC on chiral stationary phase to separate various CTB and cryptophane derivatives.[187] At that time, the increased applications of cryptophanes as chiral hosts rendered it important to develop a new analytical tool for their optical resolution. Chiralpak OT-(+) was used as the stationary phase to separate these compounds but this stationary phase suffers from low stability over time. Nevertheless, several CTB and cryptophanes were efficiently resolved as pointed previously. Table 4 summarizes the results obtained for few cryptophane derivatives. For instance, cryptophane-A, **58** was efficiently resolved into its enantiomers *M*-(+) and *P*-(-) using methanol as an eluent. The two enantiomers of cryptophane-A, *PP*-cryptophane-A and *MM*-cryptophane-A appear at 22.1 and 30.0 min, respectively.

Symmetry	**R**	**Bridges**	**Retention time (min)**	
D_3	OMe	$O(CH_2)_2O$	22.1(+)	30.0(-)
D_3	OMe	$O(CH_2)_3O$	27.4(+)	37.6(-)
D_3	OMe	$O(CH_2)_4O$	30.3(+)	75.3(-)
D_3	OMe	$O(CH_2)_6O$	38.9(+)	54.9(-)

Table 4: analysis of D_3-cryptophanes by chiral pack-OT (+), the (+) and (-) signs correspond to the SOR sign recorded at 589 nm.

Chiralpak OT-(+) was also employed to separate enantiopure cryptophane bearing aromatic bridged linkers. Thus, *anti*-cryptophane **94** bearing three ortho-substituted aromatic linkers was resolved using the latter chiral column. The two enantiomers appeared at 23.7 and 39.4 minutes, respectively. Same conditions were used to get cryptophane **95** with retention times 36.5 and 73.0 minutes, Figure 100. These molecules were used to encapsulate various ammonium salts.[35,188]

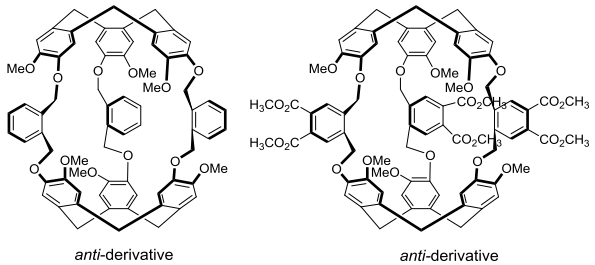

Figure 100: optically resolved cryptophane bearing benzyl substituted linkers.

More recenly, enantiopure nona, **66** and dodecamethoxy **96** cryptophanes were resolved using new chiral HPLC columns. The *anti* and *syn*-isomers of cryptophane **66** show an inherently chiral structure (C_3-symmetry). For *anti*-**66**-cryptophane, an efficient separation was obtained using Chiralpak IB with ee ≥ 99.5% for both enantiomers. On the other hand, the two enantiomers of the the *syn*-diastereomer have been separated by using a Chiralpak IA column chromatography (ee ≥ 98.5%). In the case of cryptophane **96**, only the *anti*-diastereomer is chiral and has a D_3 symmetry. The two enantiomers of this derivative were separated by using Chiralpak ID column chromatography. Typically, a separation performed on a semi-preparative column allows to isolate few hundreds of mg of enantiopure compounds, which are sufficient to achieve a thourough study of chiroptical properties.[176]

Cryptophane with C_2-symmetry have also been separated by chiral column chromatography. For instance, compounds **60** and **61** bearing one and two propylenedioxy linkers have been separated

with chiralpak IA column. A detailed study of chiroptical properties has been reported by polarimetry, ECD, VCD and ROA and it will be discussed later.[189]

Interestingly, using a Chiralpak ID column, cryptophane derivatives with no substituents have been successfully separated. Thus, several hundreds of mg of the two enantiomers of cryptophane-[111] **97** and cryptophane-[222] **98** have been obtained. This allowed a detailed description of the chiroptical properties of these two derivatives, Figure 101.[190, 191]

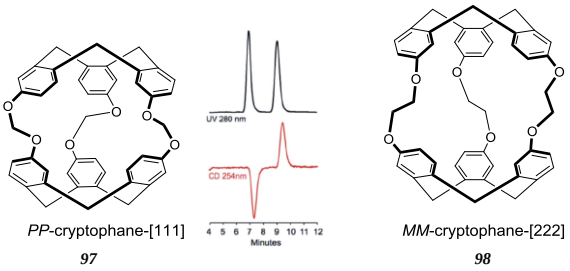

Figure 101: structure of cryptophane-[111] **97** and the corresponding retention time of each enantiomer. On the right shown the structure of cryptophane-[222] **98**.

Optical resolution of dually functionalized cryptophane **12** bearing a unique secondary alcohol on its propylenedioxy linker was also reported using chiral HPLC with high ee ≥ 99.5%. This cage showed a high affinity towards Cs^+ and Tl^+ cations, Figure 41.[64]

Cryptophane-[222] $(OH)_5$, **99** is an interesting molecular host capable of binding a large range of guest molecules. For this purpose, the two enantiomers of this molecule were separated in order to investigate how the presence of a guest molecule affects its chiroptical properties. Two different approaches have been used to get the two enantiomers of compound **99**. The first approach lies on the separation of two diastereomeric compounds as described previously in the above section. This method is time consuming but it allows us to obtain these compounds with high ee and in fair quantities to perform the chiroptical studies. More recently, a simplified time saving approach was used instead, based on chiral HPLC separation of the penta-acetate

derivative **100**. This derivative, which is the protected version of compound **99**, was chosen due to its enhanced solubility. Thus, a Whelk-O1 column was used as the stationary chiral phase to offer the two enantiomers of the compound **100** with excellent ee ≥ 99%. The latter was then subjected to an alkaline hydrolysis to give the targeted enantiopure cryptophane derivative.[61, 60] It is noteworthy that in this example the descriptors of compound **99** and **100** are inverted. Thus *PP*-**100** gives rise to the *MM*-**99,** Figure 102.

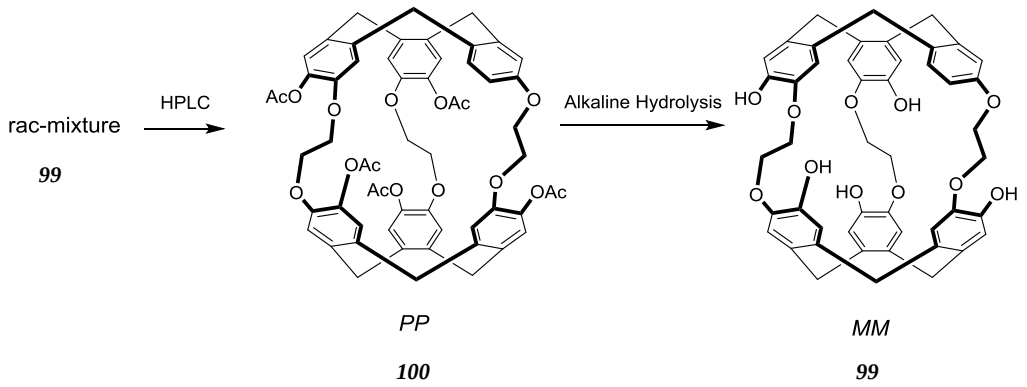

Figure 102: synthesis of enantiopure hepta-hydroxyl cryptophane-[222].

2.5. Synthesis of Chiral Metallo-Cryptophanes:

The synthesis of multi-dimensional supramolecular structures can be achieved by different methods and coordination driven self-assembly is one of them. A particular interest is given to metallo-cages, which are made up of multi-dentate ligands and metal cations due to their potential applications in catalysis, separation, molecular recognition, and nanoscale vessels.[192,193] The first described self-assembled coordination driven cryptophane cage was reported in 2001 by Zhong and co-workers. In this paper, racemic pyridyl CTB derivative, **101** was self-assembled into $[Pd_3\mathbf{101}_2]^{6+}$ as the *meso-syn* cryptophane, **103** and chiral *anti*-cryptophanes **104** by the coordination with *cis*-protected palladium salts, **102**. Inter conversion between these two *syn* and

anti-structures was observed and fastened by increasing the molar ratio of the **101** with respect to the metal source Figure 103. The tunable character of these cages is advantageous as they would change their properties in response to the guest molecule.[194]

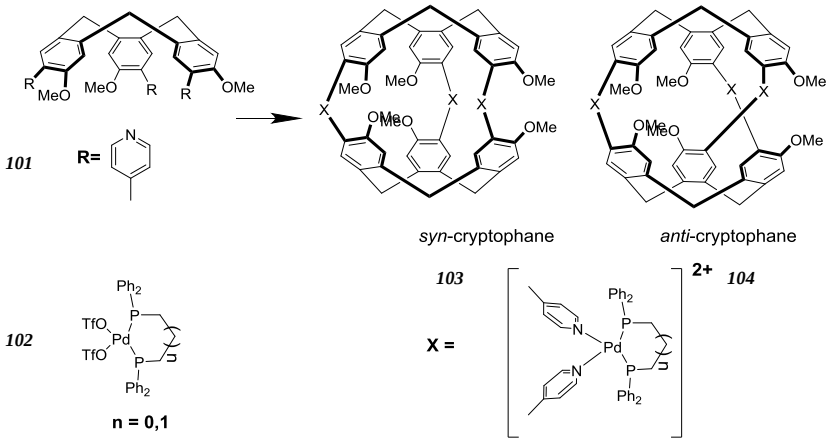

Figure 103: synthesis of Pd-based metallo cryptophanes.

In another example Hardie and co-workers reported the synthesis of emissive Ir^{3+} metallo-cryptophanes starting from CTB derived ligands **105** shown in Figure 104 and (L,D)-[Ir-$(ppy)_2(MeCN)_2]\cdot X$ ($X=PF_6$, BF_4), **106** as the metal source. These molecules undergo homochiral self-sorting of the ligands in solution and in the solid state leading to chiral *anti*-cryptophanes **107**, Figure 104. This process is enhanced in the presence of enantiopure chiral guest like *R*-camphor.[195]

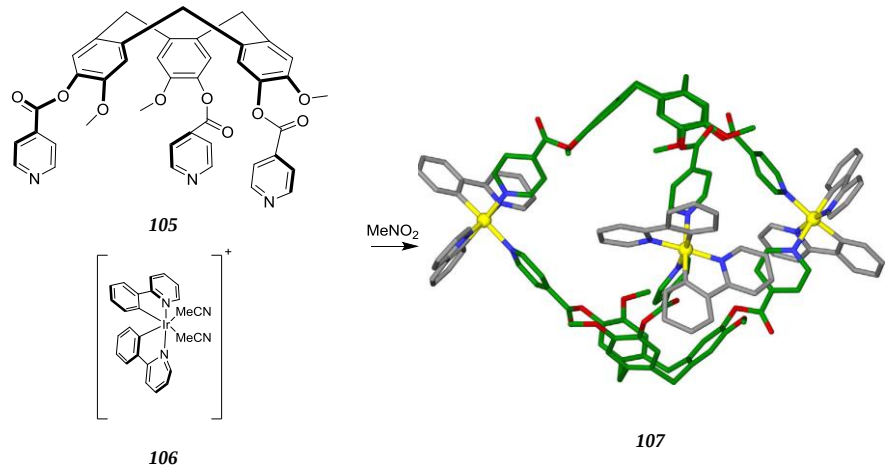

Figure 104: synthesis and crystal structure of emissive *anti*-cryptophane.

Finally, Chambron and co-workers reported the synthesis of chiral *trans*-metallo-cages resulting from the reaction of nitrile-functionalized CTB, **108**, with $[Pd(dppp)][OTf]_2$. The reaction was completely stereoselective favoring the *anti*-$[Pd_3(dppp)_3(\mathbf{108})_2][OTf]_6$ as proved by proton and carbon NMR and crystal structure. The homochirality of these cages is due to the satisfaction of the square planar geometry of the palladium and the platinum centers by the coordination with the triply coordinated **108** derivatives, Figure 105.[196]

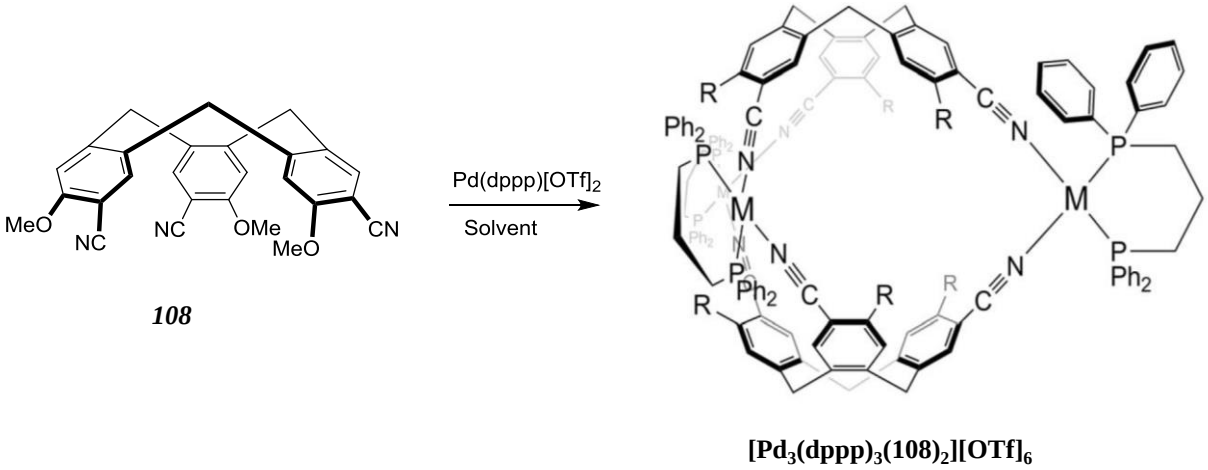

Figure 105: nitrile-functionalized CTB unit and the synthesis of metallo *anti*-cryptophane derivative.

3. Chiroptical Properties of Cryptophane Derivatives and Their Complexes

The access of enantiomerically pure cryptophanes allows us to investigate their chiroptical properties. These properties have been heavily exploited to assign the absolute configuration of cryptophanes and to gain insights about the conformation of these molecules in solution. Finally, the presence of a guest inside the cavity of the host might also modify the overall chiroptical properties of the host molecule. Interestingly, a large range of techniques such as ECD, VCD, ROA and ORD and X-ray crystallography can be used to study the chiroptical properties of these molecules. We will describe in the appendix section briefly the principle of these spectroscopic techniques. Through selected examples, which have been reported in the literature, we would like to show how these chiroptical techniques serve to characterize cryptophanes and their complexes. ECD spectroscopy is one of the earliest chiroptical methods used to study enantiopure cryptophane derivatives. Collet, Gotarelli and co-workers pioneered this work by studying enantiomerically enriched cryptophanes with D_3 and C_3-symmetry. Based on the Kuhn-Kirkwood-coupled oscillator model, these authors were able to predict the shape of the ECD spectra of cryptophane-A and its congeners. For instance, in the case of the cryptophane-A derivative with D_3-symmetry, this model predicts that each transitions ^1L_b, ^1L_a and ^1B_b (Platt's notation) visible on the UV-visible spectrum (210-310 nm) can be decomposed into three excited states due to the resulting excitonic coupling. Each of these excited states possesses its own rotational strength that determines the intensity and the sign of the ECD bands. The obtained ECD spectrum is the result of the contribution of all these excited states. The ECD spectrum of *PP*-cryptophane-A has been reported in Figure 106. This ECD spectrum shows several Cotton bands with positive or negative signs. The two first bands observed between 260 and 310 nm can

be assigned to the Cotton bands of the ^1L_b transition. Then, the negative-positive bisignate (230-260 nm) corresponds to the ECD bands of ^1L_a transition. It has been observed, by analogy, with other cryptophane-A congeners that this bisignate can be extremely useful to assign the absolute configuration of cryptophane derivative in organic solvents. Indeed, in contrast to the ECD bands of the ^1L_b transitions, which are very sensitive to structural modifications and other external factors, the sign of this bisignate is robust and characteristic of the absolute configuration of the molecule. The negative-positive bisignate observed in Figure 106 allows us to assign the *PP* absolute configuration to the (+)-cryptophane-A derivative. Finally, the strong ECD band observed in the region of 220 nm corresponds to the ^1B_b transition.

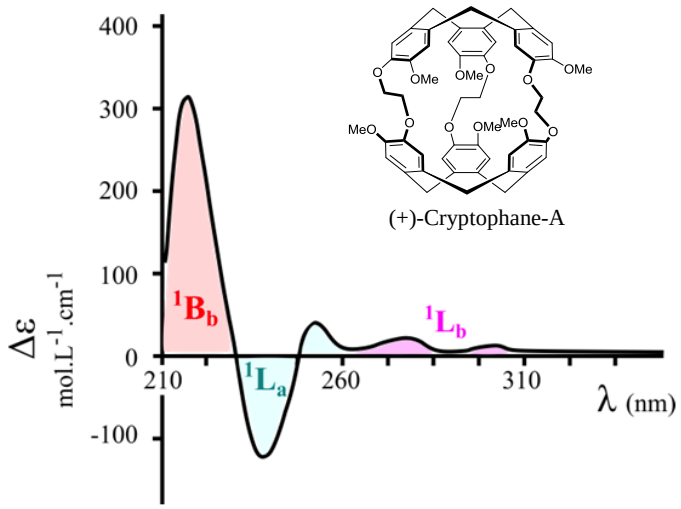

Figure 106: ECD of (+)-cryptophane-A spectrum of 1,4-dioxane.

Since the work of Collet and co-workers, numerous enantiopure cryptophane derivatives have been studied by ECD spectroscopy both in organic solvents and in aqueous solutions. Thus, numerous cryptophane derivatives having different symmetry have been investigated and in some

cases their ECD spectra have been predicted thanks to the use of TD-DFT calculations.[71] From a general point of view, it has been observed that ECD spectra recorded in organic solvents are not very sensitive to a change of the nature of the solvent.[183] Spectral ECD modifications take place mainly in the ^1L_b and ^1B_b regions of the ECD spectrum and a change in the nature of the organic solvent slightly affects the ECD spectra. Moreover, more pronounced changes are sometimes observed with the SOR values in terms of sign and magnitude. At first sight, this may appear surprising since the ECD and SOR values are strongly related. An interesting example is observed with cryptophane-[222], **98** devoid of any substituents whose ECD spectra recorded in several organic solvents are almost identical in shape and intensities. In contrast, the SOR values recorded in the same solvents show large variation in intensities. In addition, the sign of these SOR values can be different depending on the solvent and wavelength.[191] This behavior has been attributed to tiny conformational changes that the molecule can adopt in solution. Interestingly, this unusual example reveals that in the case of cryptophane derivatives, polarimetry or ORD spectroscopy is much more sensitive to reveal small conformational changes in organic solvent. Another interesting example will be discussed in the next chapter that describes the unusual behavior of cryptophane derivatives subjected to self-encapsulation.

It is noteworthy that this situation can be different in aqueous solution. For instance, it has been observed that the ECD spectra of enantiopure cryptophanes **90** bearing six phenol groups can be extremely sensitive to the nature of guest molecule and the nature of the aqueous solution. An example is reported in Figure 107 that shows ECD modifications upon complexation in LiOH solution. In Figure 107, it can be noticed that large spectral modifications occur in ^1L_b and the ^1B_b regions of the spectrum depending on the nature of the guest. For instance, in presence of $CHCl_3$, the ECD spectrum shows between 270 and 330 nm a broad negative ECD band whereas several positive and negative Cotton bands are observed in absence of a solvent molecule or in presence

of CH_2Cl_2. Large spectroscopic changes are also observed in the ^1B_b region of the spectrum. These spectral changes are the consequences of conformational changes induced by the nature of the encapsulated guest. Indeed, the nature of the guest and in particular its molecular volume imposes the host molecule to change its molecular conformation to maximize interactions. Additional hydrophobic effect may contribute to these changes.[184]

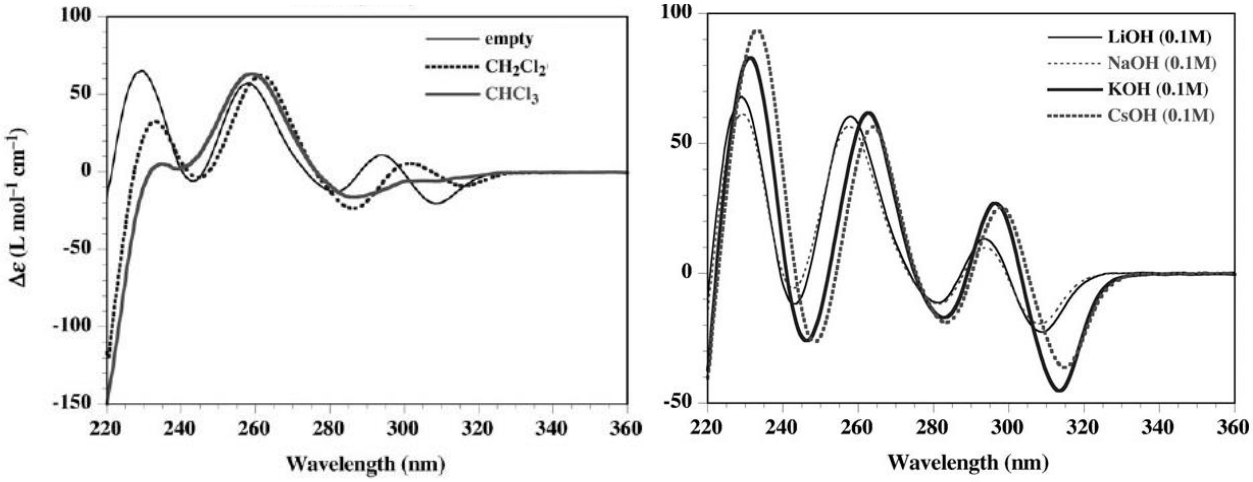

Figure 107: ECD spectra of empty free *MM*-**90** and in the presence of CH_2Cl_2 and $CHCl_3$ in LiOH (0.1 M) shown on the left. On right is shown the ECD spectra of *MM*-**90** in solutions of LiOH, NaOH, KOH, and CsOH in H_2O (0.1m).

It has also been observed that a change of the nature of the solvent had a tremendous effect on the shape of these ECD spectra. Replacing, LiOH by CsOH solution resulted in important spectral changes. For instance, we observed a slight bathochromic shift of the whole ECD spectrum but we also noticed that this ECD spectrum remains unchanged upon addition of CH_2Cl_2 or $CHCl_3$. Subsequent investigations have revealed that cationic species such as rubidium, cesium and even thallium are strongly encapsulated. For instance, ITC experiments allow us to measure very high binding constants $K = 3.80 \times 10^8\ M^{-1}$ and $K = 2.39 \times 10^9\ M^{-1}$ in LiOH (0.1 M) for cesium and thallium cations, respectively.

The strong affinity of host **99** bearing five hydroxyl groups for cesium and thallium cations can be assessed by ECD spectroscopy. Indeed, upon addition of these cationic species a strong change of the whole spectrum takes place. These spectral changes are strongly dependent on the experimental conditions. Figure 108 shows the differences observed when the initial cage is empty or when it contains a chloroform molecule inside the cavity. Particularly, upon addition of cesium cations to a free cryptophane cage, a bathochromic shift was observed along with an increase of the ECD component located at 315 nm and a decrease of the component located at 300 nm in the $^{1}L_{b}$ region is observed. A change in the $^{1}B_{b}$ transition is also detected. The obtained isobestic points indicate the formation of the cesium complexes. Addition of cesium to a chloroform saturated cage induces huge spectral changes especially in the $^{1}B_{b}$ region, where the latter significantly decreased upon cesium complexation. This spectral region allows us to extract information about the conformational changes taking place upon the replacement of chloroform by the smaller cesium cation. Since then, this work has been extended to study the complexation of cationic species by other cryptophane derivatives.[197,64,52]

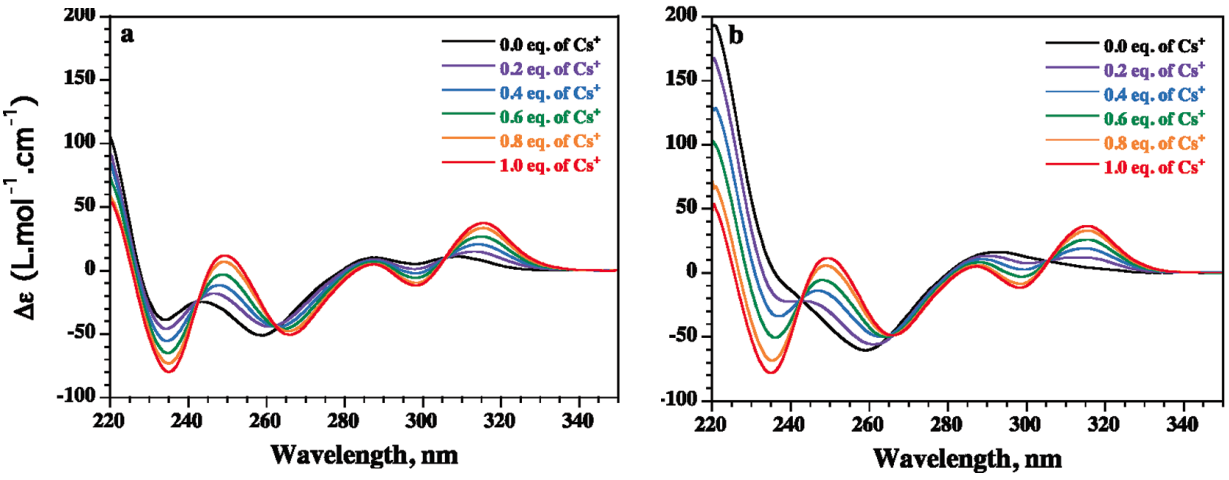

Figure 108: ECD spectra recorded at 293 K of *PP*-**99** (from 6.5 to 8.5 × 10^{-5} M): (a) in LiOH/H_2O solution (0.1 M) in the presence of different amounts of a CsOH/H_2O solution; (b) in a saturated solution of $CHCl_3$ in LiOH/H_2O in presence of different amounts of a CsOH/H_2O solution. [197]

Besides these studies involving cationic species, water-soluble enantiopure cryptophanes have been used to study the encapsulation of small chiral molecules. Due to their small molecular volume, small oxirane derivatives are well adapted to perform these studies. For instance, it has been shown that methyl oxirane and its congeners fit well the cavity of the penta-hydroxy derivative **99**. Interestingly, it has been demonstrated that this cryptophane was able to achieve in basic aqueous solution enantioselective encapsulation. This enantioselective complexation can be easily detected by ^{1}H NMR spectroscopy thanks to the high-shielding effect induced by the six aromatic rings surrounding the guest molecule. In addition, it has been observed that the different diastereomeric complexes give rise to different ECD spectra. Even though these differences are small they cannot be the consequence of artifact, Figure 109.

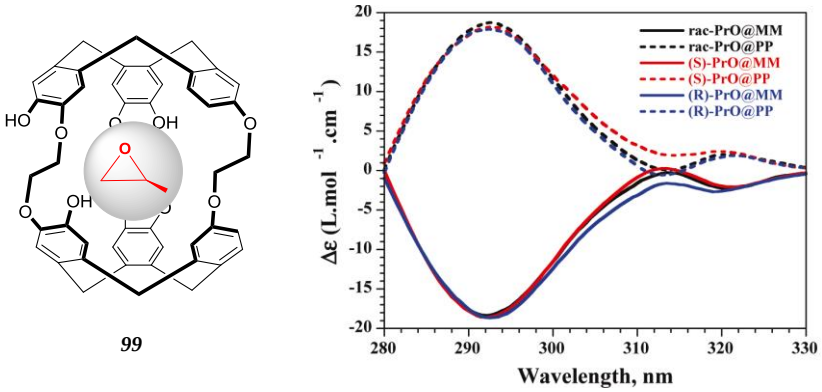

Figure 109: structure of (*S*)-methyl oxirane@*MM*-cryptophane **99**, and the corresponding ECD spectra of *MM*- **99** and *PP*-**99** in the presence of *rac*-oxirane, (*S*)-oxirane, and (*R*)-oxirane in NaOH/H_2O solution (0.1 M) at 293 K. The concentration of *MM*-**99** and *PP*-**99** was taken in the range 5×10^{-5} and 5×10^{-4} M.

Another example has been reported with cryptophane **99** and bioxirane. Bioxirane is an interesting example since this compound possesses two stereogenic centers; hence there exist three isomers, the *RR*, *SS* and *meso*-bioxirane. Thus, in presence of enantiopure compound **99**, three different diastereomeric complexes can be formed in solution. As for the methyl oxirane

complexes, ^{1}H NMR and ECD spectroscopies allows us to distinguish the three diastreomers formed in solution, Figure 110.[61, 60]

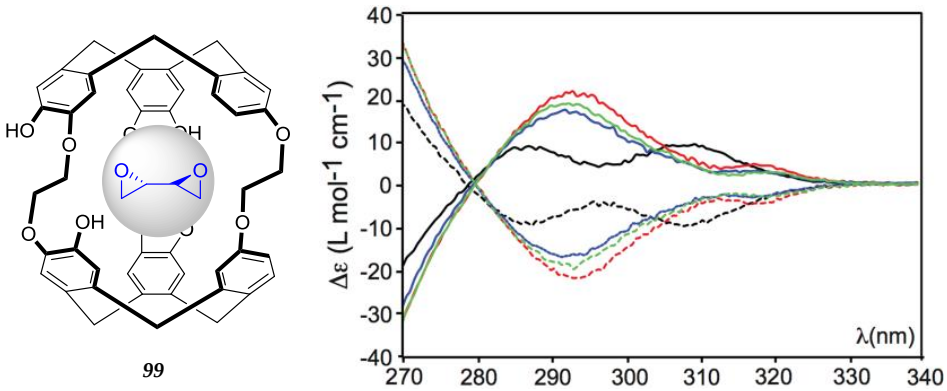

Figure 110: structure of (*S*,*S*)@*MM*-**99** complex, ECD spectra of (*R*,*R*)-bioxirane@*PP*-**99** (red), (*S*,*S*)-bioxirane@*PP*-**99** (blue), *meso*-bioxirane@*PP*-**99** (green), and guest-free *PP*-**99** (black spectrum). ECD spectra of (*S*,*S*)- bioxirane@*MM*-**99** (red dashes), (*R*, *R*)-bioxirane@*MM*-**99** (blue dashes), meso-bioxirane@*MM*-**99** (green dashes), and guest-free *MM*-**99** (black dashes). The spectra were recorded at 278 K in NaOH/H_2O (0.08 M) solution. [Host] = (6.2–8.8) × 10^{-5} M, [guest] = 0.06 M.

Vibrational Circular Dichroism is another powerful technique that has raised considerable interest over the two last decades.[198] This technique has been largely used to characterize enantiopure cryptophane derivatives. For instance, Brotin and co-workers reported in 2006 the first VCD spectra of the two enantiomers of cryptophane-A derivative, Figure 111. This study represented the first direct determination of the absolute configuration of this derivative thanks to the use of DFT calculations aimed at reproducing the experimental spectrum. Thus, from these experiments the *MM* absolute configuration could be attributed to the $(-)_{589}$-cryptophane-A derivative. In turn, the *PP* absolute configuration could be attributed to the $(+)_{589}$-cryptophane-A.[199] It is noteworthy that the absolute configuration of this derivative was previously determined indirectly from the knowledge of the absolute configuration of the corresponding CTB unit.[34] Besides, this study allowed us to gain information about the conformation of the linkers in solution. This study was somehow complicated and time demanding considering all the possible conformations that the

three linkers can adopt in solution. In this example, our results reveal that the linkers of the $CHCl_3$@cryptophane-A complex adopt mainly an all *trans* conformation. This conclusion is reasonable considering the large molecular volume of the guest (V_{vdw} = 72 $Å^3$). Cryptophane-[111], **97** bearing three methylenedioxy bridges constitutes the simplest case and a model molecule to be studied by VCD spectroscopy. Indeed, this molecule offered many advantages because no solvent molecule can enter its cavity and this compound has limited number of conformations that simplifies the DFT analysis. Thus, this compound was very easy to analyze and the DFT calculation reproduces very well the experimental VCD spectrum.[190]

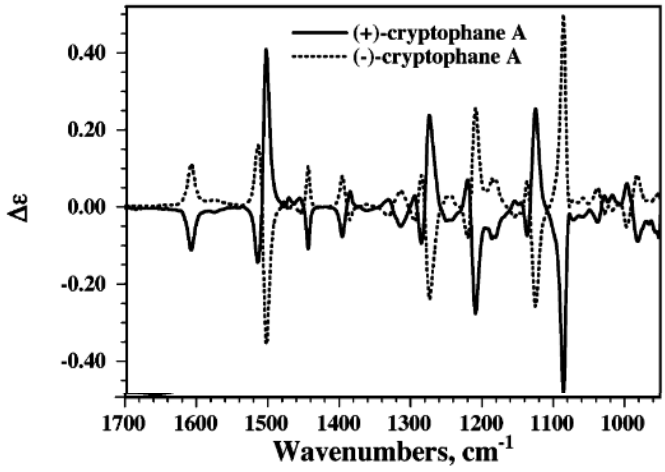

Figure 111: VCD spectrum of cryptophane-A in $CDCl_3$.

Since then many other cryptophane derivatives have been studied by VCD spectroscopy. From a general point of view, the VCD spectra are not very sensitive to a structural change of the cryptophane skeleton. For instance, a series of cryptophane-A congener with C_1-symmetry results in a very similar VCD spectra.[200] The same trend was also observed with cryptophane derivatives with C_2-symmetry such as cryptophane-[223] **60** and cryptophane-[233] **61** bearing different linkers. [189] Highly substituted cryptophane also resulted in a very similar spectra.[71] To date, the only cryptophane derivative leading to pronounced VCD changes was the cryptophane-[222] **98**

devoid of methoxy substituents. In this case, the authors have noticed large differences between the VCD spectrum of cryptophane-A and that of cryptophane-[222]. It is noteworthy that this cryptophane shows a very flexible skeleton that complicates the prediction of its conformation in solution by DFT calculation.[191]

In aqueous solution the recording of VCD spectra is more complicated due to the strong absorption of infra-red radiation by water molecules. Nevertheless, good quality VCD spectra in aqueous solution can be recorded by reducing significantly the path-length of the cell. In the case of water-soluble cryptophane derivatives, VCD spectra have been recorded to study the encapsulation of solvent molecules, xenon or cationic species. For instance, it has been shown in the case of cryptophane **90** that the encapsulation of guest molecules with different size resulted in large spectroscopic changes, Figure 112. These spectral modifications are characteristic of the conformational changes of the host molecule upon binding.[184]

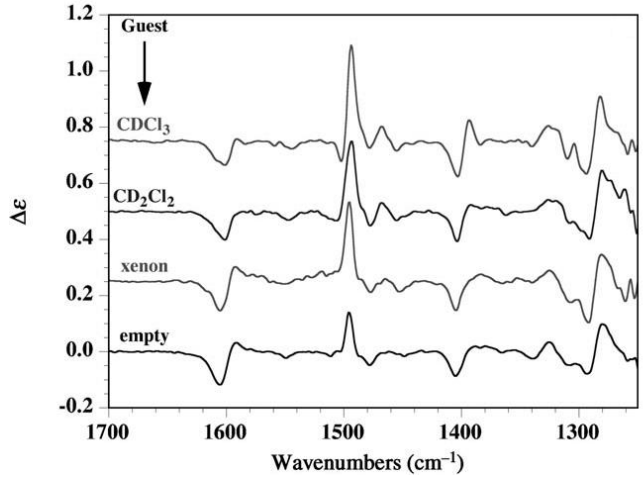

Figure 112: comparison of the VCD spectra of *PP*-compound **90** dissolved in D_2O in the presence and the absence of a guest molecule.

Raman Optical Activity (ROA) is another technique, which has been used extensively to characterize cryptophane derivatives. Readers interested in this chiroptical technique can refer to

some selected references.[201, 202] ROA spectroscopy allows us to investigate the near infra-red region and typically ROA spectra can be recorded up to 100 cm^{-1}. This represents an undeniable advantage compared to VCD spectroscopy. In the case of cryptophane derivative, ROA spectroscopy has been used as a complementary technique to determine the absolute configuration of cryptophane derivatives even though DFT calculations are more complicated to perform.

An interesting example has recently been reported with cryptophane-[111], **97**. In this example, Buffeteau and co-workers showed that ROA spectroscopy could be used to characterize the xenon@**97** complex. Figure 113 shows the ROA spectra of cryptophane-[111] recorded in the absence and in the presence of xenon. It can be noted that these two spectra are superimposable over a very large spectral range except a 190 cm^{-1}, where a clear difference can be observed. DFT calculations reveal that this vibration mode can be interpreted as the *breathing mode* of the host molecule. Upon the presence of xenon inside the cavity this mode is altered. This example clearly shows that ROA can be a useful complementary tool to characterize cryptophane molecules and their complexes.[190]

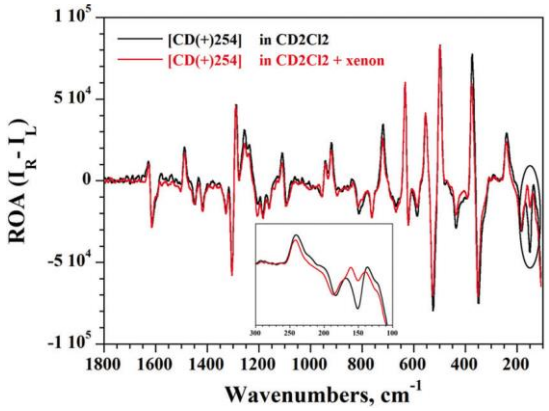

Figure 113: comparison of experimental ROA spectra of [CD(+)254]-**97** in CD_2Cl_2 solution in presence (red spectrum) or not (black spectrum) of xenon.

4. Objectives

Cryptophanes chiroptical properties have enormously served to determine their absolute configuration, and study their different conformations. In particular, a better vision of cryptophanes conformations facilitates the understanding of their complexation properties. For example depending on the guests' size and shape cryptophanes' arms can adopt different conformations to maximize host-guest interactions.

During our journey in the development of new cryptophane-[223] type derivatives bearing a functionalized propylenedioxy linker, we have evidenced a new conformation adopted by these cryptophanes. This phenomenon is referred to as "self-encapsulation", in which the molecule tends to fill its cavity by its own functionalized propylenedioxy arm in the absence of a potential guest. This phenomenon is solvent dependent and takes place at room temperature, Figure 114. An in-depth investigation of the effect of this phenomenon on the cryptophanes chiroptical properties will be delivered using different chiroptical techniques. This will allow evaluating the robustness of these chiroptical techniques in response to this particular conformational change.

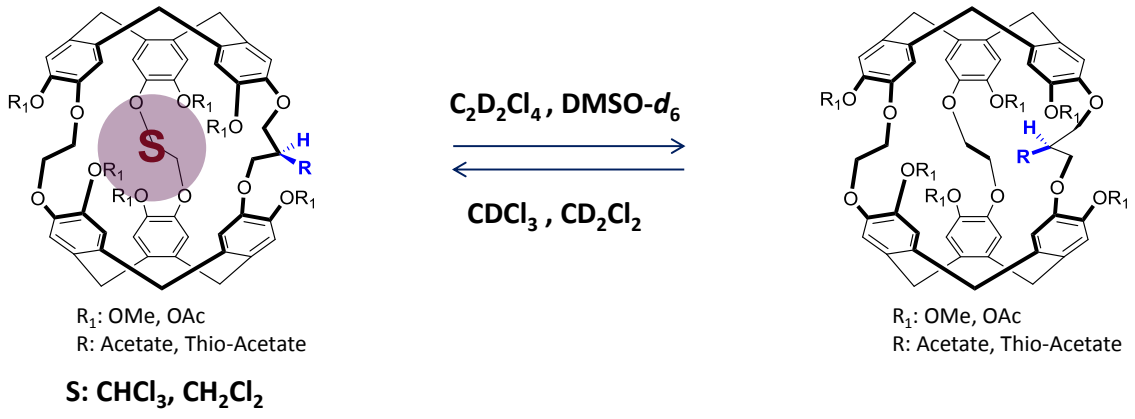

Figure 114: solvent dependent self-encapsulation phenomenon of cryptophane-[223] derivatives.

Chapter II: Self-Encapsulation: Chiroptical Aspects

1. Evidencing a New Conformation of Cryptophanes

Cryptophanes are flexible molecular cages that adopt different conformations depending on their structures and experimental conditions applied. In the introductory chapter of the first part, we have presented the several conformations that cryptophanes' CTB units can take in solution or in the solid state. Most of these conformations form when the molecule is stored for a long time in the solid state or when heated at elevated temperature. These conformations are also easily obtained if the cage has sufficiently long linkers, which imposes higher flexibility. Surprisingly, we have also observed that the presence of bulky substituents (benzyl esters for instance) on the CTB units facilitates the formation of the imploded form known as crown-saddle. Most of cryptophanes conformations are heavily described by means of ^{1}H NMR and X-ray crystallography, where a clear understanding of this arrangement is delivered, however, none of these studies investigated the impact of these conformational changes on their chiroptical properties.[47,49]

Recently, our group reported the synthesis of a cryptophane-[223] derivatives with functionalized propylenedioxy arm for xenon biosensing applications.[41] Particularly, a cryptophane-[223] platform bearing seven acetate groups, compound **109**, showed an unusual behavior upon xenon complexation. Compared to its structural congener **13**, compound **109** showed a broadened ^{129}Xe NMR signal in 1,1,2,2-tetrachloroethane-d_2. This strange behavior is characteristic of a fast in-out exchange kinetics of xenon and can be rationalized by the fact that cryptophane's cavity is less accessible to xenon. This result seems to indicate that the cage is adopting a conformation that makes its cavity less accessible to xenon, Figure 115.

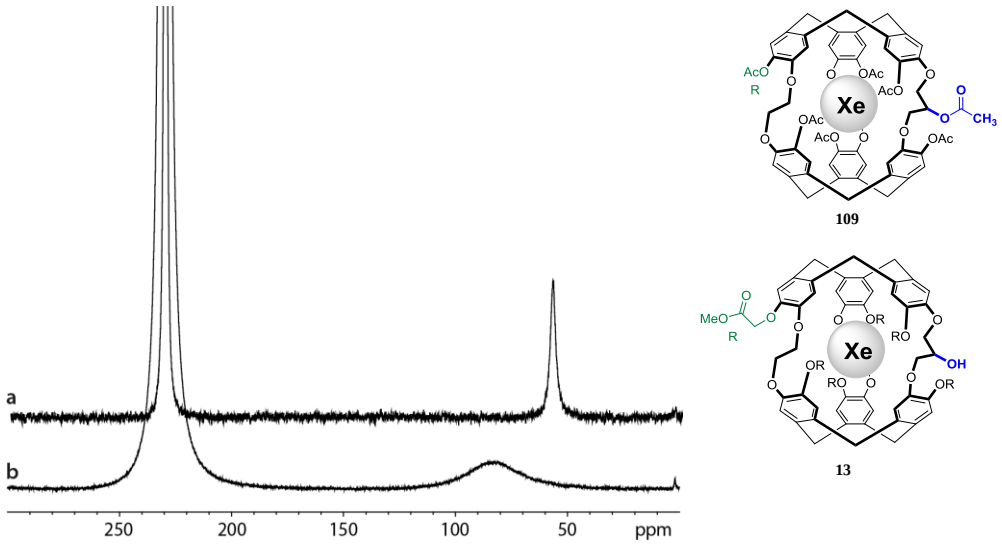

Figure 115: one-scan ^{129}Xe NMR spectra recorded at 298 K on solutions in $C_2D_2Cl_4$ of cryptophane **13** (a) and cryptophane **109** (b).

Particularly, compound **109** is vulnerable to undergo a self-encapsulation phenomenon, in which its central acetate group enters the cavity in the absence of a potential guest. This self-encapsulation behavior have been previously described for other molecular hosts like cyclodextrins and pillar[5]arene, however it is the first time, we observe this phenomenon in cryptophane derivatives.[203, 204, 205] This interesting finding triggered us to see first the effect of the self-encapsulation on the cryptophane's physical properties in solution by ^1H NMR. Since this cage is chiral, we wanted also to see the effect of this solvent-dependent conformation on the overall chiroptical properties. Investigating other cryptophane-[223] cages with similar structure, by ^1H NMR spectroscopy, like cryptophane **110** bearing six methoxy groups and one central secondary acetate, compound **111** bearing a primary acetate or compound **29** bearing a thio-acetate moiety, revealed that these molecules are also capable of performing self-encapsulation, Figure 116. It is worth mentioning that the properties of compound **29** has been only studied by ^1H NMR but other compounds were subjected to a full investigation. Having these molecules in hand, we were able then to separate their enantiomers and compare their chiroptical properties

with compound **109** to test whether we have a general trend in the chiroptical properties variation upon self-encapsulation. The physical properties of cryptophanes **109**, **110** and **111** were then compared with cryptophane-[223] $(OAc)_6$, **112,** which has no function at the propylenedioxy arm and hence does not undergo self-encapsulation. In the following sections, we will deliver an in-depth study of this phenomenon and its effect on the overall chiroptical properties. The majority of this work has been recently published in the *Chirality journal*. (Baydoun et al, *Chirality*, **2019**, *31*, (7), 481-491. DOI: 10.1002/chir.23079)

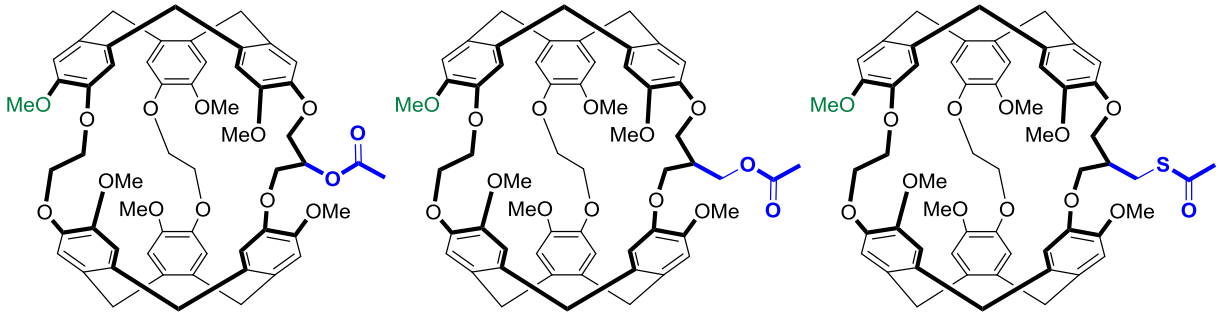

Figure 116: structure of cryptophane derivatives subjected to self-encapsulation phenomenon.

2. Synthesis and Separation of Two Enantiomers of Cryptophanes 109, 110, 111 and 112

The synthesis of cryptophane **109** has been previously reported in literature,[41] starting from cryptophane **12**, where a hepta-acylation step in pyridine provided compound **109** in a good yield (74%). The two enantiomers of cryptophane **109** were then separated on a semi-preparative HPLC on a Chiralpak-IC column. A racemic mixture of 460 mg of cryptophane-**109** provided the enantiomer [CD(-)$_{254}$]-**109** first (180 mg) and the [CD(+)$_{254}$]-**109** as a second fraction (200 mg). An enantiomeric excess ee > 99.5% and ee > 99% have been measured for [CD(-)$_{254}$]-**109** and [CD(+)$_{254}$]-**109**, respectively.

Cryptophane **110** has been obtained by a single acylation reaction of the central hydroxyl group of cryptophane **8** where it was obtained in a good yield (71%). Similar to compound **109**, the two enantiomers of cryptophane **110** were also separated using semi-preparative chiral HPLC but this time using (*S,S*)-Whelk-O1 column as a stationary phase. This provided the [CD(-)$_{254}$]-**110** and [CD(+)$_{254}$]-**110**.

Similarly, cryptophane **111** was obtained by an acylation step of compound **27** and it was obtained in a good yield (70%). The two enantiomers of compound **111** were separated (*S,S*)-Whelk-O1.

Cryptophane **112** which has no central function on its propylenedioxy arm has been prepared using a known procedure and it was obtained in a good yield (71%). The two enantiomers were separated using a (*S,S*)-Whelk-O1 column.[111] It is worth mentioning that compound **112** tends to partially implode upon separation.

An additional purification step on silica gel was performed to ensure the purity of these compounds.

3. ^{1}H NMR Analysis of Cryptophanes

The ^{1}H NMR spectra of cryptophanes **109**, **110**, **111**, **29** and **112** were recorded in different solvents that can either enter their cavities like CD_2Cl_2 and $CDCl_3$ or solvents that have low affinity to cryptophanes like DMSO-d_6, benzene-d_6 and $C_2D_2Cl_4$,. Table 5 shows the chemical shifts of the central acetate or thio-acetate groups in different solvents.

Solvent	CD_2Cl_2	$CDCl_3$	DMSO-d_6,	$C_2D_2Cl_4$	Benzene-d_6
109 δ(ppm)	2.08 (s)	2 (v.b)	0.18 (b)	-0.506 (b)	-
110 δ(ppm)	2.23 (s)	2.16	1.9 (b)	-1.74 (b)	-1.55
111 δ(ppm)	2.08 (s)	2.07 (s)	2.07 (b)	-1.35	-1.6
29 δ(ppm)	2.35 (s)	2.34	2.4	-1.1	-1.3

Table 5: chemical shift variation (ppm; ref: TMS) of the methyl function of the central acetate group in different solvents.

In cryptophane **109** for example, the comparison of these spectra revealed large differences specifically in the signal corresponding to the methyl group of the central acetate moiety. For instance, the ^1H NMR spectrum in CD_2Cl_2 clearly reveals a sharp signal at 2.08 ppm corresponding to the central acetate group grafted on the propylenedioxy arm. In $CDCl_3$, however, this signal is replaced by another broadened signal, which can be barely seen. Interestingly in solvents that do not fit the cavity, like DMSO-d_6, $C_2D_2Cl_4$ the signal appearing at 2.08 ppm is replaced by another shielded signal, which appears at 0.18 and -0.15 ppm, respectively with a chemical shift difference of about 2.59 ppm.

Compounds **110**, **111** and **29** showed a similar behavior, but interestingly, the signal appearing at almost 2 ppm is now more shielded (~3.9 ppm difference in CD_2Cl_2 and $C_2D_2Cl_4$) and it appears at -1.74, -1.35 and -1.1 ppm, respectively for each compound. In Figure 117, we have specifically shown the ^1H spectra of compound **110** in different solvents to clearly illustrate the chemical shift differences as a function of solvents.

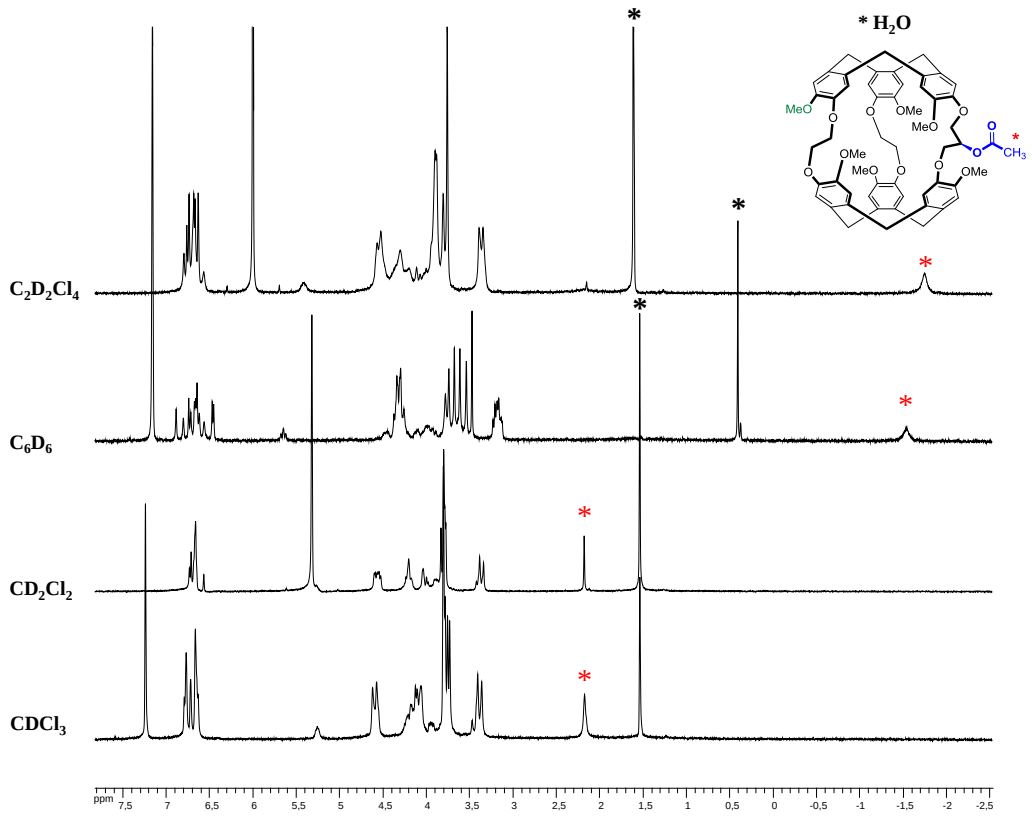

Figure 117: ^{1}H NMR spectra of compound **110** in different organic solvents.

The ^{1}H NMR spectra of compound **112** do not show any modification upon varying the solvents, this is because the molecule does not carry a central acetate moiety and thus does not seems to undergo a self-encapsulation phenomenon.

4. Polarimetry and ECD spectroscopy

The specific optical rotation (SOR) values of compounds **109**, **110**, **111** and **112** were recorded by polarimetry in different solvents (CD_2Cl_2, $CDCl_3$, DMSO-d_6, $C_2D_2Cl_4$) at five different wavelengths (589, 577, 546, 435, and 365 nm).

The SOR values of enantiopure compounds [CD(-)$_{254}$]-**109** and [CD(+)$_{254}$]-**109** show a solvent dependent behavior at these wavelength, different from that observed for compounds **110**, **111** and **112**. For example, the SOR values of [CD(-)$_{254}$]-**109** in CH_2Cl_2 are positive and similar to

that obtained in $CHCl_3$ but the latter are lower in values. In contrast, a complete inversion of SOR values sign is observed in DMSO and $C_2H_2Cl_4$, where they show low negative SOR values ($[\alpha]_{589} = -7.6 \times 10^{-1}$ deg cm^2 g^{-1} and $[\alpha]_{589} = -10.4 \times 10^{-1}$ deg cm^2 g^{-1} at 25°C in DMSO and $C_2H_2Cl_4$, respectively). It is worth mentioning that the [CD(+)$_{254}$]-**109** has the same SOR values with opposite signs, Figure 118.

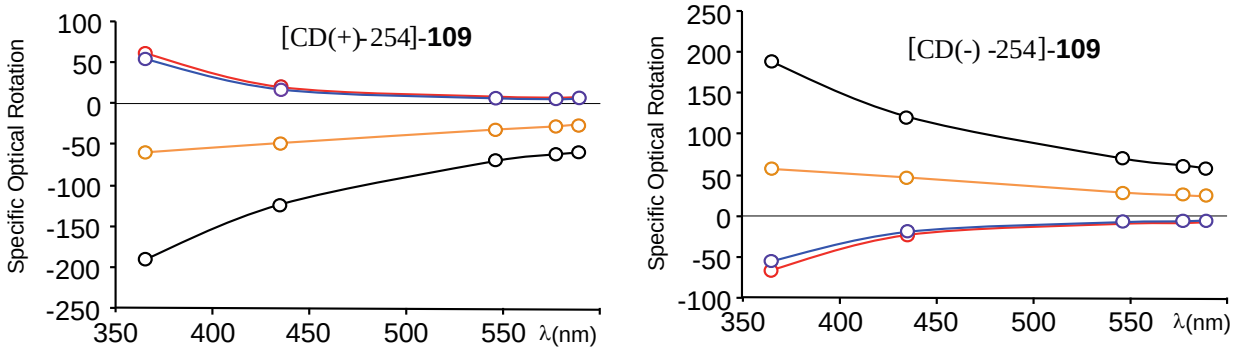

Figure 118: plot of the SOR values of [CD(+)$_{254}$]-**109** and [CD(-)254]-**109** as a function of the nature of the solvent: black (CH_2Cl_2), orange ($CHCl_3$), blue (DMSO), red ($C_2H_2Cl_4$).

In comparison to **109**, compounds **110** and **111** show a usual behavior in which no change in the sign of the SOR values is observed as a function of solvent. For example, the [CD(+)$_{254}$]-**110** and [CD(+)$_{254}$]-**111** has positive SOR values in all these solvents. Interestingly, these values are higher in magnitude compared to the ones of compound **109**, for example, the SOR value of [CD(+)$_{254}$]-**110** in $C_2H_2Cl_4$ at 589 nm is equal to $[\alpha]_{589} = 199.0 \times 10^{-1}$ deg cm^2 g^{-1} and that of [CD(+)$_{254}$]-**111** is equal to $[\alpha]_{589} = 207 \times 10^{-1}$ deg cm^2 g^{-1}.

Similarly, the two enantiomers of compound **112** have the same sign of SOR values whatever the nature of the solvent. The magnitude of these values however is comparable to that observed with compound **109**, Figure 119.

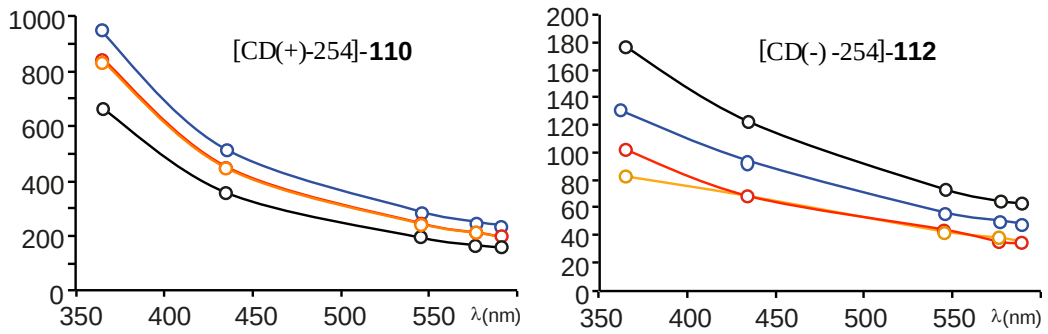

Figure 119: plot of the SOR values of [CD(+)$_{254}$]-**110** and [CD(-)$_{254}$]-**112** as a function of the nature of the solvent: black (CH_2Cl_2), orange ($CHCl_3$), blue (DMSO), red ($C_2H_2Cl_4$).

The ECD spectra of the enantiopure compounds **109**, **110**, **111** and **112** were recorded in different solvents like CH_3CN, DMSO, $C_2H_2Cl_4$, THF, CH_2Cl_2 and $CHCl_3$. These molecules showed a good solubility in all solvents except CH_3CN. Recording ECD spectra in CH_3CN and THF allows us to access a large spectral range of the absorption spectrum reaching 210 nm, which includes the ^1B_b, ^1L_a and ^1L_b transitions. In CH_2Cl_2 and $CHCl_3$ the cut-off is around 230 nm, which allows the detection of the ^1L_a and ^1L_b transitions. However, in DMSO and $C_2H_2Cl_4$ only the ^1L_b transition is observed.

The ECD spectra of [CD(+)$_{254}$]-**109** in CH_2Cl_2 revealed two negative-positive bisignate signals from low to high wavelength (Figure 120, A). The first bisignate corresponds to the ^1L_a transition, which lies between 230 and 260 nm and the second lies between 260 and 310 corresponds to the ^1L_b transition. In THF, an ECD band of the ^1B_b transition is observed as a negative Cotton band. Upon varying the nature of the solvent, no spectral modifications were observed and the spectra are nearly superimposable except in the case of $C_2H_2Cl_4$, where a decrease in the intensity of the ECD component at 290 nm is detected, Figure 120, B. Similarly, no detectable variation was observed in the ECD spectra of compound **112** in different solvents.

For compounds **110** and **111**, the ECD spectra are different from that recorded for compounds **109** and **112**. In particular, the ^1L_b transition is now composed of three Cotton bands instead of two. Unlike the first two described compounds, the ECD bands of the ^1L_b transition is more responsive to the change of the nature of the solvent, where modifications in its shape and intensity are observed especially in the ECD components between 285 and 310 nm, Figure 120, C and D.

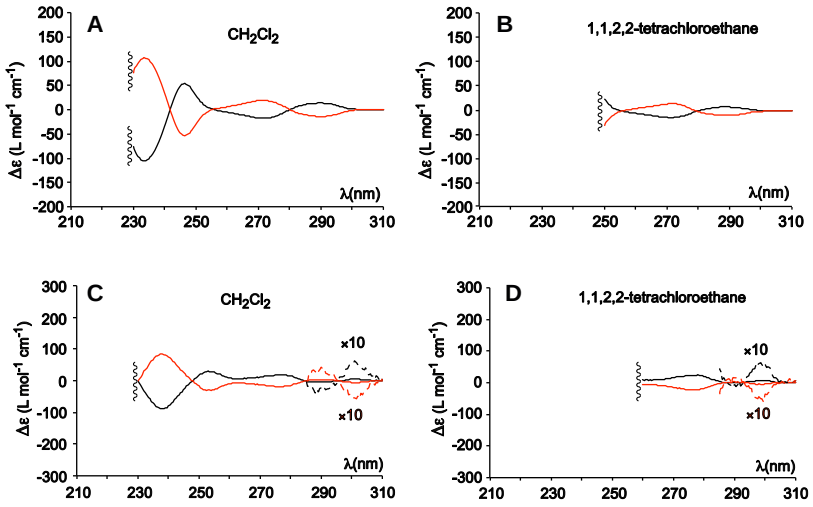

Figure 120: ECD spectra of [CD(+)254]-**109** (black spectra) and [CD(-)254]-**109** (red spectra) recorded in A) CH_2Cl_2 B) $C_2H_2Cl_4$ at 20 °C. ECD spectra of [CD(+)254]-**110** (black spectra) and [CD(-)254]-**110** (red spectra) recorded in C) CH_2Cl_2 D) $C_2H_2Cl_4$ at 20 °C.

5. IR and VCD spectroscopy

The chiroptical properties of cryptophanes **109**, **110** and **112** were also studied by VCD spectroscopy in different solvents, along with the infrared spectroscopy, which offered insight data about the self-encapsulation phenomenon.

The IR spectra recorded in different solvents are relevant to that reported previously with cryptophane-[223] derivatives.[111, 64] These spectra displayed at 1750 and 1160 cm^{-1} reflect the ν*C=O* stretching vibration and the ester asymmetric and symmetric ν*C-O-C* stretching vibrations.

The νC=O stretching vibration is of particular interest because it reflects the environment and the behavior of the carbonyl groups in the molecules in different solvents. For example, the intensity of this signal is dependent on the number of the acetate groups in the molecule. In compounds **109** and **112**, for instance, this peak is more intense because they bear seven and six acetate groups, respectively. A closer look at this spectral region informs us a lot about the self-encapsulation phenomenon. For example, the νC=O signal of compound **109** and **112** are equal to 1762 cm^{-1} in $CHCl_3$ and 1758 cm^{-1} in $C_2H_2Cl_4$. Thus, these peaks correspond to the six acetate groups grafted on the CTB units. In compound **109**, however an additional shoulder is observed at 1746 cm^{-1} that might correspond to the central acetate group. In this compound, it is hard to extract data about self-encapsulation due to the contribution of the other six acetate available moieties, Figure 121, A and C.

Interestingly, in compound **110** which bears a unique central acetate group, more information about the self-encapsulation process can be extracted from the νC=O IR band. In $CHCl_3$ and CH_2Cl_2 for example, this stretching vibration appears as a single peak around 1740 cm^{-1}. In $C_2H_2Cl_4$ where self-encapsulation takes place, a new signal appears at higher energy, 1752 cm^{-1} in addition to the initial signal appearing at 1738 cm^{-1}. This new peak can be assigned to the acetate group pointing inside the cavity. It is worth mentioning that the new signal is double in intensity compared to the initially observed signal at 1739 cm^{-1}. The new observed peak has a higher energy and this indicates that it interacts less with the surrounding environment. To confirm this result, additional experiment was performed in $C_2H_2Cl_4$ with xenon, which is a competitive guest. Upon xenon addition, the intensity of the two peaks are reversed, in which the peak observed at 1739 cm^{-1} that corresponds to the acetate group out the cavity, is now predominant. This result can be explained by the fact that once xenon enters the cavity it expels

the acetate group out of it and hence clearly illustrates the self-encapsulation phenomenon, Figure 121, B.

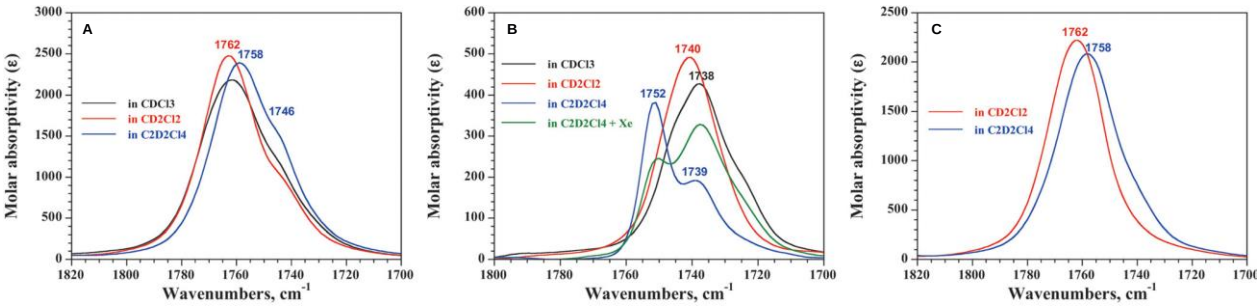

Figure 121: IR spectra in the ester νC═O spectral range of (A) **109**, (B) **110**, and (C) **112** in $CDCl_3$ (black spectra), CD_2Cl_2 (red spectra), and $C_2D_2Cl_4$ (blue spectra) solvents (15 mM, 250 μm path length). Additional IR spectrum of **110** in $C_2D_2Cl_4$ in the presence of xenon (green spectrum in B).

The VCD spectra of enantiopure compounds [CD(+)$_{254}$]-**109**, [CD(+)$_{254}$]-**110**, and [CD(+)$_{254}$]-**112** were also recorded in different solvents. The comparison of the VCD spectra in these solvents is shown in Figure 122. Generally speaking, upon changing the nature of the solvent, the overall shape of the VCD spectra does not vary. However, a slight decrease in the intensity of the peaks is observed when using $C_2H_2Cl_4$ as a solvent. Since this feature is observed in all the three compounds, which either undergo (**109** and **110**) or does not (**112**) self-encapsulation, then it seems that these modifications are not specific to this process but rather to the solvent effect. The latter behavior has been also observed previously for cryptophane-[222] with methoxy substituents, where it was related to the conformational changes of the linkers. When the cryptophane cage is complexing a guest molecule such as $CHCl_3$, the *trans* conformation of the linkers is favored. However, in the absence of a suitable guest, the molecule tends to have different conformations and an overall conformational equilibrium is observed. This in turn gives rise to different VCD spectra. Additionally, a deep observation of the VCD spectra of compounds [CD(+)$_{254}$]-**109** and [CD(+)$_{254}$]-**112** revealed a negative positive bisignate signal from low to high

wavenumbers which is referred to as an excitonic coupling of the acetate groups. Specifically it arises from the coupling pair of oriented C═O dipoles and has been already observed for cryptophane derivative bearing six carboxylic acid groups Figure 122, A and C.

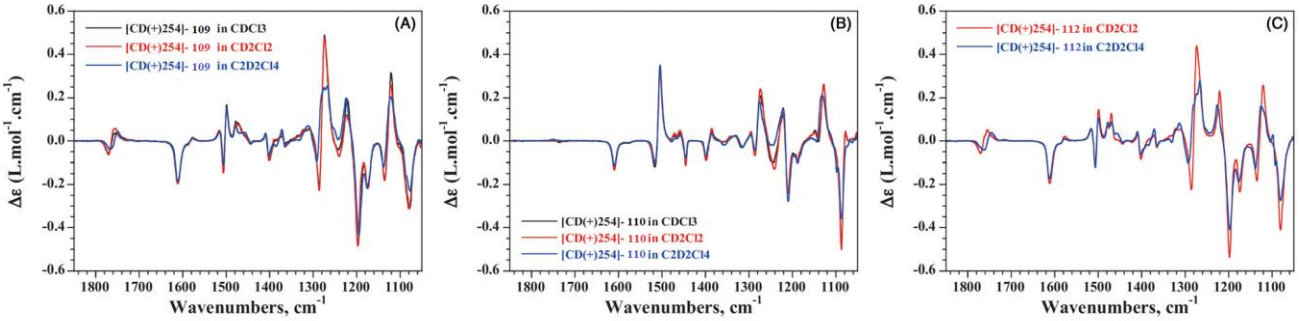

Figure 122: VCD spectra in the 1850 to 1050 cm^{-1} spectral range of (A) [CD(+)254]-**109**, (B) [CD(+)254]-**110**, and (C) [CD(+)254]-**112** in $CDCl_3$ (black spectra), CD_2Cl_2 (red spectra), and $C_2D_2Cl_4$ (blue spectra) solvents (15 mM, 250 µm path length).

6. Determination of the Absolute Configuration of Cryptophane 109, 110, 111 and 112

Determination of cryptophane's absolute configuration (AC) has been assessed using different chiroptical techniques and specifically polarimetry at 589 nm, which constitutes the simplest and the most used technique to determine the AC of cryptophanes.[111,71] For example, *PP*-cryptophane-A and its derivatives have a positive SOR value at 589 nm regardless the nature of the solvent. This value is also associated with a positive CD band at 254 nm. In case of compound **109**, a direct attribution of the AC using polarimetry is rendered impossible because the sign of the SOR values depends on the nature of the solvent. This is not the case for compounds **110**, **111** and **112** and compound **109** is the first reported cryptophane that shows this behavior.

For the determination of the AC of compound **109**, complementary chiroptical tools like ECD and VCD spectroscopy are thus necessary. ECD spectroscopy in organic solvents has proved its efficiency to attribute the AC of cryptophane derivatives. In particular, the ECD bands of the ^1L_a transition can be exploited with confidence to attribute cryptophane's AC. This is because, the ECD bands of the ^1L_a transition are quite robust towards structural and experimental conditions like a change of the solvent. As discussed in the introductory chapter, the ECD bands of the *PP*-cryptophane-A show a negative-positive bisignate ^1L_a transition from high to low energy. The *MM*-cryptophane-A shows obviously opposite ECD Cotton bands. In case of an *anti*-cryptophane derivative bearing six acetate groups, the descriptors *M* and *P* will be inversed due to the change of priority of the groups (Prelog's rules). Based on this, and by analogy with the results observed with enantiopure cryptophane-A, enantiopure *MM*-**109** will display a negative-positive bisignate for the ECD bands of the ^1L_a transition. Consequently, the [CD(+)$_{254}$]-**109** corresponds to the *MM*-cryptophane-**109**, whereas the [CD(-)$_{254}$]-**109** corresponds to the *PP*-descriptor. The SOR value obtained at 589 nm is no longer reliable to determine the AC since it changes its sign in different solvents. Thus, in compound **109** it is important to specify the nature of the solvent to complete the assignment of the AC. Hence, we can conclude that the *MM*-**109** is the (+)$_{589}$-*MM*-**109** in $C_2H_2Cl_4$ and (-)$_{589}$-*MM*-**109** in CH_2Cl_2, Figure 123.

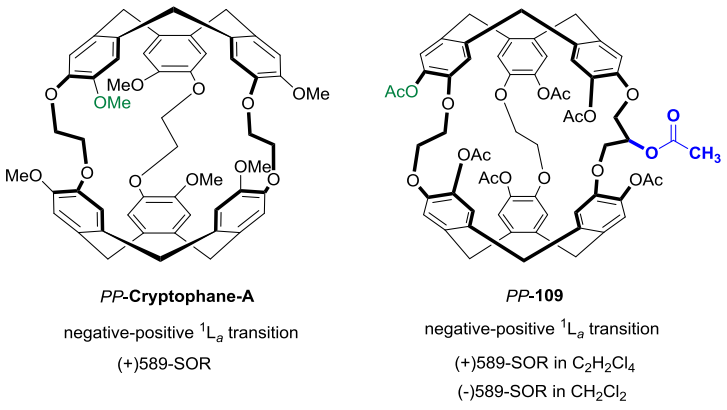

Figure 123: comparison between the *PP*-cryptophane-A and *PP*-**109**.

For compounds **110**, **111** and **112**, the case is simpler, since no change in the SOR values is observed upon varying the nature of the solvents. For example, [CD(-)$_{254}$]-**110** and [CD(-)$_{254}$]-**111** can be attributed to the *MM*-**110** and *MM*-**111** which have a negative SOR at 589 nm and a positive-negative bisignate ^1L_a transition. The *PP*-**112** is attributed to [CD(-)$_{254}$]-**112** and to (+)$_{589}$-*PP*-**112**, Figure 124.

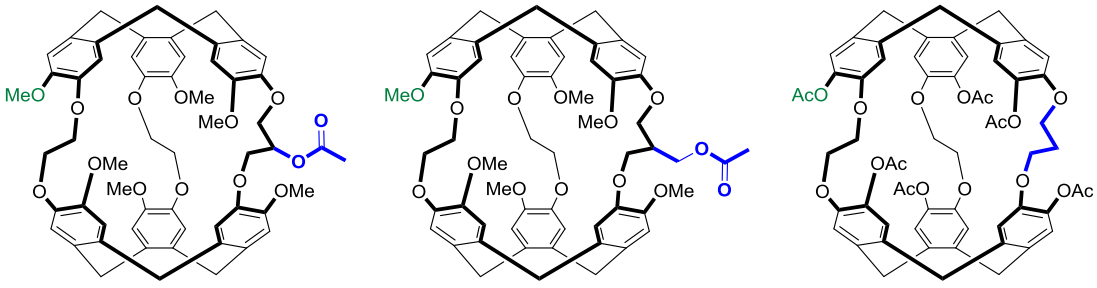

***MM*-110**
[CD(-)254]

***MM*-111**
[CD(-)254]

***PP*-112**
[CD(-)254]

Figure 124: attributed absolute configuration of cryptophanes **110**, **111** and **112**.

To confirm the absolute configuration of cryptophanes derivatives, VCD spectroscopy combined with ab initio calculations at the DFT level have been performed for compounds **109** and **110**. The geometries of *PP*-**109** and *MM*-**110** were optimized at the B3LYP/6-31G** level, and harmonic vibrational frequencies were calculated at the same level. Calculations were performed assuming *trans* and *gauche-gauche* conformations for the ethylenedioxy and propylenedioxy linkers, respectively, and considering that the acetate group grafted on the propylenedioxy linker points toward or outward the cavity. The comparison of the experimental VCD spectrum of [CD(-)$_{254}$]-**109** and those calculated for *PP*-**109** configuration are reported in Figure 125. The VCD spectra calculated for the *PP* configuration of **109**, whatever the orientation of the acetate group grafted on the propylenedioxy linker, reproduce the sign of most of the bands observed in the experimental VCD spectrum for the [CD(-)$_{254}$]-**109** enantiomer, thus confirming the absolute configuration [CD(-)$_{254}$]-*PP* for **109**. Similarly, the comparison of the experimental VCD

spectrum of [CD(-)$_{254}$]-**110** and those calculated for the *MM*-**110** configuration, confirms the absolute configuration [CD(-)$_{254}$]-*MM* for **110**.

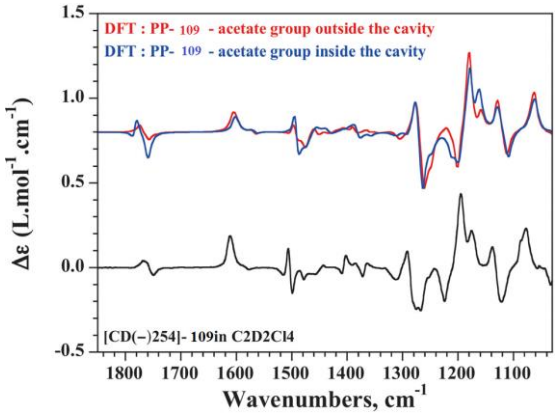

Figure 125: Comparison of experimental VCD spectrum of [CD(−)254]-**109** in $C_2D_2Cl_4$ solution (15 mM, 250 µm path length) and VCD spectra of *PP*-**109** calculated at the B3LYP/6-31G** level (IEFPCM = $C_2H_2Cl_4$) for the *trans* and *gauche*-*gauche* conformations of the ethylenedioxy and propylenedioxy linkers, respectively, and for the acetate group grafted on the propylenedioxy linker pointing toward (blue spectrum) or outward (red spectrum) the cavity.

7. Self-Encapsulation Confirmation by ^{1}H NMR and IR

Among the different spectroscopic methods used to characterize the self-encapsulation process, ^{1}H NMR and IR confirmed with confidence this conformation. For instance, ^{1}H NMR spectra revealed a clear chemical shift change of the central acetate or thio-acetate group in solvents that fill or do not fill the cavity. In large solvents like DMSO and $C_2H_2Cl_4$, the central acetate group tends to fill cryptophanes cavity leading to high shielding. In the presence of a potential guest like $CHCl_3$ and CH_2Cl_2, the acetate group will be expelled out and the guest molecule will occupy the cavity.

Compound **109** shows a shielding of about 2.58 ppm in $C_2H_2Cl_4$, this value suggests that the acetate group is not completely encapsulated. For compounds **110**, **111** and **29**, the acetate group is shielded by about 4 ppm. This value is comparable to that observed with cryptophane guests and it suggests a better complexation event.[206,53] This can be explained by the fact that the acetate

groups bordering cryptophane-**109** skeleton are now replaced by less hindered methoxy groups which in turn enhance the flexibility of the cage allowing better conformational rearrangement.

Infrared spectroscopy has also served to confirm this phenomenon, specifically in compound **110** that bears only one acetate group. For example, the peak observed at 1752 cm^{-1} in $C_2H_2Cl_4$ can be clearly associated with the acetate group pointing inward the cavity. This stretching vibration appears at higher wavenumber compared to the acetate group pointing outward (1739 cm^{-1}) because it interacts less with surrounding solvent environment. DFT calculations have also served to reproduce these IR spectra, in which an increase of the stretching vibration wavenumber by about 13 cm^{-1} is calculated for acetate pointing inward the cavity. This has been also confirmed by a competition experiment with xenon that expels the acetate group, thus restores the initial signal which appears at 1739 cm^{-1} and decrease the one at 1752 cm^{-1}.

It is worth mentioning, that self-encapsulation is a new conformation that is used by cryptophanes to fill their cavities in the absence of a guest. Normally, cryptophanes use imploded conformation as an alternative tool to occupy their cavities, but this conformation is energetically demanding or it forms when the cryptophane is stored for a long time in the solid state. The latter case is observed for compound **112** which even implodes in solution.

8. Effect of Self-Encapsulation on Chiroptical Properties

Self-encapsulation induces large conformational changes of cryptophane linkers. These changes were readily confirmed by ^{1}HNMR and IR spectroscopy (see above). Different chiroptical tools were also employed to characterize this phenomenon. Despite the fact that compounds **109**, **110** and **111** undergo self-encapsulation, they have completely different chiroptical properties in different solvents. Investigating the chiroptical properties by ECD spectroscopy revealed little variations in different solvents.[183] This result is in agreement with our

previously reported results, which show that the Cotton bands are less responsive to conformational changes in organic solvents. This lack of sensitivity can be explained in part because the benzene chromophores are inserted into two independent rigid structures. Thus, the chromophores and their relative orientation seem to be moderately affected by the conformational rearrangement of the linkers. The ECD spectral results of enantiopure compound **109** are quite surprising, because the SOR are strongly modified under the same experimental conditions. It is also noteworthy that ECD and SOR (ORD) are related by Kramers-Kronigs relationships (see Appendix). Consequently, a change of the SOR (ORD) values must have an impact on the overall ECD spectrum.

To explain this lack of sensitivity several hypotheses can be proposed. One of the proposed hypothesis is the contribution of high-energy excited states, which cannot be accessed in our case by conventional ECD spectrometer (< 220 nm). These high-energy excited states can contribute to the SOR values recorded for compound **109**. This assumption is however difficult to check experimentally because we do not have access to the whole ECD spectrum of compound **109**. Synchrotron Radiation Circular Dichroism (SRCD) allows extending the spectral range, but even in this case, it will be difficult to confirm this hypothesis. Such a study has been performed in the case of cryptophane-[222], **98**, that shows a large variation of the SOR (ORD) values as a function of the nature of the solvent.[191]

Another assumption to explain this unusual behavior will be to consider a participation of the solvent. Indeed, it has been shown in some cases that the solvent may contribute to the sign of the SOR values measured.[207] Thus, a contribution of the solvent cannot be totally excluded, but this effect is also difficult to verify experimentally or by quantum calculations since the use of an explicit model would require large computation times, considering the molecular size of

compound **109**, the number of possible conformations adopted and the number of solvent molecules surrounding the host molecule. Nevertheless, this surprising effect cannot be solely attributed to the self-encapsulation process since other compounds such as **110** and **111** show a different behavior.

Compared to ECD, VCD spectroscopy revealed a higher sensitivity to conformational changes. For example, the VCD spectra of [CD(+)$_{254}$]-**109** and [CD(+)$_{254}$]-**110** enantiomers are dependent on the fact that the solvent can enter ($CDCl_3$ or CD_2Cl_2) or not ($C_2D_2Cl_4$) the cavity of the host. Particularly the spectral regions lying between 1480 and 1450 cm^{-1} associated with the δCH_2 bending vibration and in the 1300 to 1250 cm^{-1} related to the wagging and twisting modes of methylene groups are mostly affected by the nature of the solvent. However, these spectral modifications do not give any clue about self-encapsulation since they are also observed with compound **112**, which does not undergo self-encapsulation.

As observed with many different enantiopure cryptophane derivatives studied by our group, polarimetry appears to be the most sensitive technique to detect small conformational changes, when recorded in organic solvent. In contrast, ECD spectroscopy appears much less sensitive in studying these conformational changes due to the particular arrangement of the six benzene chromophores. VCD spectroscopy can also be useful to detect such type of conformational variations, with an additional advantage of being easily calculated using quantum mechanics equations. In addition, VCD spectroscopy combined with DFT calculations remain the methods of choice to determine, with confidence, the absolute configuration of these derivatives. This technique was proved to be efficient in the case of compound **109**, where the direct determination of the absolute configuration was found complicated.

Conclusion

Conclusion of Part II

Through the run of this part, we have delivered a non-exhaustive description of some chiral cryptophane derivatives. The different chiroptical properties of these cages were also discussed to offer a better understanding of cryptophanes' configurations and conformational variations of cryptophanes and their complexes. Importantly, we also highlighted the main chiroptical tools used in this domain and described the major functions of each tool, their advantages and inconveniences. Exploiting these tools along with ^{1}H NMR spectroscopy, we were particularly interested in studying the behavior of the cryptophanes-[223] derivatives subjected to "self-encapsulation". This phenomenon is characterized by a conformational change of the central group lying on the propylenedioxy arm, which points inward the inner cavity of the host in the absence of a competitor guest. The chiroptical properties of these cages revealed that compound **109** has a unique behavior, since its SOR values invert depending on the nature of the solvent. To our knowledge, this family of compounds gathers the first examples of cryptophane derivatives that give rise to a self-encapsulation phenomenon. The self-encapsulation process appears as a convenient way to fill the cavity in absence of guest molecules. This process occurs spontaneously in solution, and it requires less energy than the CTB implosion that is usually observed upon heating the compound in solution or in the solid state. In contrast, compound **112** that does not possess appropriate substituent on the linker gives more easily the imploded form.

Experimental Part

Experimental Details:

Polarimetric, UV-Vis, and ECD measurements

Optical rotations of the two enantiomers of **109**, **110**, **111** and **112** were measured in four solvents ($CHCl_3$, CH_2Cl_2, DMSO, and $C_2H_2Cl_4$) at 589, 577, 546, 435, and 365 nm using a polarimeter with a 10 cm path length cell, thermostated at 25°C. Concentrations used for the polarimetric measurements were typically in the range 0.22 to 0.3 g/100 mL. ECD spectra of the two enantiomers of **109**, **110**, **111** and **112** recorded on a Chirascan spectrometer (Applied Photophysics) in six solvents ($CHCl_3$, CH_2Cl_2, THF, CH_3CN, $C_2H_2Cl_4$, and DMSO) at 20 °C with a 0.2 cm path length quartz cell (concentrations were in the range 0.1 to 1.0 × 10^{-4} M). Spectra were recorded between 210 and 350 nm (THF, CH_3CN), 230 and 350 nm (CH_2Cl_2 and $CHCl_3$), and 250 and 350 nm (DMSO, $C_2H_2Cl_4$) with a 0.5 nm increment and a 1 second integration time. Spectra were processed with standard spectrometer software, baseline corrected, and slightly smoothed by using a third-order least square polynomial fit. UV-Vis spectra of compounds **109**, **110**, **111** and **112** were recorded in THF (210-350 nm) at 25°C with a 1 cm path length quartz cell.

IR and VCD measurements

The IR and VCD spectra were recorded on a FTIR spectrometer equipped with a VCD optical bench. IR absorption and VCD spectra were recorded at a resolution of 4 cm^{-1}, by coadding 50 and 24000 scans (8 h acquisition time), respectively. Samples were held in a 250 μm path length cell with BaF2 windows. IR and VCD spectra of the two enantiomers of **109**, **110** and **112** were measured in $CDCl_3$, CD_2Cl_2, and $C_2D_2Cl_4$ solvents at a concentration of 15 mM. Additional IR spectrum of **110** was measured in $C_2D_2Cl_4$ in the presence of xenon.

DFT calculations

The geometry optimizations, vibrational frequencies and absorption intensities were calculated by the Gaussian 09 program on the DELL cluster of the MCIA computing centre of the Bordeaux University. Calculations of the optimized geometry of *PP*-**109** and *MM*-**110** enantiomers were performed at the density functional theory (DFT) level using B3LYP functional and 6-31G** basis set with the use of IEFPCM model of solvent ($C_2H_2Cl_4$ described with parameters $\varepsilon = 7.096$ and $\varepsilon\infty = 2.21$). First, a conformational search of the two compounds was performed at the molecular mechanics level (MMFF94 force fields incorporated in compute VOA software, 8 kcal mol^{-1} limit) on the optimized structure of cryptophane-[223] as a starting point, on which acetate substituents were added. Two structures with, respectively, *trans*, *trans*, and *gauche-gauche* conformations for the two ethylenedioxy and propylenedioxy linkers, with the acetate group grafted on the latter pointing inward and outward the cavity, were optimized. Vibrational frequencies and IR intensities were calculated at the same level of theory. For comparison with experiments, the calculated frequencies were scaled by 0.968 and the calculated intensities were converted to Lorentzian bands with a half-width of 7 cm^{-1}.

Experimental part

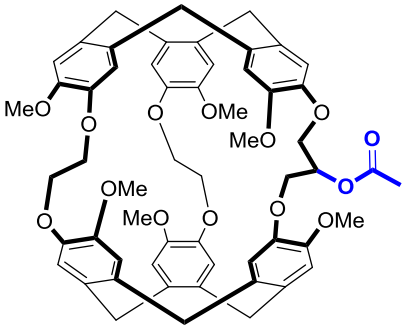

110

Synthesis of cryptophane 110: Acetic anhydride (0.7 mL, 7.4 mmol, 10 equiv.) was added dropwise at 0 °C to a solution of cryptophane **8** (0.7 g, 0.75 mmol) in freshly distilled CH_2Cl_2 (23 mL) and pyridine (3.5 mL). The reaction mixture was stirred for 48 hours at room temperature. The solution was then quenched at 0 °C with concentrated $NaHCO_3$ (10 ml) for 10 minutes and then poured in 20 mL of H_2O. The aqueous layer was extracted 5 times with CH_2Cl_2 and then dried over Na_2SO_4. After filtration the solvent was evaporated under reduced pressure. The crude product was subjected to column chromatography on silica gel (CH_2Cl_2/acetone: 85/15) to give rise to compound **110** as a white product (0.52 g, 71%).

^{1}H NMR (400 MHz, $CDCl_3$, 25 °C): 6.63-6.79 (12 s, 12 H), 4.58-4.62 (m, 6H), 4.02-4.2 (m, 11H), 3.93 (m, 1 H), 3.73- 3.8 (6s, 18 H), 3.47 (m, 1H), 3.36-3.41 (m, 6 H), 2.17 (s, 3H).

^{13}C {^{1}H} NMR (100.6 MHz, $CDCl_3$, 25 °C): 170.6, 149.6 (2C), 149.55, 149.4, 148.8, 148.1, 146.8, 146.7 (2 C), 146.6, 146.5 (2 C), 134.1, 134.1, 133.8, 133.8, 133.3, 132.8, 132.1, 131.9, 131.5, 131.4, 131.35, 131.3, 120.3, 120.2 (3 C), 117.2, 115.1, 114.2 (2 C), 113.9, 113.7, 113.35, 113.2, 70.8, 69.6, 69.5, 69.1, 68.9 (2 C), 66.6, 56.3, 56.3, 55.7, 55.65(2 C), 55.6, 36.5, 36.4; 36.2 (4 C), 21.2.

HRMS(ESI-TOF) *m/z* $[M + Na]^+$ calcd for $C_{57}H_{58}O_{14}Na$ 989.3724, found 989.3719.

Experimental part

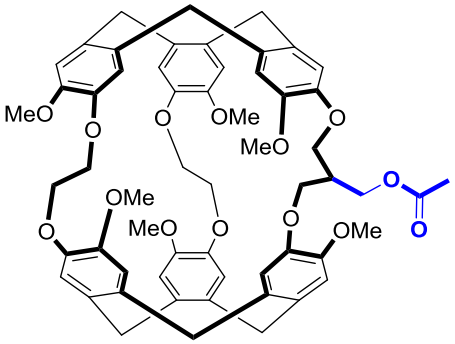

111

Synthesis of cryptophane 111: Acetic anhydride (0.3 mL, 3.1 mmol, 5 equiv.) was added dropwise at 0 °C to a solution of cryptophane **27** (0.6 g, 0.63 mmol) in freshly distilled pyridine (8 mL). The reaction mixture was stirred for 48 hours at room temperature. The solution was then quenched at 0 °C with concentrated $NaHCO_3$ (10 ml) for 10 minutes and then poured in 20 mL of H_2O. The aqueous layer was extracted 5 times with CH_2Cl_2 and then dried over Na_2SO_4. After filtration the solvent was evaporated under reduced pressure. The crude product was subjected to column chromatography on silica gel (CH_2Cl_2/acetone: 95/5) to give rise to compound **111** as a white product (0.57 g, 70%).

^{1}H NMR (400 MHz, $CDCl_3$, 25 °C): 6.76-6.52 (12 s, 12 H), 4.62-4.55 (m, 6H), 4.45-3.95 (m, 11H), 3.79 (1s, 9 H), 3.76 (1s, 3H), 3.74 (1s, 3H), 3.44-3.35 (m, 6 H), 2.63 (s, 1H), 2.07 (s, 3H).

^{13}C {^{1}H} NMR (100.6 MHz, $CDCl_3$, 25 °C): 171.1, 149.5, 149.4 (2C), 149.3, 147.8, 147.5, 147.0, 146.9, 146.7, 146.56, 146.54, 133.9 (2C), 133.8 (3C), 132.3, 132.2, 131.6, 131.5, 131.4, 130 (2C), 120.4 (2C), 120.38, 120.1, 113.9 (2C), 113.6, 113.4, 112.9, 112.9, 112.3, 112.2, 69.65, 69.5, 68.9 (2C), 64.92, 64.2, 62.56, 56.19, 55.7, 55.52 (2C), 55.4, 39.6 (2C), 36 (2C), 35.9 (2C), 20.9.

HRMS(ESI-TOF) *m/z* $[M + Na]^+$ calcd for $C_{58}H_{60}O_{14}Na$ 1003.3880, found 1003.3875

Experimental part

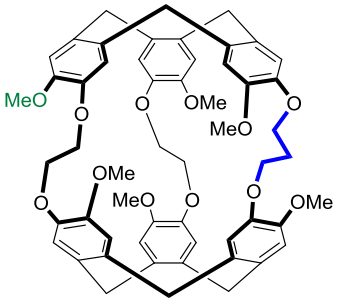

112

Synthesis of cryptophane 112: Acetic anhydride (2.2 mL, 41 mmol) was added dropwise at 0 °C to a solution of cryptophane223 $(OH)_6$ (0.35g, 0.42 mmol) in Pyridine (5 mL). The reaction was stirred at room temperature for 16 hours under an argon atmosphere. Then, the reaction was quenched with a solution of sodium bicarbonate at 0 °C. The solution was then extracted 5 times with CH_2Cl_2. The combined organic layers were dried over sodium sulfate. A filtration, followed by evaporation of the solvents under reduced pressure, gives rise to compound **112** as a white product. The solid was then washed on a frit with an Et_2O/CH_2Cl_2: 75/25 mixture to give compound **112** as a clean white solid (0.31g, 71%).

^{1}H NMR (400 MHz, $CDCl_3$, 25 °C): 6.94 (s, 2 H), 6.91(2 H), 6.89 (2 H), 6.87 (2 H), 6.86(2 H), 6.62 (2 H), 4.65-4.58 (m, 6 H), 4.28-4.286 (2 H, m), 4.16-4.15 (m, 2 H), 4.04 - 3.8 (m, 8 H), 3.5-3.4 (m, 6H), 2.31 (s, 6 H), 2.29 (s, 6 H), 2.25 (s, 6 H), 2.09 (m, 2 H).

^{13}C {^{1}H} NMR (100.6 MHz, $CDCl_3$, 25 °C): 168.5 (4 C), 168.3 (2 C), 149.3 (2 C), 149.25 (2 C), 149.0 (2 C), 140.5 (2 C), 140.3 (2 C), 138.7 (2 C), 138.6 (2 C), 137.8 (2 C), 136.7 (2 C), 133.6 (2 C), 133.4 (2 C), 131.2 (2 C), 124.4 (2 C), 124.0 (2 C), 123.3 (2 C), 120.9 (2 C), 120.7 (2 C), 113.6 (2 C), 69.8 (2 C), 69.1 (2 C), 63.7 (2 C), 36.4 (2 C), 36.1 (4 C), 20.7 (4 C), 20.6 (2 C).

HRMS (ESI-TOF) *m/z* $[M + Na]^+$ calcd for $C_{61}H_{56}O_{18}Na$ 1099.3364, found 1099.3359.

Analytical separation for compound **109**

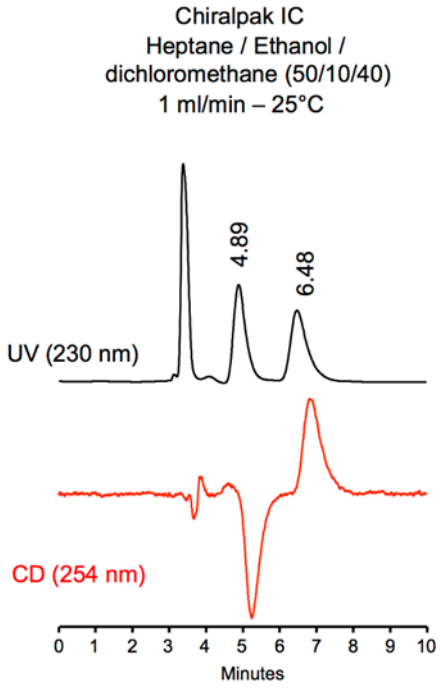

Column	Mobile Phase	t_1	k_1	t_2	k_2	α	Rs
Chiralpak IC	heptane/EtOH/CH_2Cl_2 (50/10/40)	4.89 (-)	0.63	6.48 (+)	1.16	1.84	2.23

Figure 126: chromatograms (Chiralpak IC, 250 x 4.6 mm, heptane/ethanol/CH_2Cl_2: 50/10/40, 1 mL/min at 25 °C) of the (rac)-**109** before preparative separation on Chiralpak IC (250 x 10 mm, heptane/ethanol/CH_2Cl_2: 50/10/40, 5 mL/min).

Semi-preparative separation for compound 109:

Sample preparation: About 460 mg of compound (rac)-**109** are dissolved in 18 mL of dichloromethane. Chromatographic conditions: Chiralpak IC (250 x 10 mm), hexane/ethanol/dichloromethane (5/1/4) as mobile phase, flow-rate = 5 ml/min, UV detection at 230 nm. Injections (stacked): 180 times 100 µL, every 5 minutes. The first eluted enantiomer is collected between 4.2 and 5.2 minutes and the second one between 6 and 7.5 minutes. First fraction: 180 mg of the first eluted [$CD(-)_{254}$]-**109** with ee > 99.5% on Jasco CD-1595 circular dichroism detector at 254 nm. Second fraction: 200 mg of the second eluted [$CD(+)_{254}$]-**109** with ee > 99% on Jasco CD-1595 circular dichroism detector at 254 nm.

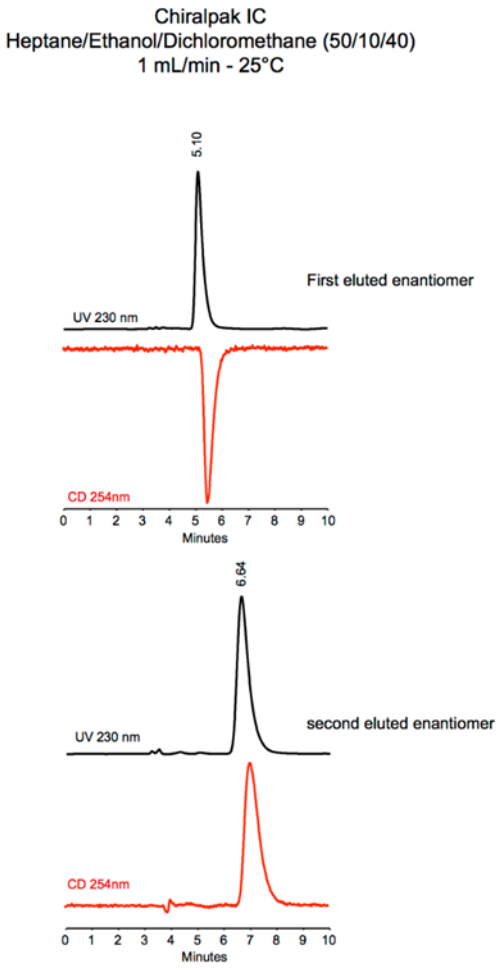

Figure 127: chromatograms (Chiralpak IC, 250 x 4.6 mm, heptane/ethanol/CH_2Cl_2: 50/10/40, 1 mL/min at 25 °C) of the collected [$CD(-)_{254}$]-**109** and [$CD(+)_{254}$]-**109** after preparative separation on Chiralpak IC (250 x 10 mm, heptane/ethanol/CH_2Cl_2: 50/10/40, 5 mL/min). Detection performed by UV-Vis spectroscopy at 230 nm (black chromatograms) and CD spectroscopy at 254 nm (red chromatograms).

Analytical separation for compound **110**

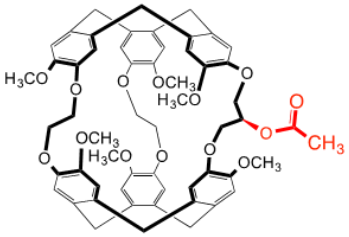

(S,S)-Whelk-O_1
Heptane/ethanol/CH_2Cl_2
(20/40/40)
1 ml/min – 25°C

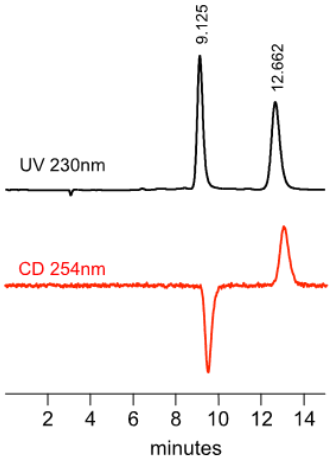

Column	Mobile Phase	t_1	k_1	t_2	k_2	α	Rs
(*S,S*)-Whelk-O_1	heptane/EtOH/CH_2Cl_2 20/40/40	9.13 (-)	2.10	12.67 (+)	3.29	1.57	5.72

Figure 128: chromatograms ((*S,S*)-Whelk-O_1, 250 x 4.6 mm, heptane/ethanol/CH_2Cl_2: 20/40/40, 1 mL/min at 25 °C) of the (rac)-**110** before preparative separation on (*S,S*)-Whelk-O_1 (250 x 10 mm, heptane/ethanol/CH_2Cl_2: 20/40/40, 5 mL/min).

Experimental part

Semi-preparative separation for compound 110:

Sample preparation: About 580 mg of (rac)-**110** are dissolved in 6 mL of dichloromethane. Chromatographic conditions: (*S*,*S*)-Whelk-O1 (250 x 10 mm), heptane/ethanol/ dichloromethane (20/40/40) as mobile phase, flow-rate = 5 mL/min, UV detection at 230 nm. Injections (stacked): 20 times 300 µL, every 13.8 minutes. First fraction: 255 mg of the first eluted [CD(-)$_{254}$]-**110** with ee > 99.5% on Jasco CD-1595 circular dichroism detector at 254 nm. Second fraction: 240 mg of the second eluted [CD(+)$_{254}$]-**2** with ee > 99.5% on Jasco CD-1595 circular dichroism detector at 254 nm.

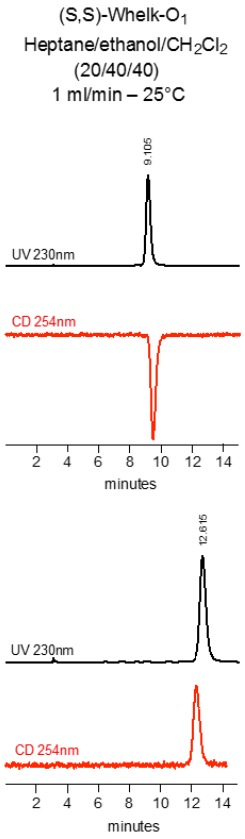

Figure 129: chromatograms ((*S*,*S*)-Whelk-O$_1$, 250 x 4.6 mm, heptane/ethanol/CH_2Cl_2: 20/40/40, 1 mL/min at 25 °C) of the collected [CD(-)$_{254}$]-**110** and [CD(+)$_{254}$]-**110** after preparative separation on (*S*,*S*)-Whelk-O$_1$ (250 x 10 mm, heptane/ethanol/CH_2Cl_2: 20/40/40, 5 mL/min). Detection performed by UV-Vis spectroscopy at 230 nm (black chromatograms) and CD spectroscopy at 254 nm (red chromatograms).

Analytical separation for compound **111**

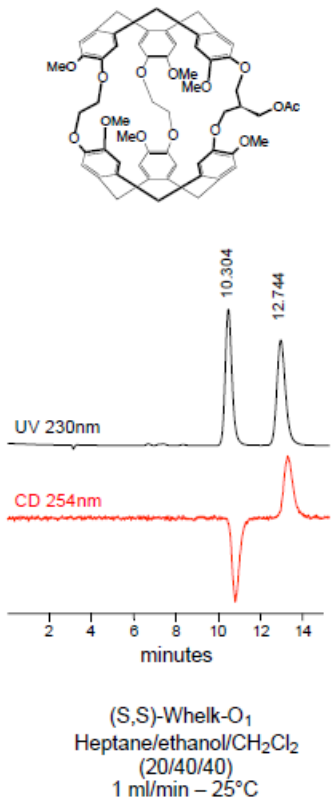

Column	Mobile Phase	t1	k1	t2	k2	α	Rs
(*S*,*S*)-Whelk-O1	Heptane/EtOH/CH_2Cl_2 20/40/40	10.30 (-)	2.49	12.74 (+)	3.32	1.33	3.79

Figure 130: chromatograms ((*S*,*S*)-Whelk-O_1, 250 x 4.6 mm, heptane/ethanol/CH_2Cl_2: 20/40/40, 1 mL/min at 25 °C) of the (rac)-**111** before preparative separation on (*S*,*S*)-Whelk-O_1 (250 x 10 mm, heptane/ethanol/CH_2Cl_2: 20/40/40, 5 mL/min).

Experimental part

Semi-preparative separation for compound 111:

Sample preparation: About 530 mg of compound **111** are dissolved in 7 mL of dichloromethane. Chromatographic conditions: (*S*,*S*)-Whelk-O1 (250 x 10 mm), heptane/ethanol/dichloromethane (20/40/40) as mobile phase, flow-rate = 5 mL/min, UV detection at 260 nm. Injections (stacked): 28 times 250 µL, every 14 minutes. First fraction: 220 mg of the first eluted ((-)-CD 254nm)-enantiomer) with ee > 99.5%. Second fraction: 240 mg of the second eluted ((+)-CD 254nm)-enantiomer) with ee > 99.5%.

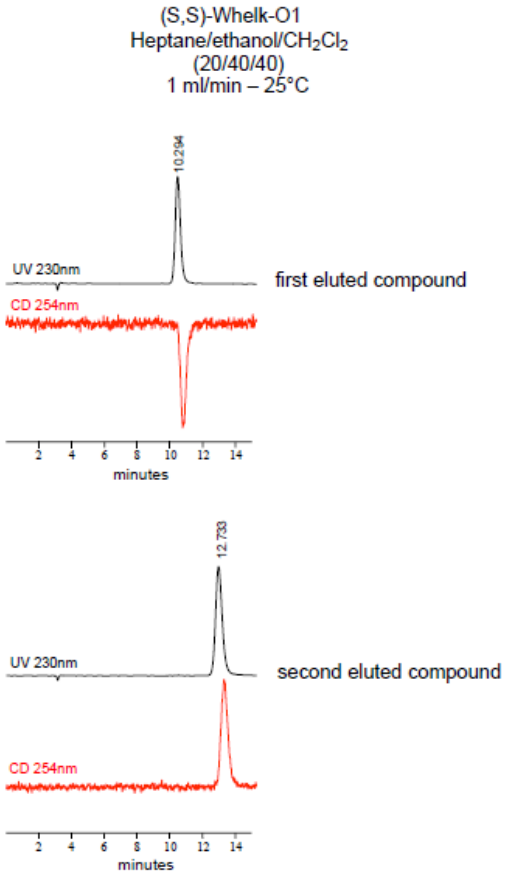

Figure 131: chromatograms ((*S*,*S*)-Whelk-O_1, 250 x 4.6 mm, heptane/ethanol/CH_2Cl_2: 20/40/40, 1 mL/min at 25 °C) of the collected [CD(-)$_{254}$]-**111** and [CD(+)$_{254}$]-**111** after preparative separation on (*S*,*S*)-Whelk-O_1 (250 x 10 mm, heptane/ethanol/CH_2Cl_2: 20/40/40, 5 mL/min). Detection performed by UV-Vis spectroscopy at 230 nm (black chromatograms) and CD spectroscopy at 254 nm (red chromatograms).

Analytical separation for compound **112**

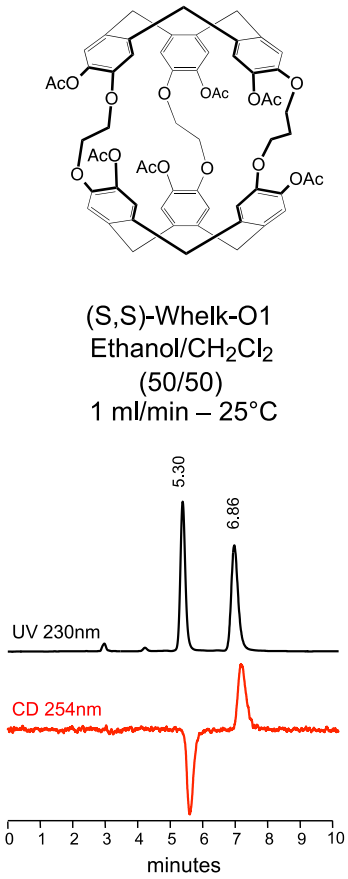

Column	Mobile Phase	t_1	k_1	t_2	k_2	α	Rs
(*S*,*S*)-Whelk-O1	ethanol/CH_2Cl_2 50/50	5.30 (-)	0.80	6.86 (+)	1.32	1.67	4.81

Figure 132: chromatograms ((*S*,*S*)-Whelk-O_1, 250 x 4.6 mm, ethanol/CH_2Cl_2: 50/50, 1 mL/min at 25 °C) of the (rac)-**112** before preparative separation on (*S*,*S*)-Whelk-O_1 (250 x 10 mm, heptane/ethanol/CH_2Cl_2: 35/65, 5 mL/min).

Semi-preparative separation for compound 112

Sample preparation: About 575 mg of compound (rac)-**112** are dissolved in 170 mL of a mixture of ethanol/dichloromethane (30/70). Chromatographic conditions: (*S*,*S*)-Whelk-O_1 (250 x 10 mm), ethanol/dichloromethane (35/65) as mobile phase, flow-rate = 5 ml/min, UV detection at 230 nm. Injections (stacked): 340 times 500 µL, every 4.4 minutes. First fraction: 235 mg of the first eluted [$CD(-)_{254}$]-**112** with ee > 99% on Jasco CD-1595 circular dichroism detector at 254 nm. Second fraction: 200 mg of the second eluted [$CD(+)_{254}$]-**112** with ee > 99.5% on Jasco CD-1595 circular dichroism detector at 254 nm.

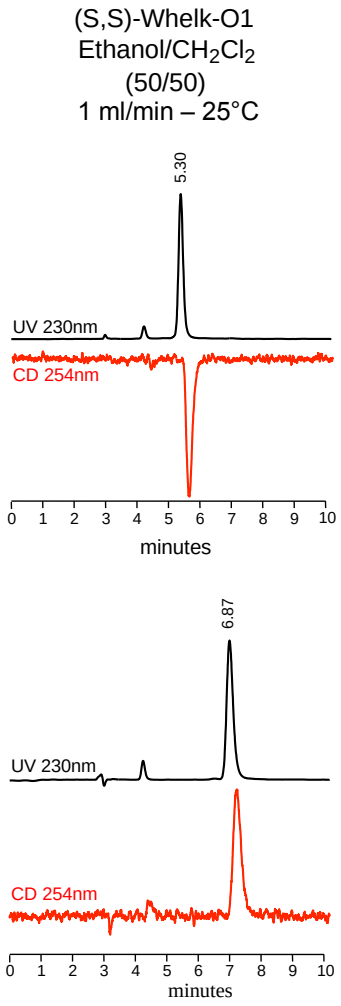

Figure 133: chromatograms ((*S*,*S*)-Whelk-O_1, 250 x 4.6 mm, ethanol/CH_2Cl_2: 50/50, 1 mL/min at 25 °C) of the collected [$CD(-)_{254}$]-**112** and [$CD(+)_{254}$]-**112** after preparative separation on (*S*,*S*)-Whelk-O_1 (250 x 10 mm, ethanol/CH_2Cl_2: 50/50, 5 mL/min). Detection performed by UV-Vis spectroscopy at 230 nm (black chromatograms) and CD spectroscopy at 254 nm (red chromatograms).

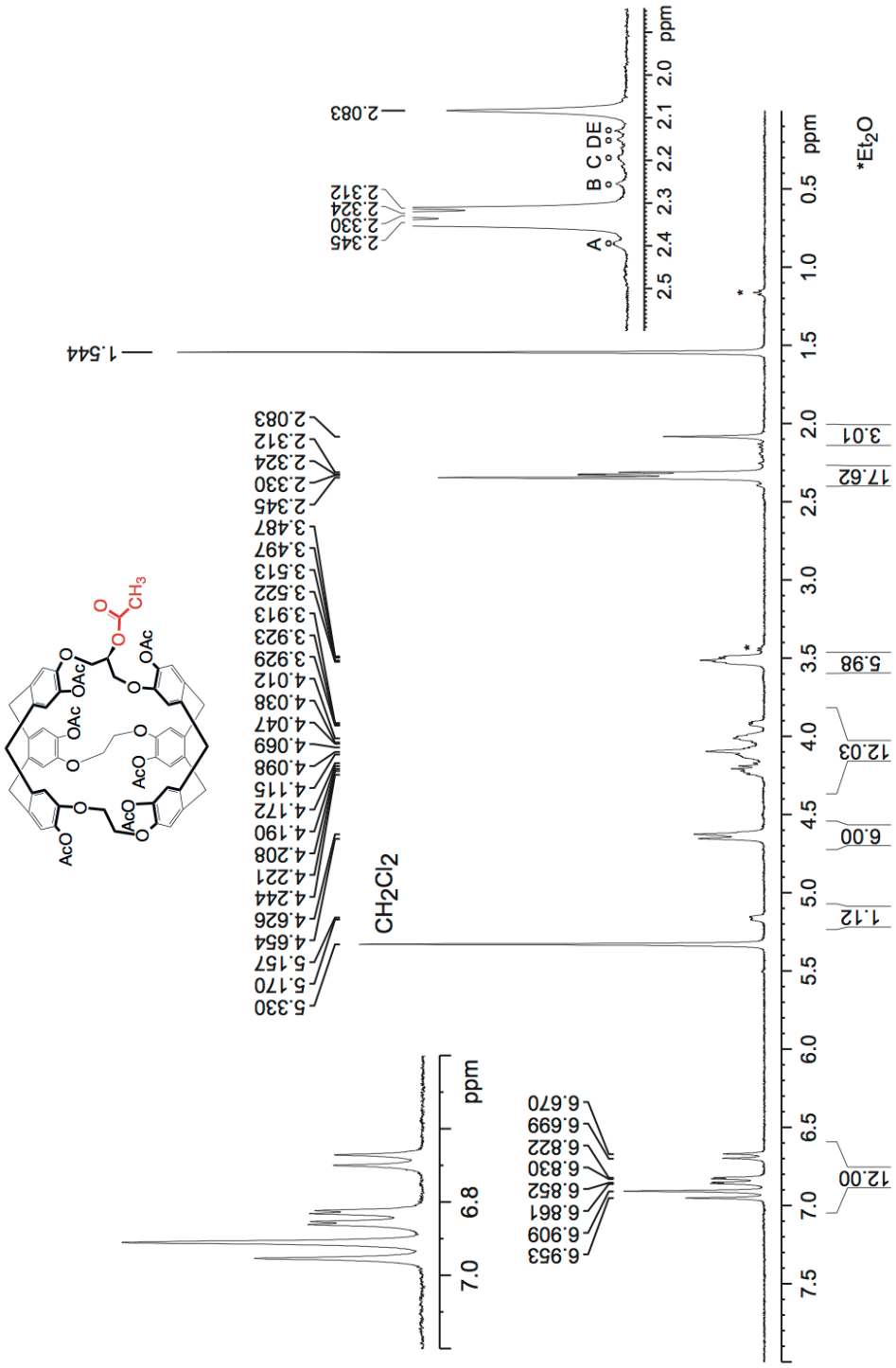

Figure 134: ^{1}H NMR spectrum (300 MHz) of (rac)-**109** recorded in CD_2Cl_2 at 25 °C. The letters A,B,C,D,E show protons signals related to the imploded form.

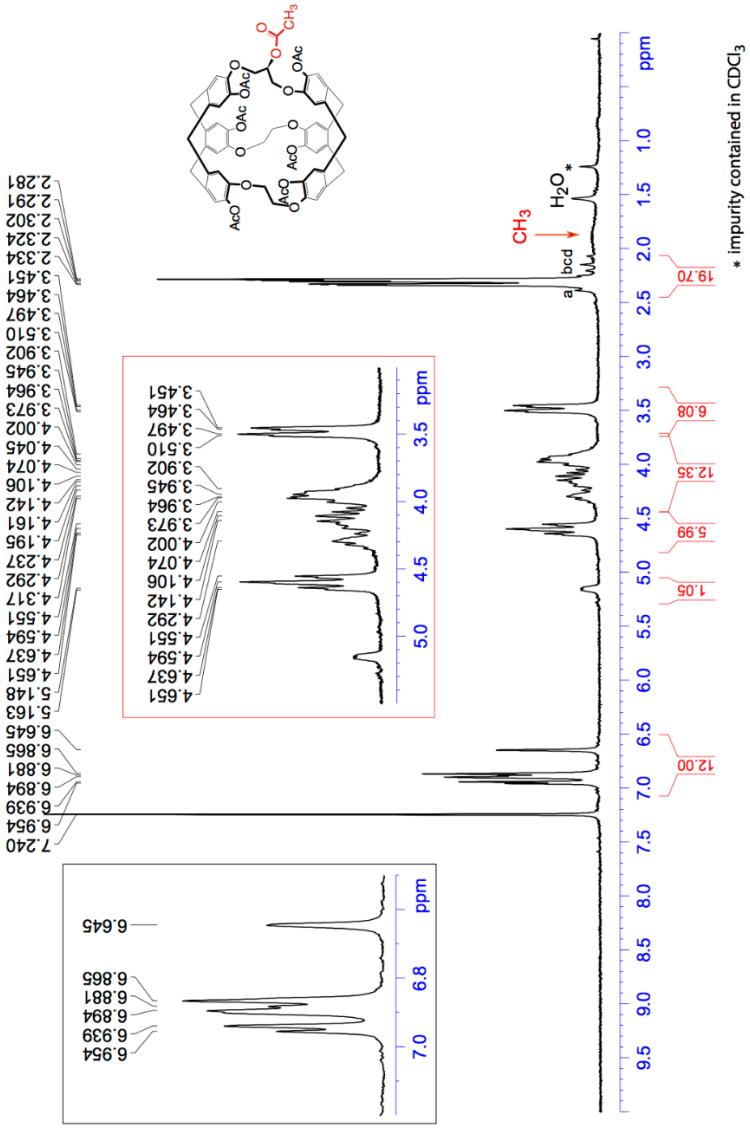

Figure 135: ^{1}H NMR spectrum (300 MHz) of (rac)-**109** recorded in $CDCl_3$ at 25 °C. The letters A,B,C,D show protons signals related to the imploded form.

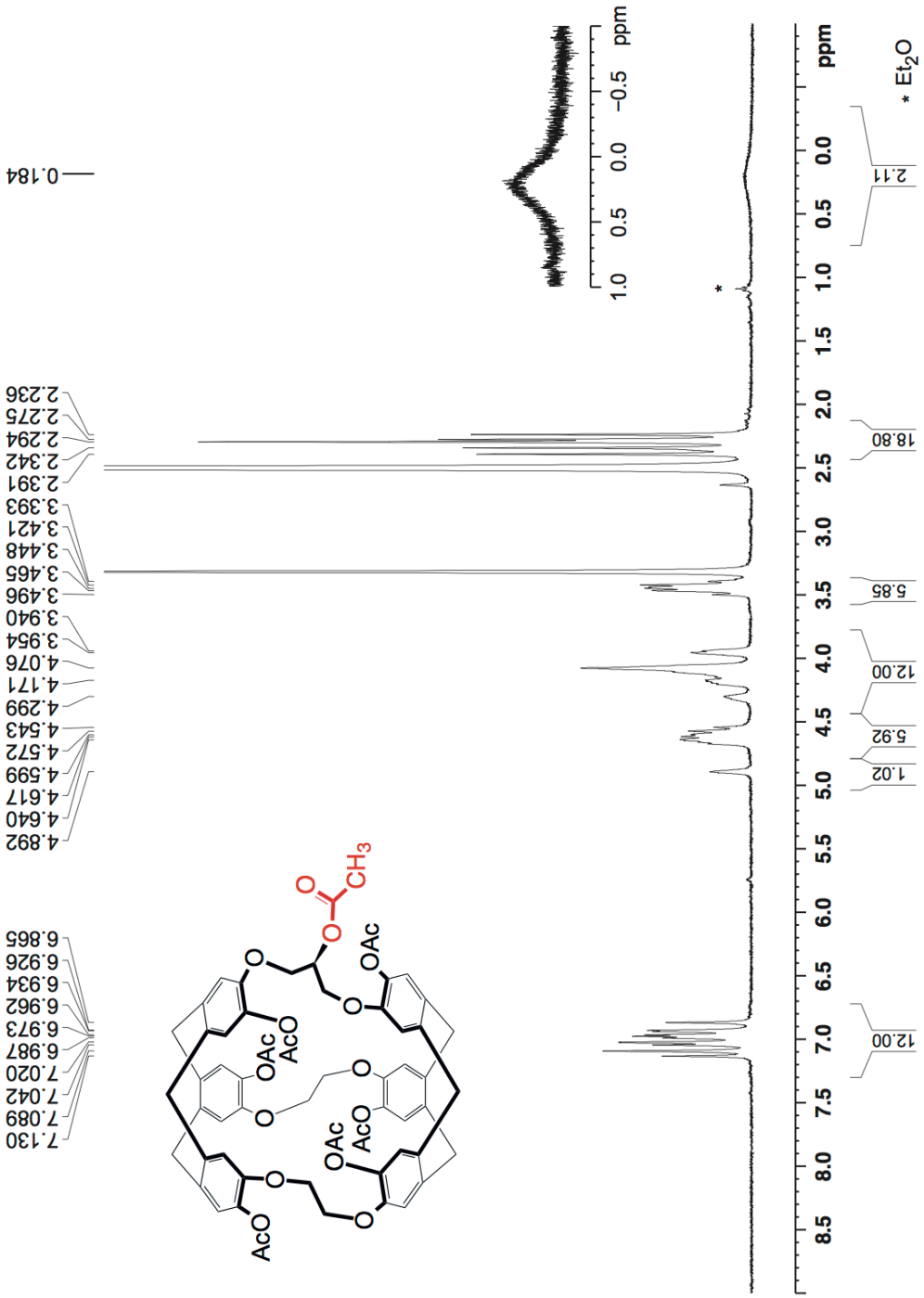

Figure 136: ^{1}H NMR spectrum (300 MHz) of (rac)-**109** recorded in DMSO-d_6 at 25 °C.

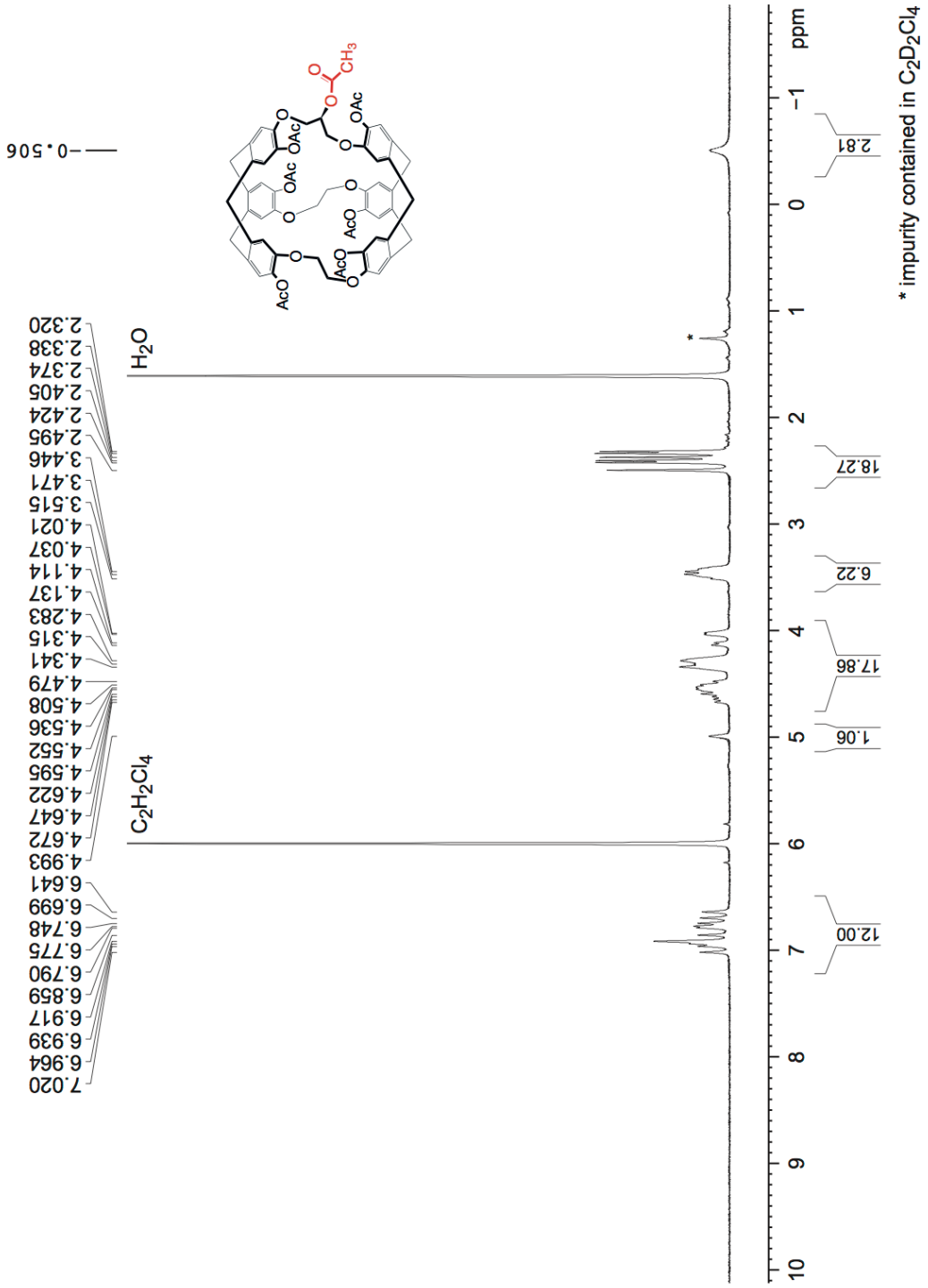

Figure 137: ^{1}H NMR spectrum (300 MHz) of (rac)-**109** recorded in 1,1,2,2-tetrachloroethane-d_2 at 25 °C.

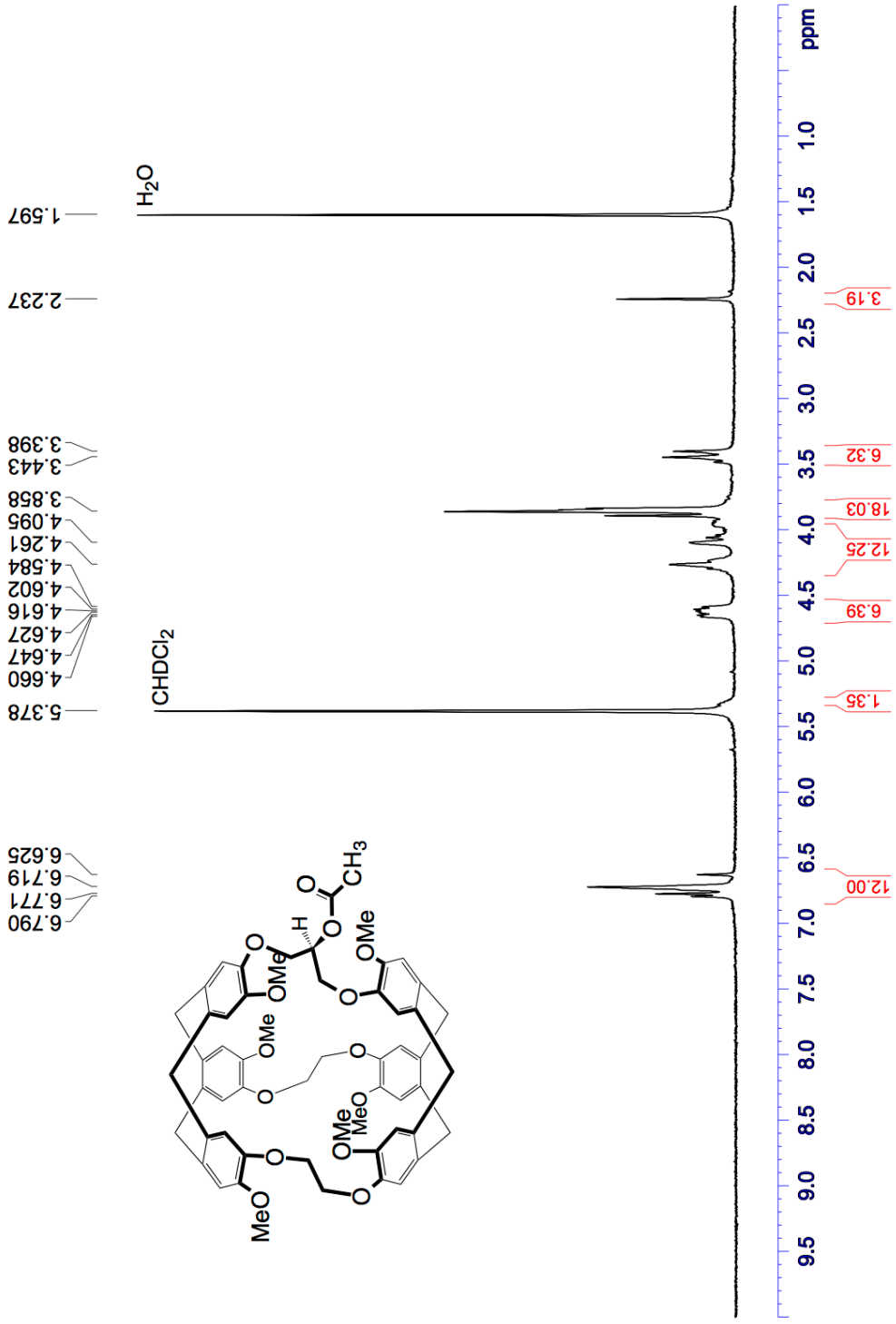

Figure 138: ^{1}H NMR spectrum (300 MHz) of (rac)-**110** recorded in CD_2Cl_2 at 25 °C.

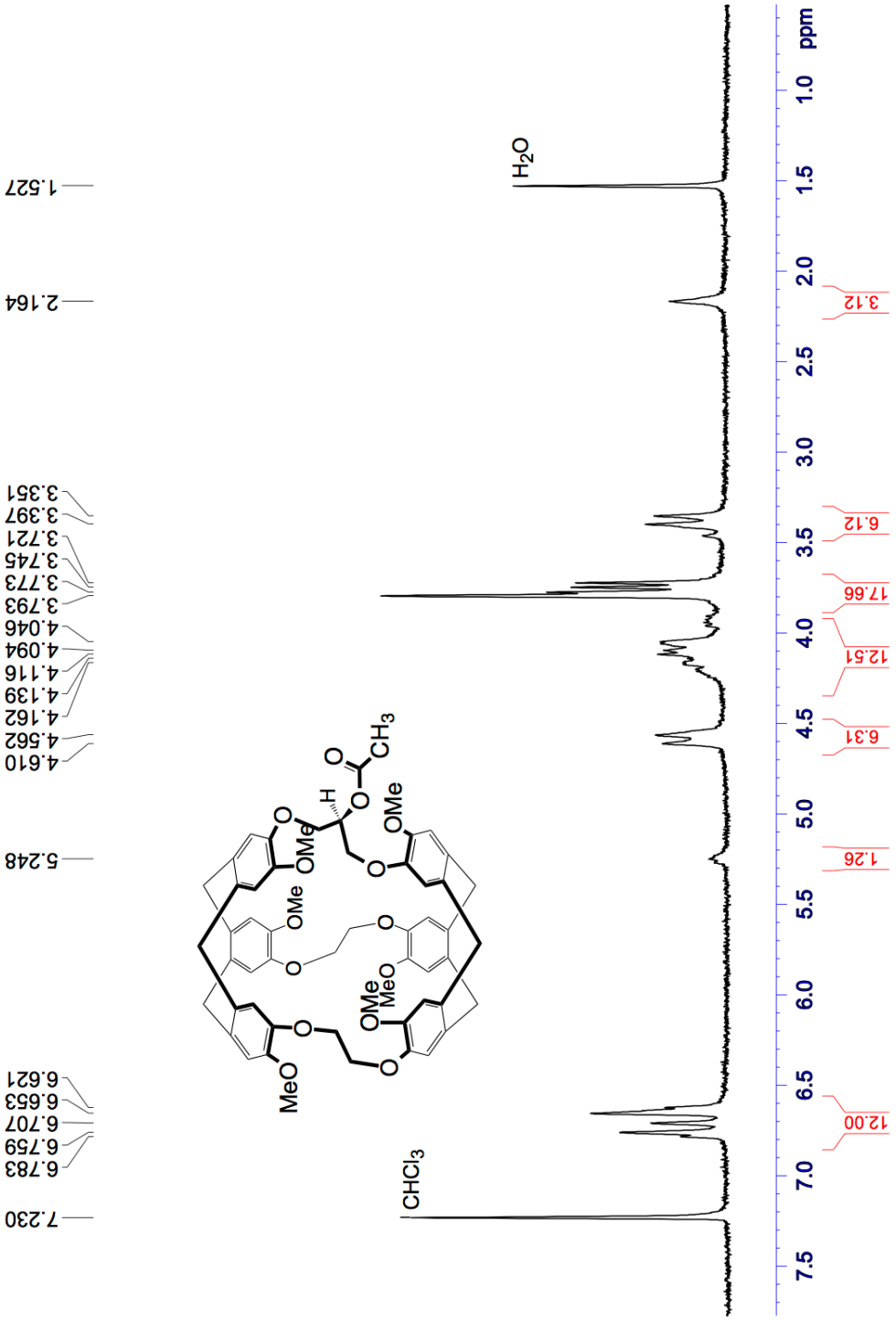

Figure 139: ^{1}H NMR spectrum (300 MHz) of (rac)-**110** recorded in $CDCl_3$ at 25 °C.

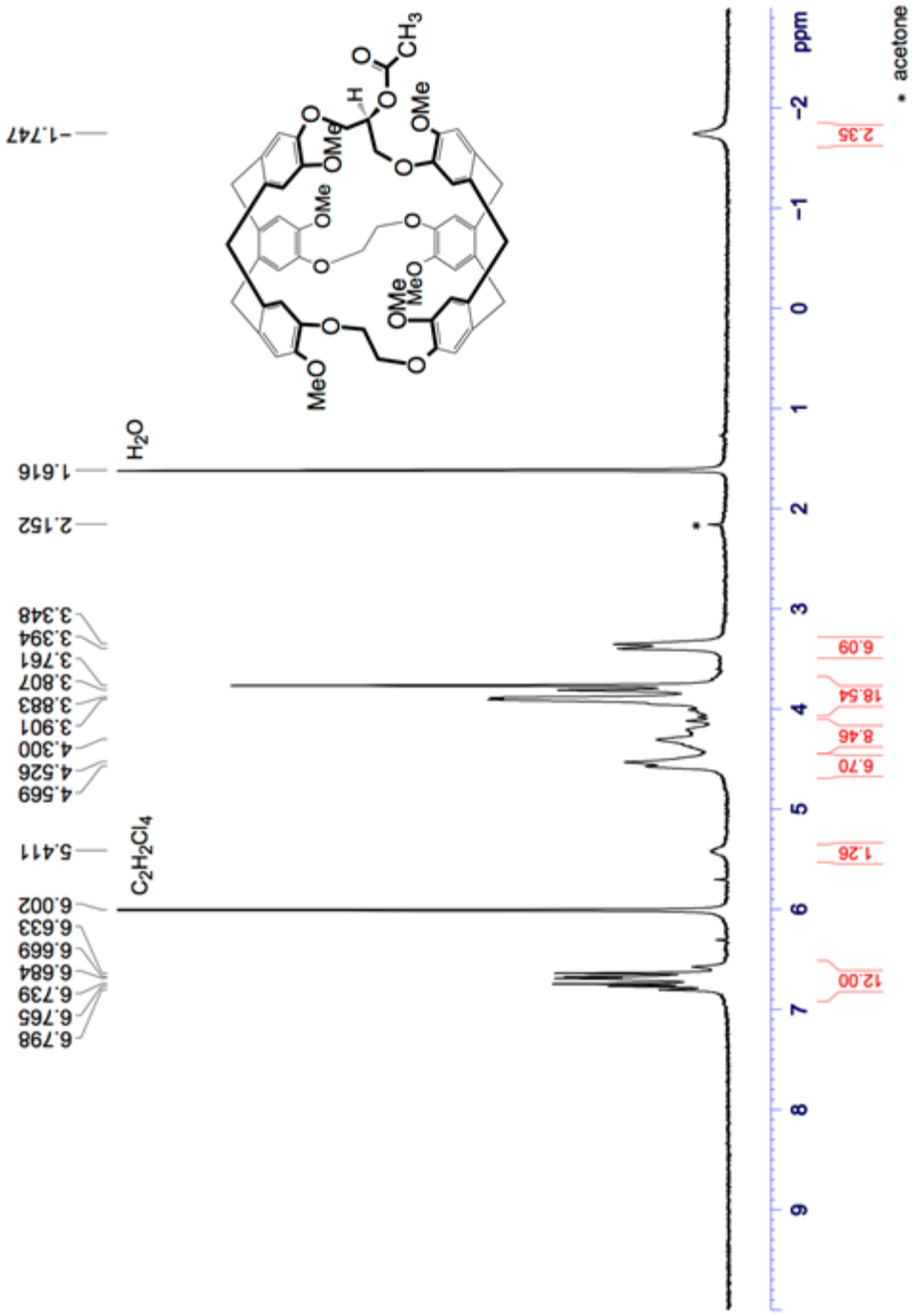

Figure 140: ^{1}H NMR spectrum (300 MHz) of (rac)-**110** recorded in 1,1,2,2-tetrachloroethane-d_2 at 25 °C.

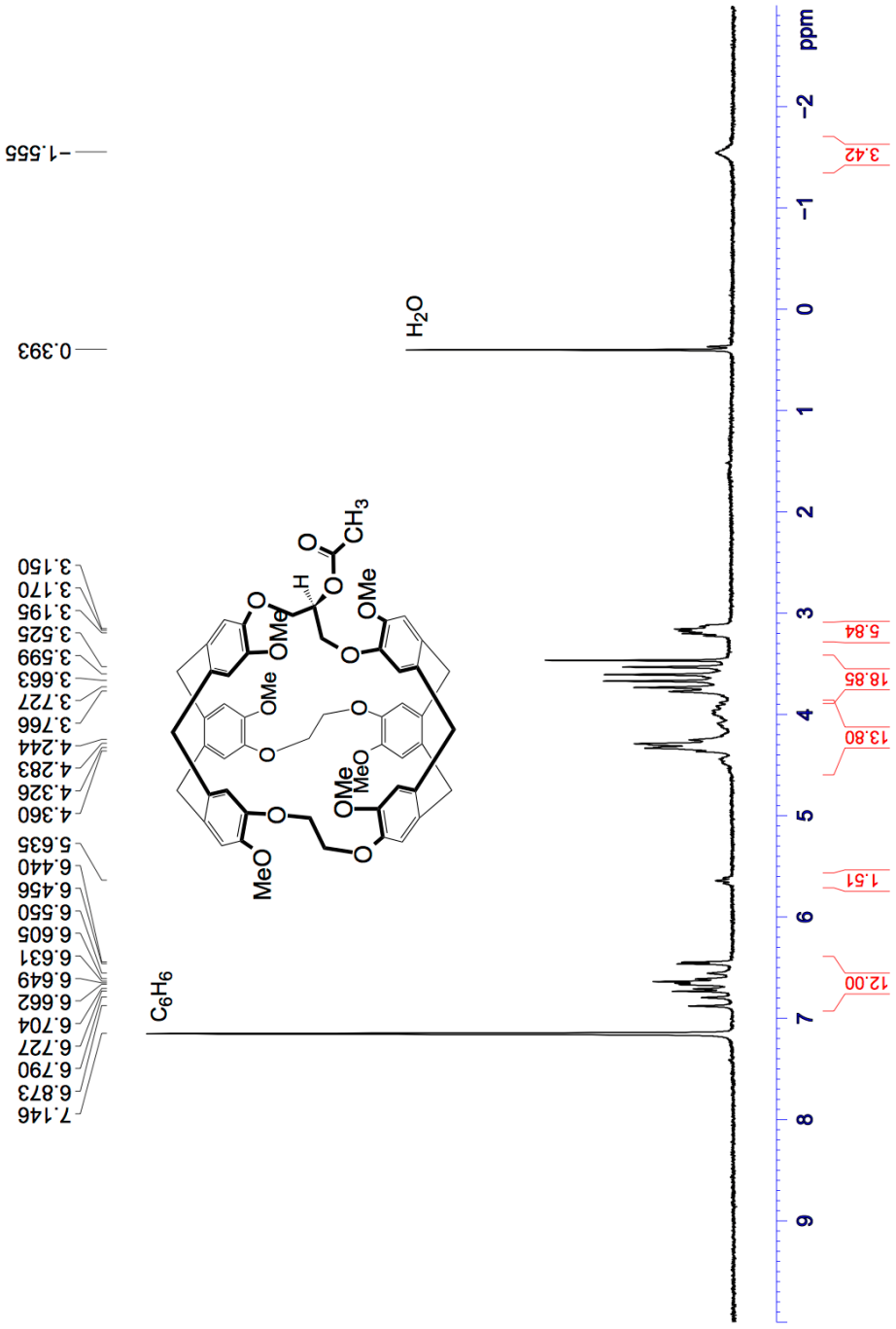

Figure 141: ^{1}H NMR spectrum (300 MHz) of (rac)-**110** recorded in benzene-d_6 at 25 °C.

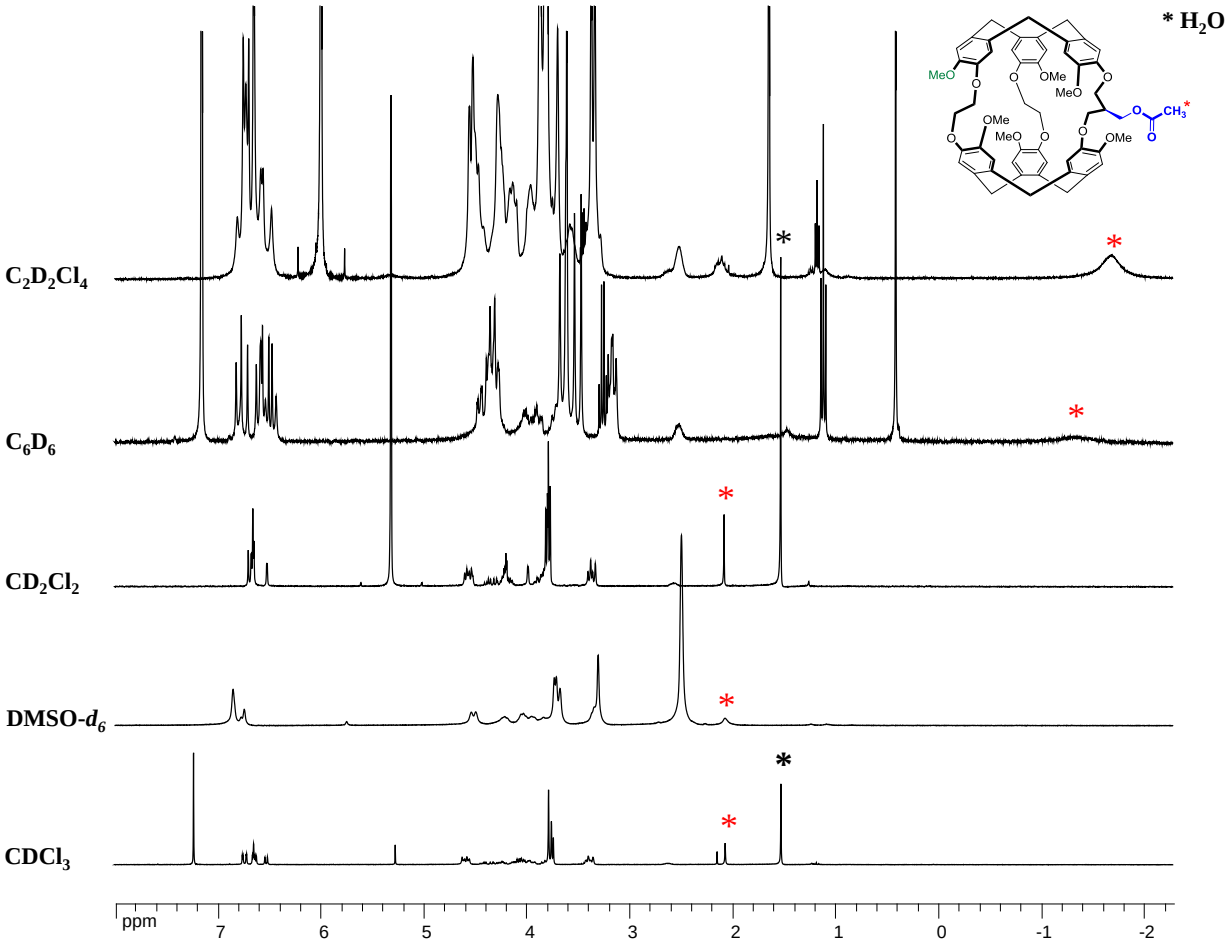

Figure 142: ^{1}H NMR spectrum (300 MHz) of (rac)-**111** recorded in different solvents at 25 °C.

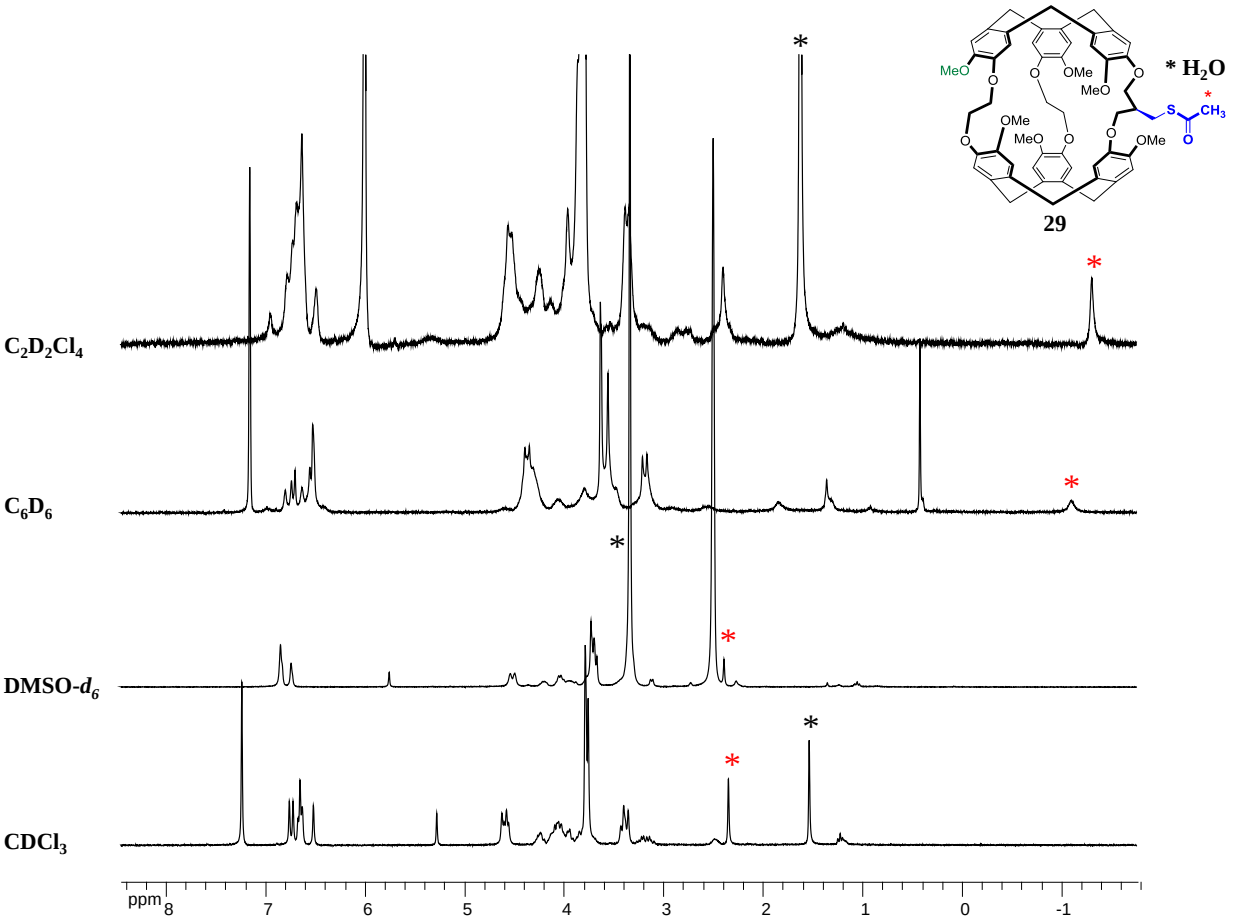

Figure 143: ^{1}H NMR spectrum (300 MHz) of (rac)-**29** recorded in different solvents at 25 °C.

Solvent	Conc.	$[\alpha]_{589}$	$[\alpha]_{577}$	$[\alpha]_{546}$	$[\alpha]_{435}$	$[\alpha]_{365}$
CH_2Cl_2	0.21	-60.1	-62.3	-70.3	-123.4	-190.9
$CHCl_3$	0.23	-25.4	-28.3	-32.1	-48.5	-59.8
DMSO	0.26	+7.2	+7.0	+8.0	+19.9	+61.4
$C_2H_2Cl_4$	0.26	+8.1	+9.1	+12.0	+23.4	+66.3

Specific optical rotation values measured for $[CD(+)_{254}]$-**109** in different solvents at 25 °C.

Solvent	Conc.	$[\alpha]_{589}$	$[\alpha]_{577}$	$[\alpha]_{546}$	$[\alpha]_{435}$	$[\alpha]_{365}$
CH_2Cl_2	0.21	+58.4	+62.0	+70.3	+121.2	+188.2
$CHCl_3$	0.25	+23.9	+24.9	+28.4	+46.9	+57.3
DMSO	0.26	-7.6	-8.9	-9.7	-23.4	-66.1
$C_2H_2Cl_4$	0.29	-10.4	-9.8	-13.6	-26.2	-64.4

Specific optical rotation values measured for $[CD(-)_{254}]$-**109** in different solvents at 25 °C.

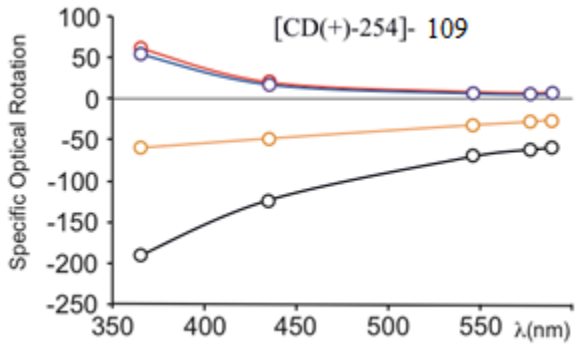

Figure 144: plot of the SOR (10^{-1} deg cm^2 g^{-1}) values versus λ (nm) for the $[CD(+)_{254}]$-**109** enantiomer in CH_2Cl_2 (black), $CHCl_3$ (orange), DMSO (blue) and $C_2H_2Cl_4$ (red) at 25 °C.

Solvent	Conc.	$[\alpha]_{589}$	$[\alpha]_{577}$	$[\alpha]_{546}$	$[\alpha]_{435}$	$[\alpha]_{365}$
CH_2Cl_2	0.19	+159.0	+168.0	+194.5	+359.0	+664.5
$CHCl_3$	0.26	+201.0	+214.1	+246.5	+453.5	+845.1
DMSO	0.31	+228.3	+241.1	+278.8	+510.4	+943.5
$C_2H_2Cl_4$	0.21	+199.0	+213.0	+244.5	+448.0	+835.5

Specific optical rotation values measured for $[CD(+)_{254}]$-**110** in different solvents at 25 °C.

Solvent	Conc.	$[\alpha]_{589}$	$[\alpha]_{577}$	$[\alpha]_{546}$	$[\alpha]_{435}$	$[\alpha]_{365}$
CH_2Cl_2	0.24	-155.0	-163.0	-189.0	-347.0	-652.0
$CHCl_3$	0.27	-200.2	-211.0	-245.0	-446.4	-823.4
DMSO	0.30	-227.8	-239.0	-276.4	-505.0	-936.0
$C_2H_2Cl_4$	0.20	-192.5	-206.0	-236.5	-440.5	-820.0

Specific optical rotation values measured for $[CD(-)_{254}]$-**110** in different solvents at 25 °C.

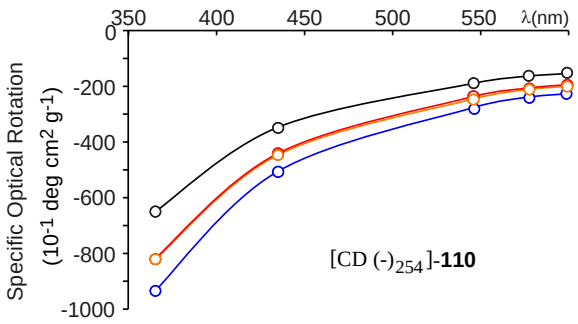

Figure 145: plot of the SOR (10^{-1} deg cm^2 g^{-1}) values versus λ (nm) for the [CD(-)$_{254}$]-**110** enantiomer in CH_2Cl_2 (black), $CHCl_3$ (orange), DMSO (blue) and $C_2H_2Cl_4$ (red) at 25 °C.

Solvent	Conc.	$[\alpha]_{589}$	$[\alpha]_{577}$	$[\alpha]_{546}$	$[\alpha]_{435}$	$[\alpha]_{365}$
CH_2Cl_2	0.28	+150.0	+158.4	+183.8	+343.8	+656.2
$CHCl_3$	0.27	+214.4	+202.3	+235.2	+431.4	+804.1
DMSO	0.25	+215.1	+226.26	+262.7	+480.8	+887.7
$C_2H_2Cl_4$	0.27	+207.1	+213.6	+251.6	+466.8	+872.7

Specific optical rotation values measured for $[CD(+)_{254}]$-**111** in different solvents at 25 °C.

Solvent	Conc.	$[\alpha]_{589}$	$[\alpha]_{577}$	$[\alpha]_{546}$	$[\alpha]_{435}$	$[\alpha]_{365}$
CH_2Cl_2	0.31	-148.8	-148.8	-180.6	-355.4	-639.1
$CHCl_3$	0.24	-190.4	-200.0	--230.2	-420.2	-775.4
DMSO	0.31	-208.5	-218.5	-252.4	-463.6	-855.2
$C_2H_2Cl_4$	0.25	-204.4	-214.5	-249.18	-459.1	-850.0

Specific optical rotation values measured for $[CD(-)_{254}]$-**111** in different solvents at 25 °C.

Solvent	Conc.	$[\alpha]_{589}$	$[\alpha]_{577}$	$[\alpha]_{546}$	$[\alpha]_{435}$	$[\alpha]_{365}$
CH_2Cl_2	0.26	-66.0	-70.1	-78.7	-131.6	-191.3
$CHCl_3$	0.24	-38.6	-40.9	-47.3	-74.5	-90.4
DMSO	0.25	-50.0	-52.9	-60.5	-101.5	-145.0
DMF	0.27	-53.9	-54.8	-61.8	-102.6	-142.3
$C_2H_2Cl_4$	0.30	-38.9	-38.3	-45.7	-75.6	-112.7

Specific optical rotation values measured for $[CD(+)_{254}]$-**112** in different solvents at 25 °C.

Solvent	Conc.	$[\alpha]_{589}$	$[\alpha]_{577}$	$[\alpha]_{546}$	$[\alpha]_{435}$	$[\alpha]_{365}$
CH_2Cl_2	0.25	+62.8	+64.5	+72.9	+122.0	+176.8
$CHCl_3$	0.29	+35.2	+38.0	+42.3	+68.0	+82.5
DMSO	0.26	+47.0	+49.0	+54.8	+92.2	+127.5
DMF	0.26	+45.3	+49.4	+55.0	+88.1	+118.5
$C_2H_2Cl_4$	0.31	+34.0	+35.1	+43.9	+68.2	+102.0

Specific optical rotation values measured for $[CD(-)_{254}]$-**112** in different solvents at 25 °C.

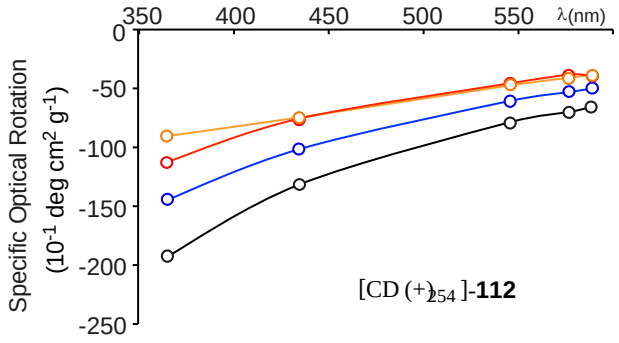

Figure 146: plot of the SOR (10^{-1} deg cm^2 g^{-1}) values versus λ (nm) for the [$CD(+)_{254}$]-**112** enantiomer.

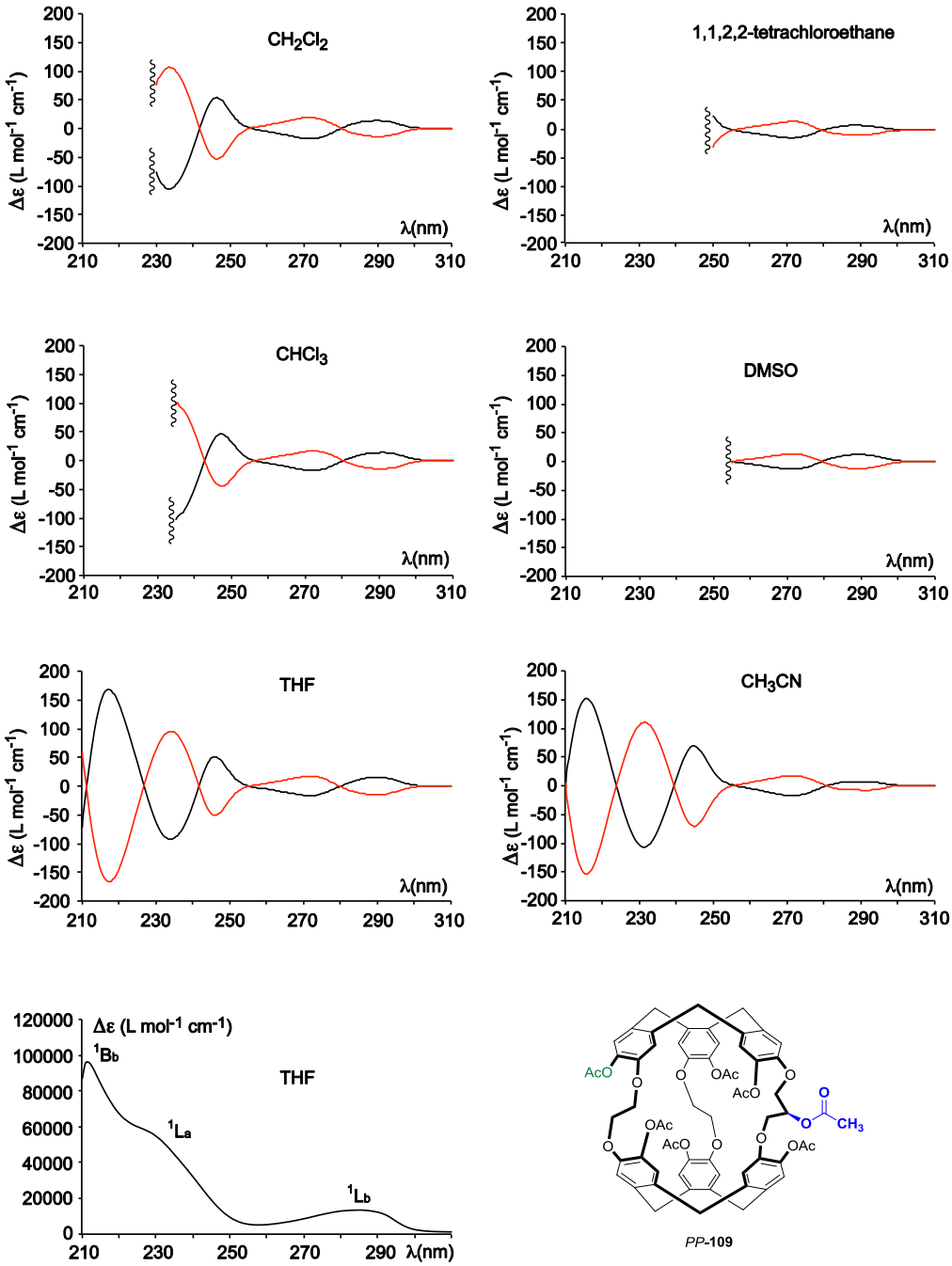

Figure 147: ECD spectra of [CD(+)$_{254}$]-**109** (black spectra) and [CD(-)$_{254}$]-**109** (red spectra) recorded in CH_2Cl_2, $CHCl_3$, THF, CH_3CN, DMSO and $C_2H_2Cl_4$ at 20 °C. (c = 10^{-4} – 10^{-5} M). UV-visible spectrum of **109** recorded in THF at 25 °C (c = 1.12 10^{-5} M).

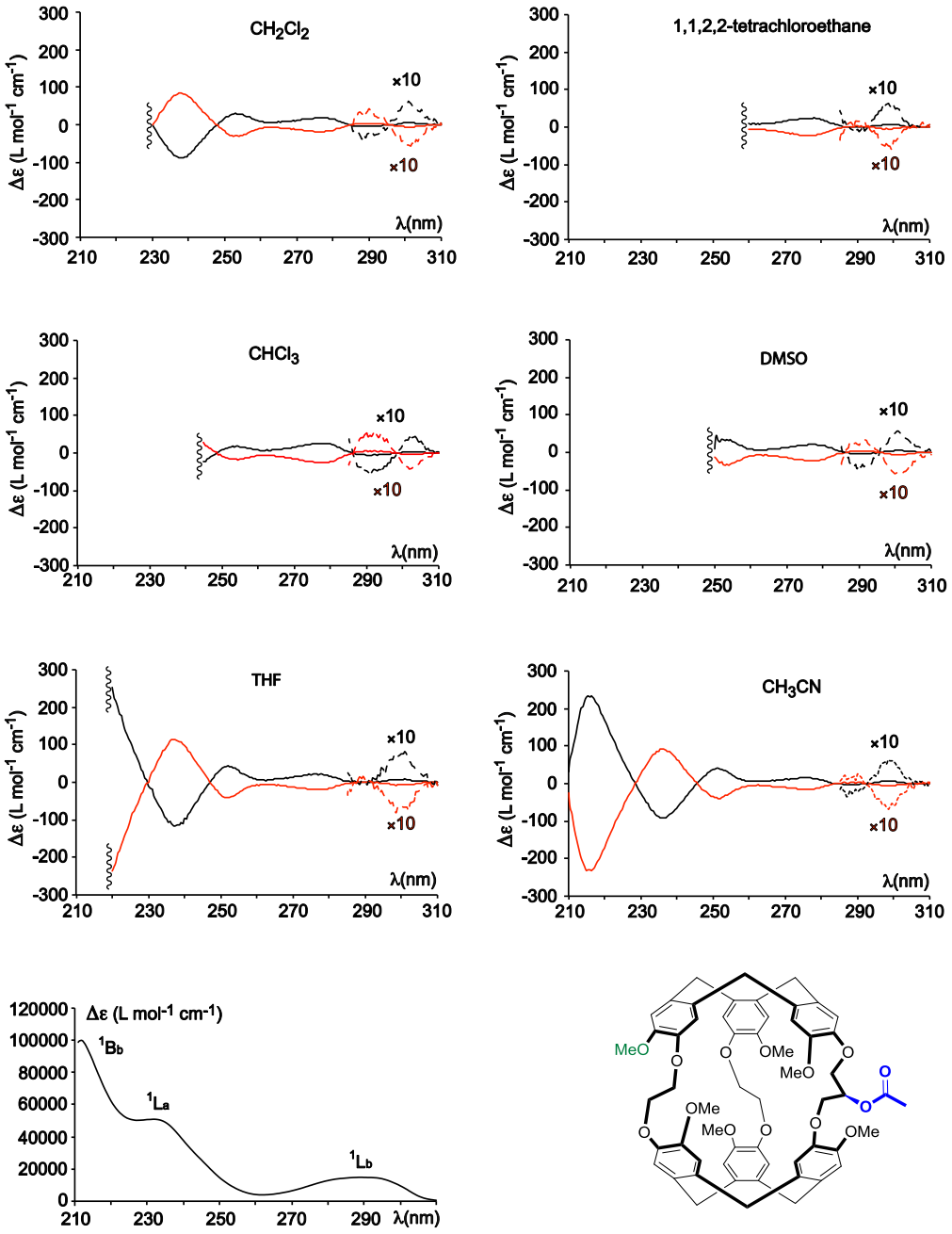

***MM*-110**

Figure 148: ECD spectra of [CD(+)$_{254}$]-**110** (black spectra) and [CD(-)$_{254}$]-**110** (red spectra) recorded in CH_2Cl_2, $CHCl_3$, THF, CH_3CN, DMSO and $C_2H_2Cl_4$ at 20 °C. (c = 10^{-4} – 10^{-5} M). UV-visible spectrum of **110** recorded in THF at 25 °C (c = 1.02 10^{-5} M).

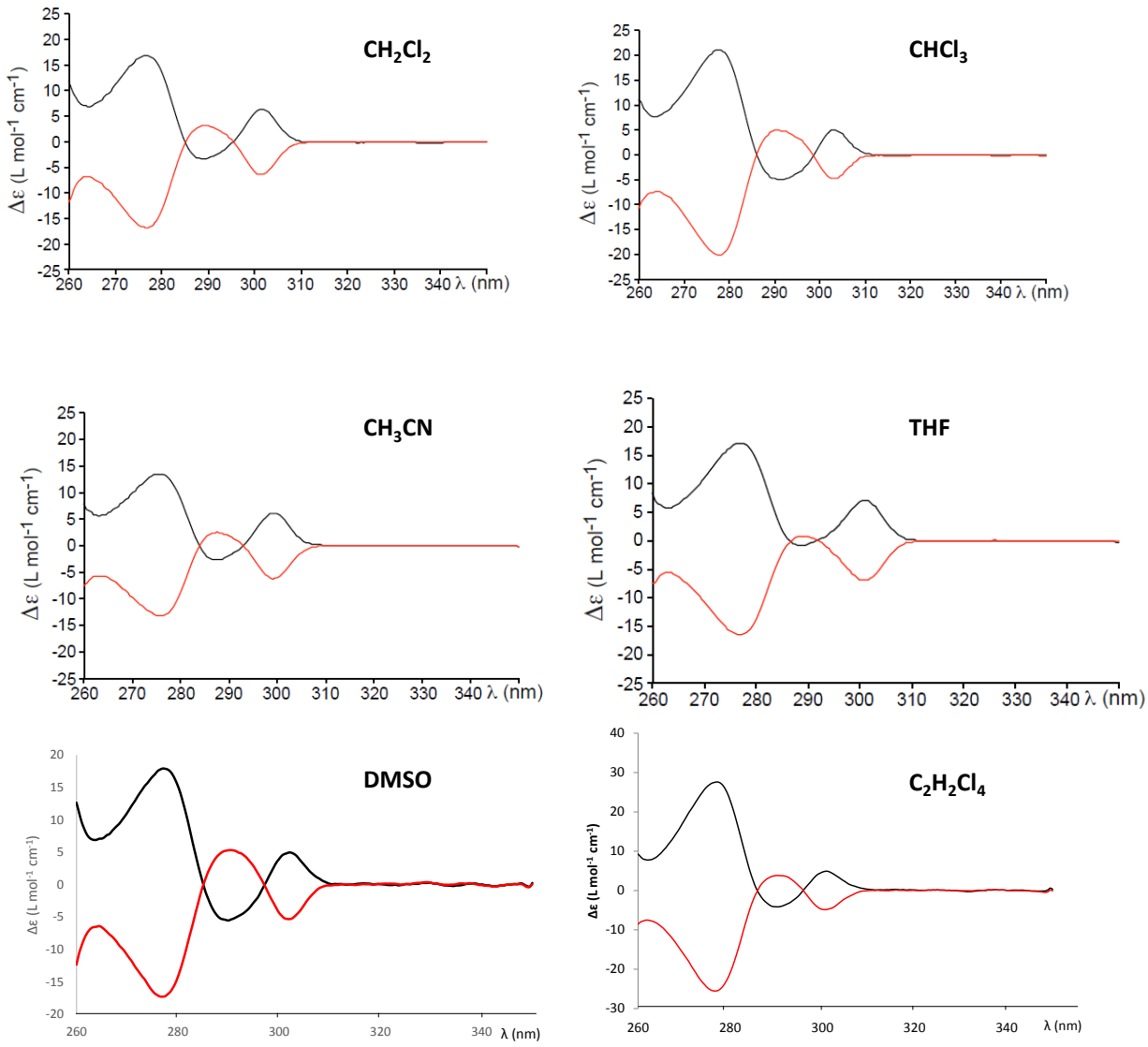

Figure 149: ^1L_b transition of the ECD spectra of [CD(+)$_{254}$]-**111** (black spectra) and [CD(-)$_{254}$]-**111** (red spectra) recorded in CH_2Cl_2, $CHCl_3$, THF, CH_3CN, DMSO and $C_2H_2Cl_4$ at 20 °C. (c = 10^{-4} – 10^{-5} M).

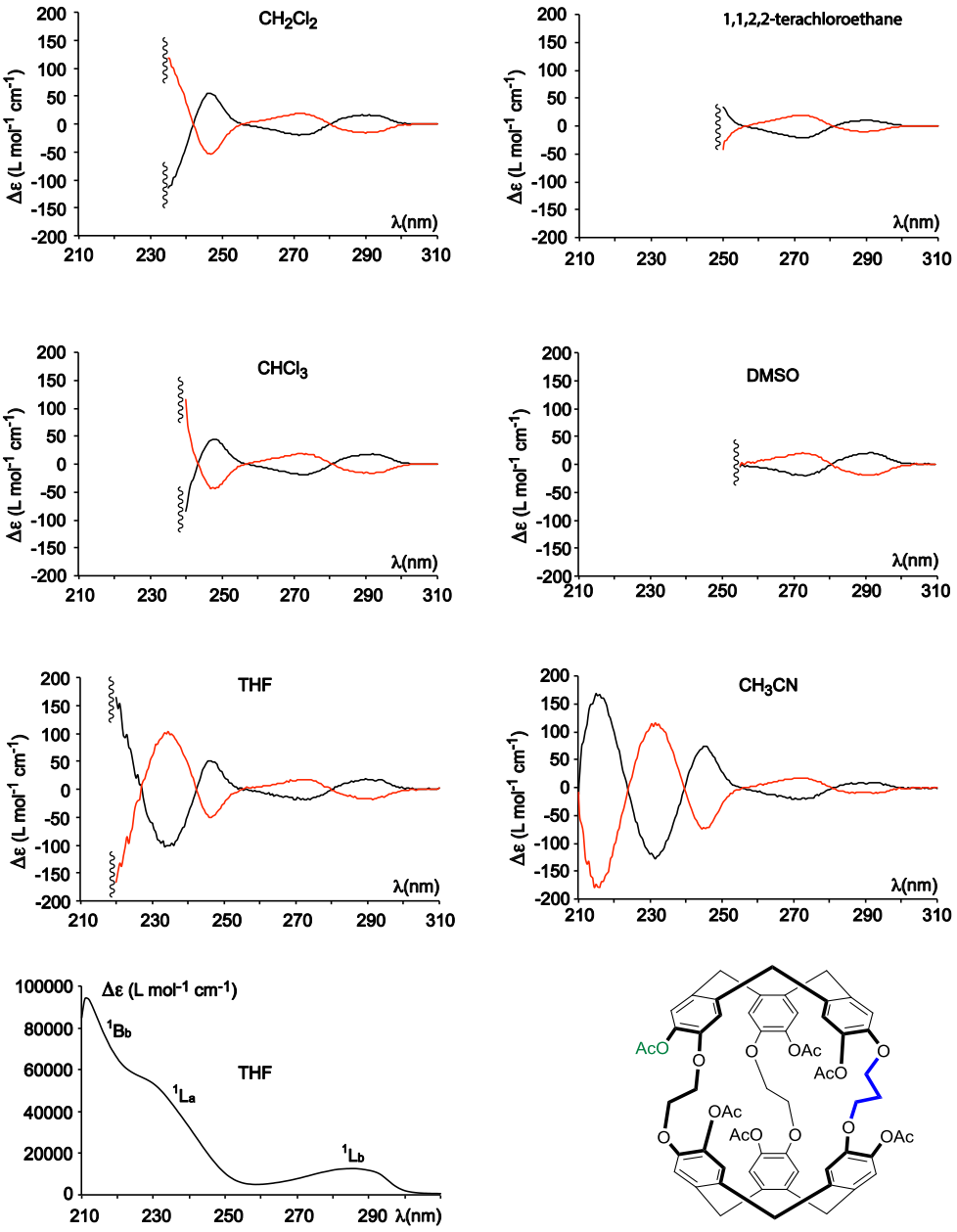

***PP*-112**

Figure 150: ECD spectra of [CD(+)$_{254}$]-**112** (black spectra) and [CD(-)$_{254}$]-**112** (red spectra) recorded in CH_2Cl_2, $CHCl_3$, THF, CH_3CN, DMSO and $C_2H_2Cl_4$ at 20 °C. (c = 10^{-4} – 10^{-5} M). UV-visible spectrum of **112** recorded in THF at 25 °C (c = 0.99 10^{-5} M).

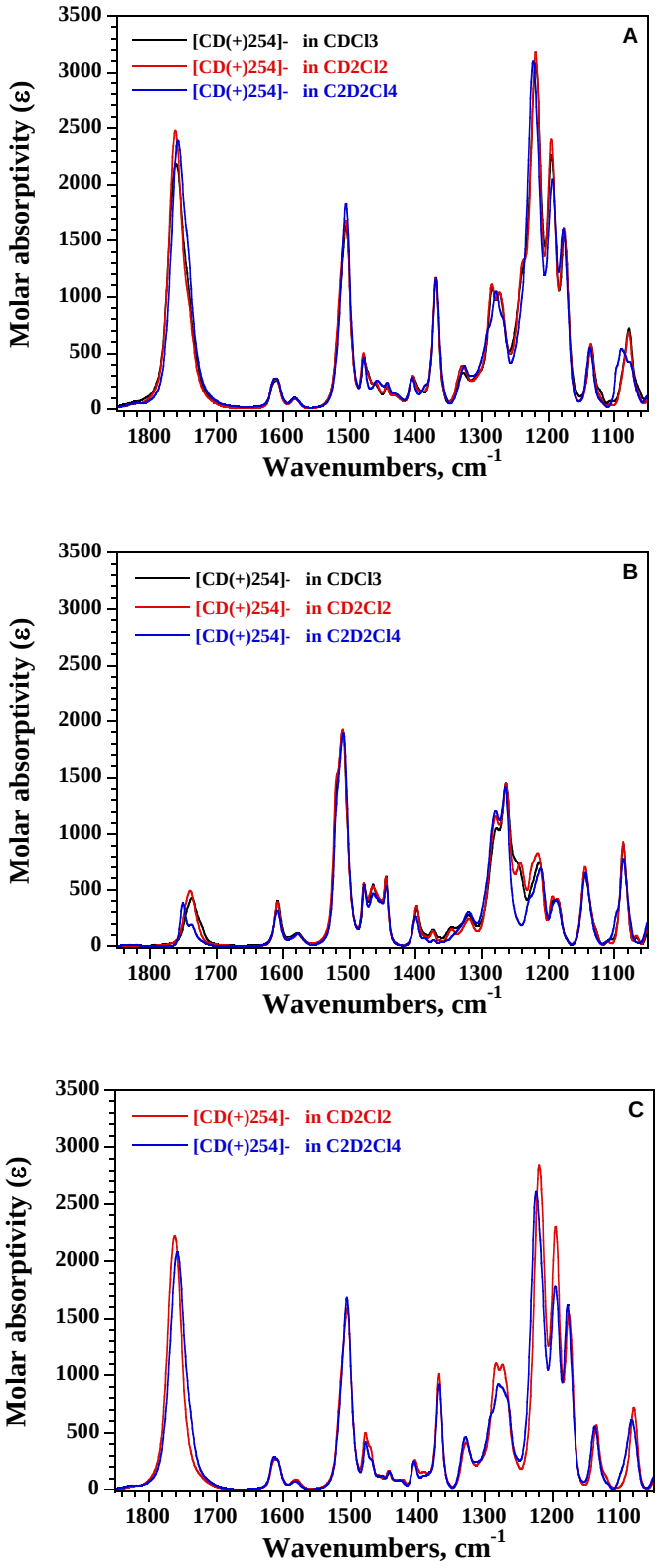

Figure 151: IR spectra of a) [CD(+)$_{254}$]-**109**, b) [CD(+)$_{254}$]-**110** and [CD(+)$_{254}$]-**112** c) in $CDCl_3$ (black spectra), CD_2Cl_2 (red spectra) and $C_2D_2Cl_4$ (blue spectra) solvents (0.015 mM, 250 µm path length).

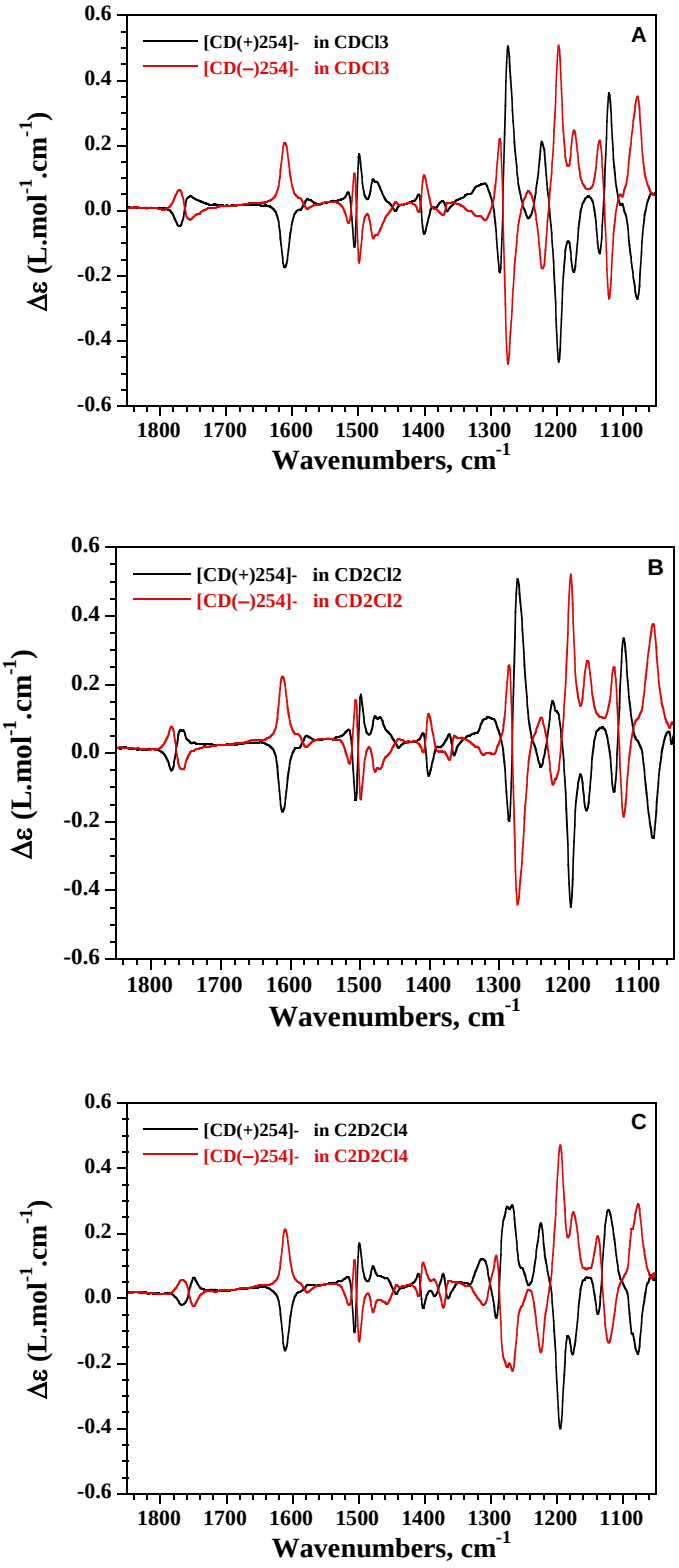

Figure 152: VCD spectra of [CD(+)$_{254}$]-**109** (black spectra) and [CD(-)$_{254}$]-**109** (red spectra) in a) $CDCl_3$, b) CD_2Cl_2, and c) $C_2D_2Cl_4$ solvents (0.015 mM, 250 µm path length).

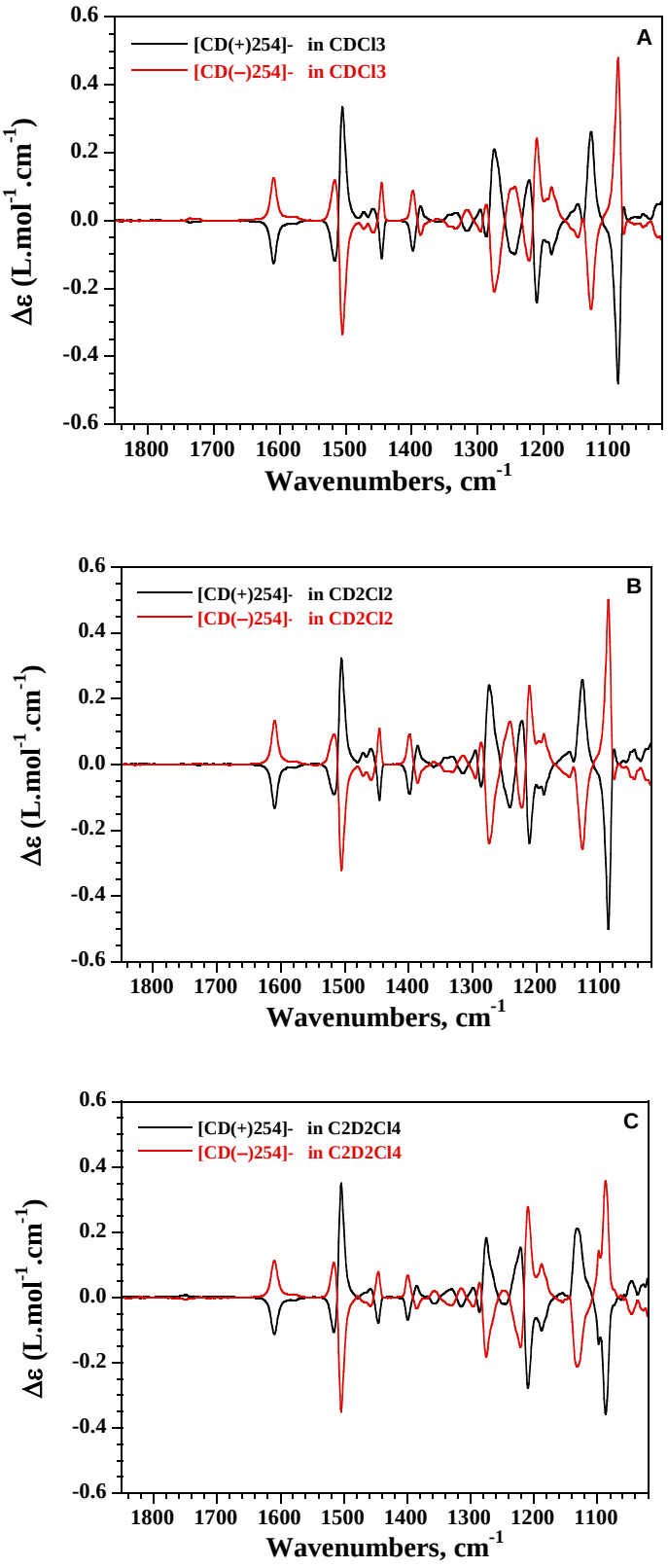

Figure 153: VCD spectra of [CD(+)$_{254}$]-**110** (black spectra) and [CD(-)$_{254}$]-**110** (red spectra) in a) $CDCl_3$, b) CD_2Cl_2, and c) $C_2D_2Cl_4$ solvents (0.015 mM, 250 µm path length).

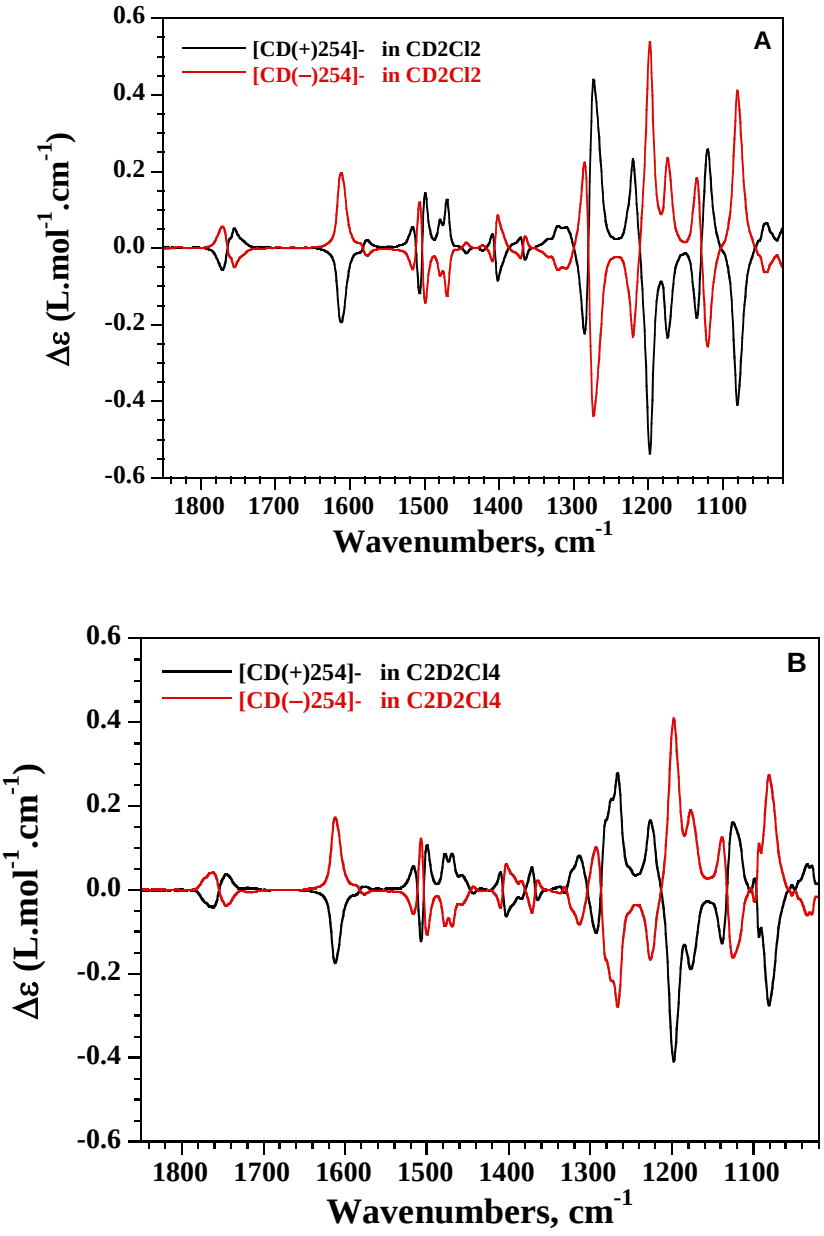

Figure 154: VCD spectra of [CD(+)$_{254}$]-**112** (black spectra) and [CD(-)$_{254}$]-**112** (red spectra) in a) CD_2Cl_2 and b) $C_2D_2Cl_4$ solvents (0.015 mM, 250 µm path length).

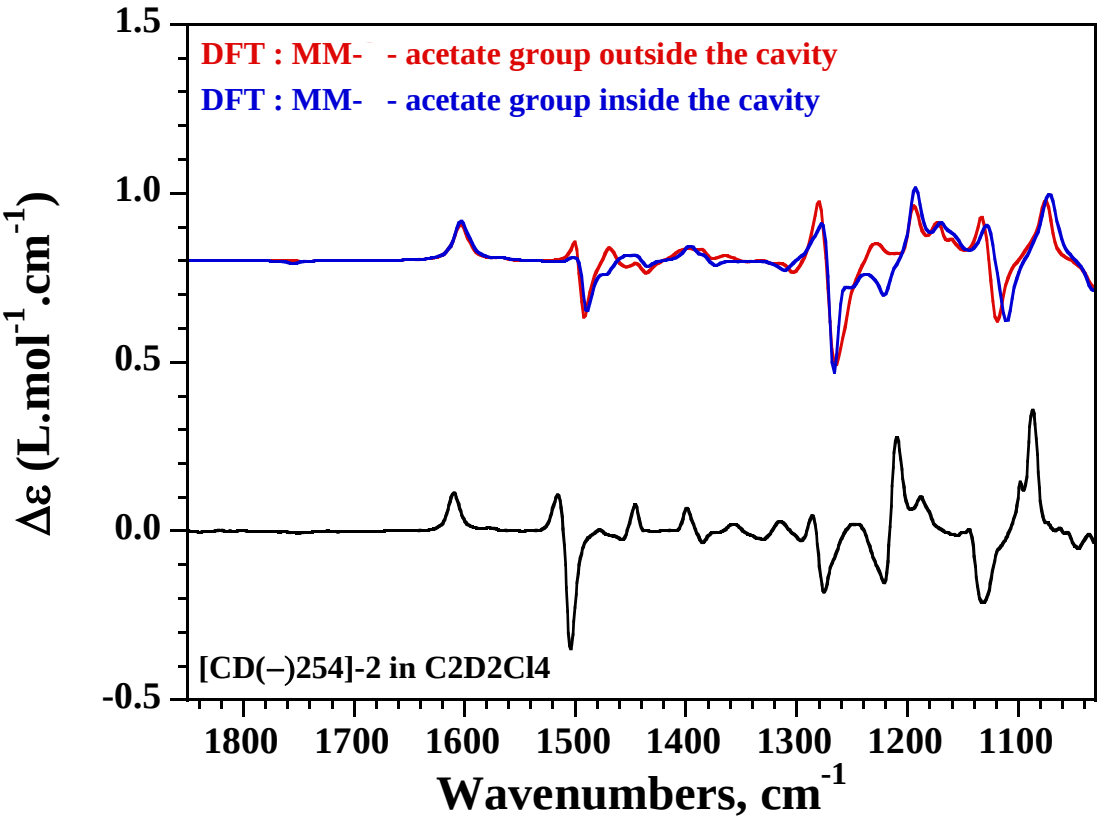

Figure 155: comparison of experimental VCD spectrum of [CD(-)$_{254}$]-**110** in $C_2D_2Cl_4$ solution (15 mM, 250 µm path length) and VCD spectra of *MM*-**110** calculated at the B3LYP/6-31G** level (IEFPCM = $C_2H_2Cl_4$) for the *trans* and *gauche-gauche* conformations of the ethylenedioxy and propylenedioxy linkers, respectively, and for the acetate group grafted on the propylenedioxy linker pointing inside (blue spectrum) or outside (red spectrum) the cavity.

	IEFPCM = CH_2Cl_2	IEFPCM = $C_2D_2Cl_4$
Acetate pointing inward the cavity	1753.58	1755.17
Acetate pointing outward the cavity	1741.42	1742.52

B3LYP/6-31G** frequencies (scaled by 0.968) of the ester ν C=O stretching vibration of *MM*-**110** (IEFPCM = CH_2Cl_2 and $C_2D_2Cl_4$) for the acetate group pointing inward or outward the cavity.

General Conclusion

General Conclusion

Cryptophanes have been first described by André Collet and widely developed in the laboratory of the ENS de Lyon. Since that time, the chemistry of cryptophanes has been limited to fundamental academic research, which focuses on the comprehension of supramolecular interactions. Since 2001, cryptophanes combined with hyperpolarized xenon have emerged as a breakthrough in molecular imaging dedicated for biological applications. Large number of xenon-cryptophane biosensors have been reported for in *vitro* and in *cellulo* imaging. The high sensitivity, fast responsiveness and exogenous nature of such sensors highlighted the chemistry of cryptophanes and triggered researchers to develop new faster routes for their synthesis in decent amounts. Most of these developed routes utilize cryptophane-[222] platform, which may suffer from low water solubility leading to non-specific interactions with cellular membranes and high symmetry making its functionalization and scaling up hard to achieve

As a solution for these two problems, we have developed a new approach to synthesize water-soluble easily functionalizable xenon cages based on cryptophane-[223] skeleton. Our platforms are dually functionalized that bear a lateral carboxylic acid moiety on their propelenedioxy arm and six ester groups as water-soluble precursors grafted on their CTB caps. With the available carboxylic acid group, successful functionalization of these platforms with different sensing arms like hydroxamic acid, APTRA unit and biotin derivative was made possible via amide coupling reaction. Elaboration of water soluble sensors was performed by an additional ester deprotection step. The obtained biosensors were produced in decent amounts and they showed acceptable solubility in water in the required concentration range. The ability of these cages to bind xenon was assessed with our collaborator Dr. Patrick Berthault in CEA, Saclay, Paris. These characterizations revealed that our molecules effectively bind xenon, as expected, with an in-out exchange dynamic suitable for performing hyper-CEST experiments. Unfortunately, the sensing

responsiveness of our sensors seems to be partially diminished compared to the reported cryptophane-[222] sensors. This is mainly due the position of the sensing unit, which is located on the propelendioxy arm. At this position, any change in the sensing units affects less the aromatic ring current, which in turn induces little changes in the magnetic field around xenon, hence will be translated as little change in xenon chemical shift. Nevertheless, our platforms can still be used as MRI tracers, when connected to a sensing unit whose affinity to the targeted analyte is very high, as seen with the biotin functionalized cage. With these results in hands, we can conclude that the position of the sensing unit is of particular importance to tune the responsiveness of xenon-biosensors. The next step in this subject involves the optimization of the some synthetic steps and functionalization of our platforms by different biologically active units to target biological events.

Our cryptophane-[223] derivatives show a unique solvent-dependent self-encapsulation behavior of their central function. Unlike the imploded form, which is energetically demanding, self-encapsulation takes place spontaneously at room temperature in the absence of a potential guest. This interesting phenomenon induces large conformational changes, which were successfully proved by ^{1}H NMR and IR spectroscopy. The chiroptical study of these enantiopure cages, which were separated by our collaborator at Aix Marseilles University, Dr. Nicolas Vanthuyne, revealed that the overall chiroptical properties of these cages were modified under the effect of self-encapsulation. Specifically, polarimetry appears to be the most sensitive technique to small conformational variations in organic solvents. Other spectroscopic techniques like ECD and VCD combined with DFT calculation, which were performed with our collaborators Dr. Thierry Buffeteau and Dr. Nicolas Daugey in Bordeaux, have mainly served in the determination of the AC of cryptophanes, where the direct determination of AC is hard to assess.

Appendix

Appendix

1. Nuclear Magnetic Resonance (NMR) Spectroscopy Principles

Any nucleus with an odd number of protons and/or neutrons has a charge with a characteristic spin *(I)* of (m_I) different orientations of (2*I*+1) values varying from *–I, 2I+1* to *+I* states, all of which are degenerate (have the same energy). A proton, for example, has an (*I*) =1/2 which means, it has two allowed spin states (m_I) of 1/2 and -1/2. The spinning of this nucleus creates a characteristic magnetic field with a magnetic moment (μ) which is related to (*I*) by an intrinsic constant, gyromagnetic ratio (γ), characteristic to each nucleus (eq. 1), Figure 156.

$$\mu = \hbar \gamma I \qquad \text{eq. 1}$$

ħ: reduced planks constant

In the presence of an external uniform magnetic field B_0, the randomly orientated nuclei will align themselves in the direction of the applied magnetic field and they will lose their degeneracy due to the interaction of their magnetic moments with external applied field (Zeeman energy levels). Nuclei with lower energy, α state, orient themselves with the direction of the field, whereas nuclei with higher energy align in the opposite direction, β state. The energy values of each state are linear values to B_0 and it is given in (eq. 2).

$$E = -\hbar \gamma m_I B_0 \qquad \text{eq. 2}$$

The thermal population distribution between the two states is based on Boltzmann distribution coefficient given in (eq.3) where *N* represents the number of nuclei residing in the lower and higher energy states, N_α and N_β, respectively, *K* is the Boltzmann constant and *T* is temperature.

$$N_\beta / N_\alpha = e^{\Delta E/KT} = e^{(-\hbar \gamma B0)/KT} \qquad \text{eq.3}$$

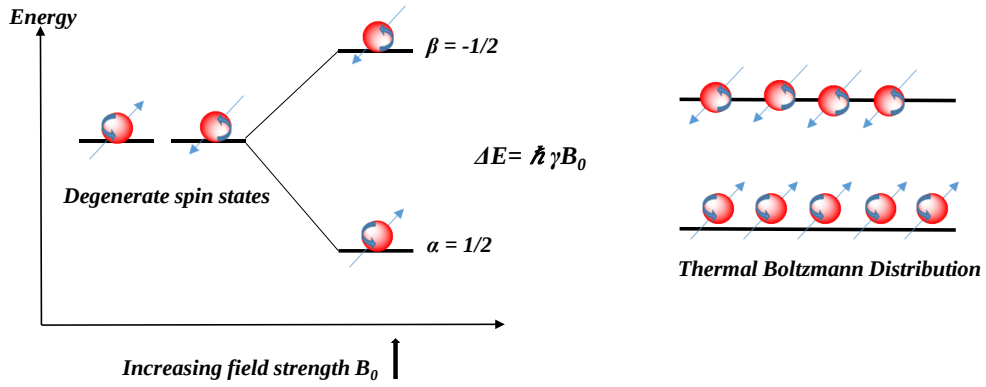

Figure 156: population distribution of spins at equilibrium state.

For protons in 1.41 T magnet, the distribution coefficient between the two states is equal to 0.9999382 which means that there is a slight excess on nuclei in the lower energy state directed parallel to the magnetic field. The difference in population between the two states is referred to as polarization (*P)* and it is expressed in (eq. 4).

$$P = N_\alpha - N_\beta / N_\alpha + N_\beta \approx (\hbar \gamma B_0) / 2KT \qquad \text{eq.4}$$

This will be expressed as a net longitudinal magnetization M_0 in the direction of the applied field B_0, (eq. 5) where N_s represents the excess of population residing in the α state.

$$M_0 = (N_S \hbar \gamma P)/2 \qquad \text{eq.5}$$

The nuclei at this stage are known to precess in the direction of B_0 because they cannot be really oriented parallel or anti-parallel to it. The precession frequency is the known Larmor frequency $G\mathcal{O}_0$ and it is expressed in (eq. 6).

$$G\mathcal{O}_0 = \gamma B_0 \qquad \text{eq. 6}$$

Once a radio frequency pulse is applied, excess of nuclei in the lower energy will be excited to a higher energy sate, and they will coherently precess, creating a transverse magnetization along

the y-axis. Once the pulse is removed the nuclei relax back to their initial state first by a spin-spin or transverse T_2 relaxation resulting from the collision of the nuclei, and then a spin-lattice relaxation or longitudinal T_1 relaxation resulting a dissipation of the thermal energy from one spin to the surrounding lattice environment and thus re-growing the initial longitudinal magnetization M_0. The energy emitted after this process is detected as free induction decay (FID) and can be converted to a spectrum as a function of frequency by a Fourier transform, Figure 157.[208]

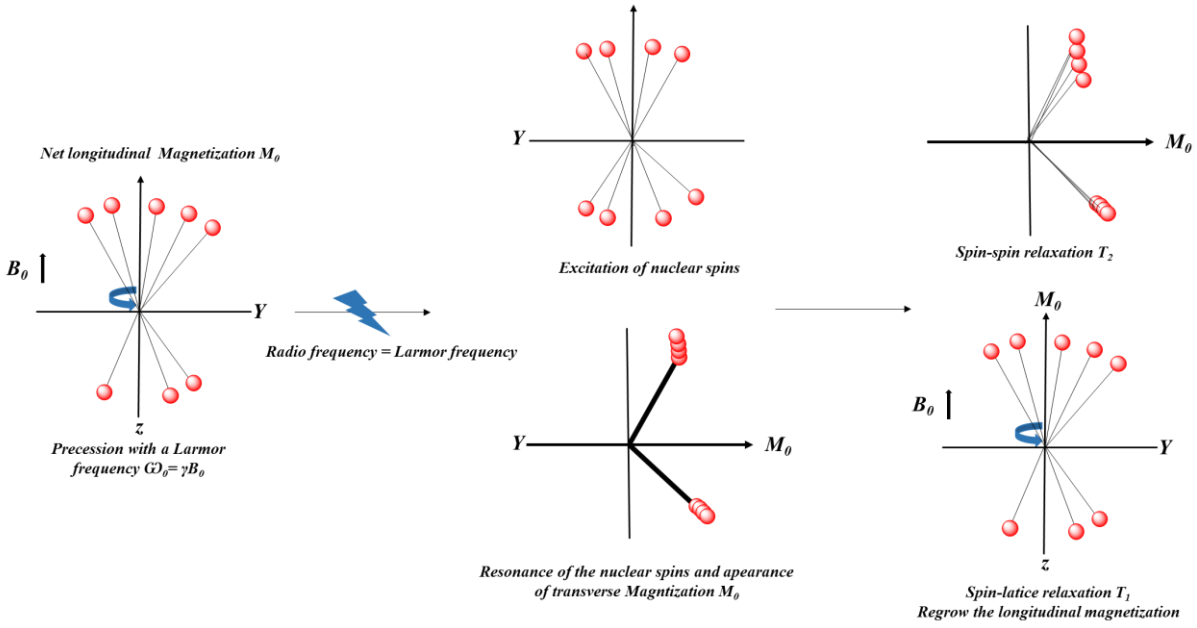

Figure 157: NMR principle.

The key factor affecting the sensitivity of the NMR signals is the polarization of the nuclei between the two states. Higher polarization results in a higher longitudinal magnetization M_0, enhancing thus the sensitivity. Back to (eq.4) enhancing the polarization can be reached by increasing the magnetic field (high costs) or by decreasing sample's temperature (not suitable for biological samples). A last way to improve the sensitivity is to play by the nuclear polarization

itself, by disturbing the thermal Boltzmann equilibrium of nuclei between the different states into a non-equilibrated polarization or the so-called hyperpolarization which will be detailed throughout the introductory chapter of the first part.

2. Optical Activity of Chiral Molecules and the Spectroscopic Tools

The optical activity of chiral molecules originates from their differential interaction with contra-rotational components of the plane polarized light i.e. left and right circularly components. In other word, chiral molecules tend to affect the respective velocities and intensities of left and right polarized lights. These effects are the origin of what is known as the optical rotation and circular dichroism.

2.1.Optical Rotatory Dispersion ORD and Polarimetry:

When passed through a chiral sample, the two compartments of circularly polarized light are transmitted at different velocities. This will lead to a rotation of their resultant plane polarized light by an angle noted α. The difference in left and right circularly polarized light velocities originates from the difference in the refractive indices of these two components in a chiral sample. This phenomenon is the origin of optical rotation.

$$\boldsymbol{\alpha = \frac{180l\,(nL-nR)}{\lambda}}$$

Optical rotation angle α is expressed in the above equation where l is path length, n is the refractive index and λ is the wavelength. This equation shows that α is proportional to the difference in the refractive indices and it is inversely proportional to the wavelength.

This angle can be measured by a polarimeter at a well-defined wavelength. The sodium D-line transition at 589 nm is the most common used. To characterize each sample a correction with respect to the concentration is needed. Thus, the Specific Optical Rotation (SOR) $[\alpha]_{\lambda\ (nm)}$

characterizes each enantiopure compound. Since $[\alpha]_{589}$ is also dependent on the temperature and concentration effect, these parameters have to be carefully mentioned. Concentration C is usually reported in g/100 mL of solvent and l' is cell length which is usually equal to 1 dm.

$$[\alpha]_{\lambda} = \frac{\alpha}{l'C}$$

Another way to measure SOR values as a function of the wavelength is the Optical Rotation Dispersion (ORD) and it can be extended to the UV-visible spectral regions (on-resonance). Two different parts of the ORD spectrum can be discussed. In the off-resonant spectral region (the molecule does not absorb light), the ORD curves tend to show a monotonous behavior. In addition the SOR values tend to increase negatively or positively as we get close to an absorption wavelength. In some other cases a change of the sign of the SOR values can be sometimes observed. In the on-resonant spectral region (the molecule absorbs light), the ORD spectrum shows a dispersion band (bisignate). This effect is called the anomalous effect (AORD). This effect is translated by the appearance of maximal peaks and minimal troughs. A quantum theoretical description of ORD spectroscopy can be found in some reviews and articles, Figure 158.[209, 210]

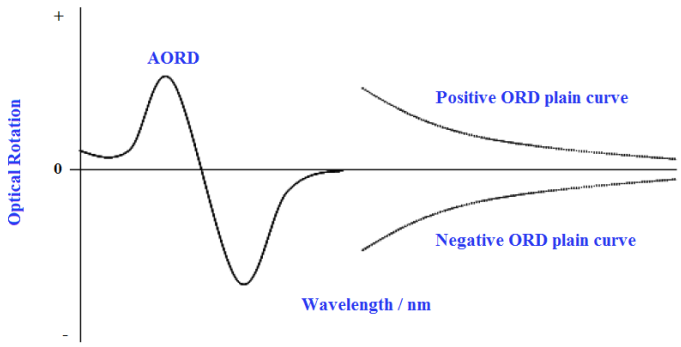

Figure 158: plain and anomalous ORD curves.

2.2. Electronic Circular Dichroism ECD Spectroscopy:

Circular dichroism results from a differential absorption of the left and right circularly polarized light by chiral molecules. In the classical approach, this difference affects the respective intensities of these two components creating an elliptical polarized light whose ellipticity is described by an angle θ which is characteristic of the chiral material studied. In an ECD spectrum, the difference in the absorptivity of the left and right circularly polarized light ($\Delta\varepsilon = \varepsilon_L - \varepsilon_R$) is traced as a function of the wavelength. Each excited state visible on the ECD spectrum has a characteristic *Rotational Strength* R_{ij} that determines its intensity and sign. The shape of the ECD spectrum is the result of the summation of all contributed rotational strengths of each electronic transition. It is worth mentioning that the sum of the rotational strengths extended to all the excited states is equal to zero. Nevertheless, it is important to note that the experimentalists do not have access to the whole ECD spectrum. Usually, the spectral range that is accessible depends on many different factors: the molecule it-self, the solvent, the concentration, and the spectrophotometer used. For instance, it is now possible to extend the spectral range by using Synchrotron Radiation circular Dichroism Spectroscopy.

It is worth to note that ORD and ECD are strongly related via Kramers–Kronig relationship.[211] Thus, theoretically these two spectra can be deduced from each other but practically this is difficult to achieve since we cannot have access to the whole ECD or ORD spectra. In recent years, numerous studies have been undertaken to predict ORD curves from partial ECD spectra, Figure 159.

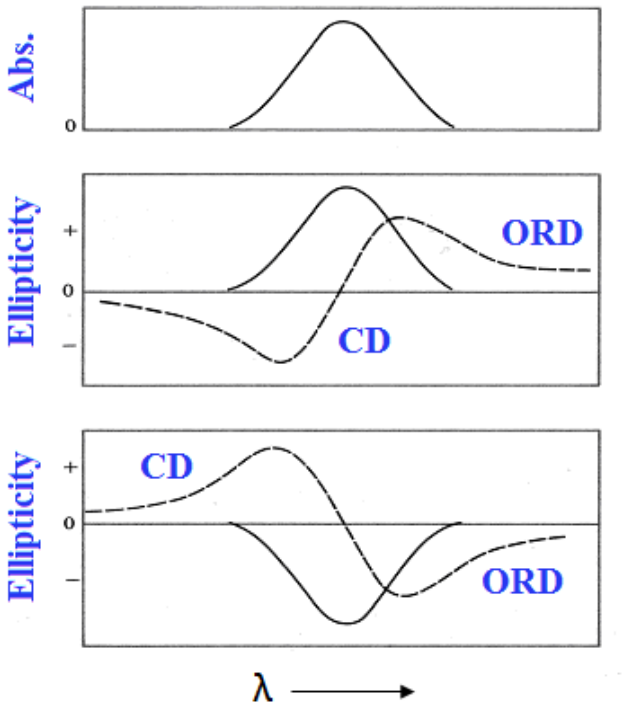

Figure 159: ORD curves and the corresponding ECD Cotton bands.

The presence of more than one chromophore in cryptophane molecules, in close vicinity to each other and with proper orientations results in the interaction between them. This is called the excitonic coupling. This phenomenon is defined as the delocalization of the electronic excitation along the chromophores array, rather being confined on one chromophore. The process generates coupling interactions of the initial excited states to form new excitonic states, which are slightly shifted in frequency with respect to the initial excited state. Absorption of light in the ECD spectrum results in a bisignate band (positive-negative or negative-positive). For two chromophores interacting with each other, the sign of these ECD bands can be easily interpreted by the excitonic coupling method developed by Nakanishi and co-workers.[212] It is noteworthy that in the case of cryptophane derivatives where six chromophore are involved a direct interpretation of their excitonic coupling is more complicated and can only understood by using quantum calculations, Figure 160.

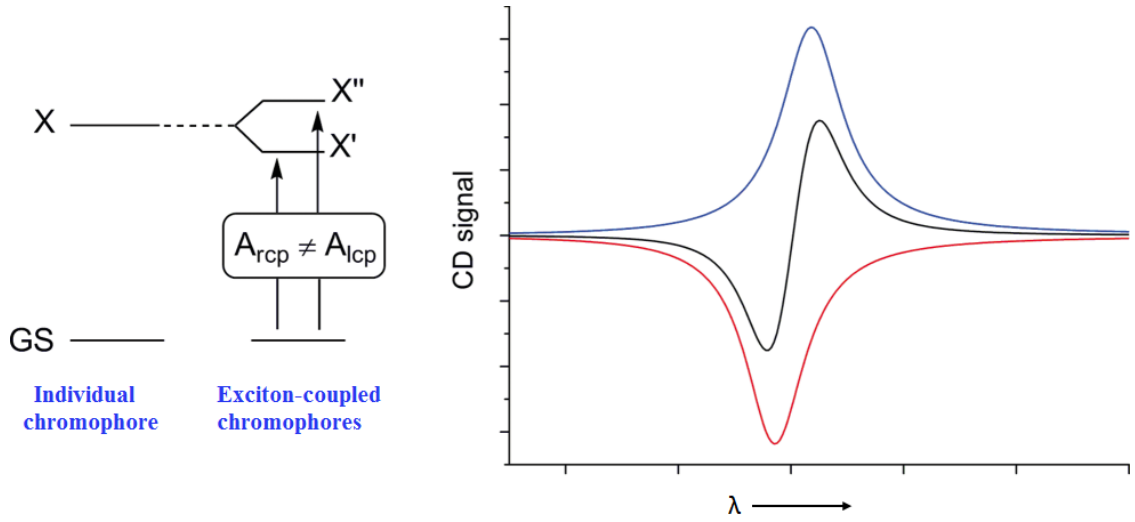

Figure 160: Differential absorption of left and right polarized light by the exciton coupled chromophores and the corresponding excitonic couplets (black curve) which is a summation of the positive (blue curve) and negative (red curve) Cotton effects.

Since, ECD spectroscopy depends on geometrical factors this technique is highly sensitive to conformational changes of the chiral molecules. Thus, a change of the conformation induced by external factors such as the nature of the solvent, temperature or in the case of the cryptophane derivatives the presence of a guest molecule inside its cavity can have a large impact on the ECD spectrum. ECD spectroscopy can also be used to determine the absolute configuration of chiral molecules.

ECD spectra can be reproduced by quantum calculations by using TD-DFT. However, these theoretical spectra are quite difficult to reproduce because we need to consider many excited states. These simulated spectra give better results if we consider the role of the solvent (implicit or explicit model). However, this increases the complexity of such simulation and considerably increases the computational time.

2.3. Vibrational Circular Dichroism VCD Spectroscopy:

Similar to the above described ECD spectroscopy, vibrational circular dichroism is the measurement of the differential absorption of left and right circularly polarized light in the infrared region. The obtained VCD spectra of two enantiomers are equal in magnitude but opposite in signs just like ECD spectra. In contrast to ECD spectroscopy, VCD spectra are more complicated in shape since each vibrational mode possess its own rotational strength. Thus numerous transitions can be detected on the VCD spectra of organic molecules. Nevertheless, solvent absorption often decreases the spectral window accessible. Thus the choice of the organic solvent is critical to record such spectra. Usually, CD_2Cl_2, $CDCl_3$, 1,1,2,2-terachloroethane-d_2 or even DMSO-d_6 can be used to record spectra between 1800 cm^{-1} and 1000 cm^{-1}. Despite the strong absorption of water, VCD experiments can also be performed in deuterated water but these experiments usually require small path-length compared to organic solvents. This spectral region contains numerous bands and that can be useful to get information about the absolute configuration of the molecule of interest and its conformation in solution. Interestingly, this technique gives rise to VCD spectra, which are the sum of all conformations adopted by the molecule in solution. This may complicate the analysis of these spectra in the case of highly flexible molecules. VCD spectra can be reproduced by DFT calculation. A comparison of the experimental and calculated spectra allows the determination of the absolute configuration of the molecule. In addition it gives insights about the conformation adopted by the molecule in solution. Sometimes, a weighted sum of theoretical VCD spectra is necessary to reproduce the experimental VCD spectrum. VCD spectroscopy only requires calculation performed on the ground state contrary to ECD spectroscopy. This represents an undeniable advantage to perform these calculations. VCD spectra are more difficult to record than ECD spectra. Consequently,

they require specific skills to obtain VCD spectra of good quality and avoid misinterpretation of the results. This is the reason why we have undertaken collaboration with Thierry Buffeteau and co-workers at the University of Bordeaux.[198]

List of Main Compounds Synthesized and Their Corresponding Numbers

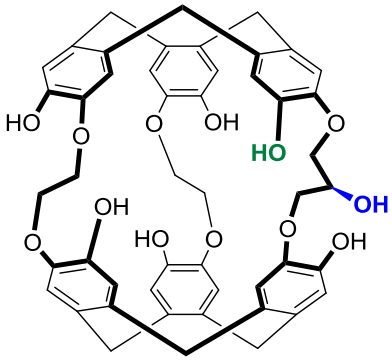

12

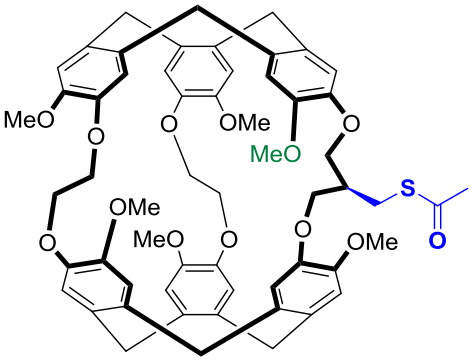

29

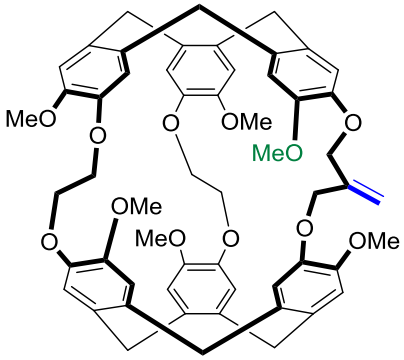

26

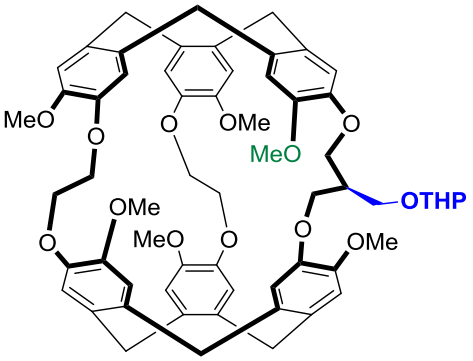

34

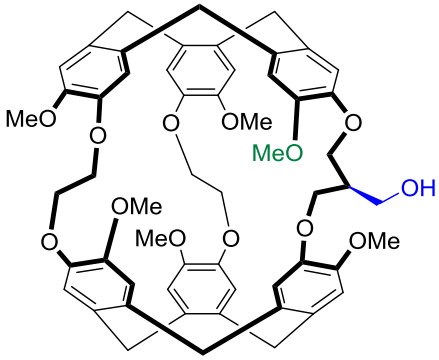

27

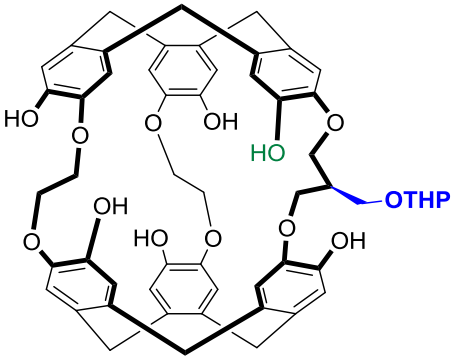

35

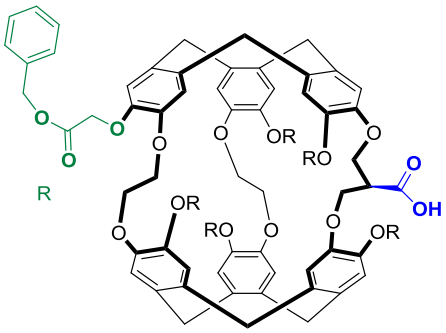

43 R =

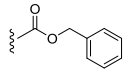

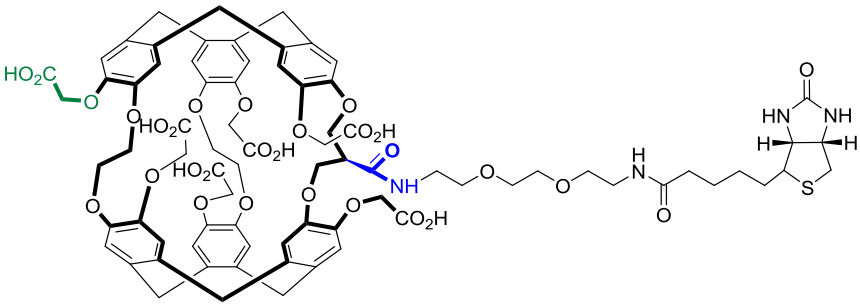

57

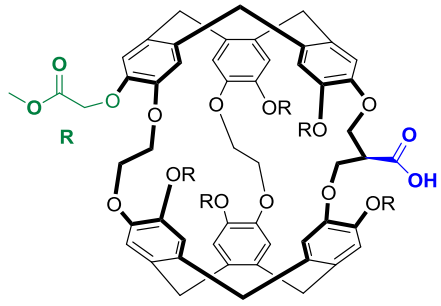

44 R =

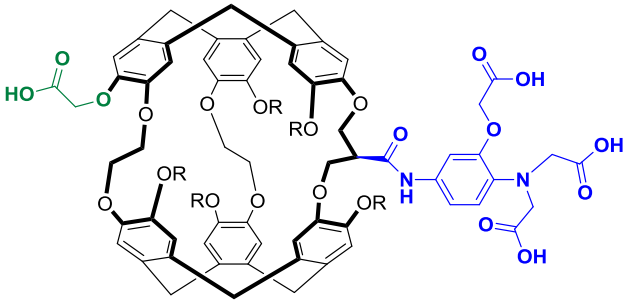

55

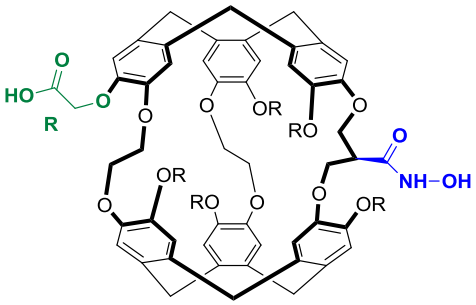

48

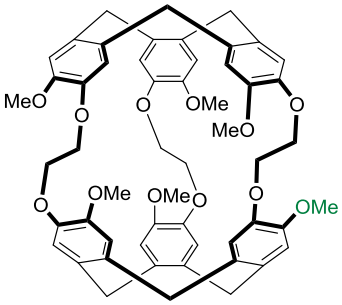

58

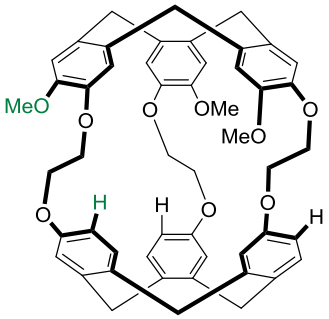

59

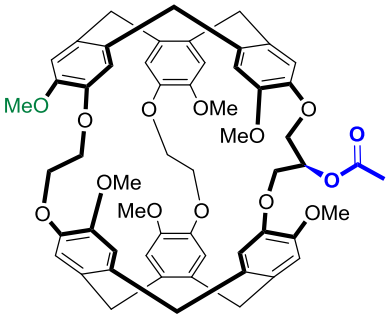

110

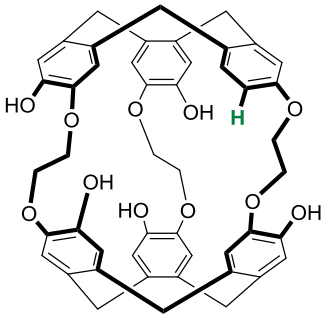

99

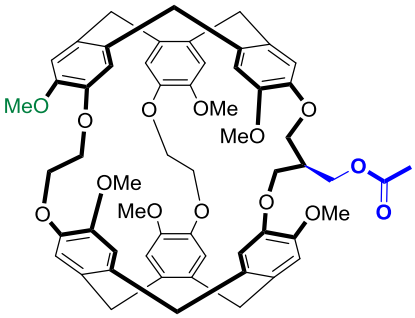

111

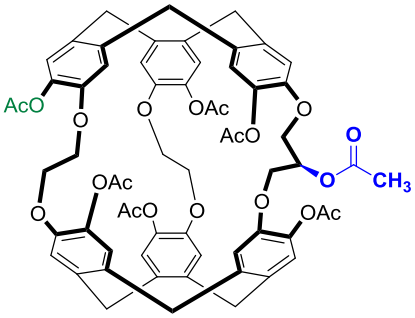

109

References

References

(1) Cram, D. J. International Edition in English. *Angew. Chemie Int. Ed. English* **1985**, *24* (10), 799–810.

(2) Lehn, J. M. Cryptates: Inclusion Complexes of Macropolycyclic Receptor Molecules. *Pure Appl. Chem.* **2007**, *50* (9–10), 871–892. https://doi.org/10.1351/pac197850090871.

(3) Lehn, J. M. Towards Complex Matter: Supramolecular Chemistry and Self-Organization. *Eur. Rev.* **2009**, *17* (2), 263–280. https://doi.org/10.1017/S1062798709000805.

(4) Kyba, E. P.; Helgeson, R. C.; Madan, K.; Gokel, G. W.; Tarnowski, T. L.; Moore, S. S.; Cram, D. J. Host-Guest Complexation. 1. Concept and Illustration. *J. Am. Chem. Soc.* **1977**, *99* (8), 2564–2571. https://doi.org/10.1021/ja00450a026.

(5) Fischer, E. Einfluss der Configuration auf die Wirkung der Enzyme. *Berichte der deutschen chemischen Gesellschaft* **1984**, *27*(3), 2985-2993.

(6) Schneider, H. J. Limitations and Extensions of the Lock-and-Key Principle: Differences between Gas State, Solution and Solid State Structures. *Int. J. Mol. Sci.* **2015**, *16* (4), 6694–6717. https://doi.org/10.3390/ijms16046694.

(7) Cram, D. J. Molecular Container Compounds. *Nature* **1992**, *356* (6364), 29–36. https://doi.org/10.1038/356029a0.

(8) Pedersen, C. J. Cyclic Polyethers and Their Complexes with Metal Salts. *J. Am. Chem. Soc.* **1967**, *89* (26), 7017–7036. https://doi.org/10.1021/ja01002a035.

(9) Dietrich, B.; Lehn, J. M.; Sauvage, J. P. Diaza-Polyoxa-Macrocycles et Macrobicycles. *Tetrahedron Lett.* **1969**, *10* (34), 2885–2888. https://doi.org/10.1016/S0040-4039(01)88299-X.

(10) Kyba, E. B.; Koga, K.; Sousa, L. R.; Siegel, M. G.; Cram, D. J. Chiral Recognition in Molecular Complexing. *J. Am. Chem. Soc.* **1973**, *95* (8), 2692–2693. https://doi.org/10.1021/ja00789a051.

(11) Shi, Y.; Cai, K.; Xiao, H.; Liu, Z.; Zhou, J.; Shen, D.; Qiu, Y.; Guo, Q. H.; Stern, C.; Wasielewski, M. R.; Diederich, F. Selective Extraction of C70 by a Tetragonal Prismatic Porphyrin Cage. *J. Am. Chem. Soc.* **2018**, *140* (42), 13835–13842. https://doi.org/10.1021/jacs.8b08555.

(12) Ballester, P.; Fujita, M.; Rebek, J. Molecular Containers. *Chem. Soc. Rev.* **2015**, *44* (2), 392–393. https://doi.org/10.1039/c4cs90101k.

(13) Moran, J.R., Karbach, S. Cram, D.J. Cavitands: Synthetic Molecular Vessels. *J. Am. Chem. Soc.* **1982**, *104* (21), 5826-5828.

(14) Turner, D. R.; Pastor, A.; Alajarin, M.; Steed, J. W. Molecular Containers: Design Approaches and Applications **2012**, *108*, 97–168. https://doi.org/10.1007/b14138.

(15) Bryant, J. A.; Blanda, M. T.; Vincenti, M.; Cram, D. J. Host-Guest Complexation. 55. Guest Capture during Shell Closure. *J. Am. Chem. Soc.* **2005**, *113* (6), 2167–2172. https://doi.org/10.1021/ja00006a040.

References

(16) Liu, F.; Wang, H.; Houk, K. N. Gated Container Molecules. *Sci. China Chem.* **2011**, *54* (12), 2038–2044. https://doi.org/10.1007/s11426-011-4429-1.

(17) Rudkevich, D. M. Nanoscale Molecular Containers. *Bull. Chem. Soc. Jpn.* **2002**, *75* (3), 393–413. https://doi.org/10.1246/bcsj.75.393.

(18) Gabard J.; Collet A. Synthesis of a (D_3)-Bis(cyclotriveratrylenyl) Macrocage by Stereospecific Replication of a (C_3)-Subunit. *Chem. Comm.* **1981**, *21*, 1137–1139.

(19) Sherman, J. C.; Knobler, C. B.; Cram, D. J. Syntheses and Properties of Soluble Carceplexes. *J. Am. Chem. Soc.* **1991**, *113* (6), 2194–2204. https://doi.org/10.1021/ja00006a043.

(20) Szejtli, J. Introduction and General Overview of Cyclodextrin Chemistry. *Chem. Rev.* **2002**, *98* (5), 1743–1754. https://doi.org/10.1021/cr970022c.

(21) Zhang, D., Martinez, A., Dutasta, JP. Emergence of Hemicryptophanes: From Synthesis to Applications for Recognition, Molecular Machines, and Supramolecular Catalysis. *Chem. rev.* **2017**, *117*(6), 4900-42.

(22) Szejtli, J. Introduction and General Overview of Cyclodextrin Chemistry. *Chem. Rev.* **1998**, *98* (5), 1743–1754. https://doi.org/10.1021/cr970022c.

(23) Zyryanov, G. V.; Rudkevich, D. M.; Organo, V. G.; Leontiev, A. V.; Kang, Y. Molecular Containers for NOX Gases. *Supramol. Chem.* **2004**, *17* (1–2), 93–99. https://doi.org/10.1080/10610270412331328808.

(24) Warmuth, R. The Inner Phase of Molecular Container Compounds as a Novel Reaction Environment. *J. Incl. Phenom. Macrocycl. Chem.* **2000**, *37*, 1–38.

(25) Collet, A. Cyclotriveratrylenes and Cryptophanes. *Tetrahedron* **1987**, *43* (24), 5725–5759. https://doi.org/10.1016/S0040-4020(01)87780-2.

(26) Brotin, T.; Dutasta, J. P. Cryptophanes and Their Complexes - Present and Future. *Chem. Rev* **2009**, *40* (19), 88–130. https://doi.org/10.1002/chin.200919253.

(27) El-Ayle, G.; Holman, K. T. *Cryptophanes* 2017; Vol. 6. https://doi.org/10.1016/B978-0-12-409547-2.13925-3.

(28) Lindsey, A. S. The Structure of Cyclotriveratrylene (10,15-Dyhydro-2,3,7,8,12,13-Hexamethpxy-5H-Tribenzo[a,d,g]Cyclononene) and Related Compounds. *J. Am. Chem. Soc.* **1965**, *1965*, 1685–1692.

(29) Canceill, J.; Lacombe, L.; Collet, A. Analytical Optical Resolution of Bromochlorofluoromethane by Enantioselective Inclusion into a Tailor-Made "Cryptophane" and Determination of Its Maximum Rotation. *J. Am. Chem. Soc.* **1985**, *107* (24), 6993–6996.

(30) Steed, J. W.; Junk, P. C.; Atwood, J. L.; Barnes, M. J.; Raston, C. L.; Burkhalter, R. S. Ball and Socket Nanostructures: New Supramolecular Chemistry Based on Cyclotriveratrylene. *J. Am. Chem. Soc.* **1994**, *116* (22), 10346–10347. https://doi.org/10.1021/ja00101a083.

References

(31) Jurisson, S. S.; Mitchell, A. R.; Burkhalter, R. S.; Holman, K. T.; Steed, J. W.; Halihan, M. M.; Atwood, J. L. Inclusion of Neutral and Anionic Guests within the Cavity of π-Metalated Cyclotriveratrylenes. *J. Am. Chem. Soc.* **2002**, *118* (40), 9567–9576. https://doi.org/10.1021/ja961655w.

(32) Canceill, J.; Collet, A.; Gabard, J.; Kotzyba-Hibert, F.; Lehn, J. M. Speleands. Macropolycyclic Receptor Cages Based on Binding and Shaping Sub-units. Synthesis and Properties of Macrocycle Cyclotriveratrylene Combinations. Preliminary Communication. *Helv. Chim. Acta* **1982**, *65* (6), 1894–1897. https://doi.org/10.1002/hlca.19820650623.

(33) Gabard, J.; Canceill, J.; Collét, A. New D_3 and C_{3h} Cryptophanes with Ethelynic Bridges Structural Assignments, Absolute Confugrations and Circular Dichriosm of D_3 Isomers. *Tetrahedron* **1987**, *43* (20), 4531–4538.

(34) Canceill, J.; Collét, A.; Gottarelli, G.; Palmieri, P. Synthesis and Exciton Optical Activity of D3-Cryptophanes. *J. Am. Chem. Soc.* **1987**, *109* (21), 6454–6464. https://doi.org/10.1021/ja00255a035.

(35) Akabori, S.; Takeda, M.; Miura, M. The Complexing Abilities of Diethyleneoxy- and Xylene-Bridged Cryptophanes with Alkanes. *Supramol. Chem.* **1999**, *10* (4), 253–262. https://doi.org/10.1080/10610279908054509.

(36) Mulatier, J. C.; Jeanneau, E.; Berthault, P.; Léonce, E.; Pitrat, D.; Brotin, T. Synthesis of Cryptophane-B: Crystal Structure and Study of Its Complex with Xenon. *J. Org. Chem.* **2018**, *83* (23), 14465–14471. https://doi.org/10.1021/acs.joc.8b02246.

(37) Canceill, J.; Collet, A. Two Step Synthesis of D_3 and C_{3h} Cryptophanes. *Chem. Commun.* **1988**, No. 582, 582–584.

(38) Huber, G.; Baydoun, O.; De Rycke, N.; Léonce, E.; Berthault, P.; Brotin, T. Unsaturated Cryptophanes: Toward Dual PHIP/Hyperpolarised Xenon Sensors. *Magn. Reson. Chem.* **2017**, *56* (7), 672–678. https://doi.org/10.1002/mrc.4691.

(39) Collet, A.; Barron, L. D.; Costante, J.; Hecht, L.; Polavarapu, P. L. Absolute Configuration of Bromochlorofluoromethane from Experimental and Ab Initio Theoretical Vibrational Raman Optical Activity. *Angew. Chemie Int. Ed. English* **2004**, *36* (8), 885–887. https://doi.org/10.1002/anie.199708851.

(40) Berthault, P.; Léonce, E.; Dognon, J.; Pitrat, D.; Mulatier, J.; Brotin, T. Accurate PH Sensing via Hyperpolarized Xe NMR. *Chem. - A Eur. J.* **2018**, *24*, 6534–6537.

(41) Chapellet, L. L.; Cochrane, J. R.; Mari, E.; Boutin, C.; Berthault, P.; Brotin, T. Synthesis of Cryptophanes with Two Different Reaction Sites: Chemical Platforms for Xenon Biosensing. *J. Org. Chem.* **2015**, *80* (12), 6143–6151. https://doi.org/10.1021/acs.joc.5b00653.

(42) Malthete, J.; Collet, A. Inversion of the Cyclotribenzylene Cone in a Columnar Mesophase: A Potential Way to Ferroelectric Materials. *J. Am. Chem. Soc.* **1987**, *109* (24), 7544–7545. https://doi.org/10.1021/ja00258a057.

(43) Dale, J. Multistep Conformational Interconversion Mechanisms. *Topics in Stereochemistry* **1976**, *9*, 200-265.

(44) Markopoulos, G.; Henneicke, L.; Shen, J.; Okamoto, Y.; Jones, P. G.; Hopf, H. Tribenzotriquinacene: A Versatile Synthesis and C3-Chiral Platforms. *Angew. Chemie - Int. Ed.* **2012**, *51* (51), 12884–12887. https://doi.org/10.1002/anie.201207220.

(45) Niu, W. X.; Wang, T.; Hou, Q. Q.; Li, Z. Y.; Cao, X. P.; Kuck, D. Synthesis and Optical Resolution of Inherently Chiral Difunctionalized Tribenzotriquinacenes. *J. Org. Chem.* **2010**, *75* (19), 6704–6707. https://doi.org/10.1021/jo101106k.

(46) Wang, T.; Zhang, Y. F.; Hou, Q. Q.; Xu, W. R.; Cao, X. P.; Chow, H. F.; Kuck, D. C3-Symmetrical Tribenzotriquinacene Derivatives: Optical Resolution through Cryptophane Synthesis and Supramolecular Self-Assembly into Nanotubes. *J. Org. Chem.* **2013**, *78* (3), 1062–1069. https://doi.org/10.1021/jo302470v.

(47) Mough, S. T.; Goeltz, J. C.; Holman, K. T. Isolation and Structure of an "Imploded" Cryptophane. *Angew. Chemie - Int. Ed.* **2004**, *43* (42), 5631–5635. https://doi.org/10.1002/anie.200460866.

(48) Haberhauer, G.; Woitschetzki, S.; Bandmann, H. Strongly Underestimated Dispersion Energy in Cryptophanes and Their Complexes. *Nat. Commun.* **2014**, *5*, 1–7. https://doi.org/10.1038/ncomms4542.

(49) Thorp-Greenwood, F. L.; Howard, M. J.; Kuhn, L. T.; Hardie, M. J. Fully Collapsed Imploded Cryptophanes in Solution and in the Solid State. *Chem. - A Eur. J.* **2019**, *25*, 1–6. https://doi.org/10.1002/chem.201900269.

(50) Huber, G.; Brotin, T.; Dubois, L.; Desvaux, H.; Dutasta, J. P.; Berthault, P. Water Soluble Cryptophanes Showing Unprecedented Affinity for Xenon: Candidates as NMR-Based Biosensors. *J. Am. Chem. Soc.* **2006**, *128* (18), 6239–6246. https://doi.org/10.1021/ja060266r.

(51) Mecozzi, S.; Rebek, J. The 55% Solution: A Formula for Molecular Recognition in the Liquid State. *Chem. - A Eur. J.* **1998**, *4* (6), 1016–1022. https://doi.org/10.1002/(SICI)15213765(19980615)4:6<1016::AIDCHEM1016>3.0.CO;2-B.

(52) Brotin, T.; Cavagnat, D.; Berthault, P.; Montserret, R.; Buffeteau, T. Water-Soluble Molecular Capsule for the Complexation of Cesium and Thallium Cations. *J. Phys. Chem. B* **2012**, *116* (35), 10905–10914. https://doi.org/10.1021/jp305110k.

(53) Canceill, J.; Cesario, M.; Collet, A.; Guilhem, J.; Lacombe, L.; L.; BknPdicte, C. P. Structure and Properties of the Cryptophane-E/$CHCl_3$, Complex, a Stable van Der Waals Molecule. *Angew. Chem.* **1989**, *28* (3), 1246–1248.

(54) Little, M. A.; Donkin, J.; Fisher, J.; Halcrow, M. A.; Loder, J.; Hardie, M. J. Synthesis and Methane-Binding Properties of Disulfide-Linked Cryptophane-0.0.0. *Angew. Chemie - Int. Ed.* **2012**, *51* (3), 764–766. https://doi.org/10.1002/anie.201106512.

(55) Fogarty, H. A.; Berthault, P.; Brotin, T.; Huber, G.; Desvaux, H.; Dutasta, J. P. A Cryptophane Core Optimized for Xenon Encapsulation. *J. Am. Chem. Soc.* **2007**, *129* (34), 10332–10333. https://doi.org/10.1021/ja073771c.

(56) Garel L.; Dutasta J. P.; Collet, A. Complexation of Methane and Chlorofluoro-Carbons by

Cryptophane-A in Organic Solution. *Angew. Chem.*, **1993**, *32* (8), 1169–1171.

(57) Soulard, P.; Asselin, P.; Cuisset, A.; Moreno, A.; Huet, J. R.; Petitprez, T. R.; Petitprez, D.; Demaison, J.; Freedman, T. B.; Cao, X.; Nafie, L. A.; Crassous, J. Chlorofluoroiodomethane as a Potential Candidate for Parity Violation Measurements. *Phys. Chem. Chem. Phys.* **2006**, *8* (1), 79–92. https://doi.org/10.1039/b510675c.

(58) Cram, D. J.; Tanner, M. E.; Keipert, S. J.; Knobler, C. B. Two Chiral [1.1.1] Orthocyclophane Units Bridged by Three Biacetylene Units as a Host Which Binds Medium-Sized Organic Guests. *J. Am. Chem. Soc.* **1991**, *113* (23), 8909–8916. https://doi.org/10.1021/ja00023a044.

(59) Holman, K. T. Encyclopedia of Supramolecular Chemistry, Volume 2. *Encycl. Supramol. Chem. 1* **2004**, *340*. https://doi.org/10.1081/E-ESMC.

(60) Bouchet, A.; Brotin, T.; Linares, M.; Ågren, H.; Cavagnat, D.; Buffeteau, T. Enantioselective Complexation of Chiral Propylene Oxide by an Enantiopure Water-Soluble Cryptophane. *J. Org. Chem.* **2011**, *76* (10), 4178–4181. https://doi.org/10.1021/jo200519r.

(61) De Rycke, N.; Jean, M.; Vanthuyne, N.; Buffeteau, T.; Brotin, T. Enantioselective Complexation of Chiral Oxirane Derivatives by an Enantiopure Cryptophane in Water. *Eur. J. Org. Chem.* **2018**, *2018* (13), 1601–1607. https://doi.org/10.1002/ejoc.201800142.

(62) Garel, L.; Lozach, B.; Dutasta, J. P.; Collet, A. Remarkable Effect of Receptor Size in the Binding of Acetylcholine and Related Ammonium Ions to Water-Soluble Cryptophanes. *J. Am. Chem. Soc.* **1993**, *115* (24), 11652–11653. https://doi.org/10.1021/ja00077a096.

(63) Garcia, C.; Humilière, D.; Riva, N.; Collet, A.; Dutasta, J.P. Kinetic and Thermodynamic Consequences of the Substitution of SMe for OMe Substituents of Cryptophane Hosts on the Binding of Neutral and Cationic Guests. *Org. Biomol. Chem.* **2003**, *1* (12), 2207–2216. https://doi.org/10.1039/b211363e.

(64) Chapellet, L. L.; Dognon, J. P.; Jean, M.; Vanthuyne, N.; Berthault, P.; Buffeteau, T.; Brotin, T. Experimental and Theoretical Study of the Complexation of Cesium and Thallium Cations by a Water-Soluble Cryptophane. *ChemistrySelect* **2017**, *2* (19), 5292–5300. https://doi.org/10.1002/slct.201700979.

(65) Brotin, T.; Montserret, R.; Bouchet, A.; Cavagnat, D.; Linares, M.; Buffeteau, T. High Affinity of Water-Soluble Cryptophanes for Cesium Cations. *J. Org. Chem.* **2012**, *77* (2), 1198–1201. https://doi.org/10.1021/jo202259r.

(66) Brotin, T.; Cavagnat, D.; Berthault, P.; Montserret, R.; Buffeteau, T. Water-Soluble Molecular Capsule for the Complexation of Cesium and Thallium Cations. *J. Phys. Chem. B* **2012**, *116* (35), 10905–10914. https://doi.org/10.1021/jp305110k.

(67) Brotin, T.; Goncalves, S.; Berthault, P.; Cavagnat, D.; Buffeteau, T. Influence of the Cavity Size of Water-Soluble Cryptophanes on Their Binding Properties for Cesium and Thallium Cations. *J. Phys. Chem. B* **2013**, *117* (41), 12593–12601. https://doi.org/10.1021/jp4074009.

(68) Fairchild, R. M.; Holman, K. T. Selective Anion Encapsulation by a Metalated

Cryptophane with a π-Acidic Interior. *J. Am. Chem. Soc.* **2005**, *127* (47), 16364–16365. https://doi.org/10.1021/ja055560i.

(69) Akabori, S.; Miura, M.; Takeda, M.; Yuzawa, S.; Habata, Y.; Ishii, T. Syntheses of Diethyleneoxy Bridged Cryptophanes and Their Complexing Abilities with Alkali Metal and Alkylammonium Cations. *Supramol. Chem.* **1996**, *7* (3), 187–193. https://doi.org/10.1080/10610279608027515.

(70) Taratula, O.; Hill, P. A.; Bai, Y.; Khan, N. S.; Dmochowski, I. J. Shorter Synthesis of Trifunctionalized Cryptophane - A Derivatives. *Org. Lett.* **2011**, *13* (6), 1414–1417. https://doi.org/10.1021/ol200088f.

(71) Brotin, T.; Vanthuyne, N.; Cavagnat, D.; Ducasse, L.; Buffeteau, T. Chiroptical Properties of Nona- and Dodecamethoxy Cryptophanes. *J. Org. Chem.* **2014**, *79* (13), 6028–6036. https://doi.org/10.1021/jo500621g.

(72) Kotera, N.; Delacour, L.; Traoré, T.; Tassali, N.; Berthault, P.; Buisson, D. A.; Dognon, J. P.; Rousseau, B. Design and Synthesis of New Cryptophanes with Intermediate Cavity Sizes. *Org. Lett.* **2011**, *13* (9), 2153–2155. https://doi.org/10.1021/ol2005215.

(73) Holman, K. T.; Drake, S. D.; Steed, J. W.; Orr, G. W.; Atwood, J. L. Anion Binding, Aryl-Extended Cyclotriguaiacylenes and an Aryl-Bridged Cryptophane That Provides Snapshots of a Molecular Gating Mechanism. *Supramol. Chem.* **2010**, *22* (11–12), 870–890. https://doi.org/10.1080/10610278.2010.514615.

(74) Canceill, J.; Lacombe, L.; Collet, A. Water-Soluble Cryptophane Binding Lipophilic Guests in Aqueous Solution. *J. Chem. Soc. Chem. Commun.* **1987**, No. 3, 219–221. https://doi.org/10.1039/C39870000219.

(75) Darzac, M.; Brotin, T.; Rousset-Arzel, L.; Bouchu, D.; Dutasta, J.P. Synthesis and Application of Cryptophanol Hosts: ^{129}Xe NMR Spectroscopy of a Deuterium-Labeled (Xe)2@bis-Cryptophane Complex. *New J. Chem.* **2004**, *28* (4), 502. https://doi.org/10.1039/b312979a.

(76) Darzac, M.; Brotin, T.; Bouchu, D.; Dutasta, J. P. Cryptophanols, New Versatile Compounds for the Synthesis of Functionalized Cryptophanes and Polycryptophanes. *Chem. Commun.* **2002**, *2* (1), 48–49. https://doi.org/10.1039/b109301k.

(77) Mari, E.; Berthault, P. ^{129}Xe NMR-Based Sensors: Biological Applications and Recent Methods. *Analyst* **2017**, *142* (18), 3298–3308. https://doi.org/10.1039/c7an01088e.

(78) Cavagnat, D.; Buffeteau, T.; Brotin, T. Synthesis and Chiroptical Properties of Cryptophanes Having C_1-Symmetry. *J. Org. Chem.* **2008**, *73* (1), 66–75. https://doi.org/10.1021/jo701662w.

(79) Wei, Q.; Seward, G. K.; Hill, P. A.; Patton, B.; Dimitrov, I. E.; Kuzma, N. N.; Dmochowski, I. J. Designing ^{129}Xe NMR Biosensors for Matrix Metalloproteinase Detection. *J. Am. Chem. Soc.* **2006**, *128* (40), 13274–13283. https://doi.org/10.1021/ja0640501.

(80) Hill, P. A.; Wei, Q.; Eckenhoff, R. G.; Dmochowski, I. J. Thermodynamics of Xenon Binding to Cryptophane in Water and Human Plasma. *J. Am. Chem. Soc.* **2007**, *129* (30),

9262–9263. https://doi.org/10.1021/ja072965p.

(81) Delacour, L.; Kotera, N.; Traoré T.; Garcia‐Argote, S.; Puente, C.; Leteurtre, F.; Gravel, G.; Léonce, E.; Boulard, Y.; Berthault, P.; Rousseau, B. "Clickable" Hydrosoluble PEGylated Cryptophane as a Universal Platform for ^{129}Xe Magnetic Resonance Imaging Biosensors. *Chem. - A Eur. J.* **2013**, *19* (19), 6089–6093. https://doi.org/10.1002/chem.201204218.

(82) Tyagi, R.; Witte, C.; Haag, R.; Schröder, L. Dendronized Cryptophanes as Water-Soluble Xenon Hosts for ^{129}Xe Magnetic Resonance Imaging. *Org. Lett.* **2014**, *16* (17), 4436–4439. https://doi.org/10.1021/ol501951z.

(83) Jayapaul, J.; Schröder, L. Complete Generation of a ^{129}Xe Biosensor on the Solid Support by Systematic Backbone Assembly. *Bioconjug. Chem.* **2018**, *29* (12), 4004–4011. https://doi.org/10.1021/acs.bioconjchem.8b00814.

(84) Fairchild, R. M.; Joseph, A. I.; Holman, K. T.; Fogarty, H. A.; Brotin, T.; Dutasta, J. P.; Boutin, C.; Huber, G.; Berthault, P. A Water-Soluble Xe@cryptophane-111 Complex Exhibits Very High Thermodynamic Stability and a Peculiar ^{129}Xe NMR Chemical Shift. *J. Am. Chem. Soc.* **2010**, *132* (44), 15505–15507. https://doi.org/10.1021/ja1071515.

(85) Traoré, T.; Delacour, L.; Berthault, P.; Cintrat, J. C.; Rousseau, B. Scalable Synthesis of Cryptophane-1.1.1 and Its Functionalization. *Org. Lett.* **2010**, *12* (5), 960–962. https://doi.org/10.1021/ol902952h.

(86) Dubost, E.; Kotera, N.; Garcia-Argote, S.; Boulard, Y.; Léonce, E.; Boutin, C.; Berthault, P.; Dugave, C.; Rousseau, B. Synthesis of a Functionalizable Water-Soluble Cryptophane-111. *Org. Lett.* **2013**, *15* (11), 2866–2868. https://doi.org/10.1021/ol4012019.

(87) Berthault, P.; Delacour, L.; Boutin, C.; Traoré, T.; Romieu, A.; Renard, P.-Y.; Clavé, G.; Tassali, N.; Kotera, N.; Rousseau, B. The First Metal-Free Water-Soluble Cryptophane-111. *Chem. Commun.* **2011**, *47* (34), 9702. https://doi.org/10.1039/c1cc13378k.

(88) Ramsay, W.; Travers, M.W. Argon and Its Companions. *Philos. Trans. R. Soc. London. Ser. A, Contain. Pap. a Math. or Phys. Character* **1901**, *197*, 47–89.

(89) Cullen, S. C.; Gross, E. G. The Anesthetic Properties of Xenon in Animals and Human Beings, with Additional Observations on Krypton. *Science* **1951**, *113* (2942), 580–582. https://doi.org/10.1126/science.113.2942.580.

(90) Frampas, C.; Augsburger, M.; Varlet, V. Xenon: From Medical Applications to Doping Uses. *Toxicol. Anal. Clin.* **2017**, *29* (3), 309–319. https://doi.org/10.1016/j.toxac.2017.03.121.

(91) Thevis, M.; Piper, T.; Geyer, H.; Schaefer, M. S.; Schneemann, J.; Kienbaum, P.; Schänzer, W. Urine Analysis Concerning Xenon for Doping Control Purposes. *Rapid Commun. Mass Spectrom.* **2014**, *29* (1), 61–66. https://doi.org/10.1002/rcm.7080.

(92) Harris, P. D.; Barnes, R. The Uses of Helium and Xenon in Current Clinical Practice. *Anaesthesia* **2008**, *63* (3), 284–293. https://doi.org/10.1111/j.1365-2044.2007.05253.x.

(93) Raftery, D.; Chmelka, B. F. Xenon NMR Spectroscopy. *Anu. reports NMR Spectrosc.*

2006, *57*, 205–270. https://doi.org/10.1007/978-3-642-78483-5_3.

(94) Cherubini, A.; Bifone, A. Hyperpolarised Xenon in Biology. *Prog. Nucl. Magn. Reson. Spectrosc.* **2003**, *42* (1–2), 1–30. https://doi.org/10.1016/s0079-6565(02)00052-3.

(95) Anger, B. C.; Schrank, G.; Schoeck, A.; Butler, K. A.; Solum, M. S.; Pugmire, R. J.; Saam, B. Gas-Phase Spin Relaxation of Xe-129. *Phys. Rev. A - At. Mol. Opt. Phys.* **2008**, *78* (4), 1–10. https://doi.org/10.1103/PhysRevA.78.043406.

(96) Ruppert, K.; Mata, J. F.; Brookeman, J. R.; Hagspiel, K. D.; Mugler, J. P. Exploring Lung Function with Hyperpolarized 129Xe Nuclear Magnetic Resonance. *Magn. Reson. Med.* **2004**, *51* (4), 676–687. https://doi.org/10.1002/mrm.10736.

(97) Ruppert, K.; Qing, K.; Patrie, J. T.; Altes, T. A.; Mugler, J. P. Using Hyperpolarized Xenon-129 MRI to Quantify Early-Stage Lung Disease in Smokers. *Acad. Radiol.* **2019**, *26* (3), 355–366. https://doi.org/10.1016/j.acra.2018.11.005.

(98) Torres, L.; Kammerman, J.; Hahn, A. D.; Zha, W.; Nagle, S. K.; Johnson, K.; Sandbo, N.; Meyer, K.; Schiebler, M.; Fain, S. B. "Structure-Function Imaging of Lung Disease Using Ultrashort Echo Time MRI." *Acad. Radiol.* **2019**, *26* (3), 431–441. https://doi.org/10.1016/j.acra.2018.12.007.

(99) Goodson, B. M.; Song, Y.-Q. Q.; Taylor, R. E.; Schepkin, V.; Brennan, K.; Chingas, G.; Budinger, T. F.; Navon, G.; Pines, A. In Vivo NMR and MRI Using Injection Delivery of Laser-Polarized Xenon. *Proc. Natl. Acad. Sci.* **1997**, *94* (26), 14725. https://doi.org/10.1073/pnas.94.26.14725.

(100) Duhamel, G.; Choquet, P.; Grillon, E.; Lamalle, L.; Leviel, J. L.; Ziegler, A.; Constantinesco, A. Xenon-129 MR Imaging and Spectroscopy of Rat Brain Using Arterial Delivery of Hyperpolarized Xenon in a Lipid Emulsion. *Magn. Reson. Med.* **2001**, *46* (2), 208–212. https://doi.org/10.1002/mrm.1180.

(101) Bartik, K.; Luhmer, M.; Heyes, S. J.; Ottinger, R.; Reisse, J. Probing Molecular Cavities in α-Cyclodextrin Solutions by Xenon NMR. *J. Magn. Reson. Ser. B* **1995**, *109* (2), 164–168. https://doi.org/10.1006/jmrb.1995.0005.

(102) Shepelytskyi, Y.; Li, T.; Karas, S.; Wade, A.; Hane, F. T.; Prete, B. R. J.; DeBoef, B.; Albert, M. S.; Chaudhuri, S.; Peloquin, B.; Cyclodextrin-Based Pseudorotaxanes: Easily Conjugatable Scaffolds for Synthesizing Hyperpolarized Xenon-129 Magnetic Resonance Imaging Agents. *ACS Omega* **2018**, *3* (1), 677–681. https://doi.org/10.1021/acsomega.7b01744.

(103) Fukutomi, J.; Adachi, Y.; Kaneko, A.; Kimura, A.; Fujiwara, H. Inclusion Complex Formation of Thiacalix[4]Arene and Xe in Aqueous Solution Studied by Hyperpolarized 129Xe NMR. *J. Incl. Phenom. Macrocycl. Chem.* **2007**, *58* (1–2), 115–122. https://doi.org/10.1007/s10847-006-9130-1.

(104) Adiri, T.; Marciano, D.; Cohen, Y. Potential ^{129}Xe-NMR Biosensors Based on Secondary and Tertiary Complexes of a Water-Soluble Pillar[5]Arene Derivative. *Chem. Commun.* **2013**, *49* (63), 7082–7084. https://doi.org/10.1039/c3cc43253j.

(105) Kim, B. S.; Ko, Y. H.; Kim, Y.; Lee, H. J.; Selvapalam, N.; Lee, H. C.; Kim, K. Water Soluble Cucurbit[6]Uril Derivative as a Potential Xe Carrier for ^{129}Xe NMR-Based Biosensors. *Chem. Commun.* **2008**, No. 24, 2756–2758. https://doi.org/10.1039/b805724a.

(106) Wang, Y.; Dmochowski, I. J. Cucurbit[6]Uril Is an Ultrasensitive ^{129}Xe NMR Contrast Agent. *Chem. Commun.* **2015**, *51* (43), 8982–8985. https://doi.org/10.1039/c5cc01826a.

(107) Wang, Y.; Dmochowski, I. J. An Expanded Palette of Xenon-129 NMR Biosensors. *Acc. Chem. Res.* **2016**, *49* (10), 2179–2187. https://doi.org/10.1021/acs.accounts.6b00309.

(108) Truxal, A.; Wemmer, D. E.; Cao, L.; Isaacs, L.; Pines, A. Directly Functionalized Cucurbit[7]Uril as a Biosensor for the Selective Detection of Protein Interactions by ^{129}Xe HyperCEST NMR. *Chem. - A Eur. J.* **2019**. https://doi.org/10.1002/chem.201900610.

(109) Li, T.; Pellizzari, R. M.; Albert, M. S.; Hane, F. T.; Plata, J. A.; Smylie, P.; DeBoef, B. In Vivo Detection of Cucurbit[6]Uril, a Hyperpolarized Xenon Contrast Agent for a Xenon Magnetic Resonance Imaging Biosensor. *Sci. Rep.* **2017**, *7* (1), 4–10. https://doi.org/10.1038/srep41027.

(110) Bartik, K.; Luhmer, M.; Dutasta, J. P.; Collet, A.; Reisse, J. ^{129}Xe and ^{1}H NMR Study of the Reversible Trapping of Xenon by Cryptophane-A in Organic Solution. *J. Am. Chem. Soc.* **1998**, *120* (4), 784–791. https://doi.org/10.1021/ja972377j.

(111) Brotin, T.; Dutasta, J.P. Xe @ Cryptophane Complexes with C_2 Symmetry : Synthesis and Investigations by ^{129}Xe NMR of the Consequences of the Size of the Host Cavity for Xenon. *European J. Org. Chem.* **2003**, *2003* (6), 973–984.

(112) Bai, Y.; Colle, R.; Khan, N. S.; Fitzgerald, R.; Jacobson, D. R.; Dmochowski, I. J.; Laureano-Perez, L. Measurement of Radon and Xenon Binding to a Cryptophane Molecular Host. *Proc. Natl. Acad. Sci.* **2011**, *108* (27), 10969–10973. https://doi.org/10.1073/pnas.1105227108.

(113) Aru Hill, P.; Wei, Q.; Troxler, T.; Dmochowski, I. J. Substituent Effects on Xenon Binding Affinity and Solution Behaviour of Water-Soluble Cryptophanes. *J. Am. Chem. Soc.* **2009**, *131* (8), 3069–3077. https://doi.org/10.1021/ja8100566.

(114) Joseph, A. I.; El-Ayle, G.; Boutin, C.; Léonce, E.; Berthault, P.; Travis Holman, T. Rim-Functionalized Cryptophane-111 Derivatives via Heterocapping, and Their Xenon Complexes. *Chem. Commun.* **2014**, *50* (100), 15905–15908. https://doi.org/10.1039/c4cc08001g.

(115) Brotin, T.; Lesage, A.; Emsley, L.; Collet, A. ^{129}Xe NMR Spectroscopy of Deuterium-Labeled Cryptophane-A Xenon Complexes: Investigation of Host-Guest Complexation Dynamics. *J. Am. Chem. Soc.* **2000**, *122* (6), 1171–1174. https://doi.org/10.1021/ja993053t.

(116) Spence, M. M.; Ruiz, E. J.; Rubin, S. M.; Lowery, T. J.; Winssinger, N.; Schultz, P. G.; Wemmer, D. E.; Pines, A. Development of a Functionalized Xenon Biosensor. *J. Am. Chem. Soc.* **2004**, *126* (46), 15287–15294. https://doi.org/10.1021/ja0483037.

(117) Huber, J. G.; Dubois, L.; Desvaux, H.; Dutasta, J. P.; Brotin, T.; Berthault, P. NMR Study of Optically Active Monosubstituted Cryptophanes and Their Interaction with Xenon. *J. Phys. Chem. A* **2004**, *108* (44), 9608–9615. https://doi.org/10.1021/jp0472055.

(118) Dubost, E.; Dognon, J. P.; Rousseau, B.; Milanole, G.; Dugave, C.; Boulard, Y.; Léonce, E.; Boutin, C.; Berthault, P. Understanding a Host-Guest Model System Through 129Xe NMR Spectroscopic Experiments and Theoretical Studies. *Angew. Chemie - Int. Ed.* **2014**, *53* (37), 9837–9840. https://doi.org/10.1002/anie.201405349.

(119) Spence, M. M.; Rubin, S. M.; Dimitrov, I. E.; Ruiz, E. J.; Wemmer, D. E.; Pines, A.; Yao, S. Q.; Tian, F.; Schultz, P. G. Functionalized Xenon as a Biosensor. *Proc. Natl. Acad. Sci.* **2001**, *98* (19), 10654–10657. https://doi.org/10.1073/pnas.191368398.

(120) Wu, T.; Dutasta, J. P.; Lowery, T. J.; Brotin, T.; Ruiz, E. J.; Schultz, P. G.; Wemmer, D. E.; King, D. S.; Pines, A.; Chavez, L. Optimization of Xenon Biosensors for Detection of Protein Interactions. *ChemBioChem* **2005**, *7* (1), 65–73. https://doi.org/10.1002/cbic.200500327.

(121) Barskiy, D. A.; Coffey, A. M.; Nikolaou, P.; Mikhaylov, D. M.; Goodson, B. M.; Branca, R. T.; Lu, G. J.; Shapiro, M. G.; Telkki, V.-V.; Zhivonitko, V. V; NMR Hyperpolarization Techniques of Gases. *Chem. a Eur. J.* **2017**, *23* (4), 725–751. https://doi.org/10.1002/chem.201603884.

(122) Goodson, B. M. Advances in Magnetic Resonance: Nuclear Magnetic Resonance of Laser-Polarized Noble Gases in Molecules, Materials, and Organisms. *J. Magn. Reson.* **2002**, *155* (2), 157–216. https://doi.org/10.1006/jmre.2001.2341.

(123) Pietraiß, T.; Gaede, H. C. Optically Polarized ^{129}Xe in NMR Spectroscopy. *Adv. Mater.* **1995**, *7* (10), 826–838. https://doi.org/10.1002/adma.19950071003.

(124) Garcia, S.; Chavez, L.; Lowery, T. J.; Han, S. I.; Wemmer, D. E.; Pines, A. Sensitivity Enhancement by Exchange Mediated Magnetization Transfer of the Xenon Biosensor Signal. *J. Magn. Reson.* **2007**, *184* (1), 72–77. https://doi.org/10.1016/j.jmr.2006.09.010.

(125) Bar-Shir, A.; Bulte, J. W. M.; Gilad, A. A. Molecular Engineering of Nonmetallic Biosensors for CEST MRI. *ACS Chem. Biol.* **2015**, *10* (5), 1160–1170. https://doi.org/10.1021/cb500923v.

(126) Hilty, C.; Lowery, T. J.; Wemmer, D. E.; Pines, A. Spectrally Resolved Magnetic Resonance Imaging of a Xenon Biosensor. *Angew. Chemie - Int. Ed.* **2005**, *45* (1), 70–73. https://doi.org/10.1002/anie.200502693.

(127) Mynar, J. L.; Lowery, T. J.; Wemmer, D. E.; Pines, A.; Fréchet, J. M. J. Xenon Biosensor Amplification via Dendrimer-Cage Supramolecular Constructs. *J. Am. Chem. Soc.* **2006**, *128* (19), 6334–6335. https://doi.org/10.1021/ja061735s.

(128) Seim, K. L.; Palaniappan, K. K.; Francis, M. B.; Meldrum, T.; Wu, W.; Pines, A.; Wemmer, D. E.; Bajaj, V. S. A Xenon-Based Molecular Sensor Assembled on an MS2 Viral Capsid Scaffold. *J. Am. Chem. Soc.* **2010**, *132* (17), 5936–5937. https://doi.org/10.1021/ja100319f.

(129) Ramirez, R. M.; Francis, M. B.; Palaniappan, K. K.; Wemmer, D. E.; Bajaj, V. S.; Pines, A. Molecular Imaging of Cancer Cells Using a Bacteriophage-Based ^{129}Xe NMR Biosensor . *Angew. Chemie Int. Ed.* **2013**, *52* (18), 4849–4853. https://doi.org/10.1002/anie.201300170.

(130) Roy, V.; Brotin, T.; Dutasta, J. P.; Charles, M. H.; Delair, T.; Mallet, F.; Huber, G.;

Desvaux, H.; Boulard, Y.; Berthault, P. A Cryptophane Biosensor for the Detection of Specific Nucleotide Targets through Xenon NMR Spectroscopy. *ChemPhysChem* **2007**, *8* (14), 2082–2085. https://doi.org/10.1002/cphc.200700384.

(131) Boutin, C.; Stopin, A.; Lenda, F.; Brotin, T.; Dutasta, J. P.; Jamin, N.; Sanson, A.; Boulard, Y.; Leteurtre, F.; Huber, G.; Bogaert-Buchmann, A.; Tassali N.; Desvaux, H.; Carrière, M.; Berthault P. Cell Uptake of a Biosensor Detected by Hyperpolarized ^{129}Xe NMR: The Transferrin Case. *Bioorganic Med. Chem.* **2011**, *19* (13), 4135–4143. https://doi.org/10.1016/j.bmc.2011.05.002.

(132) Milanole, G.; Mari, E.; Brotin, T.; Leonce, E.; Bousmah, Y.; Erard, M.; Boutin, C.; Berthault, P. Bimodal Detection of Proteins by ^{129}Xe NMR and Fluorescence Spectroscopy. *ChemBioChem* **2019**. https://doi.org/10.1002/cbic.201800802.

(133) Kotera, N.; Dutasta, J.-P.; Boutin, C.; Brotin, T.; Gravel, E.; Milanole, G.; Arhel, N.; Doris, E.; Léonce, E.; Berthault P.; Rousseau, B. A Doubly Responsive Probe for the Detection of Cys4-Tagged Proteins. *Chem. Commun.* **2015**, *51* (57), 11482–11484. https://doi.org/10.1039/c5cc04721h.

(134) Gyejacquot, M.; Desvaux, H.; Stopin, A.; Brotin, T.; Boulard, Y.; Dutasta, J.P.; Berthault, P.; Wendlinger, T. Effect of PH and Counterions on the Encapsulation Properties of Xenon in Water-Soluble Cryptophanes. *Chem.- A Eur. J.* **2010**, *16* (43), 12941–12946. https://doi.org/10.1002/chem.201001170.

(135) Kotera, N.; Tassali, N.; Léonce, E.; Boutin, C.; Berthault, P.; Brotin, T.; Dutasta, J. P.; Delacour, L.; Traoré, T.; Buisson, D. A.; Taran, F.; Coudert, S.; Rousseau, B. A Sensitive Zinc-Activated ^{129}Xe MRI Probe. *Angew. Chemie - Int. Ed.* **2012**, *51* (17), 4100–4103. https://doi.org/10.1002/anie.201109194.

(136) Tassali, N.; Kotera, N.; Boulard, Y.; Rousseau, B.; Dubost, E.; Brotin, T.; Dutasta, J.; Berthault, P. Smart Detection of Toxic Metal Ions, Pb^{2+} and Cd^{2+}, Using a ^{129}Xe NMR-Based Sensor. *Anal. Chem.* **2014**, *86*, 1783–1788.

(137) Seward, G. K.; Wei, Q.; Dmochowski, I. J. Peptide-Mediated Cellular Uptake of Cryptophane. *Bioconjug. Chem.* **2008**, *19* (11), 2129–2135. https://doi.org/10.1021/bc8002265.

(138) Khan, N. S.; Dmochowski, I. J.; Bai, Y.; Riggle, B. A.; Seward, G. K. Cryptophane-Folate Biosensor for ^{129}Xe NMR . *Bioconjug. Chem.* **2014**, *26* (1), 101–109. https://doi.org/10.1021/bc5005526.

(139) Taratula, O.; Bai, Y.; D'Antonio, E. L.; Dmochowski, I. J. Enantiopure Cryptophane-^{129}Xe Nuclear Magnetic Resonance Biosensors Targeting Carbonic Anhydrase. *Supramol. Chem.* **2015**, *27* (February 2015), 65–71. https://doi.org/10.1080/10610278.2014.906601.

(140) Dmochowski, I. J.; Aaron, J. A.; Hill, P. A.; Christianson, D. W.; Chambers, J. M.; Han, Z.; Kuzma, N. N. Cryptophane Xenon-129 Nuclear Magnetic Resonance Biosensors Targeting Human Carbonic Anhydrase. *J. Am. Chem. Soc.* **2009**, *131* (2), 563–569. https://doi.org/10.1021/ja806092w.

(141) Riggle, B. A.; Greenberg, M. L.; Wang, Y.; Wissner, R. F.; Zemerov, S. D.; Petersson, E.

J.; Dmochowski, I. J. A Cryptophane-Based "Turn-on" ^{129}Xe NMR Biosensor for Monitoring Calmodulin. *Org. Biomol. Chem.* **2017**, *15* (42), 8883–8887. https://doi.org/10.1039/c7ob02391j.

(142) Riggle, B. A.; Wang, Y.; Dmochowski, I. J. A "Smart" ^{129}Xe NMR Biosensor for PH-Dependent Cell Labeling. *J. Am. Chem. Soc.* **2015**, *137* (16), 5542–5548. https://doi.org/10.1021/jacs.5b01938.

(143) Hennig, A.; Sloniec, J.; Schnurr, M.; Witte, C.; Resch-Genger, U.; Schröder, L. Biomembrane Interactions of Functionalized Cryptophane-A: Combined Fluorescence and 129 Xe NMR Studies of a Bimodal Contrast Agent . *Chem. - A Eur. J.* **2013**, *19* (9), 3110–3118. https://doi.org/10.1002/chem.201203773.

(144) Jayapaul, J.; Rose, H. M.; Rossella, F.; Witte, C.; Schröder, L. Design and Characterization of Two Bifunctional Cryptophane A-Based Host Molecules for Xenon Magnetic Resonance Imaging Applications. *Chempluschem* **2014**, *79* (10), 1463–1471. https://doi.org/10.1002/cplu.201402179.

(145) Klippel, S.; Dçpfert, J.; Jayapaul, J.; Kunth, M.; Rossella, F.; Schnurr, M.; Witte, C.; Freund, C., Schroder, L. Cell Tracking with Caged Xenon: Using Cryptophanes as MRI Reporters upon Cellular Internalization. *Angew. Chemie - Int. Ed.* **2014**, *126*, 503 –506. https://doi.org/10.1002/anie.201307290.

(146) Witte, C.; Martos, V.; Rose, H. M.; Reinke, S.; Klippel, S.; Schröder, L.; Hackenberger, C. P. R. Live-Cell MRI with Xenon Hyper-CEST Biosensors Targeted to Metabolically Labeled Cell-Surface Glycans. *Angew. Chemie - Int. Ed.* **2015**, *54* (9), 2806–2810. https://doi.org/10.1002/anie.201410573.

(147) Yuan, Y.; Guo, Q.; Yang, S.; Bouchard, L.-S.; Liu, M.; Luo, Q.; Ren, L.; Zhang, B.; Zhou, X.; Jiang, W. Biothiol Xenon MRI Sensor Based on Thiol-Addition Reaction. *Anal. Chem.* **2016**, *88* (11), 5835–5840. https://doi.org/10.1021/acs.analchem.6b00403.

(148) Zeng, Q.; Guo, Q.; Yuan, Y.; Yang, Y.; Zhang, B.; Ren, L.; Zhang, X.; Luo, Q.; Liu, M.; Bouchard, L. S.; Zhou X. Mitochondria Targeted and Intracellular Biothiol Triggered Hyperpolarized ^{129}Xe Magnetofluorescent Biosensor. *Anal. Chem.* **2017**, *89* (4), 2288–2295. https://doi.org/10.1021/acs.analchem.6b03742.

(149) Yang, S.; Yuan, Y.; Jiang, W.; Ren, L.; Deng, H.; Bouchard, L. S.; Zhou, X.; Liu, M. Hyperpolarized ^{129}Xe Magnetic Resonance Imaging Sensor for H_2S. *Chem. - A Eur. J.* **2017**, *23* (32), 7648–7652. https://doi.org/10.1002/chem.201605768.

(150) Guo, Q.; Zeng, Q.; Jiang, W.; Zhang, X.; Luo, Q.; Zhang, X.; Bouchard, L. S.; Liu, M.; Zhou, X. A Molecular Imaging Approach to Mercury Sensing Based on Hyperpolarized ^{129}Xe Molecular Clamp Probe. *Chem. - A Eur. J.* **2016**, *22* (12), 3967–3970. https://doi.org/10.1002/chem.201600193.

(151) Schlundt, A.; Kilian, W.; Beyermann, M.; Sticht, J.; Günther, S.; Höpner, S.; Falk, K.; Roetzschke, O.; Mitschang, L.; Freund, C. A Xenon-129 Biosensor for Monitoring MHC-Peptide Interactions. *Angew. Chemie - Int. Ed.* **2009**, *48* (23), 4142–4145. https://doi.org/10.1002/anie.200806149.

References

(152) Meersmann, T.; Thomas, N. R.; Zamberlan, F.; Lesbats, C.; Pavlovskaya, G. E.; Rogers, N. J.; Faas, H. M.; Krupa, J. L. Molecular Sensing with Hyperpolarized ^{129}Xe Using Switchable Chemical Exchange Relaxation Transfer . *ChemPhysChem* **2015**, *16* (11), 2294–2298. https://doi.org/10.1002/cphc.201500367.

(153) Brotin, T.; Devic, T.; Lesage, A.; Emsley, L.; Collet, A. Synthesis of Deuterium-Labeled Cryptophane-A and Investigation of Xe@cryptophane Complexation Dynamics by 1D-EXSY NMR Experiments. *Chem. - A Eur. J.* **2001**, *7* (7), 1561–1573. https://doi.org/10.1002/1521-3765(20010401)7:7<1561::AID-CHEM1561>3.0.CO;2-9.

(154) Canceill, J.; Collet, A.; Gottarelli, G. Optical Activity Due to Isotopic Substitution. Synthesis, Stereochemistry, and Circular Dichroism of (+)- and (−)-[2,7,12-2H3]Cyclotribenzylene. *J. Am. Chem. Soc.* **1984**, *106* (20), 5997–6003. https://doi.org/10.1021/ja00332a042.

(155) Vatèle, J. M. One-Pot Selective Oxidation/Olefination of Primary Alcohols Using TEMPO-BAIB System and Stabilized Phosphorus Ylides. *Tetrahedron Lett.* **2006**, *47* (5), 715–718. https://doi.org/10.1016/j.tetlet.2005.11.100.

(156) Dalcanale, E.; Montanari, F. Selective Oxidation of Aldehydes to Carboxylic Acids with Sodium Chlorite-Hydrogen Peroxide. *J. Org. Chem.* **1986**, *51* (4), 567–569. https://doi.org/10.1021/jo00354a037.

(157) De Luca, L.; Giacomelli, G.; Masala, S.; Porcheddu, A. Trichloroisocyanuric/TEMPO Oxidation of Alcohols under Mild Conditions: A Close Investigation. *J. Org. Chem.* **2003**, *68* (12), 4999–5001. https://doi.org/10.1021/jo034276b.

(158) Vedejs, E.; Fuchs, P. L. Inversion of Acyclic Olefins by the Phosphorus Betaine Method. Scope and Limitations. *J. Am. Chem. Soc.* **1973**, *95* (3), 822–825. https://doi.org/10.1021/ja00784a032.

(159) Yale, H. L. The Hydroxamic Acids. *Chem. Rev.* **1943**, *33* (3), 209–256. https://doi.org/10.1021/cr60106a002.

(160) Codd, R. Traversing the Coordination Chemistry and Chemical Biology of Hydroxamic Acids. *Coord. Chem. Rev.* **2008**, *252* (12–14), 1387–1408. https://doi.org/10.1016/j.ccr.2007.08.001.

(161) Pathak, A.; Blair, V. L.; Ferrero, R. L.; Junk, P. C.; Tabor, R. F.; Andrews, P. C. Synthesis and Structural Characterisation of Bismuth(III) Hydroxamates and Their Activity against Helicobacter Pylori. *Dalt. Trans.* **2015**, *44* (38), 16903–16913. https://doi.org/10.1039/c5dt02259b.

(162) Chen, X.; Wang, L.; Du, Y.; Wu, Y.; Jia, X.; Yang, Y.; Hong, B. Design, Synthesis and Biological Evaluation of Hydroxamic Acid Derivatives as Potential High Density Lipoprotein (HDL) Receptor CLA-1 up-Regulating Agents. *Molecules* **2011**, *16* (11), 9178–9193. https://doi.org/10.3390/molecules16119178.

(163) Quéléver, G.; Burlet, S.; Garino, C.; Pietrancosta, N.; Laras, Y.; Kraus, J.-L. Simple Coupling Reaction between Amino Acids and Weakly Nucleophilic Heteroaromatic Amines. *J. Comb. Chem.* **2004**, *6* (5), 695–698. https://doi.org/10.1021/cc034069p.

(164) Yin, J.; Hu, Y.; Yoon, J. Fluorescent Probes and Bioimaging: Alkali Metals, Alkaline Earth Metals and PH. *Chem. Soc. Rev.* **2015**, *44* (14), 4619–4644. https://doi.org/10.1039/c4cs00275j.

(165) Gale, E. M.; Mukherjee, S.; Liu, C.; Loving, G. S.; Caravan, P. Structure-Redox-Relaxivity Relationships for Redox Responsive Manganese-Based Magnetic Resonance Imaging Probes. *Inorg. Chem.* **2014**, *53* (19), 10748–10761. https://doi.org/10.1021/ic502005u.

(166) Levy, L. A.; Murphy, E.; Raju, B.; London, R. E. Measurement of Cytosolic Free Magnesium Ion Concentration By ^{19}F NMR. *Biochemistry* **1988**, *27* (11), 4041–4048. https://doi.org/10.1021/bi00411a021.

(167) Otten, P. A.; London, R. E.; Levy, L. A. A New Approach to the Synthesis of APTRA Indicators. *Bioconjug. Chem.* **2001**, *12* (1), 76–83. https://doi.org/10.1021/bc000069w.

(168) Metten, B.; Smet, M.; Boens, N.; Dehaen, W. Synthesis of APTRA Derivatives as Building Blocks for Low-Affinity Fluorescent Ca^{2+} Indicators. *Synthesis (Stuttg).* **2005**, *11* (11), 1838–1844. https://doi.org/10.1055/s-2005-869900.

(169) Wang, J.; Qian, X. A Series of Polyamide Receptor Based PET Fluorescent Sensor Molecules: Positively Cooperative Hg^{2+} Ion Binding with High Sensitivity. *Org. Lett.* **2006**, *8* (17), 3721–3724. https://doi.org/10.1021/ol061297u.

(170) Ferreira, C. M. H.; Pinto, I. S. S.; Soares, E. V.; Soares, H. M. V. M. (Un)Suitability of the Use of PH Buffers in Biological, Biochemical and Environmental Studies and Their Interaction with Metal Ions-a Review. *RSC Adv.* **2015**, *5* (39), 30989–31003. https://doi.org/10.1039/c4ra15453c.

(171) Harty, M.; Bearne, S. L. Measuring Benzohydroxamate Complexation with Mg^{2+}, Mn^{2+}, Co^{2+}, and Ni^{2+} Using Isothermal Titration Calorimetry. *J. Therm. Anal. Calorim.* **2016**, *123* (3), 2573–2582. https://doi.org/10.1007/s10973-016-5290-4.

(172) Liu, C. -Y; Chang, H. -J; Uang, S. -S; Sun, P. -J. Aliphatic Hydroxamic Acids as Chelating Agents; the Stability of Their Proton and Metal Complexes. *J. Chinese Chem. Soc.* **1975**, *22* (3), 225–235. https://doi.org/10.1002/jccs.197500027.

(173) Farkas, E.; Enyedy, É. A.; Micera, G.; Garribba, E. Coordination Modes of Hydroxamic Acids in Copper(II), Nickel(II) and Zinc(II) Mixed-Ligand Complexes in Aqueous Solution. *Polyhedron* **2000**, *19* (14), 1727–1736. https://doi.org/10.1016/S0277-5387(00)00453-8.

(174) Berthault, P.; Léonce, E.; Dognon, J.; Pitrat, D.; Berthault, P.; Léonce, E.; Dognon, J.; Pitrat, D.; Mulatier, J.; Brotin, T. Accurate pH Sensing via Hyperpolarized 129-Xe NMR. *Chem. a Eur. J.* **2018**, *24*, 6534–6537.

(175) Garcia, C.; Humilière, D.; Nathalie, R.; Collet, A.; Dutasta J.-P. Kinetic and Thermodynamic Consequences of the Substitution of SMe for OMe Substituents of Cryptophane Hosts on the Binding of Neutral and Cationic Guests. *Org. Biomol. Chem.* **2003**, *1* (12), 2207–2216. https://doi.org/10.1039/b211363e

(176) Brotin, T.; Cavagnat, D.; Jeanneau, E.; Buffeteau, T. Synthesis of Highly Substituted

Cryptophane Derivatives. *J. Org. Chem.* **2013**, *78* (12), 6143–6153. https://doi.org/10.1021/jo4007738.

(177) Collet, A. Chromophores Chiraux possedant la symmetrie C_3. Synthese de Derives Optiquement Actifs du Cyclotriveratrylene. *Tetrahedron Lett.* **1978**, *15* (15), 1265–1268.

(178) Spada, G. P.; Gabard, J.; Gottarelli, G.; Canceill, J.; Collet, A. Exciton Approach to the Optical Activity of C_3-Cyclotriveratrylene Derivatives. *J. Am. Chem. Soc.* **1985**, *107* (5), 1299–1308. https://doi.org/10.1021/ja00291a033.

(179) Garcia, C.; Andraud, C.; Collet, A. New Key Compounds in Cyclotriveratrylene Chemistry. Synthesis, Optical Resolution, Absolute Configuration and Circular Dichroism of C_3-Cyclotriveratrylenes with Sulfur Substituents. *Supramol. Chem.* **1992**, *1* (1), 31–45. https://doi.org/10.1080/10610279208027439.

(180) Soulard, P.; Asselin, P.; Cuisset, A.; Aviles Moreno, J. R.; Huet, T. R.; Petitprez, D.; Demaison, J.; Freedman, T. B.; Cao, X.; Nafie, L. A. Chlorofluoroiodomethane as a Potential Candidate for Parity Violation Measurements. *Phys. Chem. Chem. Phys.* **2006**, *8* (1), 79–92. https://doi.org/10.1039/b510675c.

(181) Greschner, W.; Neumann, B.; Stammler, H. G.; Gröger, H.; Kuck, D. Enantiomerically Pure Tribenzotriquinacenes through Stereoselective Synthesis. *Angew. Chemie - Int. Ed.* **2015**, *54* (46), 13764–13768. https://doi.org/10.1002/anie.201506906.

(182) Xu, D.; Warmuth, R. Edge-Directed Dynamic Covalent Synthesis of a Chiral Nanocube. *J. Am. Chem. Soc.* **2008**, *130* (24), 7520–7521. https://doi.org/10.1021/ja800803c.

(183) Brotin, T.; Barbe, R.; Darzac, M.; Dutasta, J. P. Novel Synthetic Approach for Optical Resolution of Cryptophanol-A: A Direct Access to Chiral Cryptophanes and Their Chiroptical Properties. *Chem. - A Eur. J.* **2003**, *9* (23), 5784–5792. https://doi.org/10.1002/chem.200204614.

(184) Bouchet, A.; Brotin, T.; Cavagnat, D.; Buffeteau, T. Induced Chiroptical Changes of a Water-Soluble Cryptophane by Encapsulation of Guest Molecules and Counterion Effects. *Chem. - A Eur. J.* **2010**, *16* (15), 4507–4518. https://doi.org/10.1002/chem.200902740.

(185) Bouchet, A.; Brotin, T.; Linares, M.; Cavagnat, D.; Buffeteau, T. Influence of the Chemical Structure of Water-Soluble Cryptophanes on Their Overall Chiroptical and Binding Properties. *J. Org. Chem.* **2011**, *76* (19), 7816–7825. https://doi.org/10.1021/jo201167w.

(186) Taratula, O.; Kim, M. P.; Bai, Y.; Philbin, J. P.; Riggle, B. A.; Haase, D. N.; Dmochowski, I. J. Synthesis of Enantiopure, Trisubstituted Cryptophane - A Derivatives. *Org. Lett.* **2012**, *14* (14), 3580–3583. https://doi.org/10.1021/ol300943w.

(187) Tambuté, A.; Canceill, J.; Collet, A. Optical Resolution of C3 Cyclotriveratrylenes and D3 Cryptophanes by Liquid Chromatography on Chiral Stationary Phase Chiralpak-OT(+). *Bulletin of the Chemical Society of Japan*. 1989, pp 1390–1392. https://doi.org/10.1246/bcsj.62.1390.

(188) Miura, M.; Yuzawa, S.; Takeda, M.; Takeda, M.; Habata, Y.; Tanase, T.; Akabori, S. Syntheses of Aromatic Bridged Cryptophanes and Their Complexing Abilities with Alkyl

Ammonium Cations. *Supramol. Chem.* **1996**, *8* (1), 53–66. https://doi.org/10.1080/10610279608233968.

(189) Brotin, T.; Daugey, N.; Vanthuyne, N.; Jeanneau, E.; Ducasse, L.; Buffeteau, T. Chiroptical Properties of Cryptophane-223 and -233 Investigated by ECD, VCD, and ROA Spectroscopy. *J. Phys. Chem. B* **2015**, *119* (27), 8631–8639. https://doi.org/10.1021/acs.jpcb.5b04539.

(190) Buffeteau, T.; Pitrat, D.; Daugey, N.; Calin, N.; Jean, M.; Vanthuyne, N.; Ducasse, L.; Wien, F.; Brotin, T. Chiroptical Properties of Cryptophane-111. *Phys. Chem. Chem. Phys.* **2017**, *19* (28), 18303–18310. https://doi.org/10.1039/c7cp02045g.

(191) Pitrat, D.; Daugey, N.; Jean, M.; Vanthuyne, N.; Wien, F.; Ducasse, L.; Calin, N.; Buffeteau, T.; Brotin, T. Unusual Chiroptical Properties of the Cryptophane-222 Skeleton. *J. Phys. Chem. B* **2016**, *120* (49), 12650–12659. https://doi.org/10.1021/acs.jpcb.6b09771.

(192) Zarra, S.; Wood, D. M.; Roberts, D. A.; Nitschke, J. R. Molecular Containers in Complex Chemical Systems. *Chem. Soc. Rev.* **2015**, *44* (2), 419–432. https://doi.org/10.1039/c4cs00165f.

(193) Harris, K.; Fujita, D.; Fujita, M. Giant Hollow MnL2n Spherical Complexes: Structure, Functionalisation and Applications. *Chem. Commun.* **2013**, *49* (60), 6703–6712. https://doi.org/10.1039/c3cc43191f.

(194) Zhong, Z.; Ikeda, A.; Shinkai, S.; Sakamoto, S.; Yamaguchi, K. Creation of Novel Chiral Cryptophanes by a Self-Assembling Method Utilizing a Pyridyl-Pd(II) Interaction. *Org. Lett.* **2001**, *3* (7), 1085–1087. https://doi.org/10.1021/ol0157205.

(195) Pritchard, V. E.; Rota Martir, D.; Oldknow, S.; Kai, S.; Hiraoka, S.; Cookson, N. J.; Zysman-Colman, E.; Hardie, M. J. Homochiral Self-Sorted and Emissive IrIII Metallo-Cryptophanes. *Chem. - A Eur. J.* **2017**, *23* (26), 6290–6294. https://doi.org/10.1002/chem.201701348.

(196) Schaly, A.; Rousselin, Y.; Chambron, J. C.; Aubert, E.; Espinosa, E. The Stereoselective Self-Assembly of Chiral Metallo-Organic Cryptophanes. *Eur. J. Inorg. Chem.* **2016**, *2016* (6), 832–843. https://doi.org/10.1002/ejic.201501446.

(197) Brotin, T.; Montserret, R.; Bouchet, A.; Cavagnat, D.; Linares, M.; Buffeteau, T. High Affinity of Water-Soluble Cryptophanes for Cesium Cations. *J. Org. Chem.* **2012**, *77* (2), 1198–1201. https://doi.org/10.1021/jo202259r.

(198) Stephens, P. J.; Lowe, M. A. Vibrational Circular Dichroism. *Ann. Rev. Phys. Chem.* **1985**, *36*, 213–241.

(199) Brotin, T.; Cavagnat, D.; Dutasta, J.; Buffeteau, T. Vibrational Circular Dichroism Study of Optically Pure Cryptophane-A. *J. Am. Chem. Soc.* **2006**, *128*, 5533–5540.

(200) Brotin, T.; Cavagnat, D.; Buffeteau, T. Conformational Changes in Cryptophane Having C_1-Symmetry Studied by Vibrational Circular Dichroism. *J. Phys. Chem. A* **2008**, *112* (36), 8464–8470. https://doi.org/10.1021/jp804450w.

(201) Barron, L. D.; Hecht, L.; McColl, I. H.; Blanch, E. W. Raman Optical Activity Comes of

Age. *Mol. Phys.* **2004**, *102* (8), 731–744. https://doi.org/10.1080/00268970410001704399.

(202) Nafie, L. A. Infrared and Raman Vibrational Optical Activity: Theoretical and Experimental Aspects. *Annu. Rev. Phys. Chem.* **1997**, *48* (1), 357–386. https://doi.org/10.1146/annurev.physchem.48.1.357.

(203) Hamada, F.; Murai, K.; Akihiko, U.; Susuki, I.; and Osa, T. Excimer Formation and Intramolecular Self-Complexation of Double-Armed A-Cyclodextrin. *Bull. Chem. Soc. Jpn* **1988**, *61* (10), 3758–3760.

(204) Strutt, N. L.; Zhang, H.; Giesener, M. A.; Lei, J.; Stoddart, J. F. A Self-Complexing and Self-Assembling Pillar[5]Arene. *Chem. Commun.* **2012**, *48* (11), 1647–1649. https://doi.org/10.1039/c2cc16030g.

(205) Ni, M.; Hu, X. Y.; Jiang, J.; Wang, L. The Self-Complexation of Mono-Urea-Functionalized Pillar[5]Arenes with Abnormal Urea Behaviors. *Chem. Commun.* **2014**, *50* (11), 1317–1319. https://doi.org/10.1039/c3cc47823h.

(206) Canceill, J.; Lacombe, L.; Collet, A. New Cryptophane Forming Unusually Stable Inclusion Complexes with Neutral Guests in a Lipophilic Solvent. *J. Am. Chem. Soc.* **1986**, *108* (14), 4230–4232. https://doi.org/10.1021/ja00274a067.

(207) Mukhopadhyay, P.; Zuber, G.; Wipf, P.; Beratan, D. N. Contribution of a Solute's Chiral Solvent Imprint to Optical Rotation. *Angew. Chemie - Int. Ed.* **2007**, *46* (34), 6450–6452. https://doi.org/10.1002/anie.200702273.

(208) Edwards, J. C. Principles of NMR. *Process NMR Assoc. LLC, 87A Sand Pit Rd, Danbury CT* **2009**, *6810*. https://doi.org/10.1016/0165-9936(92)80053-9.

(209) Djerassi, C. Application of Optical Rotatory Dispersion Studies to Problems in Natural Products Chemistry. *Pure Appl. Chem.* **1961**, *20* (138), 475–504. https://doi.org/10.1351/pac196102030475.

(210) Purdie, N.; Brittain, H.G. Introduction to Chiroptical Phenomena. In Analytical Applications of Circular Dichroism. *Elsevier B.V.: Bristol-Myers*, USA, **1994**, 1–13.

(211) Warnke, I.; Furche, F. Circular Dichroism: Electronic. *Wiley Interdiscip. Rev. Comput. Mol. Sci.* **2012**, *2* (1), 150–166. https://doi.org/10.1002/wcms.55.

(212) Telfer, S. G.; McLean, T. M.; Waterland, M. R. Exciton Coupling in Coordination Compounds. *Dalt. Trans.* **2011**, *40* (13), 3097–3108. https://doi.org/10.1039/c0dt01226b.